**In re: Oil Spill by the Oil Rig "Deepwater Horizon" in
the Gulf of Mexico, on April 20, 2010**
UNITED STATES DISTRICT COURT
EASTERN DISTRICT OF LOUISIANA
MDL NO. 2179, SECTION J
JUDGE BARBIER: MAGISTRATE JUDGE SHUSHAN

Well-Test Analysis

Expert Report of Alain Gringarten

May 1, 2013

Table of Contents

Scope of Work

I have been retained on behalf of BP Exploration & Production to use methodologies from a field of petroleum engineering known as well-test analysis to provide input into the calculations of my colleague Professor Martin Blunt, who is submitting a separate expert report on the amount of cumulative oil flow, as well as to provide my own assessment of that amount. My analysis yields opinions about parameters that determine the amount of oil flow, such as permeability, flow rate, original oil in place, and pressure depletion of the Macondo reservoir. Government expert witnesses have in several cases used values for these attributes that are far different from those indicated by the pressure behaviour of the Macondo reservoir, which is often the most reliable method to ascertain these values. The government expert reports do not include a rigorous well-test analysis of the Macondo pressure and flow-rate data. In this report I analyse pressure and flow-rate data collected by a tool at the bottom of the well prior to the incident to determine the permeability of the reservoir. I then use this permeability to analyse the pressure data collected after the incident and determine the cumulative volume of oil that flowed from the reservoir, the original oil in place, and the amount of pressure depletion of the Macondo reservoir.

1. Preamble and professional background

I am a petroleum engineer and professor of petroleum engineering and Director of the Centre for Petroleum studies at Imperial College London. I have an MSc (1969) and a PhD (1971) in Petroleum Engineering from Stanford University. I was a Research Fellow at the Miller Research Institute for Basic Research in Science at the University of California at Berkeley from 1970 to 1972. After Berkeley, I spent five years with the French Geological Survey in Orleans, France. I then worked for five years for Schlumberger, a service company for the oil and gas industry, first in Melun, France, then in Houston, Texas. I spent fourteen years with Scientific Software – Intercomp, a consulting and software company, in London, UK and in Denver, Colorado. I became a professor at Imperial College in 1997.

I am an expert in well-test analysis for oil fields, through which I derive reservoir properties from available pressure and flow-rate data. I have pioneered many of the techniques used in modern well-test analysis and authored numerous papers and taught courses on the subject to practitioners and to students of all levels.

I have taught the basic principles presented in this report, namely fluid flow in porous media and well-test analysis, for over 30 years. My research combines experiment, theory and numerical modelling to study the movement of fluid flow underground with application to well-test analysis of complex fluids, wells and reservoirs. I have published over 90 papers.

I am an Honorary member of the Society of Petroleum Engineers (SPE)[1]. I was elected a Distinguished Member in 2002 and served as an SPE Distinguished Lecturer in 2003. I received the SPE Formation Evaluation Award[2] in 2001, the John Franklin Carll Distinguished Professional Award[3] in 2003, and the Cedric K. Ferguson certificate in 2005 for the best paper published in 2004. I am an independent director of two companies providing services to the oil industry.

My curriculum vitae and a full publications list are provided in Appendix G of this report.

This report describes the analysis I have performed, from September 2011 to April 2013, on the Macondo reservoir to calculate the volume of oil released during the *Deepwater Horizon* incident and on related issues. One of my former PhD students at Imperial College, Dr. Olalekan Aluko, has performed additional well-test analysis work in support of the analysis under my supervision, and his contribution is mentioned explicitly in the report.

The data I have used include pressure readings in the capping stack, laboratory-measured fluid and rock properties, and information from BP reports. I have also consulted relevant scientific papers in the public domain. I interpreted pressure measurements from the Macondo reservoir, both before and during the spill, to calculate the volume of oil released.

My calculations are based on well-known reservoir engineering principles and follow standard, verified approaches employed in the oil industry. This work and my conclusions would be understood by petroleum engineers with knowledge of fluid flow in porous media and well test analysis methods.

---

[1] Honorary Membership is conferred on individuals for outstanding service to SPE and/or in recognition of distinguished scientific or engineering achievement in fields encompassed in the Society's technical scope. Honorary Membership is the highest honor the Society bestows on an individual, and it is limited to 0.1% of the Society's membership.

[2] The SPE Formation Evaluation Award recognizes outstanding achievements in or contributions to the advancement of petroleum engineering in the area of formation evaluation, encompassing core analysis, well logging, and petrophysics.

[3] The John Franklin Carll Award recognizes distinguished contribution in the application of engineering principles to petroleum development and recovery.

TREX-011696R.005

2. Summary

I estimate that the Macondo reservoir released approximately 2.4-3 million stock tank barrels (MMstb).

In addition, I also separately determine another critical property of the Macondo reservoir, its permeability. Permeability refers to the ease with which the reservoir pore space allows fluid to flow. The higher the permeability of a reservoir, the more readily the oil flows through it. For this reason, permeability is strongly and directly correlated with the total flow volume.

The government experts use a variety of permeabilities ranging from 300 to more than 800 milliDarcies (mD), and virtually all who address it insist that the number is at least 500 mD. But they do so with little (if any) analysis of this decisive question. As I will explain below, on the few occasions these experts do apply industry-accepted methods to determine permeability, they do so in a circular way—by using their assumed flow rates. Because the government experts assume high flow rates, these efforts are preordained to result in high permeabilities. The government experts regard this approach as confirmation. I will demonstrate that it was foreordained from their (incorrect) premise.

In this report I will show that the best estimate for permeability is 238 mD, less than one half to one third of what most government experts contend. For this, I use the most modern and reliable well-test analysis methods, where reservoir parameters are derived from pressure and flow-rate data. This is the standard industry approach to assessing permeability, and it is more reliable than other methods because it is based on the actual flow of the formation fluid in the reservoir.

Specifically, I use data obtained from a tool placed at the bottom of the well before the incident to collect reservoir fluid samples. As explained below in Section 3.2.1, the device precisely measured pressure and flow rate as the fluid was drawn into a container and as the pressure built back up after the container was full. This is exactly the information needed to determine key reservoir parameters, like permeability. It is axiomatic in the field of well-test analysis, which is used (at least implicitly) by all the government experts to derive permeability, that permeability cannot be determined unless the underlying data includes both pressure and flow-rate measurements. For the Macondo incident, of course, flow rates are precisely what is unknown and being sought by all these experts. But the government experts ignore the rate-dependence of their permeability estimates—which is the driver and determinant of their flow calculations. None uses the method described here. Because the fluid-sampling tool was employed prior to the incident, and collected fluid at known flow rates, I am able to deduce permeability with high reliability.

I then use the permeability derived from this work as an input into my well-test analysis of the data from during the incident and after the well was shut in. In this analysis, I again employ the most up-to-date methodologies of well-test analysis, which are described in Section 3 and utilized in Sections 4 and 5. This sets my work apart from the government experts, who use out-of-date or incorrect methods. I find that approximately 2.4-3 million barrels of oil left the reservoir during the spill. Government experts

reach higher numbers in part because of their methodologies, which I will critique in Sections 3.3.1, 3.3.3, 5.6.3, and in Section 6.

3. The well-test analysis approach used in this study

My analysis, like that of several of the government experts, uses available pressure and flow-rate measurements from Macondo to infer the properties of the Macondo reservoir. This is known in the industry as well-test analysis. Unlike these government experts, however, I employ the most up-to-date well-test analysis methods available. In fact, I invented many of these techniques. To understand the power of these techniques and why they are much better than what the government experts use, I need to provide some background on well testing. I then go on to explain the particular methods as applied to Macondo.

3.1 Well-test fundamentals

Well-test analysis uses pressure and flow-rate information to ascertain the general structure of the reservoir and other key reservoir parameters, such as permeability. Because the rate of fluid flow in the reservoir is governed by well-known equations, we can use sophisticated techniques and computers to understand what combinations of reservoir properties could produce the pressure and/or flow-rate information we have measured. After a brief discussion of the fundamentals, we will look at some of these techniques as applied to Macondo.

When a fluid is produced into a well from an underground porous rock (here, the Macondo sandstone reservoir), the pressure decreases in the reservoir. *This is called a drawdown.* The decrease in pressure increases with the production rate and is higher right at the well than in the reservoir away from the well, as shown schematically in Fig. 3.1.
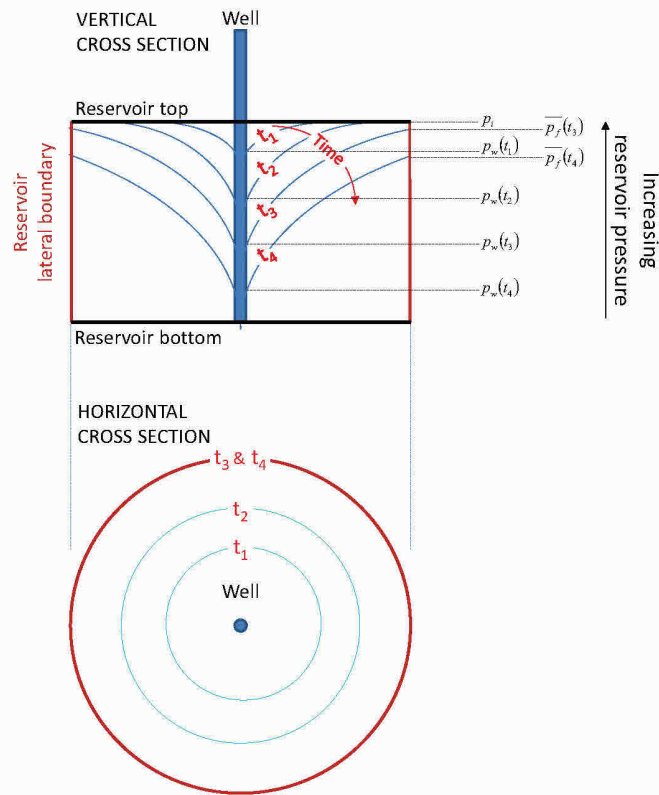
7

Figure 3.1: Schematic of pressure distribution in a closed circular reservoir during production. The top diagram shows how, as time goes on, the pressure, represented with blue lines, declines. Note how the pressure decreases most near the well, shown in the middle. The lower diagram is a view from the top showing pressure signals moving outward in a radial pattern from the well.

You can see the same thing in a draining bathtub. There is a large depression of the water right over the drain, and conditions further away are almost unchanged.
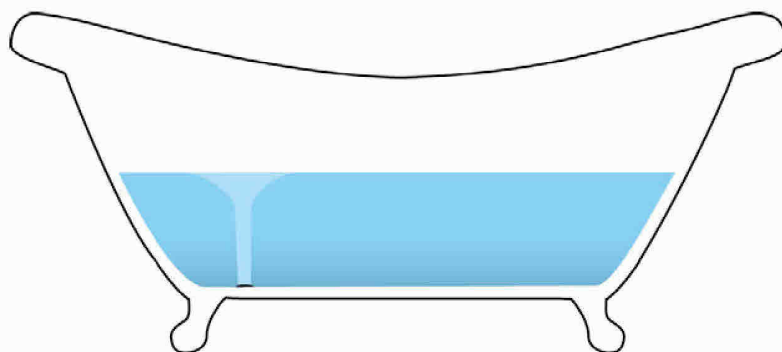

Figure 3.2: Schematic of pressure distribution in a draining bathtub.

Before production begins, the pressure everywhere in the reservoir is the initial pressure p_i of the reservoir. For Macondo, this was 11,856 pounds per square inch (psi).[4] As flow continued, the pressure in the reservoir continued to decrease. The pressure moved downward as shown on the top graph and outward on the bottom graph in Fig. 3.1.

If the well is then closed ("shut in"), the flow rate becomes zero, and the pressure in the reservoir increases. *This is called a build up* (because the pressure builds back up). One important question for us is to what pressure will this reservoir recover? This is the question of the final reservoir pressure for Macondo, and as explained in Section 3.3.1, the government experts apply incorrect methodology when arriving at their estimates of this important parameter.

3.2   Well-test data acquisition

Well-test data consist of pressure and production (flow) rate measurements. There are different types of well-tests through which this data is acquired, and they are performed at different times in the life of a well and investigate different volumes in the reservoir.

3.2.1   Wireline formation test[5]

The government experts overlooked some of the most valuable well-test data available in this case. This data includes exceptionally useful pressure and flow-rate information from testing done at the bottom of the well before the incident. This is the only set of well-test data that includes this detailed coupling of pressure and flow-rate information (measurements taken right at the edge of the reservoir itself, which makes the data still more valuable). This is crucial because well-testing cannot be used to infer the critical parameter of permeability reliably unless flow-rate history is known, which of course was not the case during the blowout. (Government experts simply assume rates, which makes their analysis of this parameter circular.)

I speak here of the *wireline formation test*, which measured pressure and flow rates right at the reservoir while gathering reservoir fluids for analysis. This is generally the first well-test to be performed in a well, and in the case of Macondo, it was the *only* well-test accompanied by contemporaneous flow-rate data. The omission of this well-test from the ambit of the government experts' analyses helps to explain why many of them ended up using a permeability that is more than double the most likely value.

---

[4] *See* BP-HZN-2179MDL03742328 (MDT Report), page 7, 22. This is at the true vertical depth of 18,056 feet below the sea surface (TVDSS).

[5] See a more detailed description in Haddad, S., Cribbs, M., Sagar, R., Viro, E., Castelijins, K., and Tang, Y., "So What is the Reservoir Permeability?", paper SPE 63138 presented at the SPE Annual Technical Conference and Exhibition, Dallas, Texas, 1-4 October 2000.

And, as we will discuss later, permeability is the property of the reservoir rock that is a directly proportional to flow rate. The government experts' incorrect determination of permeability has a direct impact on their estimates of cumulative flow. They got permeability wrong by up to and at times more than a factor of two, and thus overestimated cumulative flow.

The well-test we are focussing on now occurs when a wireline formation tester tool is run into the well to take measurements of pressure and procure samples of the reservoir fluid. This is a tool with sensors and other equipment that sends data to the surface via an electrical cable. The Macondo testing was done using a version made by Schlumberger, called MDT™.[6] During this test, a probe is inserted into the borehole wall, and a short test, called a "pre-test," is conducted to measure the formation pressure. *See* Fig. 3.3. Up to 20 cc (cubic centimetres) of mainly filtrate (essentially the liquid components of the drilling mud) is withdrawn through the probe (as with a syringe) into a pre-test chamber.
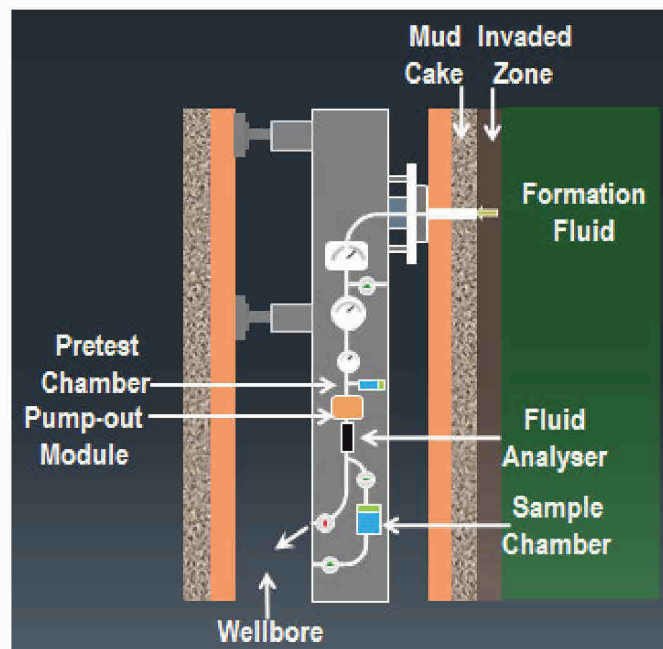

Figure 3.3: Schematic of a typical wireline formation tester

The corresponding drawdown pressure depends on the flowing fluid's "mobility," which is the permeability of the formation divided by the viscosity of the fluid and is written as $\dfrac{k}{\mu}$. At the end of the drawdown period (about 20 seconds), the pre-test chamber is full, flow stops, and a build up period starts. The time required for the pressure to build up to the formation pore pressure (usually, a few

---

[6] *See* BP-HZN-2179MDL03742328 (MDT Report).

minutes) is a function of the formation fluid mobility and producing time.[7] Further explanation is included in Appendix E. This process gives us the initial reservoir pressure, p_i.

Versions of wireline formation testers, including the Schlumberger MDT used here, have been developed to acquire formation-fluid samples. To get uncontaminated (filtrate-free) reservoir fluid, the device withdraws fluid continuously for several hours, which is then simply dropped into the wellbore. When the tool detects that the incoming fluid no longer contains contaminate, the pumped fluid is diverted to a sample chamber that is then taken to surface for further analysis. During the entire sampling process, pressure and rate are measured versus time at the probe level[8] and can be used to provide permeability estimates.[9]

In the Macondo well, three reservoir fluid samples were taken with the MDT tool, one in the M56D formation (Schlumberger's sample designated F144), one in the Upper M56E formation (F143), and the third one in the Lower M56E formation (F147). Pressure measurements were made with a quartz gauge with a 0.02 psi resolution, the smallest pressure change that the gauge can detect. The sampling MDT pressure and rate measurements in the M56D layer are shown in Fig. 3.4. Well-test analysis of the sampling MDT tests is described in Section 4 and Appendix E. From it, I deduce that the best estimate for permeability is 238 mD. This estimate is quite reliable because, among other things, I do not need to assume a flow rate that is in fact unknown, as the government experts have done with their estimates of permeability using pressure data from the incident. With my alternative method, the flow rate is obtained directly from the MDT tool. [10]

---

[7] *See* T. M. Whittle, J. Lee and A.C. Gringarten: "Will Wireline Formation Tests Replace Well Tests?", paper SPE 84086 presented at the 2003 SPE Annual Technical Conferenceand Exhibition, Denver, Colorado 5-8 October 2003.

[8] The rate is deduced from the speed at which the pre-test chamber is filled up.

[9] *See* Pimonov, E., Ayan, C., Onur, M. and Kuchuk, F., "A New Pressure/Rate-Deconvolution Algorithm to Analyze Wireline-Formation-Tester and Well-Test Data", paper SPE 123982 presented at the SPE Annual Technical Conference and Exhibition, New Orleans, Louisiana 4-7 October 2009, page 603-613.

[10] See a more detailed description in Haddad, S., Cribbs, M., Sagar, R., Viro, E., Castelijins, K., and Tang, Y.: "So What is the Reservoir Permeability?", paper SPE 63138 presented at the SPE Annual Technical Conference and Exhibition, Dallas, Texas, 1-4 October 2000.
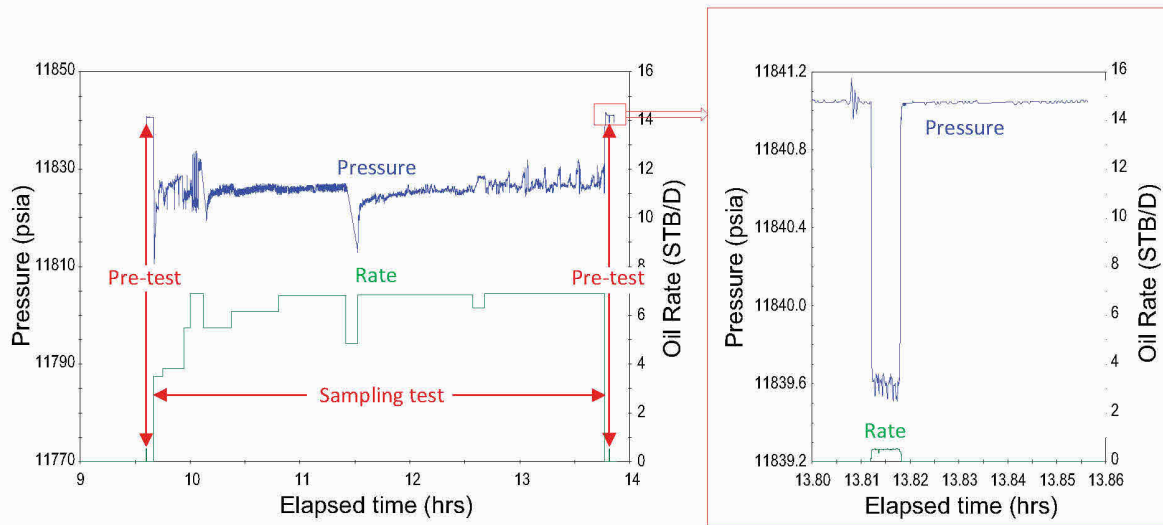
Fig. 3.4: F144 MDT sampling test in the Macondo M56D layer. It includes an initial pre-test around 9.6 hours, and a final pre-test around 13.81 hours (enlarged in the box on the right hand side)

3.2.2 Production test

Production tests are performed in wells equipped for production so that oil companies can calculate permeability and other reservoir properties using dynamic flowing data. During production, pressure is measured continuously at the wellhead, while flow rate is measured through a separator at the surface.

The period from the start of oil flow on April 20, 2010 in the Macondo well to the shut in of the well on July 15, 2010, and to the end of the corresponding build up on August 3, 2010 can be considered as a production test, though we do not know the flow rate. I analyse the associated pressure data in detail in Section 5 and Appendix F.

From the flowing pressure data I conclude that the best estimate of the total amount of oil that left the reservoir is around 2.4-3 MMstb. My analysis uses the most modern methodologies and my independent determination of permeability from the MDT analysis.

TREX-011696R.012

3.3   Well-test analysis

3.3.1   Well-test basics

Well-test analysis of pressure and rate data provides qualitative and quantitative information on the well and the reservoir. Great strides have been made in this field over the last 25 years.[11] Modern techniques and methodologies are vastly superior to what preceded them and provide powerful tools to understand reservoir parameters and structure. As already noted, well-test analysis uses measured pressure and flow-rate data to ascertain detailed information about the reservoir. To get the basic picture, think of sonar used on a submarine to detect its surroundings. The sonar system sends out a ping and then listens for the sound return reflected off of objects. From analysing the return signal, the sonar system can locate undersea objects and find their range. (Fig. 3.5) In well-testing, we send a signal into the reservoir (for example, the pressure drop caused by flowing the well) and we listen for the return signal (for example, the change in pressure over time). From this process, we can determine where the reservoir ends and various other properties of the reservoir.
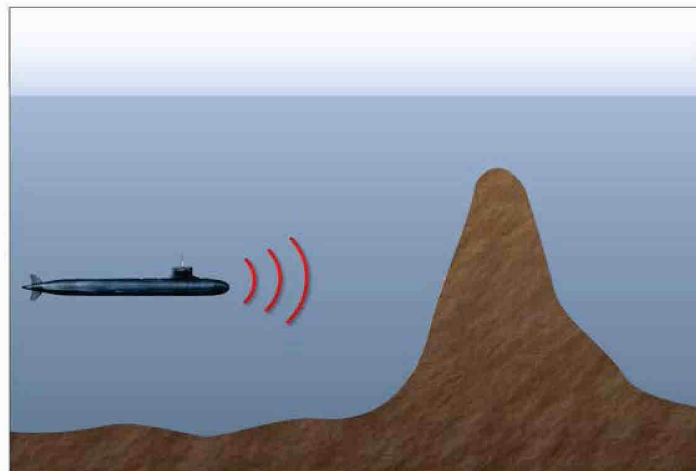

Figure 3.5: Well-test analysis can be analogized to sonar. In each case, a signal is sent out and information is obtained through analysing the returned signal

Again, just as I imagine is the case with sonar, it is important to use the most advanced tools in well-testing. Just as one would not entrust a billion dollar submarine to 1950s technology, one should not rely on outdated well-testing techniques. Yet, that is precisely what the government well-test reports have done. For example, Drs. Kelkar and Raghavan analyse the shut-in pressure data to estimate the

---

[11] *See* Gringarten, A.C., "From Straight Lines to Deconvolution: The Evolution of the State of the Art in Well Test Analysis", paper SPE 102079 presented at the 2006 SPE Annual Technical Conference and Exhibition, San Antonio, Texas, 24-27 September 2006; also marked as Exhibit 8620 (IGS075-018303).

final reservoir pressure. In doing so, they employ Mead's method, which is an empirical technique that can be used when *nothing* is known about the reservoir.[12] Yet, we know a great deal about the reservoir, and it makes no sense to ignore that. In Section 6, I examine in more detail the various well-test analysis mistakes made by the government experts.

In the standard well test, a period of constant flow rate is analysed. In practice, pressure build ups are preferred because they occur when the flow is shut off and hence the flow rate is known to be zero. Drawdowns are more difficult to interpret because of possible flow-rate fluctuations.

Analysing so-called "multi-rate tests" in which there are periods of various flow rates, including interim and final shut-ins when the flow rate is zero, is somewhat more difficult. Fig. 3.6 depicts such a test. Understanding how to analyse these tests properly is the key to modern well testing and to understanding the Macondo reservoir.
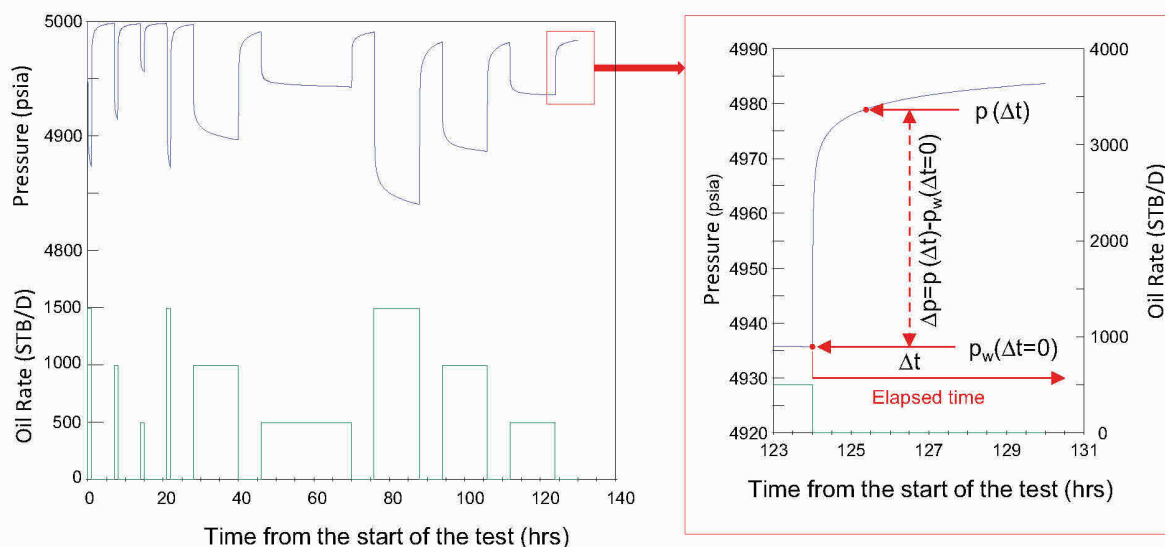

Figure 3.6: Example of a multi-rate test. The last build up is enlarged in the box on the right hand side. The signal to be interpreted by well-test analysis is Δp, which is the difference between the pressure p(Δt) after an elapsed time Δt since the start of the build up, and the pressure at the start of the build up, p(Δt=0).

One of the most important innovations in well-test analysis is use of the pressure derivative, which loosely speaking describes how fast pressure is changing at each instant. For this, we use the pressure

---

[12] *See* Haughland, T., Larsen, L., and Skjaeveland, S.M ., "Analyzing Pressure Buildup Data by the Rectangular Hyperbola Approach", paper SPE 13079 presented at the 1984 SPE Annual Technical Conference and Exhibition, Houston, Texas, 16-19 September 1984, page 1("*If nothing is known about the reservoir*, then [Mead's method] can be used to get a rough estimate of the average pressure.").

14

data and computer programs to calculate how fast the pressure is actually changing. The rigorous definition of the pressure derivative is given in Appendix C.

Use of the pressure derivate has revolutionized well-test analysis over the last 30 years.[13] It is by far the most powerful method to figure out the right reservoir interpretation model (that is, the main characteristics of the reservoir, such as its shape and size, which can be further refined later with other techniques). This can be seen by looking at the plot in Fig. 3.7, where the pressure derivative $\Delta p'(\Delta t)$ is plotted as a function of the elapsed time Δt on a log-log graph (that is, the decimal logarithm of the derivative is plotted as a function of the decimal logarithm of elapsed time).

Key aspects of the reservoir (flow regimes) can be readily seen from the graph. The time it takes the pressure to enter into these different flow regimes can be used to deduce the dimensions of the reservoir and hence its connected volume, a key parameter needed to calculate oil flow using the "material balance" method of government expert Dr. Kelkar and BP expert Prof. Blunt. The derivative analysis also provides the average reservoir pressure prior to the build up, another key parameter required in material balance calculations. Later, we will look at the pressure derivative for Macondo, but I note that the actual pressure derivative for Macondo is similar to the plot in Fig. 3.7. I chose this simplified example for precisely that reason.
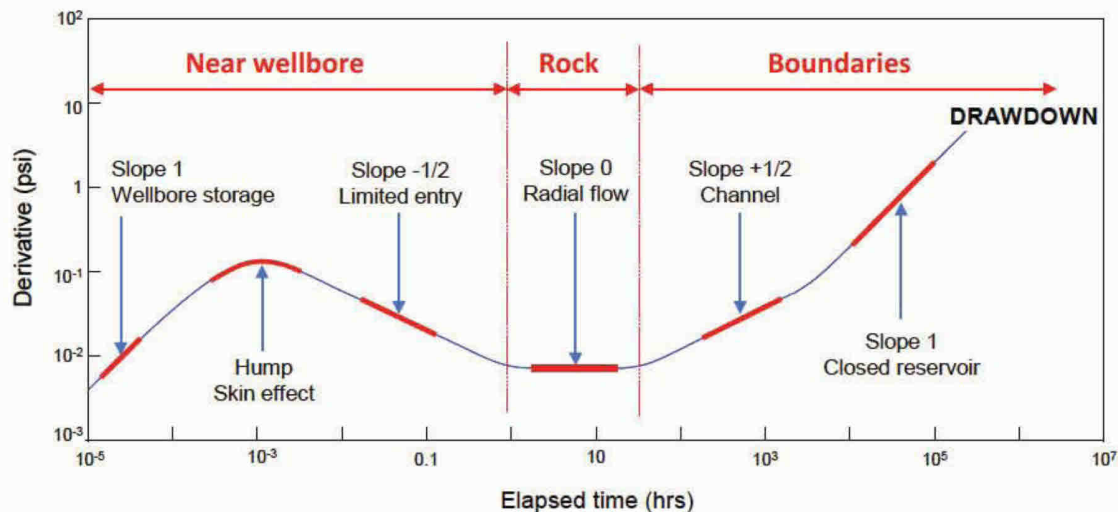

Figure 3.7: Example of a log-log plot of the pressure derivative. The elapsed time is the time since the well has been shut in. The different flow regimes and their significance are explained in the text.

---

[13] *See* Gringarten, "From Straight Lines to Deconvolution," page 42.

Wellbore storage: The first feature of interest in Fig. 3.7 is the straight line with a slope of 1 at "early times," on the left hand side of the log-log graph. This corresponds to fluid compressibility effects in the wellbore and is called *wellbore storage*. It simply means that when the well is initially opened at the wellhead to start a drawdown, the first production comes from the expansion of the fluid in the wellbore and does not come from the reservoir. This is similar to the overflow from a Coca Cola can when it is opened after having been shaken. The reverse occurs when the well is shut in at the wellhead to start a build up: although no fluid is produced at the surface, fluid is still entering into the well at the bottom and compresses the fluid already in the wellbore.

Skin: The next remarkable feature is identified as a hump in Fig. 3.7. This is caused by the *skin effect* and is related to the difference in pressure between the well and the reservoir sides of the sand face. Often, skin is an indication of extra flow resistance near the wellbore, as in the case of invasion by mud filtrate, pictured in Fig. 3.8. But the skin effect reflects flow resistance at *any* point between the reservoir side of the sand face and the location of the pressure gauge used to acquire well-test data. Where, as with Macondo, the pressure gauges are located more than 10,000 feet above the reservoir-well intersection, the skin effect could reflect pressure drops from resistance to flow through residual cement, bottom-hole equipment, or BOP rams. Indeed, we will discuss evidence that conventional skin, in the sense of mud contamination of the reservoir, was not the cause of the skin effect seen at Macondo. Thus, other flow restrictions were present between the reservoir and the capping stack (where the main well-test pressure gauge was located) that impeded flow and caused pressure drops. [14]
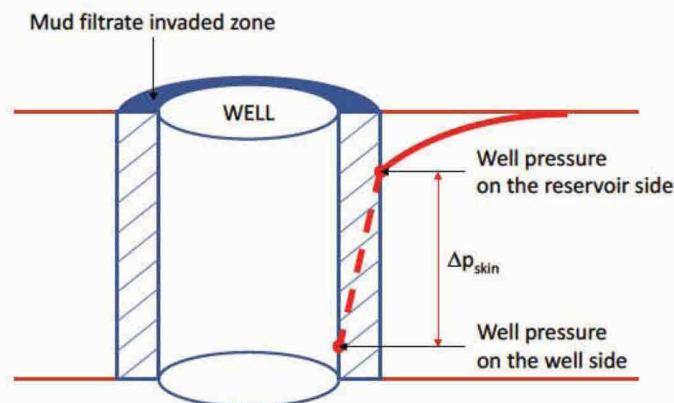

Figure 3.8: Schematic representation of the skin effect. The red curve represents the pressure distribution in the reservoir at a given time. It is similar to what is shown at the top of Fig. 3.1. The dashed red line is the additional pressure drop due to the skin effect

---

[14] My MDT analysis shows essentially no conventional skin. By contrast, my analysis of the pressure data from the spill and subsequent shut in does show skin. This implies some impediment to flow between the sandface and these gauges. This could include cement and BOP rams.

Spherical Flow: The third feature identified on Fig. 3.7 is a straight line with a slope of minus 1/2. This is characteristic of spherical flow, which occurs when only a small portion of the reservoir thickness is open to flow. This is the case in formation wireline testing, like the MDT testing in Macondo (Fig. 3.9), where the fluid entry is restricted to the probe dimension (about 1 cm).
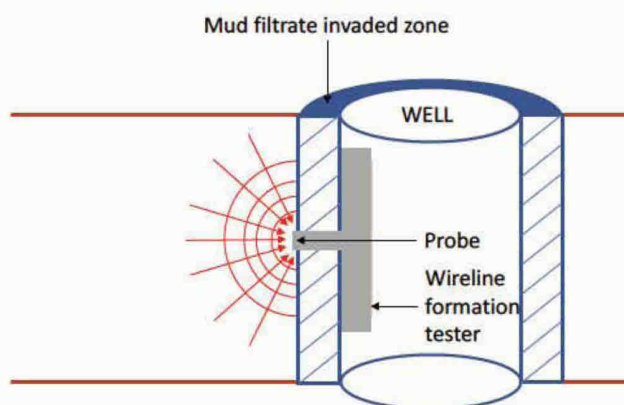

Figure 3.9: Schematic representation of spherical flow in the case of wireline formation testing

Radial Flow: These first three derivative features in Fig. 3.7 describe the region in the vicinity of the wellbore. The next feature, which occurs at "middle times," after the well has been flowing for some time, is a straight line of zero slope, known to well-test interpreters as the "derivative radial flow stabilisation," $\Delta p'_{Stabilisation}$. It is a key feature in well test analysis, as it allows calculation of the mobility-thickness product $\dfrac{kh}{\mu}$, where k is the permeability (a key variable directly related to flow rate, which the government experts have failed to estimate correctly), h is the height (usually called thickness) of the reservoir (how fat it is in feet), and μ is the viscosity of the formation fluid. We do this calculation by means of the following relationship:

$$\frac{kh}{q\,\mu} = \frac{70.6\,B}{\Delta p'_{Stabilisation}} \tag{4}$$

where q is the downhole flow rate applicable to the data being analysed, and B_o is a coefficient, called the *formation volume factor*, used to convert the flow rate from stock tank to reservoir conditions.[15] As we shall see, this feature is critical to my analysis.

---

[15] The units used in Eq. 4 are the Engineering Oil Field units, used in the upstream oil and gas industry. k is in milliDarcies (mD); h, in feet; μ, in centipoise (cp); q, in barrels per day measured at surface

Linear Flow and Boundaries: Derivative features after radial stabilisation correspond to reservoir boundaries and occur at "late times," on the right hand side of the log-log graph in Fig. 3.7. The straight line with a slope of 1/2 is characteristic of linear flow and indicates two parallel sealing boundaries (through which there is no flow), such as faults or transitions from oil-bearing sandstone to impermeable shale, as found in channel sands. Diagnosing the shape of the reservoir as a channel is crucial because it influences the equations used to analyse the pressure.

The straight line with a slope of 1 is characteristic of a "closed reservoir," that is, a reservoir surrounded by impermeable boundaries. Analysis of these data yields the distances from the well to the boundaries and the average reservoir pressure prior to shut in. In particular, the graph of the derivative shows the time at which we hit boundaries (the slope of the derivative changes there). And we can apply a simple equation to find the distance to the boundary from the time. Together, this information helps us estimate to how much oil the reservoir had initially, which is one of the inputs to the material balance equation used by expert Professor Blunt to calculate cumulative flow.

The derivative shown in Fig. 3.7 is for a drawdown. The corresponding derivative for a build up is shown in Fig. 3.10. It differs from the drawdown derivative at late times when reservoir boundaries have been reached in the preceding drawdown. In such a case, the build up pressure eventually becomes constant, stabilising at the average reservoir pressure. Therefore, its derivative becomes zero. There is no zero on a log-log graph (this is just a result of using the logarithm), hence the build up derivative drops down as shown in Fig. 3.10. The drawdown late time straight line with a slope of 1 no longer exists, and the slope of 1/2 straight line we see in the drawdown is not fully developed. As a result, the identification of boundaries with build up data alone can be quite challenging.
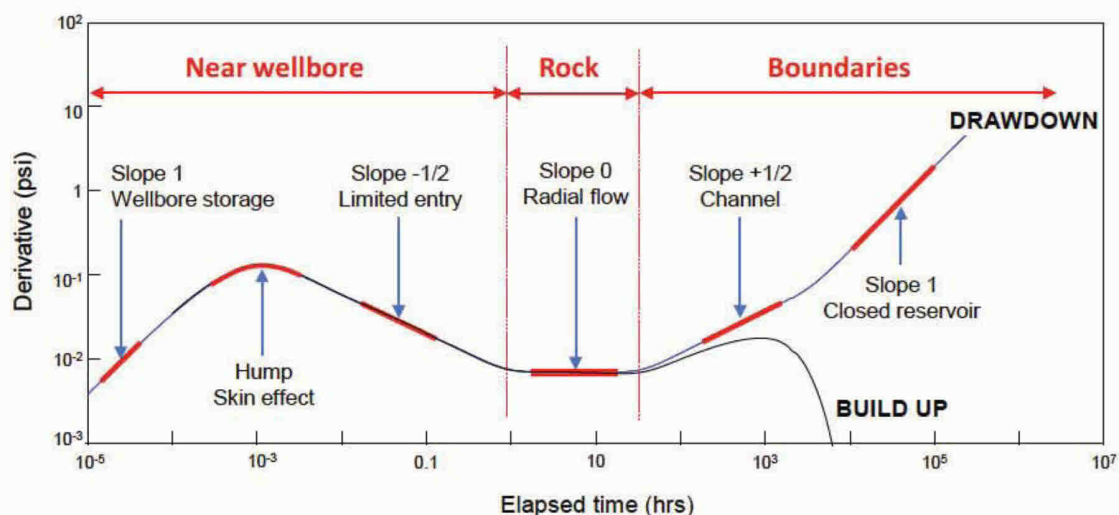
conditions (stb/day); and $\Delta p'_{stabilisation}$, in pounds per square inch (psi). 70.6 is a coefficient required to make the units consistent.

18

Figure 3.10: Example of flow regimes on a build up derivative.

3.3.2 Deconvolution

One drawback of the analysis techniques described above is that they are valid only for analysing a single period during which the rate is constant. The example in Fig. 3.6 shows that the durations of such periods are small compared to the entire duration of the test--that is, the full amount of time that the well has been flowing at various rates. Therefore, analysis of these periods in isolation can provide only a fraction of the information that is available from the entire test data.

Fortunately, there are methods that allow us to use all the data at once, and the basic approach is simple. (We will apply these to Macondo in Sections 4 and 5.) We can mathematically transform the pressure data obtained from all flow periods (including when the well is shut in and had a flow rate of zero) to what the pressure data would have been had the well undergone a single constant-rate drawdown for the entire period.

This powerful technique, known as *deconvolution*, has become the state of the art for well-test analysis and often allows the identification of the right model for the reservoir when other methods cannot. This is because the technique does not merely address a technical concern. Rather, it generally allows us to see further into the reservoir than other methods essentially by adding the different build ups and drawdowns together into a single long drawdown.

This is complicated but the basic point is essential. If we apply the right techniques, we can see much further and more clearly into the reservoir. Going back to the sonar analogy, imagine that we actually have multiple sonar signals pinging the undersea environment. The combined signal probes much further than the individual signals. Imagine that old sonar technology simply analysed each ping by itself and ignored the power of combining signals. We could improve our sonar system by understanding how to combine all these signals into one, more powerful signal. That is exactly what deconvolution does for modern well-testing.

A quick well-test illustration shows why it is useful to convert pressure data to single-drawdown pressure data. I created this example, including its rates and pressure history, based on a reservoir model to demonstrate how the pressure data can show us much more about the reservoir when it is converted from a series of isolated build ups into a single drawdown. The pressure and rate data for this reservoir model have been previously depicted in Fig. 3.6 and are depicted again below. Each rise seen in the blue pressure line, like the one magnified on the right, is a build up.
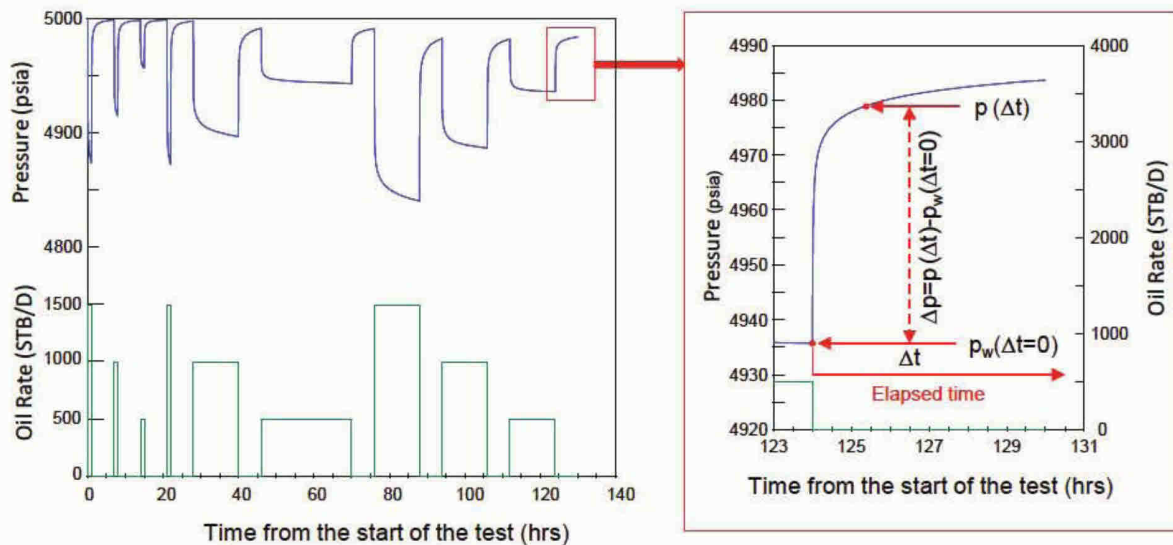
I have generated the derivatives (the way the pressure changes over time) of each build up seen in the data above. I then plotted the derivatives for each of the build ups looked at isolation from each other on the same log-log graph in Fig. 11 below.[16]
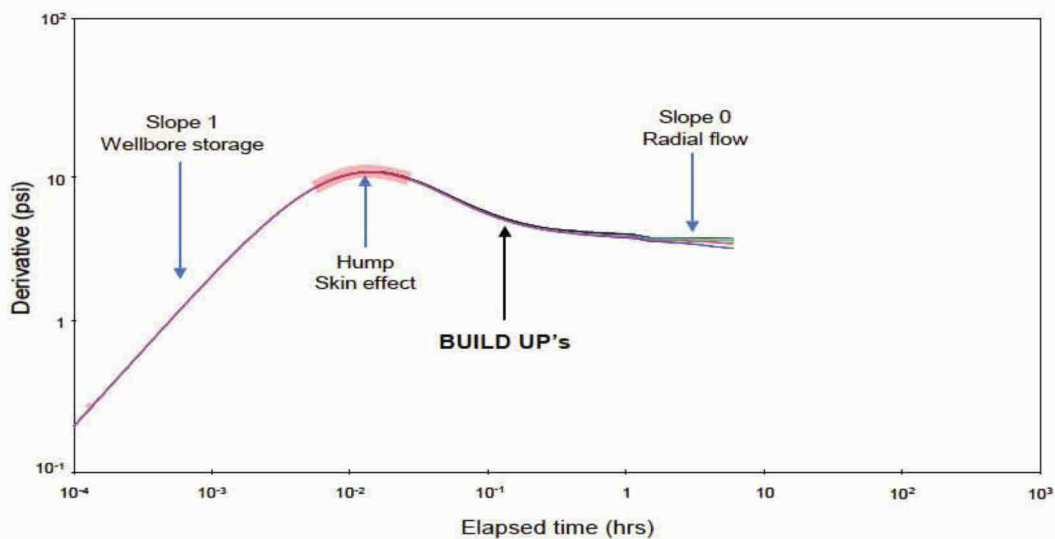

Figure 3.11: Derivatives for all the build up periods in Fig. 3.6.

---

[16] As a technical matter, to plot the derivatives from different build ups on the same graph, I have to remove the dependency on flow-rate history from each. The details are not important to a basic understanding, but to do this I divide each of the derivatives by its applicable flow rate and then multiply it by the flow rate applicable to the last build up. I have in essence removed the differences in rate history and made the derivatives directly comparable so they can be meaningfully plotted next to each other on the same graph.

20

As we can see, they are all nearly identical and fall almost entirely on top of each other. This is to be expected because the shape of the derivative is a reflection of the reservoir's properties and the amount of time of the test, and all of these build ups come from the same reservoir. Using the derivatives generated from the different build ups in isolation, even all of them, does not take advantage of all the data that we actually have. We are still treating each ping separately, to use the sonar analogy.

Note in Fig. 3.11 that none of the derivatives generated by the individual build ups show any boundaries. It would be wrong, however, to conclude that the reservoir boundaries have not been reached during the 130 hours of the entire test. In fact, once I take advantage of the full 130 hours of the data, we can see all of the reservoir boundaries. Going back to the sonar analogy, I want to combine the pings into one powerful signal that can see further. Fig. 3.12.
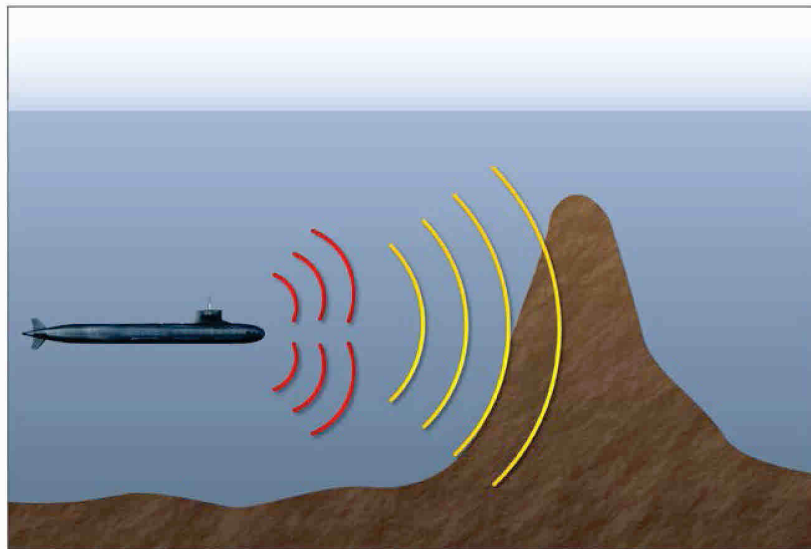
Figure 3.12: Schematic of the effect of combining pings on submarine sonar. The graphic is meant as a common-sense analogy to help the reader understand the motivation behind deconvolution.

To do this, I have also simulated a single 130-hour drawdown at constant rate. We can see the comparison in Fig. 3.13. This is what deconvolution does. It allows us to convert the data obtained from several build ups and drawdowns into equivalent data that would have been obtained from a single, constant-rate drawdown. And now instead of a number of build ups of short duration that each tells us essentially the same thing, we have a long drawdown of the entire duration that can reveal much more about the reservoir. Back to the sonar analogy: I have finally combined the pings into one powerful signal.
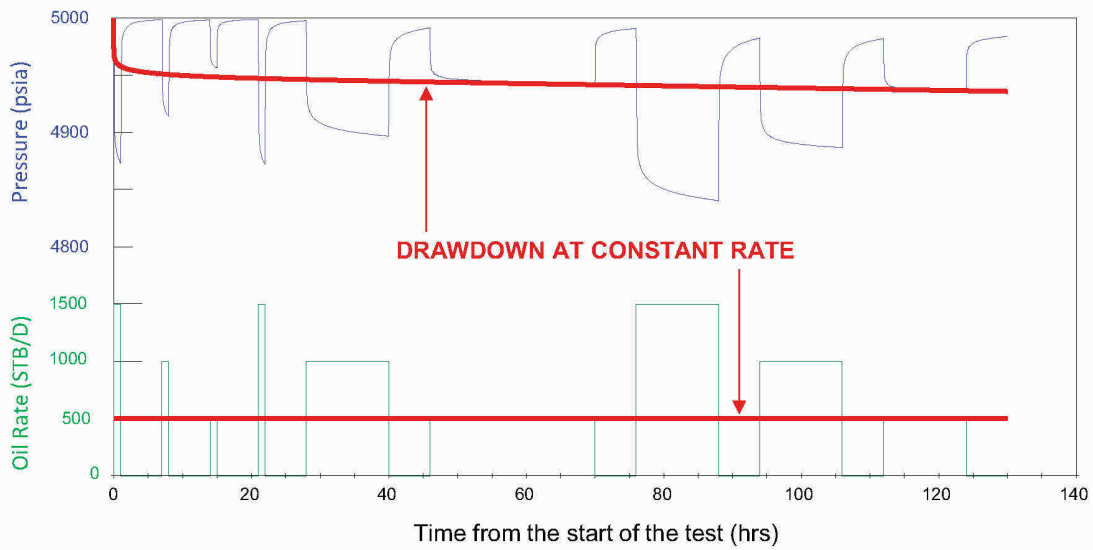
21

Figure 3.13: Using a 130-hour constant-rate drawdown instead of alternating drawdowns and build ups as in Fig. 3.5.

In Fig. 3.14, I plot both the derivatives for the individual build ups and the new derivative for the constant-rate drawdown. And we can see how the new single drawdown derivative compares to the individual build up derivatives in Fig. 3.14. Where they overlap, they are nearly identical because they are all a reflection of the same reservoir. But the power of using this combined constant-rate drawdown becomes evident at approximately the 8-hour mark where the build up derivatives stop and the constant-rate drawdown derivative continues.
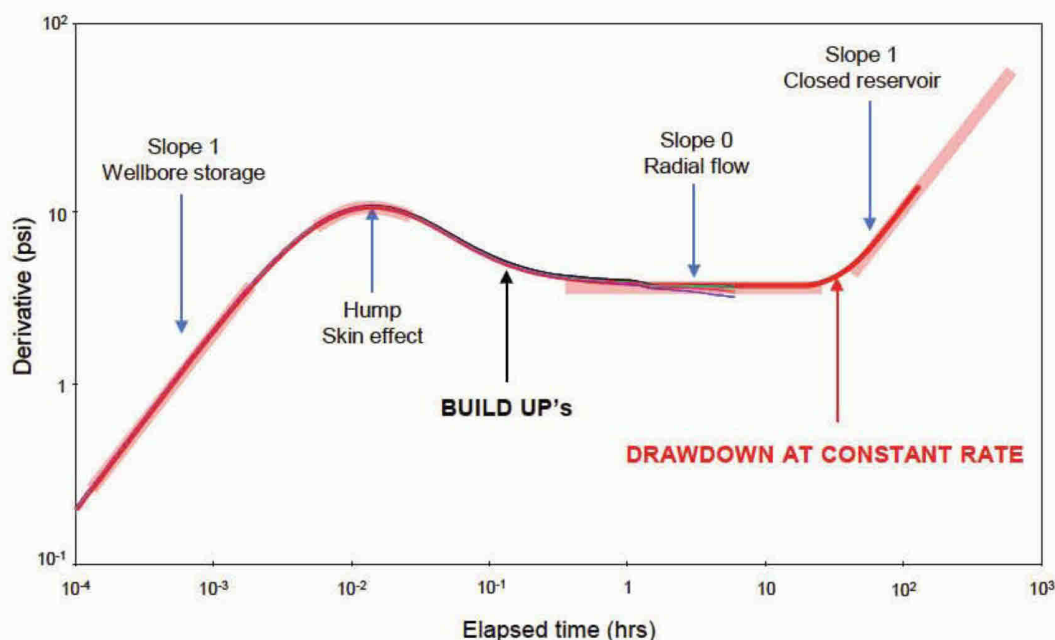
Figure 3.14: 130-hour drawdown derivative compared to build up derivatives from Fig. 3.6.

As the combined constant-rate drawdown derivative takes full advantage of all 130 hours of pressure data, we can see further into the reservoir. At approximately the 70-hour mark, the derivative rises to a slope of 1. As I discussed in Section 3.3.1, this indicates that the reservoir is of limited extent and that the pressure signal has hit all the boundaries. With this information, the size of the reservoir and the distances from the well to the boundaries can now be calculated. But without these powerful techniques, this information could have remained hidden.

In this example, I replaced the drawdowns and build ups with a single drawdown at a constant rate without using deconvolution by generating the information from my model. Deconvolution allows me to do the same thing with real-world well-test data, and I do so below for the Macondo data to determine the permeability and other reservoir parameters.[17]

When we have pressure data from when the well was flowing, deconvolution has another extremely useful function that I apply. We can use deconvolution to determine the flow-rate trend (the way the relative flow rate changed) for the period we have pressure data. Once we have the flow-rate trend, we can reconstruct the entire flow-rate history for that period as long as we can determine the flow rate at any point during that period. In Section 5, I use what I have learned through well test analysis and deconvolution to reconstruct the flow-rate history of Macondo.

---

[17] For a compressive discussion of the deconvolution technique, see Gringarten, A. C., "Practical use of well test deconvolution", paper SPE 134534 presented at the 2010 SPE Annual Technical Conference and Exhibition held in Florence, Italy, 19–22 September 2010.

Through my use of these modern and sophisticated methods, I get a much more accurate and reliable picture of the reservoir than the government experts, including its flow rates, size, and the final reservoir pressure.

3.3.3 Constructing the interpretation model

Once all the flow regimes potentially present in the data have been identified with the aid of the pressure derivative, we still need to confirm that we are correctly interpreting the data. Failure to take this step can lead to using the wrong model and misinterpreting the data and the reservoir. We do this verification by using other plots or graphical depictions that are specific to each flow regime identified on the derivative. Examples include the "Horner" (or superposition) plot for radial flow: once we have identified a potential radial-flow period on the derivative plot we need to confirm it with a Horner plot. This confirms (or disproves) our interpretation.

One we have completed this verification, we construct a mathematical expression that reflects all the verified features found in the derivative. This mathematical representation of the pressure behaviour is obtained by solving a partial differential equation, called the diffusivity equation, which models fluid flow in reservoirs. The pressure calculated by the mathematical model is then compared with the measured pressure. Then, the reservoir characteristics (permeability, shape, size, for example) are estimated by determining the values that best reproduce the measured pressure.

Critically, there may be several models that may appear to explain the same measured pressure data. A second step is therefore required, which is to verify that this interpretation model not only can reproduce the measured data, but is also consistent with any knowledge of the reservoir, and in particular with non-testing information from geology, geophysics, and petrophysics.[18] Any model that fails to be consistent with reliable information should be discarded, *no matter how well it matches the pressure*. Other possible interpretative models should then be explored.

The government experts seem to have ignored these critical steps. They fail to confirm their interpretation models before estimating reservoir parameters from them. And they tout how their models can recreate the measured pressure, and even implicitly (in the case of Dr. Pooladi-Darvish) acknowledge that many different models combining different assortments of reservoir parameters could match the measured pressure. But then they do not present an analysis that checks their inputs against the actual non-well-test measured data. For example:

- The use of 12 microsips for rock compressibility by both Kelkar/Raghavan and Hsieh, which is about twice the measured values from cores taken from the Macondo reservoir.

---

[18] Gringarten, "From Straight Lines to Deconvolution," page 44.

- The use of an oil compressibility about twice the measured values by Pooladi-Darvish in his only analytic well-test analysis presented in his report.
- The determination of values for permeability that are much higher than the measured values from logs and cores, including a best estimate of 550 mD from Pooladi-Darvish and 593 mD from Hsieh, and are inconsistent with the best well-test approach discussed in Section 4. And they fail to acknowledge that their permeability estimates depend on the flow rate during the incident, which is the very issue to be determined in this case.

Through these errors, the government experts accepted well-test interpretation models of the reservoir that clearly should have been rejected, along with the well-test parameters derived from them. And, with respect to determining permeability, their failure to use well-test data that includes flow rates caused them to overestimate permeability, at times by more than a factor of two. Their analysis of permeability, which assumes a flow rate, should be rejected as entirely circular. This is discussed further in Sections 3.3.1, 3.3.3, 5.6.3, and in Section 6.

Next, I use the MDT well-test data, which includes flow rates, to properly determine permeability. And only then do I turn to an analysis of the well-test data from the incident.

4. Determination of permeability from well-test analysis on the MDT data

4.1 Introduction: The Macondo reservoir's permeability is 238 mD

In Section 3.2.1 above, I introduced the reader to the wireline tool used to measure pressure and sample fluid at Macondo, known by its Schlumberger brand name "MDT." I explained why this is by far the best method to estimate permeability reliably at Macondo. In this Section, I analyse the MDT pressure and flow-rate data and determine as precisely as possible the formation permeability. This is a critical variable in understanding the flow rate and total flow volume, and as noted, many of the government experts repeatedly overestimate permeability by more than a factor of two. Based on the MDT data, I estimate that the formation permeability is 238 mD.

It is axiomatic in petroleum engineering that permeability is best estimated by analysing fluid flow through the reservoir, rather than by laboratory testing of rock cores. Well testing is the method used to do the former. This is because we are interested in the average permeability throughout the formation, and that is exactly what a well test can tell us, *provided we know the flow rate*. Here, I get the permeability from analysing the MDT sampling tests, where we know the pressure *and* the flow rate. None of the government experts bother to analyse the MDT well-test data, and this is one reason why my determination of permeability is far more reliable than that of the government experts.

In this Section, I first describe the radial flow equation, which allows me to calculate permeability from flow rates. Then, I discuss the determination of permeabilities for each formation layer from flow-rate

and pressure data from the MDT and other sources. Lastly, I tie all the data together to present my base case of 238 mD for the formation's permeability along with statistical analysis that clearly demonstrates that the permeabilities used by many of the government researches are much too high.

4.2   Radial flow equation and the basic plan

Much of well-test analysis is based on inferring reservoir parameters from where we see the radial flow stabilization--where we see a flat line on the derivative plot. The key mathematical relationship is set forth in equation 4:

$$\frac{k\,h}{q\,\mu} = \frac{70.6\,B}{\Delta p'_{Stabilisation}}$$ (4)

where:

- q is the downhole flow rate
- B_o is the *formation volume factor*, used to convert the flow rate from reservoir to stock tank conditions;
- h is called thickness and refers to the length of the hydrocarbon bearing formation that can be produced;
- μ is the viscosity of the hydrocarbons; and
- $\Delta p'_{stabilization}$ is the value of the derivative where it is the flat line of slope 0.

In a standard well test, the flow rate q is known and we are interested in evaluating the "mobility-thickness product," $\dfrac{k\,h}{\mu}$. Since the MDT gives me the flow rate, and because I know the reservoir thickness, h, and the fluid viscosity μ, I can calculate the permeability. We can see this by rearranging the terms in Eq. 4.

$$k = \frac{70.6\,B\,q\,\mu}{h\,\Delta p'_{stabilization}}$$

4.3   Analysis of MDT sampling tests

A schematic cross section representation of the Macondo reservoir is shown in Fig. 4.1. The reservoir is made of three layers: M56D, M56E, and M56F. M56E is divided into Upper M56E and Lower M56E. Prior to the incident, three reservoir fluid samples were taken with the MDT, one in M56D (Schlumberger's sample designated F144), one in the Upper M56E (F143), and one in the Lower M56E (F147).

26
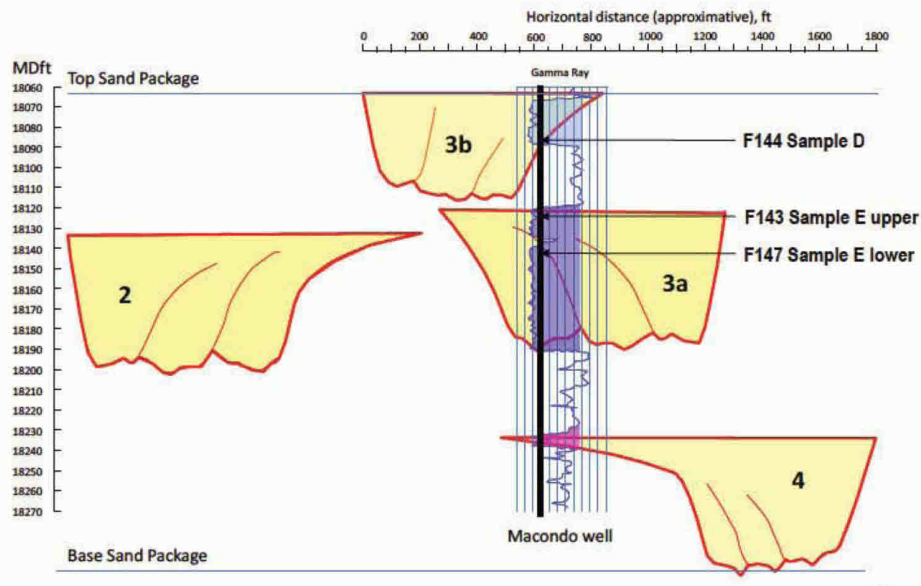
Figure 4.1: Schematic of Macondo reservoir with MDT sampling test locations.

MDT tests are conducted at the bottom of the hole, right against the actual reservoir. The pressure that is measured by the probe is therefore the actual bottomhole pressure. This simplifies our task because we do not need to convert pressures taken at the BOP or capping stack into equivalent pressures at the reservoir face. This reinforces the reliability of my determination of permeability.

Further, as discussed in Section 3.2.1, MDT sampling tests actually draw the well down for a significant amount of time in order to ensure the fluid collected in the sample chamber is contaminant-free reservoir fluid, which can then be taken to the surface and tested to determine fluid properties. This gives us a fairly long well test. Next, I look at the MDT well-test data and then analyse it with the most modern techniques to find the radial flow line and from that the permeability.

4.3.1 Data used to calculate permeability

4.3.1.1 Pressure data from the MDT tests

Although the MDT pressure gauges have a very high resolution, the data is noisy, as shown in Fig. 4.2. This is not uncommon in well test analysis - pressure data is often noisy. I can analyse the pressure using industry standard techniques of "smoothing" the data. The goal of smoothing is to reduce the noise but to leave the important information contained in the data, and thus allows us to analyse the underlying signal better.

TREX-011696R.027

I looked at two ways to smooth the data, both of which involve averaging the data over some length of time (in essence, I get moving averages aimed at maintaining the important features in the data but minimizing the noise). First, I can average over long periods, as shown with the green line in Fig. 4.2. This preserves only the trend of the data but for that reason gives the same derivative as the unsmoothed data. Second, I can average over shorter periods, as shown with the red line in Fig. 4.2. This method may not preserve the trend and so may give a different derivative, as shown in Fig. 4.3. As a result, although we do see radial flow (where the derivative is a flat line) in both approaches, the key flat line showing radial flow is higher in one than the other. This means there is some uncertainty in the level of the derivative stabilization, and therefore in the resulting mobility thickness product.
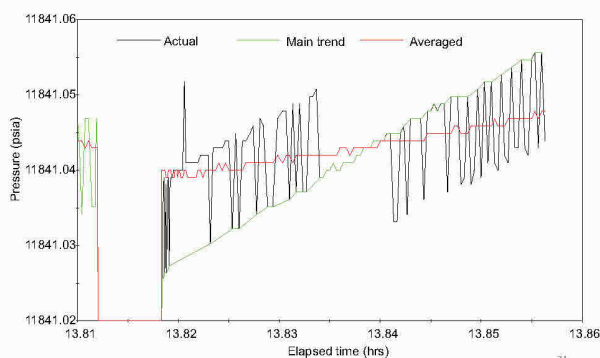
Figure 4.2: Pressure data noise in MDT sampling test F144 in M56D layer
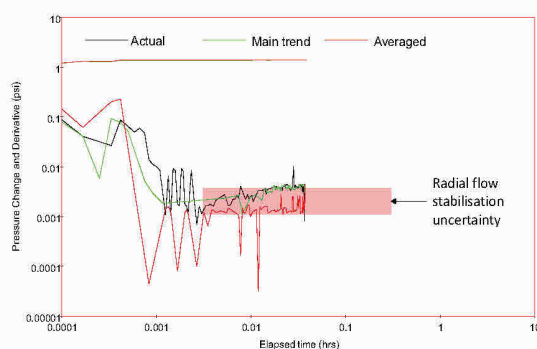
Figure 4.3: Uncertainty in derivative radial flow stabilisation in MDT sampling test F144 in M56D layer

Once I have smoothed the data, consistent with best practices for well-test analysis, I next find an interpretation model that best fits all known data. The details are given in Appendices E and F, but I use deconvolution, which is a sophisticated technique used in well-test analysis and discussed further in Section 5 and Appendices D and F, to assist in my determination of the interpretation model and flow-rate history. Applying deconvolution to the data obtained during the MDT sampling allows for the generation of the pressure derivative that sees further into the reservoir and allows for better understanding, identification and diagnosis of the reservoir features. Based on the deconvolved derivative, I conclude that the right interpretation model is a well with a limited entry into the formation, equal to the size of the probe. I can see these features on the derivative plot, and my model is also consistent with the physical system: The MDT test is conducted by drawing fluid from the reservoir into the tool through a small and restricted opening. Once I confirm that I have the right interpretation model, as explained in Section 3.3.3, I know that the flat line on the derivative plot in Fig.

28

4.3 really is the radial flow stabilization from which we can determine permeability. *See* Appendix E for more details.

4.3.1.2 Summary of data used in calculating permeability from the MDT tests

To get the permeability, we need to know the thickness of the layer h (which we get from log data) and the viscosity of the reservoir fluid μ (from PVT analysis performed by Dr. Whitson).[19] I have summarized the results of my interpretations of the MDT well-test data in Figs. 4.4 to 4.6 below. The details of my analysis are given in Appendix E. I find a permeability of 116 mD for the M56D layer, a permeability of 117 mD for Upper M56E, and a permeability of 285 mD for Lower M56E.

To arrive at these numbers, I find the radial flow stabilization (where the pressure derivative is a flat line) for each of the three MDT tests, using standard commercial well-test software. I verified that this is in fact the radial flow stabilization by building and verifying an interpretation model as described in Section 3 and by using deconvolution. Sometimes I get more than one possible match to the data, and I must analyse each. For example, there are two possible matches for M56D, as shown by the red and the green curves in Fig. 4.4, and three possible matches for Lower M56E, as shown in Fig. 4.6. For these layers, we get a range of possible radial flow stabilizations. See Appendix E for more details.

Once I confirm the radial flow stabilization line (or lines), I know the mobility-thickness of the layer, —— based on Eq. 4. But I also know h, the height of each layer, from log data,, and μ, the viscosity of the oil, from fluid analysis.[20]   I can then simply put those values in the equation and get the permeability for each layer.

The figures below summarise my results for each MDT test. The figures show the plot of the pressure derivative (the lower curves) on which we can see the radial flow stabilization. On the right-hand side of each figure, I show the probability that the permeability exceeds certain values. The P50 value is the best estimate.   I arrived at these probabilities using a standard technique called Monte-Carlo simulation.[21] In a Monte-Carlo simulation, a computer program repeatedly assigns possible values to each variable for which there is uncertainty and returns the permeability based on those values. The computer repeats this process thousands of times, and this gives us a range for the permeability and the associated probability shown on the right hand side of the figures.

---

[19] Expert Report of C. Whitson; Whitson Table, T=243-SSF-ALL.xls
[20] Expert Report of C. Whitson; Whitson Table, T=243-SSF-ALL.xls
[21] Azi, A.C., Gbo, A., Whittle, T., and Gringarten, A.C., "Evaluation of confidence intervals in well test interpretation results", paper SPE 113888 presented at the 2008 SPE Europec/EAGE Annual Conference and Exhibition,Rome, Italy, 9–12 June 2008.
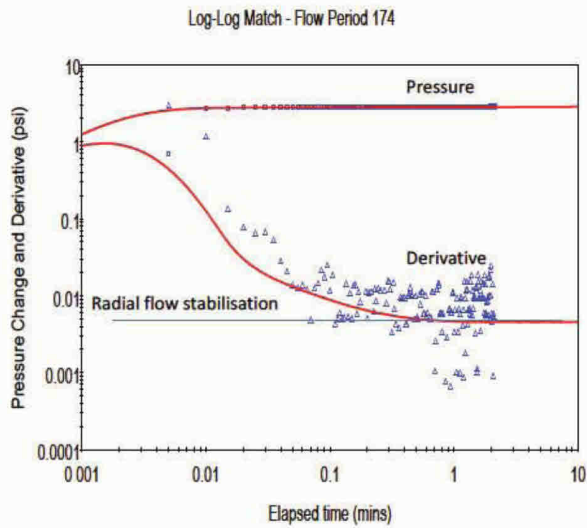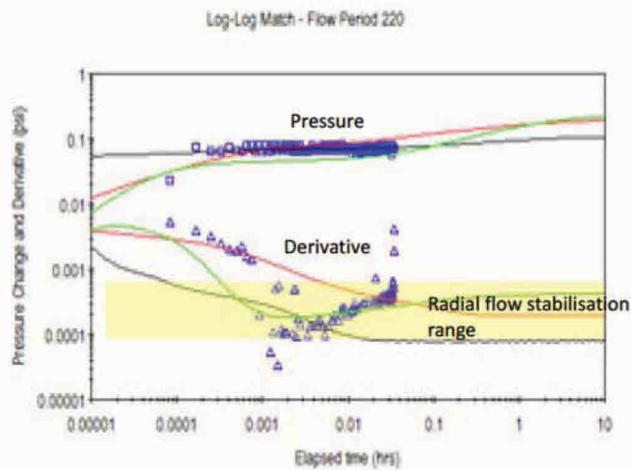
Percentiles	M56D (144)
P100	45
P90	74
P80	85
P70	95
P60	106
P50	116
P40	127
P30	138
P20	153
P10	174
P0	282
	Horizontal permeability
	mD
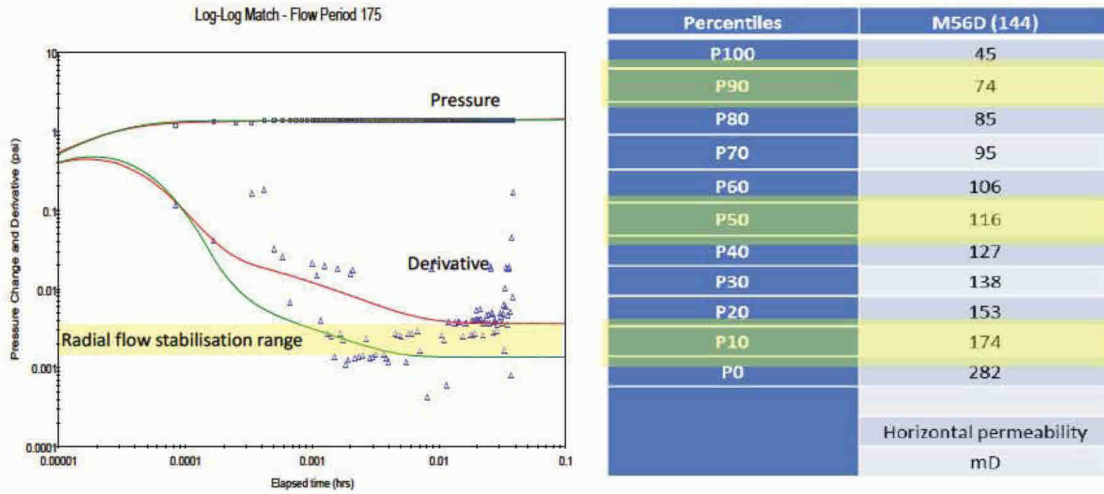
Figure 4.4: Interpretation of MDT sampling test F144 in M56D layer. The most likely value for the permeability is 116 mD (the P50).

TREX-011696R.030

Percentiles	M56E (143 Upper)
P100	73
P90	95
P80	103
P70	108
P60	112
P50	117
P40	124
P30	130
P20	137
P10	148
P0	233
	Horizontal permeability
	mD

Figure 4.5: Interpretation of MDT sampling test F143 in M56E Upper layer. The most likely value of permeability is 117 mD (the P50).

Percentiles	M56E (147 Lower)
P100	85
P90	171
P80	203
P70	230
P60	257
P50	285
P40	312
P30	343
P20	390
P10	454
P0	726
	Horizontal permeability
	mD

Figure 4.6: Interpretation of MDT sampling test F147 in M56E Lower layer. The most likely value of permeability is 285 mD (the P50).

31

4.3.2   Permeability of the M56F interval based on cores

I have found the permeability of the M56D and E (Upper and Lower) layers through analysing the MDT data as described above. One other layer may have contributed to flow, M56F. For this layer, which is only 6.5 feet thick and therefore would not contribute much to flow, we do not have an MDT test. To find an effective permeability for the reservoir as a whole, I must first estimate the permeability of M56F and then combine the permeabilities of each layer. Below, I briefly summarize these steps. The full analysis can be found in Appendix E.

To get a range for the permeability of the M56F layer, I looked at the analysis performed by BP during the incident using a standard core-log analysis. I next average the reported permeabilities of samples in the M56F layer in two different ways. First, I took the familiar (arithmetic) average. This average is appropriate where the flow stays in nice layers (laminar flow). Second, I calculated the geometric average, which applies when flow is three-dimensional and does not stay nicely layered. I look at both averages because we do not know which type of flow we have. I keep both laminar and 3-dimensional flow as possibilities. I then correct the measurements to account for the fact that the lab results determined permeability to air rather than oil. (I do not convert the highest average to an oil permeability. This likely means I have overestimated permeability, but I have done so to be conservative.) Finally, I take a probability distribution representing the highest and lowest possible values and find the mean. I take that mean, 130 mD, as the permeability for M56F. This is explained in greater depth in Appendix E.

4.3.3   Effective permeability of the Macondo Reservoir is 238 mD

The most likely total permeability of the reservoir is 238 mD based on the combination of the MDT and core permeabilities described in Sections 4.3.1 and 4.3.2. I also performed a statistical analysis of the reservoir's permeability, which shows that the government permeabilities of around 500-550 mD are implausibly high.

To calculate the overall effective permeability of the Macondo reservoir, I averaged the values from the MDT tests and cores weighted by the thickness of each one of the formation layers. I weight by the thickness (h) because thin layers, like M56F at only 6.5 feet thick, contribute much less to flow than thick layers, like M56E at almost 65 feet. The details are spelled out in Appendix E but the basic idea comes from the radial flow equation we see over and over:

$$\frac{k\,h}{q\,\mu} = \frac{70.6\,B}{\Delta p'_{Stabilisation}}$$

If we reorganize this equation slightly, we see that:

$$q = \frac{k\,h\,\Delta p'_{stabilization}}{70.6\,B}$$

32

This says that flow rate (q) is directly proportional to permeability, k, times the height, h. And thus the flow contribution of each layer will be proportional to k times h for that layer. This is why we must take the height-weighted average of permeability.

But we do not know the permeability of the layers with certainty. Rather, we have generated probability distributions for the permeability of each layer. To determine the effective permeability of the entire reservoir (and the uncertainty), I again ran a Monte-Carlo simulation.[22] Here, the computer program repeatedly assigns possible values to each layer (based on the ranges and probability distributions we have already found) and reports back the weighted average—the effective permeability of the reservoir based on specific examples of permeabilities for each layer. Again, the computer does this thousands of times. The result gives us the probability distribution of permeability for the reservoir.

I conclude that the most likely permeability for the reservoir is 238mD. The full results are depicted in Fig. 4.7.

Percentiles	MC252-Kav
P 100	99
P 90	170
P 80	192
P 70	207
P 60	223
P 50	238
P 40	253
P 30	272
P 20	295
P 10	329
P 0	519
Statistics	MC252-Kav
Trials	5000
Mean	245
Median	238
Minimum	99
Maximum	519
Mean Std. Error	0.89
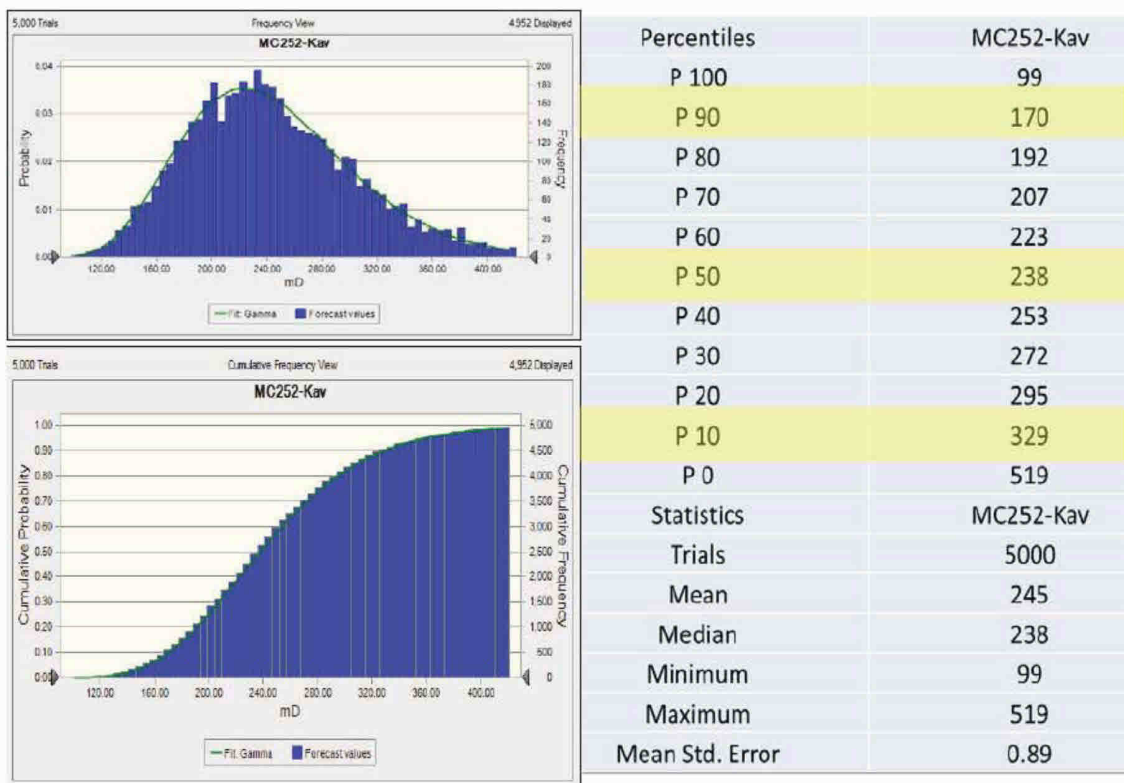
Figure 4.7: Permeability uncertainty distribution in the Macondo reservoir. The graph on the top left hand side represents the probability density function for the effective permeability of the Macondo reservoir. The graph on the bottom left hand side is the cumulative probability, which allows the construction of the table on the right hand side.

---

[22] Azi, A. C., Gbo, A., Whittle, T and Gringarten, A.C.: "Evaluation of confidence intervals in well test interpretation results," paper SPE 113888 presented at the 2008 SPE Europec/EAGE Annual Conference and Exhibition, Italy, 9–12 June 2008.

As can be seen from the chart above, this analysis demonstrates that there is less than a 5% chance that the permeability is 400 mD or higher, yet these are values used by Hsieh and also by Pooladi-Darvish in most of his models.[23]

5. Volume of oil released from the Macondo well

Next, I analyse the pressure data from PT-B—the pressure gauge at the base of the BOP—and PT-3K-2—one of the pressure gauges on the capping stack—(Fig. 5.1) using the permeability determined from my MDT analysis as an input. This allows me to estimate the total oil volume to have flowed from the reservoir during the spill at between 2.4 and 3 MMstb. I also find the reservoir size and the average pressure at shut in.
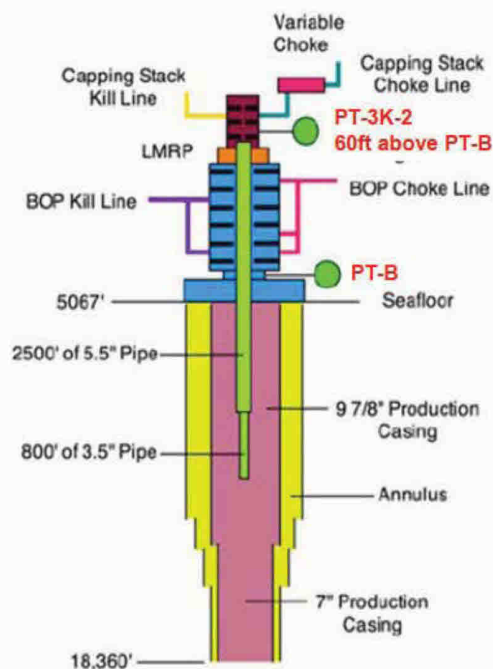
Figure 5.1: Pressure gauges used in the analysis (green circles).

My analysis proceeded in the following steps:

First, I took two assumed rate histories (Options 1 and 2) for the incident (the discussion focuses on Option 1, since the procedure is the same for each Option). These do not reflect actual flow rates although they were chosen based roughly on rate values that have been estimated for particular periods during the spill. These rate histories are used as starting points for the analysis, and, in particular, for use of deconvolution, which corrects rates based on pressure readings. I applied deconvolution to each

---

[23] *See* Hsieh, P., Computer simulation of Reservoir Depletion and Oil Flow (IGS642-000215) (2010); Expert report, "Estimate of the cumulative volume of oil released from the MC252 Macondo well," prepared by Mehran Pooladi-Darvish (2013).

34

Option using PT-B pressure data for times when the well was flowing and PT-3K-2 pressure data after the well was the shut in. I used these rates to analyse the PT-3K-2 pressure data.

Second, I took the rates obtained above and used those rates to calculate the pressure at the bottom of the well. The pressure at the bottom of the well will be higher than the pressure at the gauges, which are near the wellhead, because of the weight of the fluid and (when there is flow) the frictional forces. The pressure-changes—the "transient" —at the bottom of the well better reflect reservoir behaviour.

Third, I returned to the assumed rate history and again applied deconvolution using the new bottomhole pressure information. This, like the first step, gives me a deconvolved derivative and corrects the rates. The difference here is that the deconvolved derivative is based on bottomhole pressures instead of wellhead pressures, which should better correspond to pressure in the reservoir. I then took the corrected rates and repeated the process of applying deconvolution until I obtained a good match between the bottomhole pressures and the pressures that I calculated from the deconvolved derivative. In this case, after four iterations, the pressures were very close and the rates did not change appreciably, showing I had converged on a solution.

Fourth, I used the corrected rate histories obtained in step three to study the pressure build up that occurred after the well was shut in. For this analysis, I used post-shut-in pressure data from the PT-3K-2 gauge, which had been translated to bottomhole pressure. The deconvolved derivative allows me to build an interpretation model, as described in Section 3.

Fifth, I used the radial flow stabilization of the interpretation model to scale the flow rate history to match the permeability obtained in my MDT analysis—the permeability of the reservoir.

Sixth, I confirmed the interpretation model by verifying it can reproduce all the bottomhole pressure data during the spill and after shut in; and be verifying that the model is consistent with other information such as geology and seismic. This is necessary because often many models will appear to match the available data, and the interpreter must bring all available tools and data to bear on the problem to ensure acceptance of only an appropriate model.

My conclusions are as follows:

- The best estimate of the total volume of oil that left the reservoir during the spill is between 2.4 and 3 MMStb.
- The best estimate of the amount of oil originally in the reservoir that was connected to the wellbore is between 78 and 97 MMStb.
- The final reservoir pressure is between 10,364 and 10,460 psi.
- There is no evidence of aquifer support within the timeframe of the data available.

Dr. Blunt used a different methodology to analyse the Macondo reservoir and the cumulative flow. I have reviewed his report and I approve of his analysis.

5.1 Estimate Flow-Rate Trend Based on Wellhead Pressure

My first step was to estimate the rate history based on the wellhead pressure using deconvolution. The basic principle is that changes in pressure reflect changes in the flow rate. Deconvolution can take the pressure data we have and convert it to a flow-rate trend reflecting that pressure data. To begin this process, I must first assume a flow-rate history as a starting point. Deconvolution will correct these rates, albeit with some uncertainty. Since I want to determine the actual flow-rate history, I use two different history assumptions to start the process:

- First, I assume that the well flowed at a constant rate of 45,000 stb/d for the entire incident ("Option 1");
- Second, I also deconvolved using a starting rate assumption of 30,000 stb/d for April 20 to May 31 and 45,000 stb/d for June 1 until shut-in ("Option 2").

Later, I will discuss the differences between the rate histories I obtained. I selected these two rate histories because there is evidence that the flow rate was between 38,829 stb/d and 48,201 stb/d before shut-in started■; and that the rate was between 26,200 and 34,400 stb/d between May 13 and May 23, 2010.[25]

The flow rates that resulted from applying deconvolution to the wellhead pressure data for both cases are depicted in Figure 5.2 below. As we do not have pressure data prior to May 8, I have assumed that the pressure decreases linearly between the initial pressure and the first pressure measurement on May 8, 2010. As it turns out, these two initially corrected rate histories are similar, so they will give similar results for the analysis of PT-3K-2 pressures. They will give different downhole-converted pressures, however. I therefore analysed both Options. The discussion, however, focuses primarily on Option 1, since the process is the same for Option 2. I report the results for both.

■ ██████████████████

[25] Expert Report of M. Zaldivar.

TREX-011696R.036
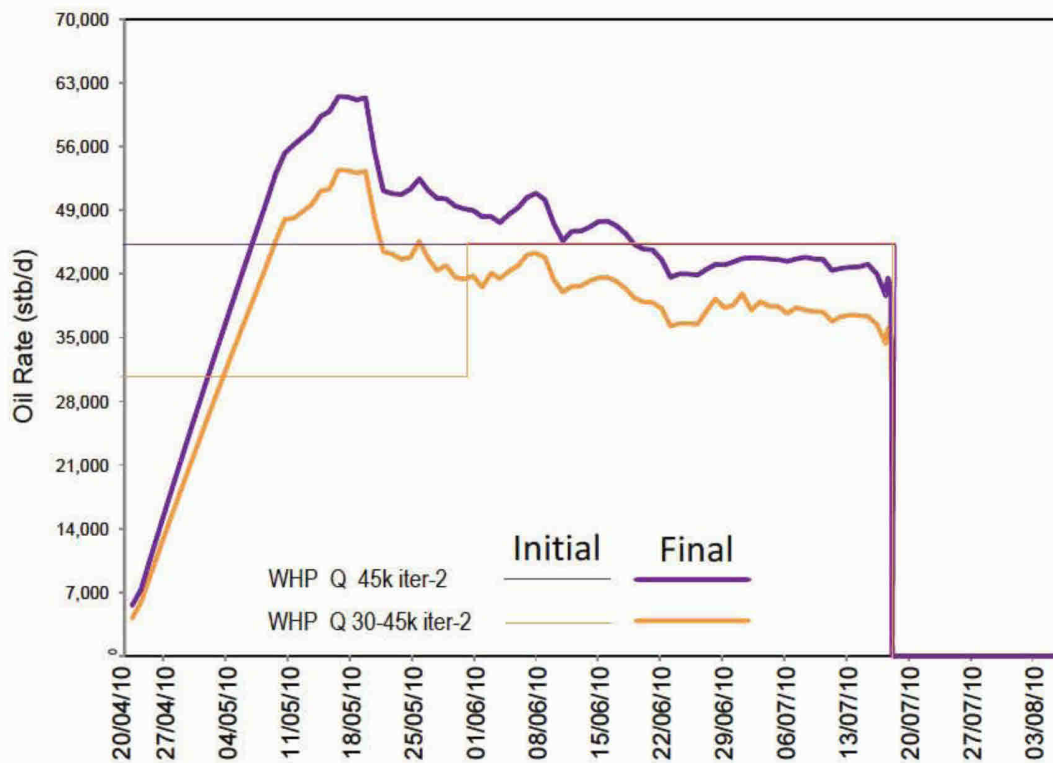
Figure 5.2: Deconvolved Rates Using PT-B and PT-3K-2 Pressure

5.2 Obtain Bottomhole Pressure

I provided the PT-B data and the flow rates between April 20 and July 15 I had estimated above to Dr. Adrian Johnson. Dr. Johnson used his model to translate those pressures to a mid-reservoir depth of 18,056 ft. TVDss.[26] I received data for both a "drill pipe high" and a "drill pipe low" scenario.[27] The difference between the two scenarios is the position of the drill pipe in the well, which apparently fell at some point. Since I do not know when, I use the pressure translations resulting from both possible locations of the drill pipe in my analysis. A schematic representation of the two drill pipe locations is shown in Figure 5.3.

---

[26] *See* Expert Report of A. Johnson; OPTION1 P and Q for Translation (26-04-13) with BHPs.xlsx; OPTION2 P and Q for Translation (26-04-13) with BHPs.xlsx.

[27] See Expert Report of A. Johnson for a description of the drill pipe high and drill pipe low scenarios.

TREX-011696R.037
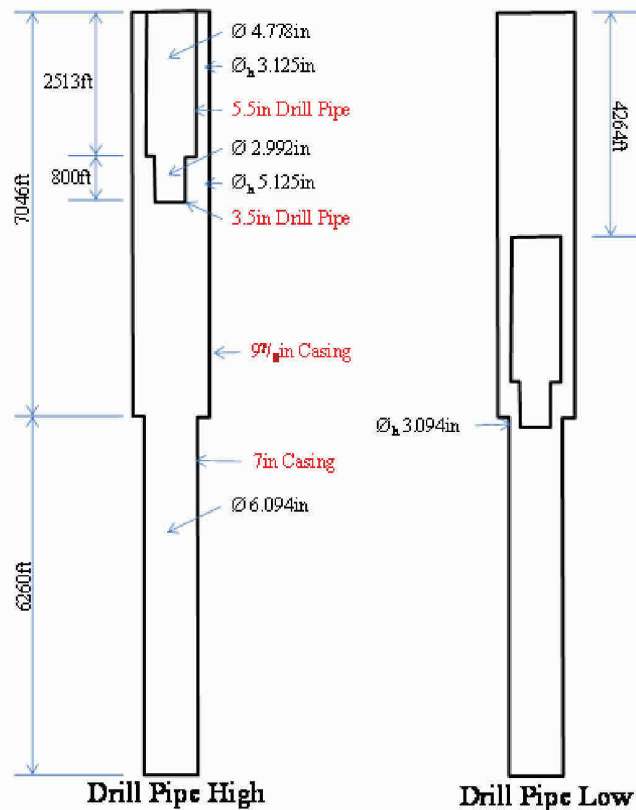
Figure 5.3: "Drill Pipe High" and "Drill Pipe Low" Scenarios[28]

I also provided a subset of the post-shut-in PT-3K-2 pressure measurements to Prof. Martin Blunt for translation to bottomhole conditions. I reviewed and agree with his method for obtaining bottomhole pressure, and I used these pressures in my further analysis.[29] Prof. Blunt provided three different equations for translating these pressures to bottomhole, each corresponding to laboratory measurements from a different fluid lab (CoreLab, Schlumberger, and Intertek). I generally use the equation for CoreLab, but I have also investigated the impact of using the equation for Schlumberger.

5.3 Estimate Flow-Rate Trend Based on Bottomhole Pressure

I then used the bottomhole pressure data to refine the flow-rate estimates I derived from the wellhead pressure data. I wanted to use bottomhole pressure data in my analysis because wellhead pressure has a tendency to overestimate permeability and skin effects.[30] It does so because of fluid compressibility

---

[28] Expert Report of A. Johnson.

[29] Expert Report of M. Blunt; OPTION1 P and Q for Translation (26-04-13) with BHPs.xlsx; OPTION2 P and Q for Translation (26-04-13) with BHPs.xlsx.

[30] Spyrou, C. E., Nurafza, P. and Gringarten, A. C.: "Well-head Pressure Transient Analysis", paper SPE 164871 to be presented at SPE Europec/EAGE Annual Conference, London, United Kingdom, 10–13 June 2013.

TREX-011696R.038

effects in the well and possible restrictions to flow between the pressure gauge and the reservoir. It is therefore important at least to compare flow-rate estimates based on wellhead conditions to those obtained from bottomhole pressure.

Once I had the bottomhole pressure data, I deconvolved the data the same way I did for the wellhead pressure data in Section 5.1, again starting with the assumed rates from my Options 1 and 2. I will use the "Option 1 - Drill Pipe High" pressure data for illustration. First, I began the deconvolution with a constant rate assumption of 45,000 stb/d. The results of my deconvolution are in Figure 5.4.
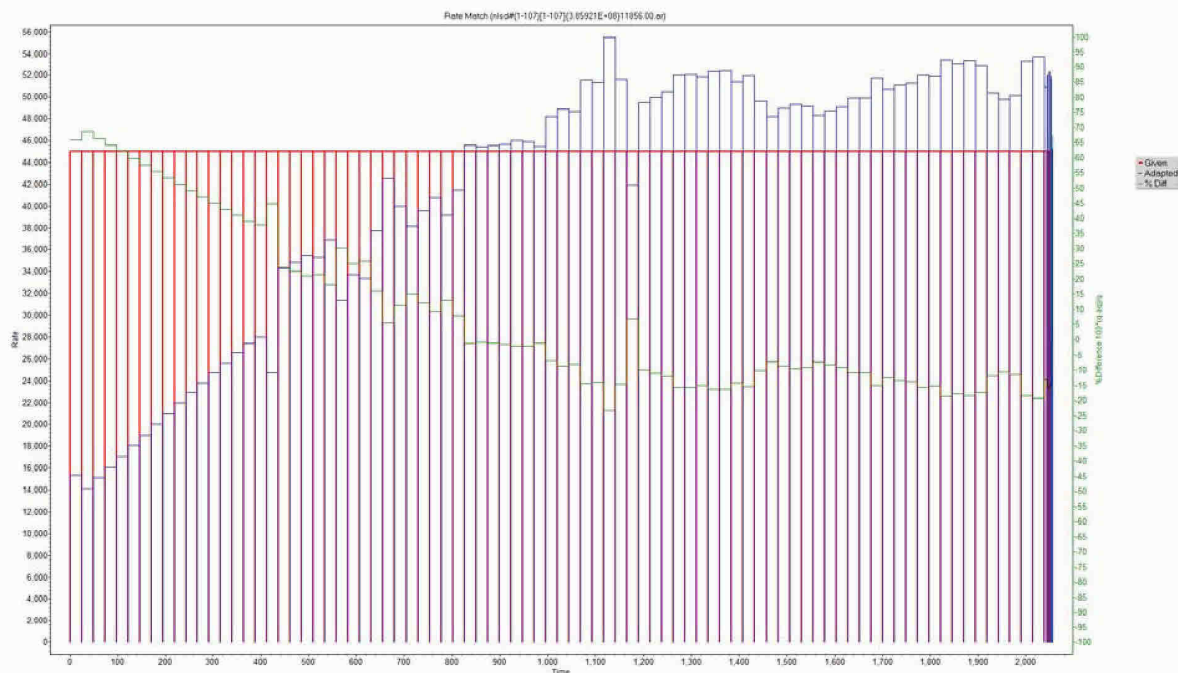
Figure 5.4: First Iteration of Deconvolved Rates Using Bottomhole Pressure (Option 1 - Drill Pipe High). Red bars show the initial assumed rates, while blue bars show the deconvolved rates resulting from deconvolution.

The red lines in Figure 5.4 show the initial assumption of a constant rate of 45,000 stb/d. The blue line shows the deconvolved rates, and the green line shows the percentage change between the initial assumption (horizontal red line) to the deconvolved rate (blue line). The vertical red lines mark the durations of the periods of constant rate.

Following standard methods, I continued to run iterations of deconvolution to refine the rates. For each successive iteration, I used the flow rates from the previous iteration as the initial assumed rates. I continued to use the same bottomhole pressures for each iteration. With each subsequent iteration, there is a smaller change from the assumed rates to the deconvolved rates. Figure 5.5 shows the results of my second iteration.

39
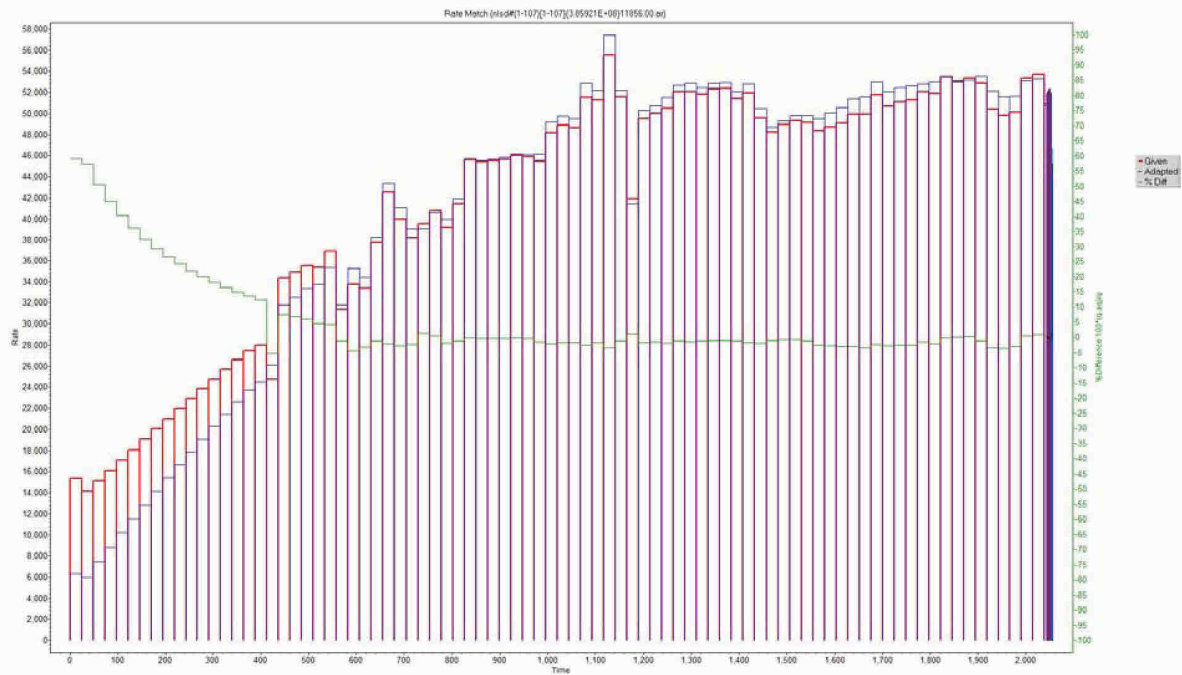
Figure 5.5: Second Iteration of Deconvolved Rates Using Bottomhole Pressure (Option 1 - Drill Pipe High)

After the second iteration, the deconvolved rates (blue lines) change much less from the assumed rates (red lines). Again, the assumed rates for this second iteration (red lines in Figure 5.5) come from the deconvolved rates for the first iteration (blue lines in Figure 5.4). By the fourth iteration of deconvolution, there was hardly any change from the initial assumption to the deconvolved rates.
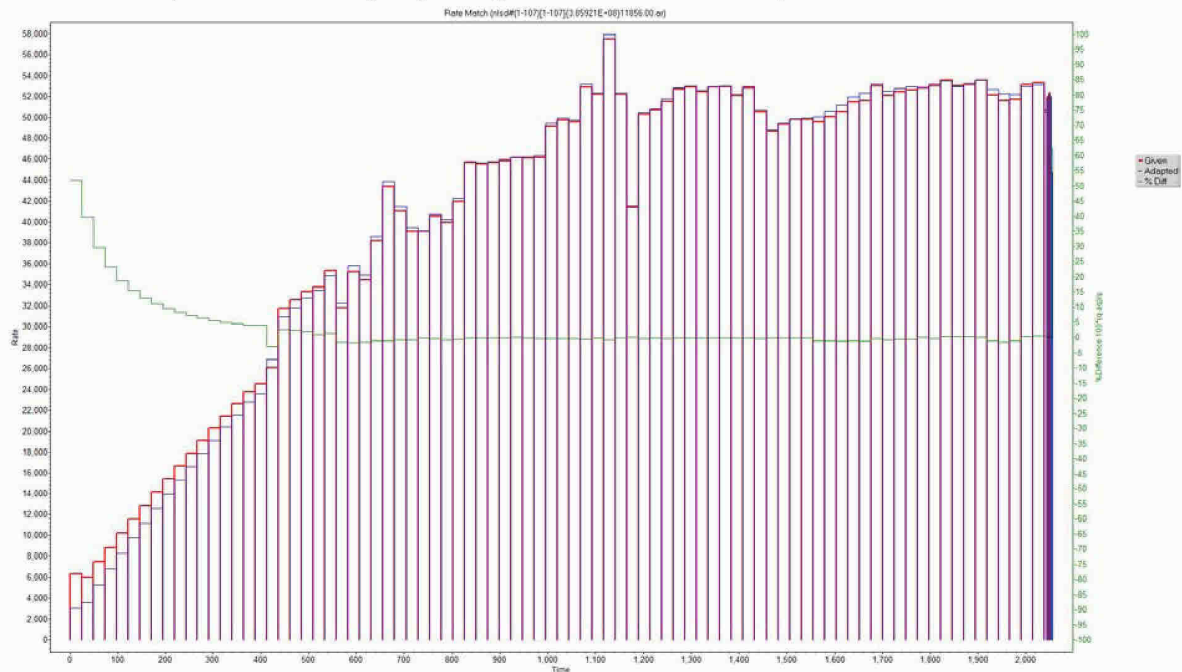
Figure 5.6: Third Iteration of Deconvolved Rates Using Bottomhole Pressure (Option 1 - Drill Pipe High)
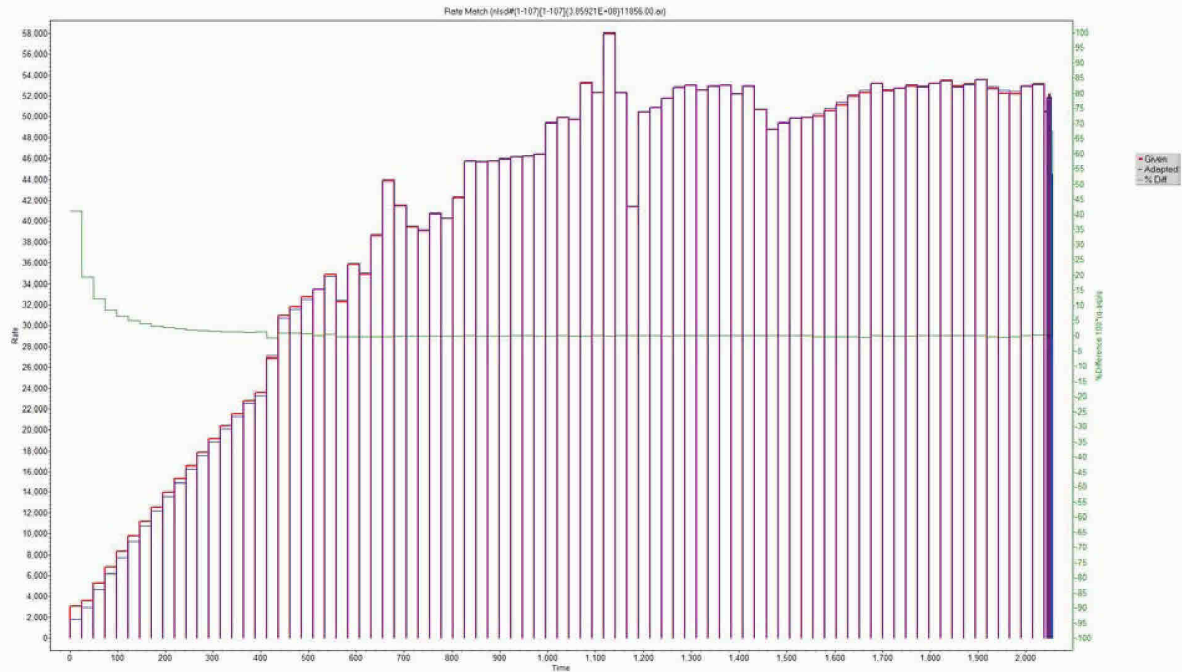
Figure 5.7: Fourth Iteration of Deconvolved Rates Using Bottomhole Pressure (Option 1 - Drill Pipe High)

The objective of this iterative process is to obtain a reliable deconvolved derivative—that is, the pressure derivative we obtain from deconvolution of pressure data. In simple terms, I can verify the reliability of the deconvolved derivative by combining the rates I have generated with the pressure derivative in a process called "convolution," which is the reverse of deconvolution. If my deconvolved derivative is reliable, I should get back pressures that closely match the bottomhole pressures. I do this at each iteration. If the deconvolved derivative is correct, then the pressure profile I generate should match the bottomhole pressures. This is, in fact, what we see in Figure 5.8 below.

41
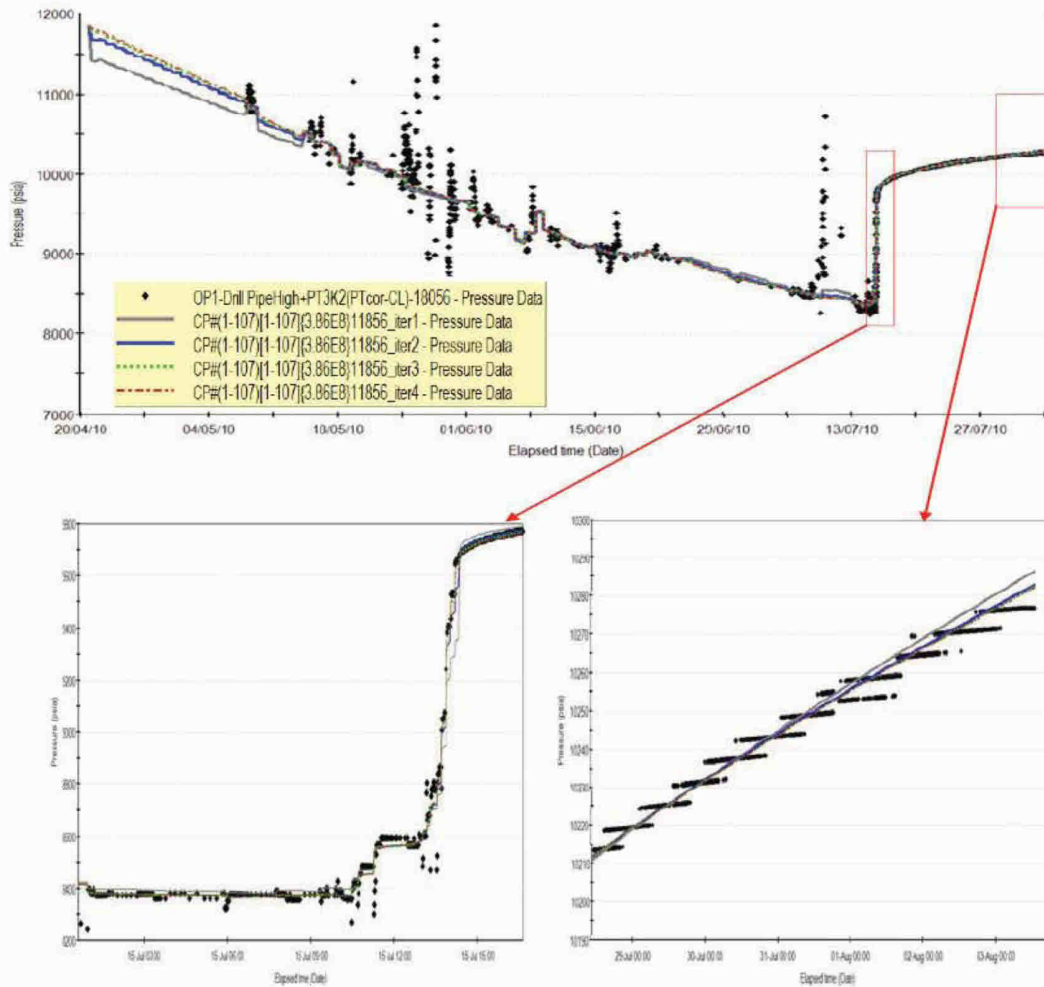
Figure 5.8: Comparison of Convolved and Measured Pressure (Option 1 - Drill Pipe High). The match between convolved pressures and measured pressures improve with the number of iterations. The measured pressure data in the bottom right graph are increasing by steps due to the low resolution of the PT-3K-2 gauge (5 psi).

We see at the top of Figure 5.8 that the first iteration, the gray line, matched the bottomhole pressure data only moderately well. But the fourth iteration, the red line, is almost indistinguishable from the bottomhole pressure data. This is even more apparent when we zoom in on the data at the top of Figure 5.8 (shown in the bottom left and bottom right graphs of Figure 5.8). This also indicates I have converged on the correct deconvolved derivative (Figure 5.9) and that I now have the correct flow-rate trend.

42
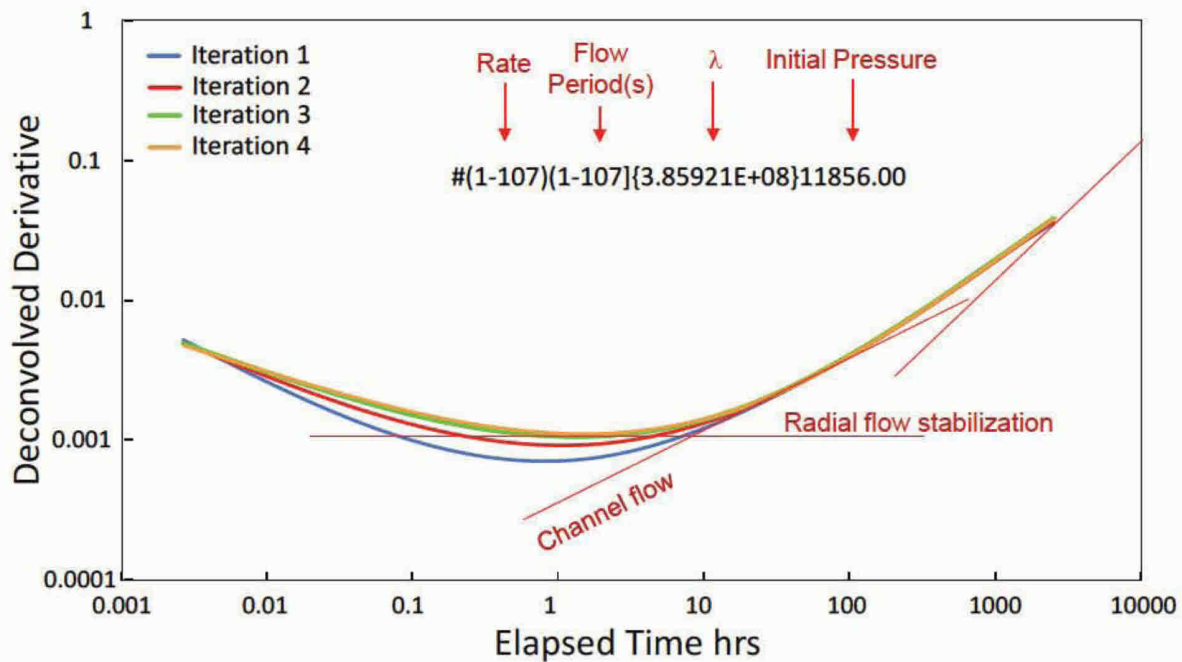
Figure 5.9: Convergence of deconvolved derivatives

I went through the above process for each of the five scenarios[31]: Option 1 - Drill Pipe High; Option 2 - Drill Pipe High, Option 2 - Drill Pipe Low (all these use the equation for downhole conversion of the shut in pressure using CoreLab fluid properties), BOP (wellhead) pressure, and Option 1 - Drill Pipe High with the downhole conversion equation using Schlumberger fluid properties. And I was able to get a well-matched pressure history for each of them.[32] This gives me confidence in the final deconvolved derivatives (which I will use to identify the interpretation model) and in the deconvolved rates (which I will use for my analyses with that interpretation model).

5.4   Identify Interpretation Model

Now that I have the flow-rate trend and the deconvolved derivative, I can build an interpretation model of the Macondo reservoir. This process involves the identification of all the various dominant flow regimes as illustrated in Figure 5.9 above, as explained in Section 3.3.1. I can see radial flow, channel flow and a closed reservoir. Hence, I determine that the reservoir has the shape of a rectangle; I can tell from the deconvolved derivative that there is no active aquifer support acting on the reservoir. The interpretation model identified from the deconvolved derivative and the deconvolved rate history are

---

[31] Option 1 - Drill Pipe Low was excluded because the pressure behaviour was anomalous just prior to shut-in. Option 1 - Drill Piple Low would have yielded the lowest cumulative flow rate; this can be inferred because Option 1 yielded a lower cumulative flow than Option 2 and Drill Pipe Low yielded a lower cumulative flow than Drill Pipe High.

[32] *See* Appendix F (Macondo Pressure Transient Analysis).

then used to analyse the actual pressure data and calculate the dimensions and other characteristics. Below, I go through some of this in more detail.

5.5   Verify Interpretation Model

The complete interpretation process is illustrated in Figure 5.10. The plot on the top left shows the bottomhole pressure change and pressure derivative. The red line on the plot is where we see radial flow stabilisation; the slope of the line is zero. I confirmed that the data where the derivative stabilises are on a straight line on the Horner plot—the red line in the plot on the middle left. My identification of the radial flow stabilisation is thus confirmed by the Horner plot. We need both: we could see a stabilisation on the derivative (maybe due to noisy data), but if there is no corresponding straight line on the Horner plot, the stabilisation on the derivative is not due to radial flow.

Further verification is illustrated by the plots on the right hand side. They show the match between the model (in red) with the data (in blue) and confirm that the model can reproduce the data. Finally, the plot at the bottom left is the skin effect versus time. The skin is 15 at the beginning of the incident and corresponds to the likely length of reservoir open to flow being 16.5 ft[33]. The skin decreases with time to a value of 4 during the spill, and zero during the shut in. The zero shut in skin indicates that the formation is not damaged and confirms the value from MDT analysis. The skin during the spill corresponds to flowing restrictions in the well.

---

[33] Expert Report of M. Emilsen.

TREX-011696R.044
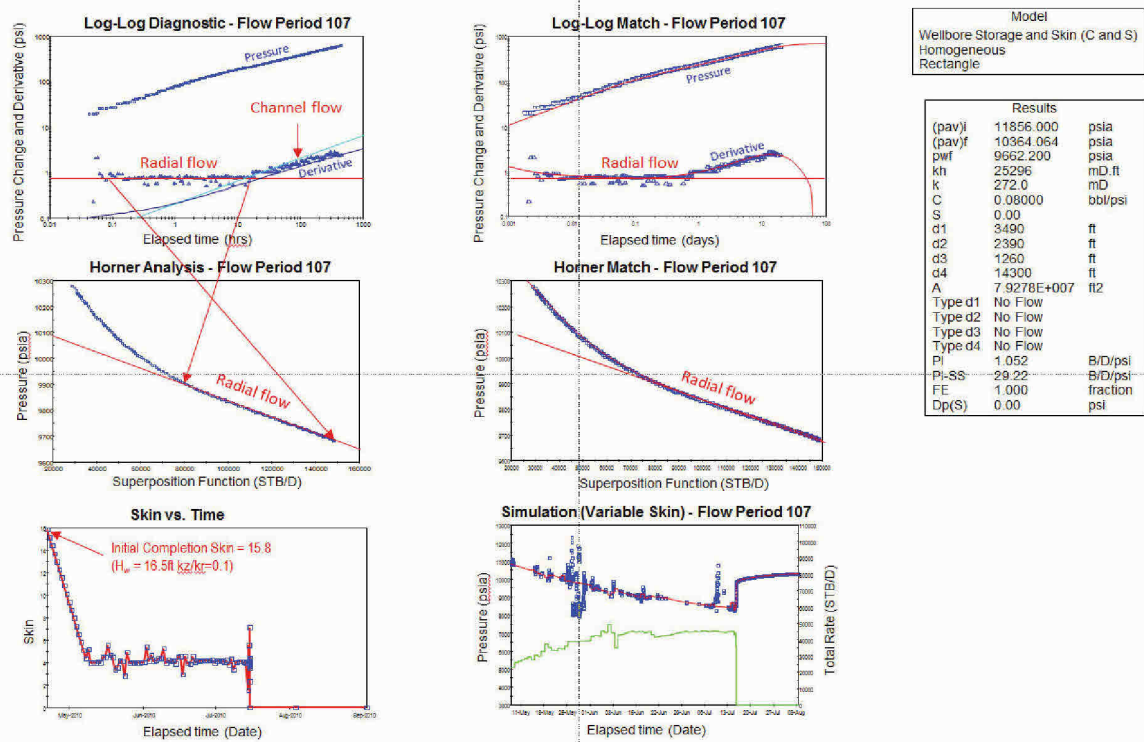
Figure 5.10: The plots on the left illustrate the computation and diagnosis of the derivative. All of the plots reflect the pressure data from shut-in until static kill on August 3, 2010; that is what we refer to as Flow Period 107 in our analysis (Option 1 - Drill Pipe High)

5.6 Scale Rate History to Permeability

As stated before, deconvolution only corrects the differences in rate from one period to the next and does not provide absolute values. Rates have therefore to be scaled. For instance, with the rate history from Fig. 5.7, the radial flow stabilisation level of the pressure build-up yields a permeability of 272 mD as can be seen in the table on the right side of Figure 5.10, not the actual permeability of Macondo. The P50 permeability I derived from the MDT analysis in Section 4 is 238 mD. To determine the rate history for Macondo, I need to scale the rate history obtained to match the 238 mD permeability of Macondo, according to Eq. 4 of Section 3.3.1. To do this, I simply multiply the rate history by (the Macondo P50 permeability)/(the unscaled permeability), 238 mD/272 mD. A comparison of the P50 flow rate history and the unscaled rate history is below in Figure 5.11. In the following subsections, I will explain why and how we use MDT permeability to scale the flow rate history.

45
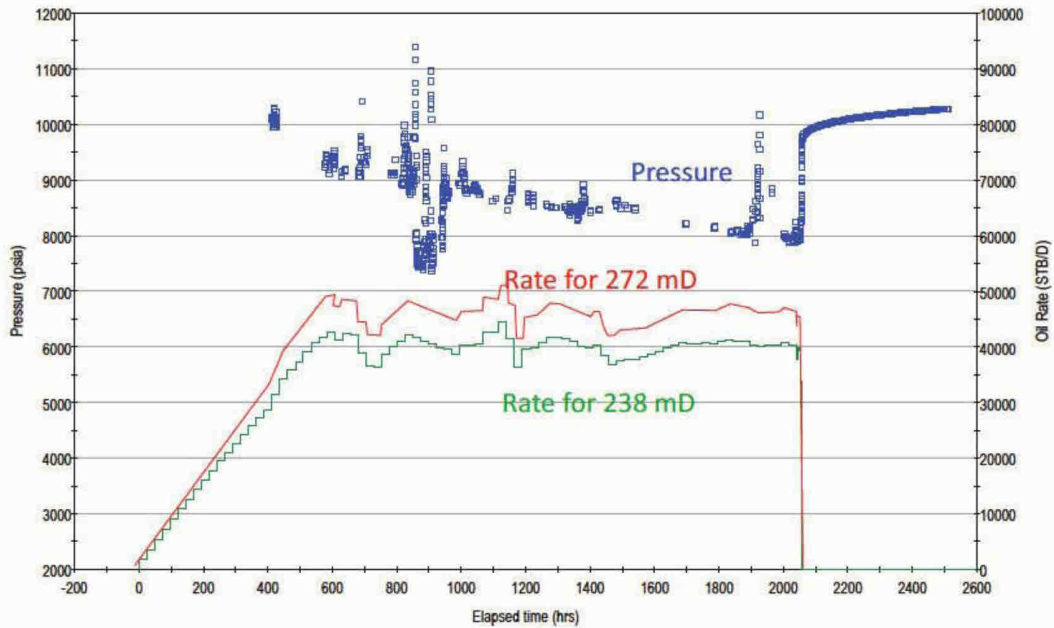
Figure 5.11: The red line is the unscaled flow-rate history. The rate history is scaled to match the Macondo P50 permeability, which was independently determined through analysis of the MDT data as discussed in Section 4.

5.6.1   The model is expressed in dimensionless variables

In order to explain how the rate history is scaled to match the MDT permeability, I need to go back to the definition of the interpretation model. As noted in Section 3.3.3, the mathematical function representing the interpretation model is expressed in terms of dimensionless variables that are functions of the reservoir parameters (for example, permeability, skin effect, distances to boundaries). These are called dimensionless because all the units cancel, and the variables are just numbers. They do not have units, like psi or milliDarcies. They therefore represent any values of reservoir parameters.

The match between model and data returns values for these dimensionless variables, and of two additional parameters, PM, called the pressure match, and TM, called the time match. These are defined as:

$$PM = \frac{kh}{141.2 \, q \, B_o \, \mu} \tag{5}$$

$$TM = 0.000264 \frac{kh}{\mu} \frac{1}{C} \tag{6}$$

(PM and TM are not dimensionless. Their units are 1/psi and 1/hour, respectively.) In the case of a well in a rectangular reservoir, the other (dimensionless) parameters are:

46

$$C_D \, e^{2S} = \frac{0.8936 \, C}{\varphi \, c_t \, h \, r_w^2} e^{2S}$$

(7)

$$A_D = \frac{A \, \varphi \, c_t \, h \, r_w^2}{0.8936 \, C} \text{ with } A = \left(d_1 + d_3\right)\left(d_2 + d_4\right)$$

(8)

$$\frac{x_e}{y_e} = \frac{d_1 + d_3}{d_2 + d_4} , \; \frac{x_w}{x_e} = \frac{d_1}{d_1 + d_3} , \; \frac{y_w}{y_e} = \frac{d_2}{d_2 + d_4}$$

(9)

C is the wellbore storage constant in barrels per psi; φ, the porosity; A, the reservoir area; and c_t, the total compressibility. d_1, d_2, d_3, and d_4 are the distances to the well to the boundaries. The other parameters have already been defined.

PM, TM and the dimensionless parameters obtained from the match between model and data in turn provide the corresponding reservoir parameters. The pressure match value is obtained from the radial flow stabilisation of the pressure derivative, $\Delta p'_{stabilisation}$ as:

$$PM = \frac{1}{2\Delta p'_{stabilisation}}$$

(10)

Substituting Eq. 10 into Eq. 5 yields Eq. 4 from Section 3.3.1:

$$\frac{k \, h}{q \, \mu} = \frac{70.6 \, B_o}{\Delta p'_{stabilisation}}$$

(4)

5.6.2 There is a direct relationship between permeability and final flow rate.

Once $\Delta p'_{stabilisation}$ is identified, the ratio k/q (the relationship between permeability and final flow rate) is fixed because h, B_o, and μ are known and constant. If we change k (permeability), we need to change q (final flow rate) to maintain the fixed k/q ratio. Therefore, to obtain the flow rates for the P50 permeability of 238 mD, I need to reduce the rate that gives me a permeability of 272 mD by the ratio 238/272. Rescaling like this will also decrease the distance to the boundaries and therefore the size of the reservoir, but will not change the dimensionless match parameters as these changes offset each other. It will not change the average reservoir pressure either, because, for a given interpretation model, the reservoir pressure depends on PM and TM[34] only. Similarly, adjusting pore volume

---

[34] The average reservoir pressure is given by $\overline{p} = p_i - \dfrac{1}{PM} p_D\left(TM \, t_p\right)$, where p_D is the mathematical function representing the interpretation model and *PM* and *TM* are dimensionless model parameters. t_p is the production time. These parameters remain constant when the permeability changes, and therefore the average pressure does not change.

47

compressibility also will not affect my flow rates because they are dependant on permeability and the pressure data only.

5.6.3   Dr. Pooladi-Darvish's analysis is flawed.

As discussed above, the model mathematical expression is written in what are called "dimensionless terms," so it is applicable to various combinations of reservoir parameter values. One important strength of this approach is that it is easy to see whether two models are in essence the same model as often happens in reservoir analysis when one is not careful. Indeed, failure to convert to dimensionless terms can lead one to look at the same model over and over thinking it represents different models.

Once we have a match, that match will be maintained for any value of permeability and rate as long as the permeability-to-rate ratio remains constant. The higher the permeability, the higher the rate, and the larger the reservoir. But the dimensionless match parameters remain the same. In other words, all the analyses of Dr. Pooladi-Darvish are really only one in dimensionless terms. He has in essence run the exact same model over and over; it is not surprising that he gets basically the same results each time. Nor is it informative. This is further illustrated in Section 6.

This is why it is mandatory to have an independent evaluation of the reservoir parameters to constrain the results. Here, we have bounded the value of permeability by interpreting the MDT data. This allows us to bound the rates and therefore the total amount of oil released during the Macondo spill.

5.6.4   The flow rate history is scaled for P10 and P90 permeabilities.

The same process as described above for the P50 permeability is repeated for the P10 and P90 permeabilities. The rate multiplier for the P10 permeability is 329/272. That for the P90 permeability is 170/272. Recall that the P10 value means that there is a 10% chance that the actual value of the variable is at least that high, and the P90 means that there is a 90% chance.

The analysis results for the P10, P50 and P90 permeabilities are given in Figure 5.12. As discussed above, the permeability and reservoir size decrease from P10 to P90, but the dimensionless match parameters do not change, meaning that there is a single match between the model and the data.

TREX-011696R.048

Parameter	P10	P50	P90	Unit
(pav)i	11856	11856	11856	psia
(pav)f	10364	10364	10364	psia
pwf	9662.2	9662.2	9662.2	psia
kh	30597	22131	15808	mD.ft
k	329	238	170	mD
C	0.097	0.070	0.050	bbl/psi
S	0.0	0.2	0.3	
d1	3517	2991	2528	ft
d2	2409	2049	1731	ft
d3	1270	1080	913	ft
d4	14412	12257	10359	ft
A	8.05E+07	5.82E+07	4.16E+07	ft2
PM	0.6692	0.6692	0.6692	1/psi
TM	440.1	440.1	440.1	1/hr
Log CDe2S	3.25	3.25	3.25	
(A)D	3.55E+05	3.55E+05	3.55E+05	
xe/ye	0.2846	0.2846	0.2846	
xw/xe	-0.4695	-0.4695	-0.4695	
yw/ye	0.7136	0.7136	0.7136	

Figure 5.12: Reservoir parameters for P10, P50 and P90 permeabilities in the case of Option 1, Drill Pipe High

5.6.5   Cumulative flow can be determined from the scaled flow rate histories.

Having determined the rate multipliers for the P10, P50 and P90 permeabilities, I can then calculate the P10, P50 and P90 cumulative productions. The P50 is the best estimate of total volume of all the oil that left the reservoir, converted to a volume at surface (stock tank) conditions of 60°F and 1 atmosphere pressure. It includes any oil burnt or collected, for example. Results are shown in Figures 5.13 and 5.14. The results also include rates scaled to the mean permeability and the permeability corresponding to a flow rate just before shut-in of approximately 45,000 stb/d in ███████████ ███████████ ████████████████████. The P10 and P90 cases set the upper and lower bounds respectively though.

49

Parameters	P 90	P 50	P 10	Mean K	K-281
Initial Pressure @ Reservoir Depth (18,056 ft TVDss) psia	11,856	11,856	11,856	11,856	11,856
Final Pressure @ Reservoir Depth (18,056 ft TVDss) psia	10,364	10,364	10,364	10,364	10,364
Depletion (psi)	1,492.00	1,492.00	1,492.00	1,492.00	1,492.00
Reservoir Permeability (mD)	170	238	329	245	281
Skin	20 → 0	20 → 0	20 → 0	20 → 0	20 → 0
Boundary1 (d1) – ft	2,528	2,991	3,517	3,035	3,253
Boundary2 (d2) – ft	1,731	2,049	2,409	2,079	2,228
Boundary3 (d3) – ft	913	1,080	1,270	1,096	1,174
Boundary4 (d4) - ft	10,359	12,257	14,412	12,438	13,328
Reservoir Width - ft	3,441	4,071	4,787	4,131	4,427
Reservoir Length - ft	12,090	14,306	16,821	14,517	15,556
Area (MM ft^2)	41.6	58.2	80.5	60.0	68.9
Area (Acres)	955	1,337	1,848	1,377	1,581
STOIIP (MMstb)	57	79	110	82	94
Cumulative Production (MMstb)	1.78	2.49	3.45	2.57	2.95

Figure 5.13: Analysis results of Option 1 Drill Pipe High
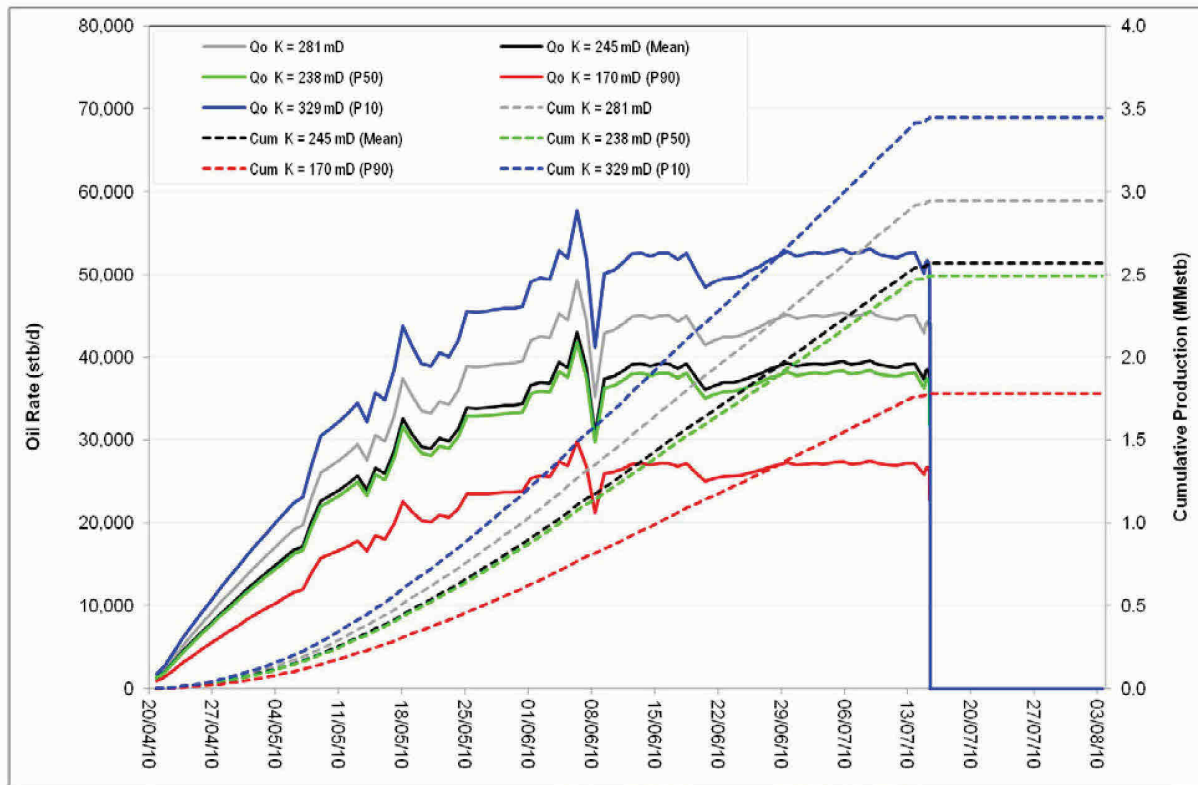
Figure 5.14: Flow rates for Option 1 Drill Pipe High. The dashed lines represent cumulative flow for their respective permeabilities.

I also apply the same procedure to the other cases: Option 2 Drill Pipe High, and Options 2 Drill Pipe Low.

Parameters	P 90	P 50	P 10	Mean K	K-264
Initial Pressure @ Reservoir Depth (18,056 ft TVDss) psia	11,856	11,856	11,856	11,856	11,856
Final Pressure @ Reservoir Depth (18,056 ft TVDss) psia	10,381	10,381	10,381	10,381	10,381
Depletion (psi)	1,475.00	1,475.00	1,475.00	1,475.00	1,475.00
Reservoir Permeability (mD)	170	238	329	245	264
Skin	20 → 4	20 → 4	20 → 4	20 → 4	20 → 4
Boundary1 (d1) – ft	2,825	3,342	3,930	3,391	3,518
Boundary2 (d2) – ft	1,730	2,047	2,407	2,077	2,155
Boundary3 (d3) – ft	1,137	1,346	1,582	1,365	1,417
Boundary4 (d4) - ft	11,059	13,086	15,385	13,276	13,776
Reservoir Width - ft	3,962	4,688	5,512	4,756	4,935
Reservoir Length - ft	12,789	15,133	17,792	15,353	15,931
Area (MM ft^2)	50.7	70.9	98.1	73.0	78.6
Area (Acres)	1,163	1,629	2,251	1,676	1,805
STOIIP (MMstb)	69	97	133	99	107
Cumulative Production (MMstb)	2.15	3.00	4.15	3.09	3.33

Figure 5.15: Analysis results of Option 2 Drill Pipe High

TREX-011696R.052
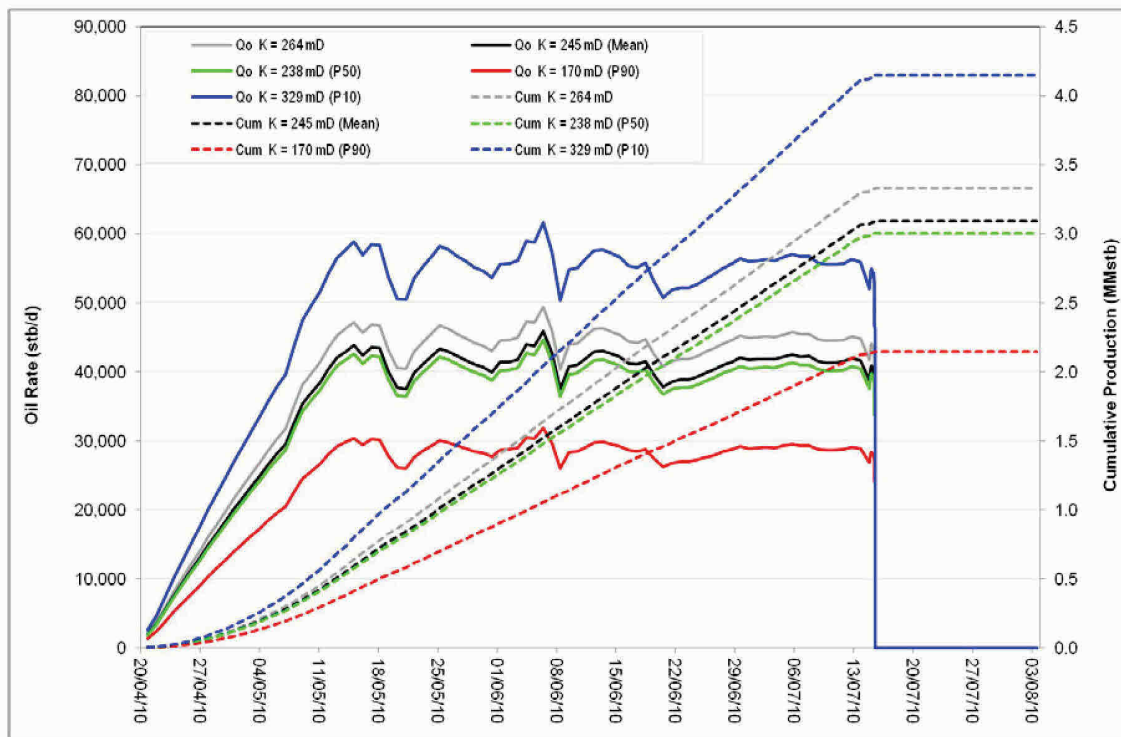
Figure 5.16: Flow rates for Option 2 Drill Pipe High. The dashed lines represent cumulative flow for their respective permeabilities.

Parameters	P 90	P 50	P 10	Mean K	K-321
Initial Pressure @ Reservoir Depth (18,056 ft TVDss) psia	11,856	11,856	11,856	11,856	11,856
Final Pressure @ Reservoir Depth (18,056 ft TVDss) psia	10,374	10,374	10,374	10,374	10,374
Depletion (psi)	1,482.00	1,482.00	1,482.00	1,482.00	1,482.00
Reservoir Permeability (mD)	170	238	329	245	321
Skin	20 → 2	20 → 2	20 → 2	20 → 2	20 → 2
Boundary1 (d1) – ft	2,402	2,842	3,342	2,884	3,299
Boundary2 (d2) – ft	1,574	1,863	2,190	1,890	2,162
Boundary3 (d3) – ft	869	1,028	1,208	1,043	1,193
Boundary4 (d4) - ft	10,902	12,899	15,166	13,088	14,973
Reservoir Width - ft	3,271	3,870	4,550	3,927	4,492
Reservoir Length - ft	12,476	14,762	17,356	14,978	17,135
Area (MM ft^2)	40.8	57.1	79.0	58.8	77.0
Area (Acres)	937	1,312	1,813	1,350	1,767
STOIIP (MMstb)	56	78	107	80	105
Cumulative Production (MMstb)	1.74	2.43	3.36	2.50	3.27

Figure 5.17: Analysis results of Option 2 Drill Pipe Low
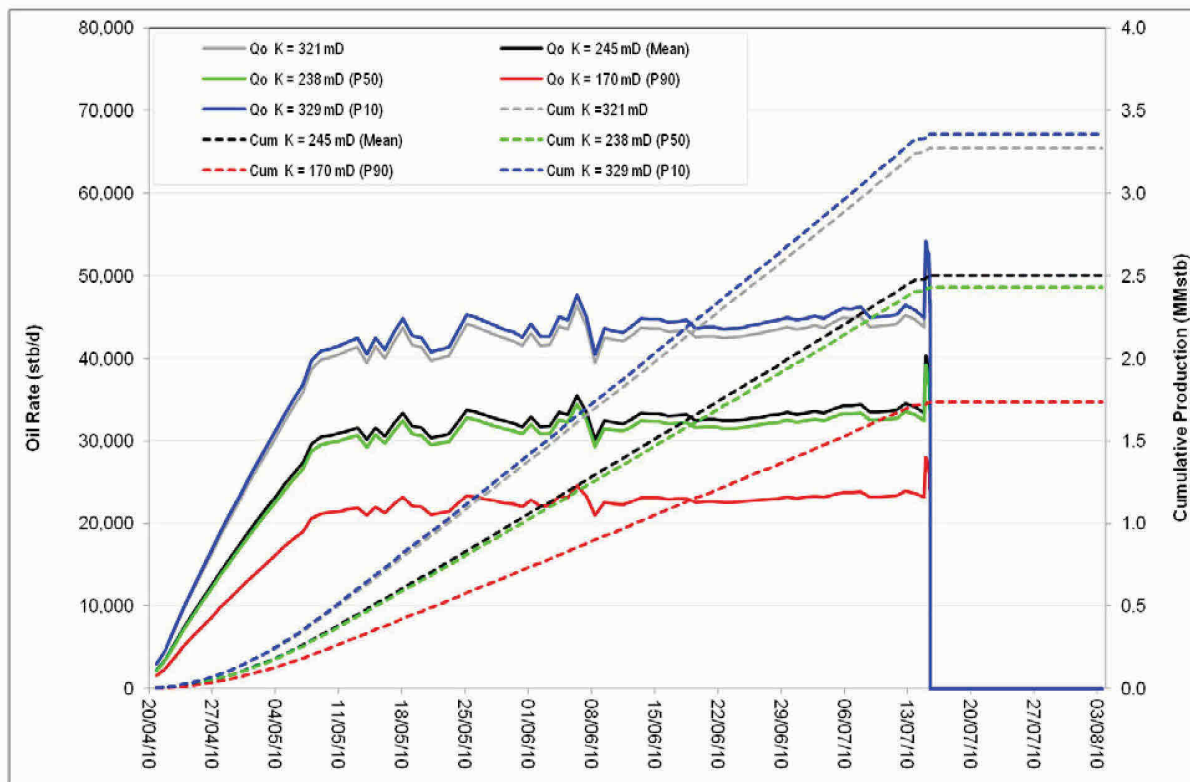
Figure 5.18: Flow rates for Option 2 Drill Pipe Low. The dashed lines represent cumulative flow for their respective permeabilities.

For comparison, I ran the same analysis described above in Sections 5.3-5.6, but I used wellhead pressure instead of bottomhole pressure. I used PT-B pressure data for the pre-shut-in period and PT-3K-2 pressure data for the post-shut-in period. The PT-3K-2 data was adjusted to the depth of the PT-B gauge (4,972 ft. TVDss) as described in Appendix F.

55

Parameters	P 90	P 50	P 10	Mean K	K-333
Initial Pressure @ BOP Depth (4,972 ft TVDss) psia	8,570	8,570	8,570	8,570	8,570
Final Pressure @ BOP Depth (4,972 ft TVDss) psia	7,046	7,046	7,046	7,046	7,046
Depletion (psi)	1,524.00	1,524.00	1,524.00	1,524.00	1,524.00
Reservoir Permeability (mD)	170	238	329	245	333
Skin	21	21	21	21	21
Boundary1 (d1) – ft	1,608	1,902	2,236	1,930	2,250
Boundary2 (d2) – ft	2,133	2,524	2,967	2,560	2,985
Boundary3 (d3) – ft	1,901	2,249	2,644	2,282	2,660
Boundary4 (d4) - ft	10,496	12,419	14,601	12,600	14,690
Reservoir Width - ft	3,509	4,151	4,880	4,212	4,910
Reservoir Length - ft	12,629	14,943	17,568	15,160	17,675
Area (MM ft^2)	44.3	62.0	85.7	63.9	86.8
Area (Acres)	1,017	1,424	1,968	1,466	1,992
STOIIP (MMstb)	60	84	117	87	118
Cumulative Production (MMstb)	1.94	2.71	3.75	2.79	3.80

Figure 5.19: Analysis results of Wellhead Pressure
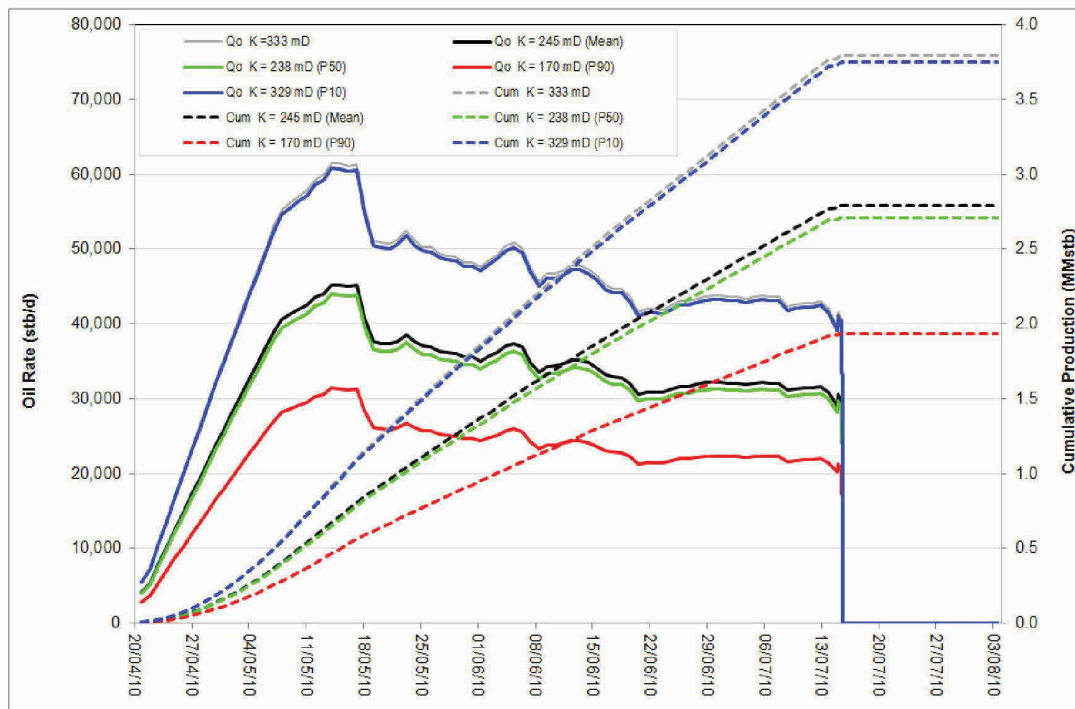
Figure 5.20: Flow rates for Wellhead Pressure. The dashed lines represent cumulative flow for their respective permeabilities.

5.6.6 Effect of fluid properties

As stated in Section 5.2, the conversion of PT-3K-2 build-up data to downhole depends on the values of the fluid properties. This is clear in Fig. 5.15, which shows the downhole-converted shut-in pressures calculated with fluid properties from CoreLab, Schlumberger, and Intertek.
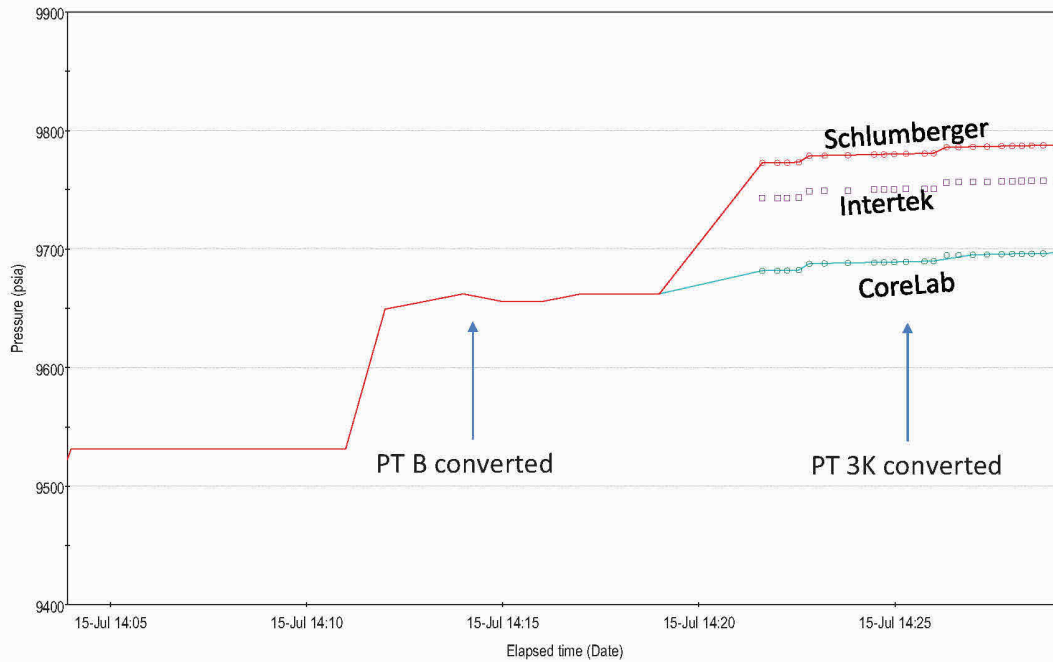
Figure 5.21: Effect of fluid properties on downhole conversion of PT-3K-2 pressure data

The analysis presented so far has been performed with PT-3K-2 data converted using CoreLab fluid properties. Using Schlumberger fluid properties yields slightly different results for the Option 1 Drill Pipe High (Fig. 5.13). Specifically, the reservoir is slightly bigger, but the cumulative production is unchanged at 2.49 MM. The average reservoir pressure is 10,460 psia under this scenario, instead of 10,364 psia (from using CoreLab data), which gives a measure of the uncertainty in the average pressure. As can be seen from Figure 5.21, the CoreLab data correspond to the lowest shut-in pressure, and the Schlumberger data correspond to the highest. Thus, the CoreLab and Schlumberger analysis puts bounds on the final pressure.

TREX-011696R.058

Model
Wellbore Storage and Skin (C and S)
Homogeneous
Rectangle

Results		
(pav)i	11856.000	psia
(pav)f	10466.449	psia
pwf	9662.200	psia
kh	22134	mD.ft
k	238.0	mD
C	0.07000	bbl/psi
S	20.62	
d1	3112.87	ft
d2	1959.27	ft
d3	1153.37	ft
d4	12700	ft
A	6.254E+007	ft2
Type d1	No Flow	
Type d2	No Flow	
Type d3	No Flow	
Type d4	No Flow	
PI	0.5806	B/D/psi
PI-SS	9.410	B/D/psi
FE	0.3791	fraction
Dp(S)	30.81	psi

Figure 5.22: Well test analysis results for Option 1, Drill Pipe High with PT-3K-2 downhole-converted shut-in pressures using Schlumberger fluid properties.

I note that I do not see any evidence of aquifer support within the timeframe of the data available. Aquifer support refers to situations in which bodies of pressurized water next to the reservoir are able to maintain the pressure of the reservoir. I reach this conclusion because deconvolution allows me to see that the reservoir is surrounded by impermeable boundaries. If there were aquifer support, I would expect to see either what is called a constant-pressure boundary (which is easy to see when plotting the pressure derivative) or a change in mobility (which is also easy to see with the pressure derivative). Here we see neither.
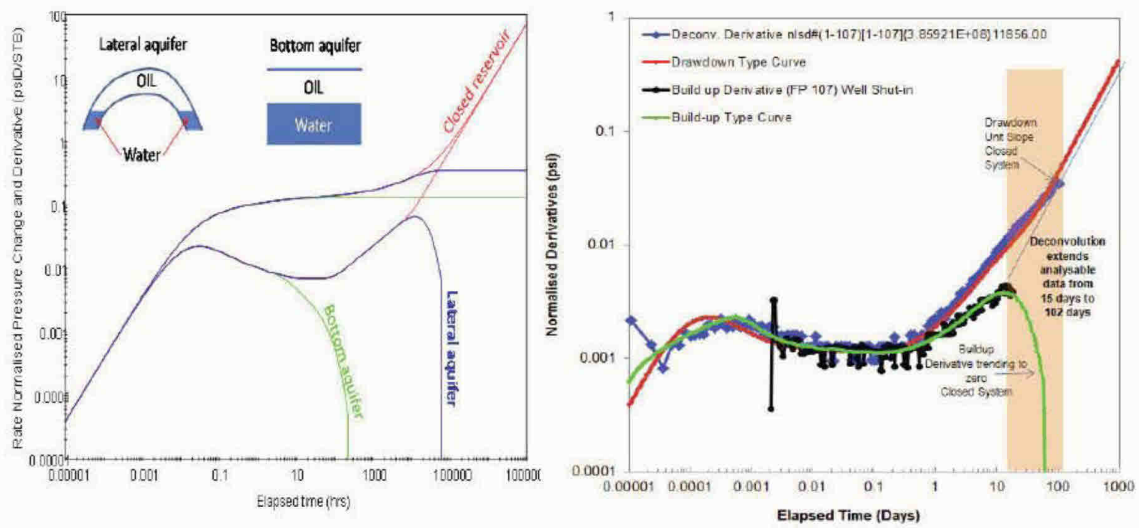
Figure 5.23: The plot on the left depicts derivatives of a reservoir with aquifer support. The red line and boxes on the plot on the right depicts the derivative for Macondo. We can see that the derivative for a reservoir with aquifer support (the blue and red lines on the plot) on the left trend sharply downward. The deconvolved derivative for Macondo, on the other hand, continues on an upwards trend from an elapsed time of 0.1 days on, which indicates a closed reservoir as depicted by the red line on the plot on the left.

60

6. Critique of Government Expert Reports

6.1 The Pooladi-Darvish report

Dr. Pooladi-Darvish has used an analytical solution and a numerical model to match the shut-in pressure converted to downhole conditions. He has run his model with different sets of assumed parameters. He claims the models matched the pressure response at the capping stack after choke closure with an average error of less than 0.1% and predicted the volumes of oil collected within 25%. These "good match" models have a cumulative volume of oil released of between 5 and 5.3 MMstb.

Dr. Pooladi-Darvish's approach was to select a model, set parameters arbitrarily, and force a match on the data. This wrong approach is also used by Dr. Hsieh. The approach is unreliable, as it is possible to achieve a good match with the data with a completely wrong model. In addition, most of his permeability values are outside the range of available rock sample measurements, and definitely, outside the values deemed possible from MDT well test interpretation.

6.2 The Kelkar-Raghavan Report

The authors use old methods to calculate the reservoir pressure (Muskat, (1937); Larson, (1963)). These methods were developed before modern well-test analysis techniques were developed and before powerful personal computers became available to use them. Consequently, the authors had to make simplifying assumptions and use approximations. Even the method by Kuchuk, (1999) is an approximation.

The proper approach is again by obtaining an interpretation model. The final average reservoir pressure is obtained by simulating a build up of infinite duration. Kelkar-Raghavan show a derivative, which seems to indicate they have done well-test analysis. Their derivative, however, is incorrect as can be seen from Fig. 6.1 below. This figure compares my derivative with theirs. Their derivative does not show the radial flow stabilisation, and there is definitely something wrong with their pressure.

Although Kelkar and Raghavan imply they have done a build-up analysis—which should yield a value for permability—they still use BP's estimate of 300 mD for the permeability. According to my study, this is not the correct value.
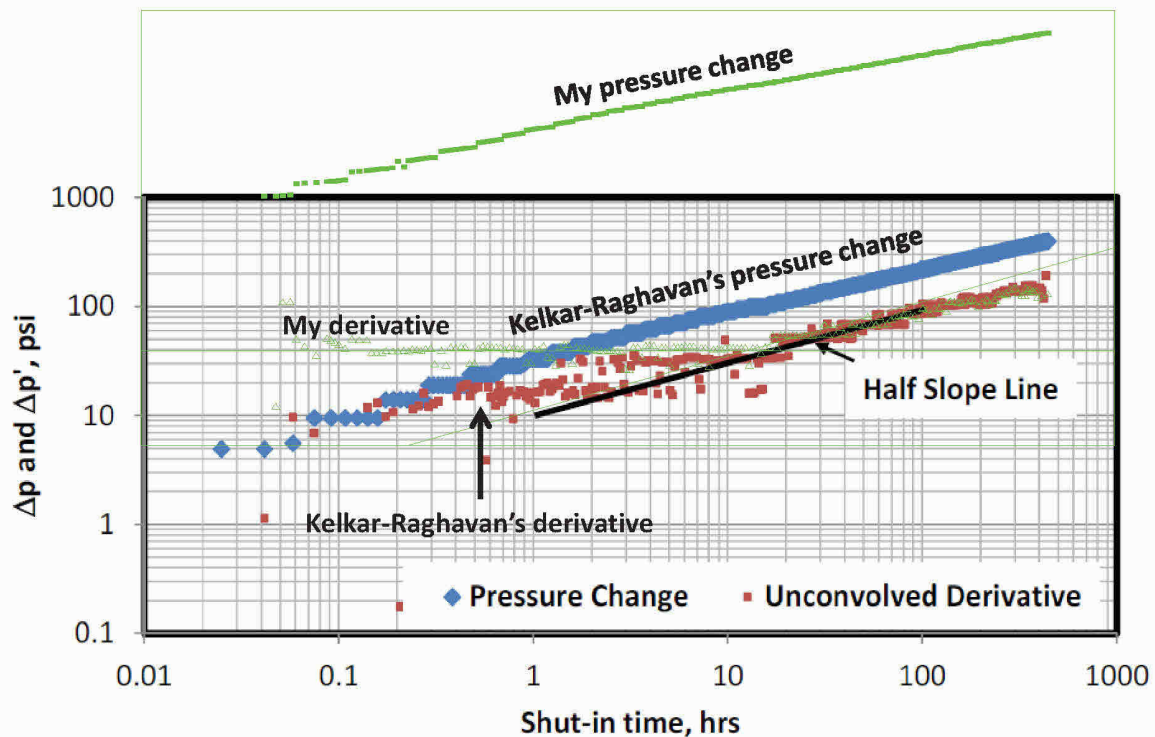
Figure 6.1: Comparison between Kelkar-Raghavan's derivative plot and mine.

Conclusion

Based on the analysis I have conducted and described in this report and the accompanying appendices, I estimate 2.4 to 3 MMstb of total oil volume flowed from the Macondo reservoir during the spill. That range does not subtract any oil that was, for example, collected before entering the Gulf of Mexico.

This report contains all my analysis, my conclusions and the reasons for them. The opinions that I have expressed are based on my review of the documents referred to in this report,[35] in the light of my education and experience.[36] I may do further analysis to supplement my findings after receiving any subsequent government expert reports or other relevant information. I am receiving £280 per hour for my work on this case, though I understand that the contracting agency of my university, by whom I am paid, receives £350 per hour.[37]

---

[35] A complete bibliographic list of the documents referred to in forming my opinion is provided in Appendix H.

[36] My CV and publication list is provided in Appendix G.

[37] I have not testified as an expert witness at trial or deposition over the past four years.

TREX-011696R.062

Alain C. Guiganter

APPENDIX A

1 FLUID DATA ANALYSIS

1.1 Introduction and Data Sources

This Appendix provides details of the analysis of fluid properties for the Macondo MDT and Capping Stack well test analysis.

I have relied on data directly provided from fluid tables (ECL Black Oil Tables - T=243F-SSF-ALL.xls) generated from tuned fluid models (EoS). The EoS models were tuned to 4 sets of experimental data provided by the following independent service laboratories: Core Labs (2 data sets), Schlumberger (1 data set) and Intertek (1 data set). The data provided were all quality checked to ensure the trends of the fluid properties as a function of pressure are consistent with what is normally observed for similar petroleum fluids. By using a standard reservoir engineering equation (Eq. 1), the oil compressibility is determined as a function of pressure.

Equation 1

$$C_o = \frac{B_o - B_{oi}}{B_{oi} \Delta p}$$

1.1.1 Macondo Fluid Properties at Initial and Final Reservoir Conditions

Tables 1 and 2 show the average and minimum to maximum range of the Macondo fluid properties both at initial and final reservoir conditions respectively. The corresponding plots are shown in Figures 1 to 4.

Reference Av. Property Values	Pressure, psia	Oil Formation Volume Factor, RB/STB	Solution Gas-Oil Ratio, Mscf/STB	Oil Viscosity, cp	Oil Compressibility, psi
Initial Reservoir Pressure	11856	2.316	2.850	0.243	1.321E-05
Final Reservoir Pressure	10400	2.366	2.850	0.212	1.462E-05

Table 1: Macondo Average Fluid Properties at Initial and Final Reservoir Conditions

Reference Av. Property Values	Pressure, psia	Oil Formation Volume Factor, RB/STB		Solution Gas-Oil Ratio, Mscf/STB		Oil Viscosity, cp		Oil Compressibility, psi	
		min	max	min	max	min	max	min	max
Initial Reservoir Pressure	11856	2.240	2.396	2.744	2.952	0.236	0.249	1.28E-05	1.36E-05

1

Final Reservoir Pressure	10400	2.284	2.450	2.744	2.952	0.205	0.218	1.41E-05	1.51E-05

Table 2: Minimum and Maximum Range of Macondo Fluid Properties at Initial and Final Reservoir Conditions
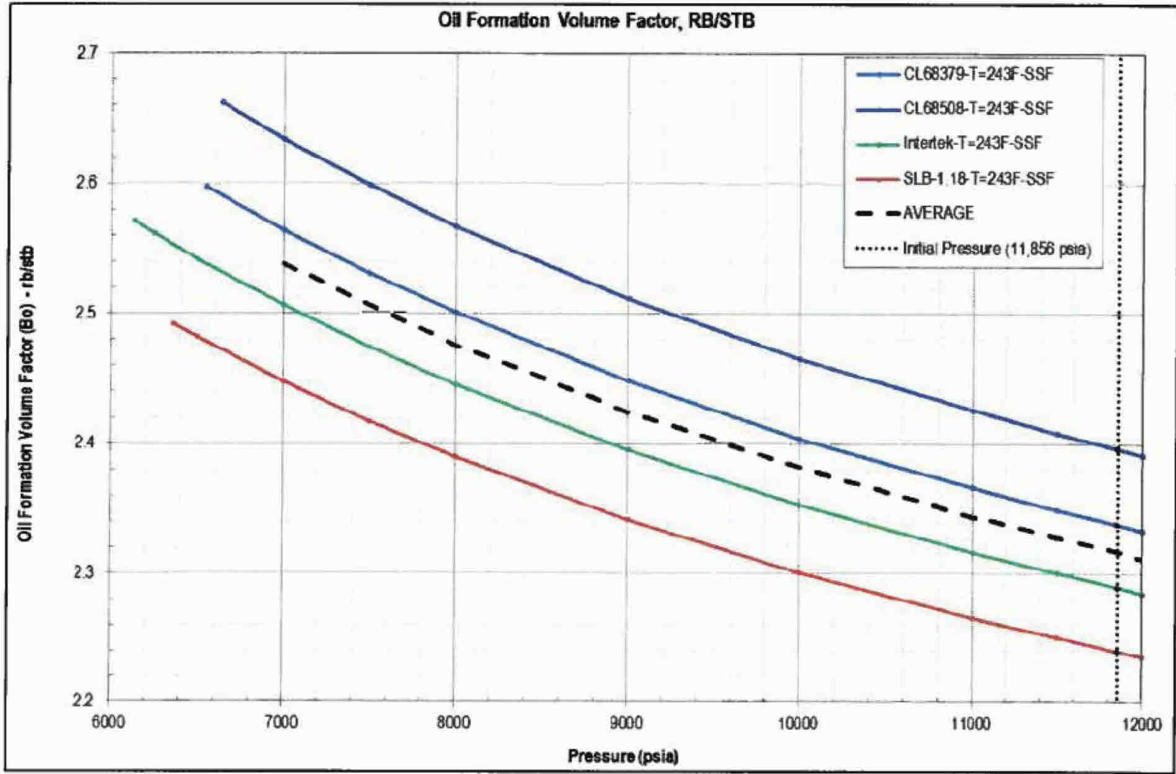
Figure 1: Macondo Oil Formation Volume Factor (B_o)

2
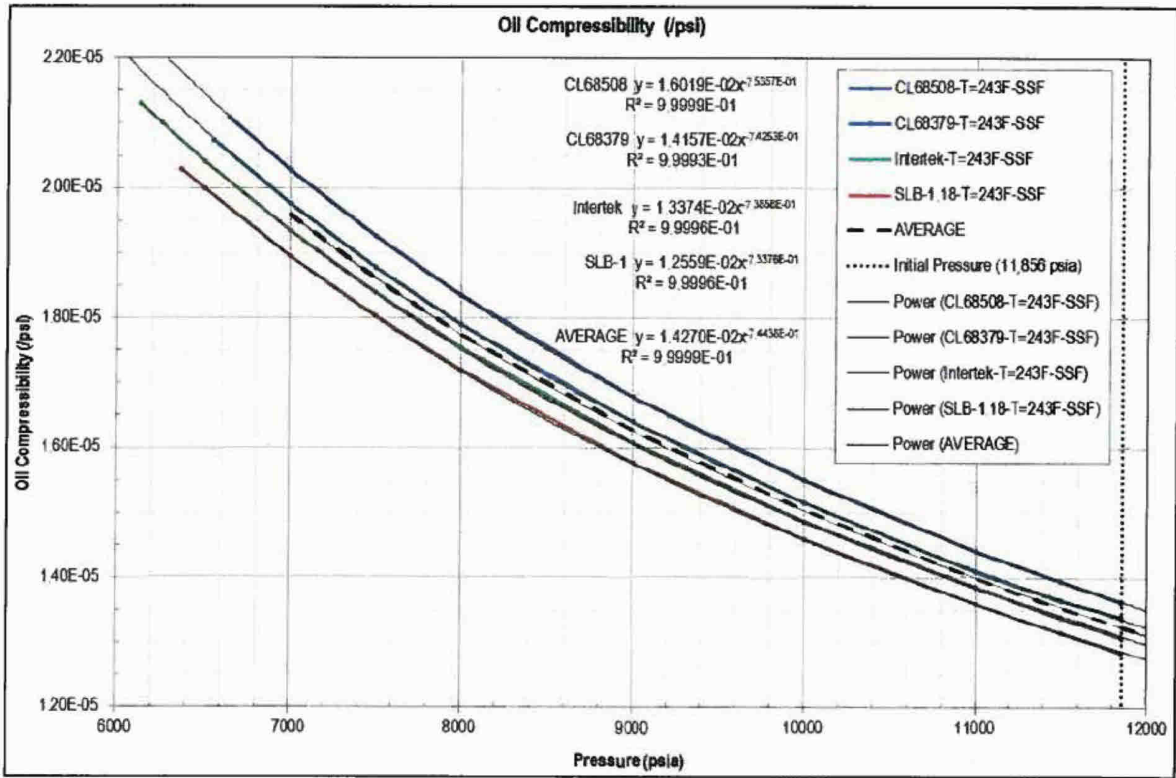
Figure 2: Macondo Oil Compressibility (C_o)
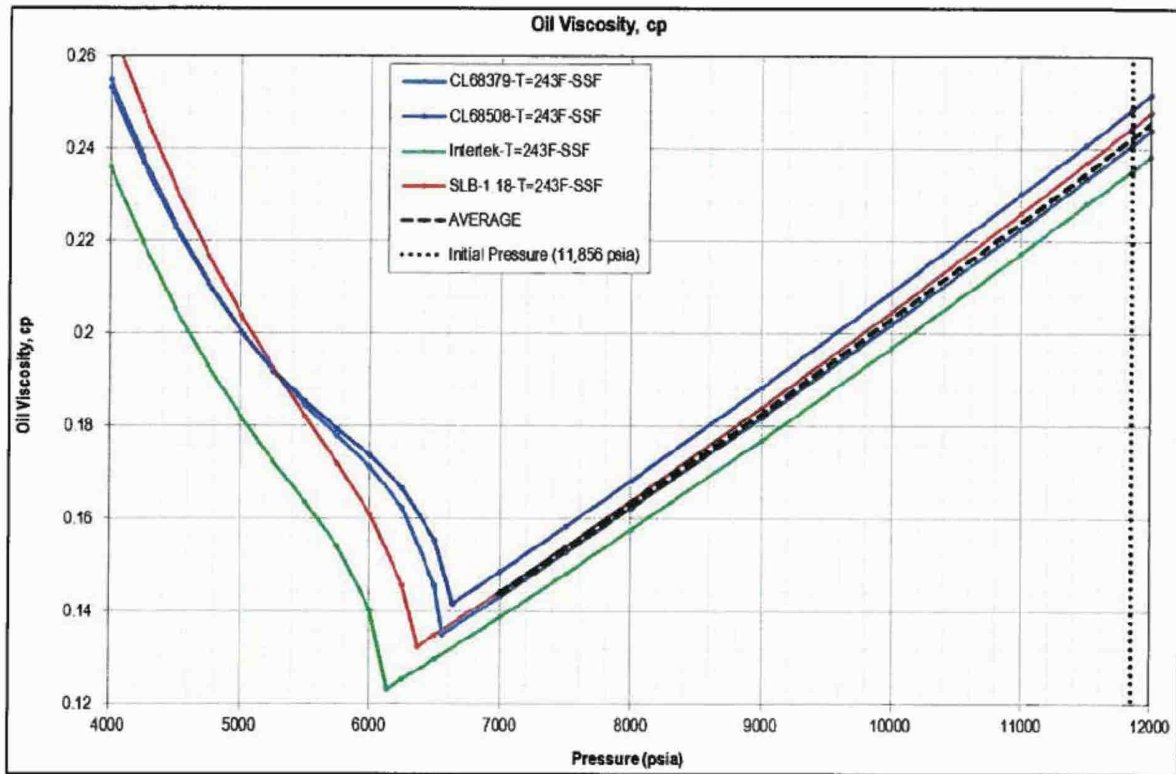
Figure 3: Macondo Oil Viscosity (μ_o)

3
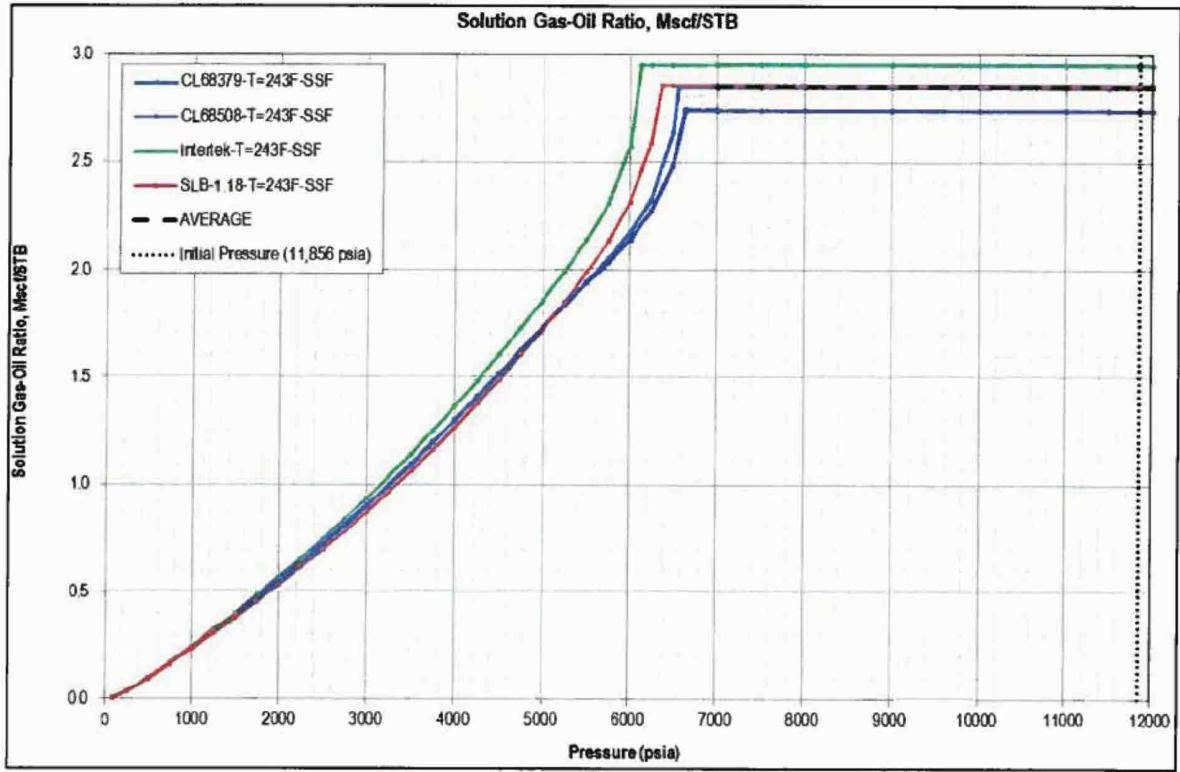
Figure 4: Macondo Solution Gas-Oil Ratio (Rs)

4

APPENDIX B

DETERMINATION OF TOTAL COMPRESSIBILITY

The total compressibility is for the Macondo system (reservoir and fluids) is defined as:

$$C_t = S_o x C_o + S_w x C_w + C_f \qquad \text{Equation 1}$$

Where C denotes compressibility and the subscripts o, w and f are oil, water and formation

The distances to boundaries (and hence the volume) computed from well test analysis are very dependent on the Total Compressibility (C_t) of the Macondo system. For example, to estimate the distance (d) to al linear discontinuity (e.g. edge of the channel or fault), we can use the intersection time (t_x) of two straight lines on the Horner plot[1] or the midpoint of the transition from radial flow stabilisation to the fault stabilisation on the derivative plot and calculate the distance as:

$$d = 0.01217 \left(\frac{kt_x}{\mu c_t}\right)^{-0.5} \qquad \text{Equation 2}$$

B.1   Total Compressibility Calculations

B.1.1   **Macondo Fluid Saturations.** The average net pay water saturation (S_w) based on the BP post drill petrophysical analysis are:

- M56D: S_w is 0.172, which gives an oil saturation ($S_o=1-S_w$) of 0.828
- M56E: S_w is 0.097, which gives an oil saturation ($S_o=1-S_w$) of 0.903
- M56F: S_w is 0.219, which gives an oil saturation ($S_o=1-S_w$) of 0.781

B.1.2   **Macondo Water Compressibility (Initial Conditions – 11,856 psia): 2.78 microsips.** The BP post drill petrophysical analysis assumed a formation water resistivity (Rw) of 0.021 Ohmm at bottom hole temperature (243 degF), which translates to a total dissolved solids of 1.2% in weight. From Figure 1 above the formation water compressibility at reservoir conditions is 2.8×10^{-6} /psi (or 2.8 microsips).
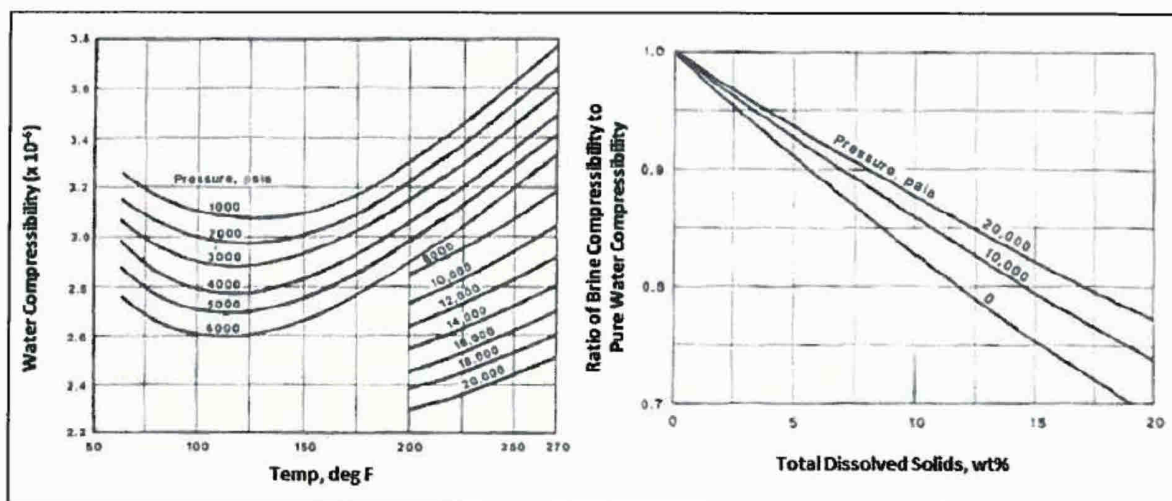
Figure 1: Water Compressibility Charts[2]

1

*B.1.3 **Macondo Oil Compressibility (Initial Conditions): 13.2 microsips.** Based on the review of the fluid properties tables (ECL Black Oil Tables - T=243F-SSF-ALL.xls) from the generated tuned fluid models (EoS), the oil average oil compressibility at reservoir condition for the various reservoirs are shown in Table 1.*

Formation	Depth	Pressure	Average	Minimum	Maximum
	(ft. MD)	(psia)	microsips		
M56D (All)	11,086	11,841	13.22	12.86	13.59
M56E (Upper)	18,124	11,850	13.22	12.85	13.58
M56E (Lower)	18,142	11,856	13.21	12.84	13.58

Table 2: Macondo Oil Compressibilites at Initial Reservoir Conditions

B.1.4 Macondo Formation Compressibility: 6.35 microsips. The mean value of 6.35 microsips is calculated[3] based on the average of the pore volume (formation) compressibilites from three samples obtained by Weatherford[4]. The calculated formation compressibilites from samples 3-16R, 3-22R and 3-6R are 4.34, 6.14 and 8.57 microsips respectively. The determined[5] range of formation compressibilites is 4.34 – 8.57 microsips.

B.1.5 Macondo Total Compressibilites at Initial Conditions: (M56D 17.8; M56E 18.6microsips).

Formation	Sw	Cw (e-6 /psi)	So	Co (e-6 /psi)	Cf (e-6 /psi)	**Ct (e-6 /psi)**
	fraction	microsips	fraction	microsips	microsips	**microsips**
M56D	0.172	2.8	0.828	13.2	6.35	17.8
M56E	0.097	2.8	0.903	13.2	6.35	18.6

Table 1: Macondo Total Compressibilites at Initial Reservoir Conditions

B.2 Uncertainty Range & Analysis for Macondo Total Compressibility

Monte Carlo simulation using Oracle's Crystal Ball was used to quantify the uncertainty in Macondo's total fluid compressibility. Monte Carlo simulation is a computerized mathematical technique that allows people to account for uncertainty in quantitative analysis. The technique is used by professionals in many industries, including the oil and gas industry. Monte Carlo simulation performs risk or uncertainty analysis by building models of possible results by substituting a range of values (a probability distribution) for any factor that has inherent uncertainty. It then calculates results over and over, each time using a different set of random values from the probability functions. Monte Carlo simulation produces distributions of possible outcome values.

A 'triangular' distribution was used to define the probability distribution of the fluid saturations and compressibilites. A triangular distribution is defined by minimum, most likely, and maximum values and values around the most likely are more likely to occur.

B.2.1 Total Compressibility at Initial Conditions

Table 3 shows the input parameter ranges and distributions for the Macondo total compressibility (at initial reservoir conditions) uncertainty analysis based on 2000 Monte Carlo calculations.

Property	Distribution	Comments	M56D			M56E		
			Min	Most Likely (ML)	Max	Min	Most Likely (ML)	Max
Water Saturation S_w (fraction)	Triangular	ML -/+ 0.3	0.142	0.172	0.202	0.067	0.097	0.127
Water Compressibility C_w (microsips)		Correlations*	2.37	2.78	3.25	2.37	2.78	3.25
Oil Saturation S_o (fraction)		ML -/+ 0.3	0.798	0.828	0.858	0.873	0.903	0.933
Oil Compressibility C_o (microsips)		BO Tables**	12.86	13.22	13.59	12.84	13.22	13.58
Formation Compressibility C_f (microsips)		Ref 4,5***	4.34	6.35	8.57	4.34	6.35	8.57

* Minimum determined from Osif Correlation (Kappa PVT Converter)

* ML Based on McCain1 correlation

* Maximum determined from Constant Correlation (Kappa PVT Converter)

** Min and Max Based on BO tables, ML based on Average of BO tables

*** Based on Weatherford Core and Independent Calculations

Table 3: Parameter ranges and distributions for the Macondo total compressibility uncertainty analysis (initial conditions)

The triangular distributions for the M56D oil compressibility and oil saturation are shown for illustration in Figure 2. The range of total compressibilites and percentiles based on 2000 Monte Carlo calculations are shown in Figure 3 and Table 4.
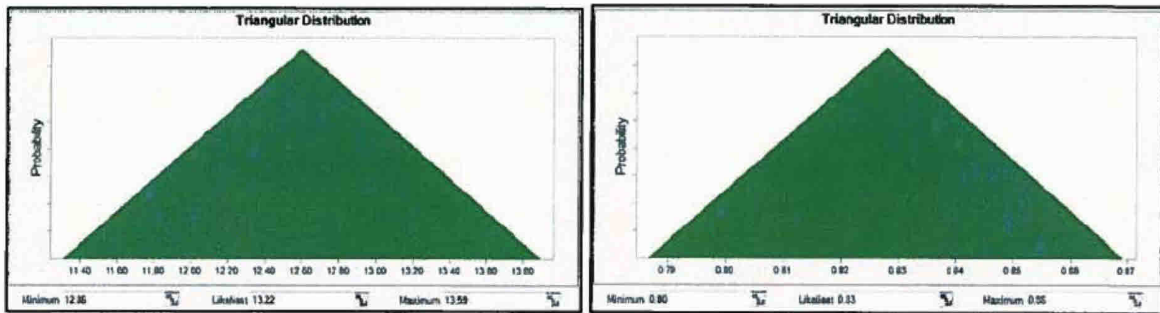
Figure 2: Triangular Distribution for M56D Oil Compressibility and Saturation.

3
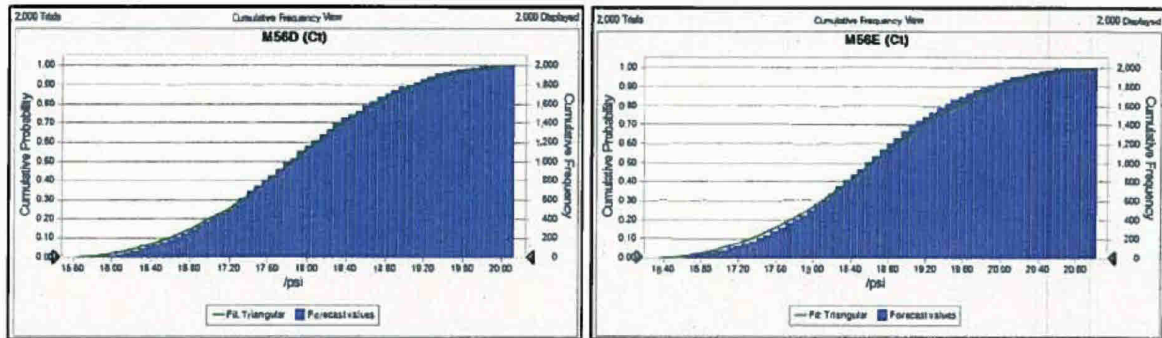
Figure 3: Cumulative Probability Density Function for the M56D and M56E Total Compressibilites (Initial Conditions)

Percentiles	M56D (Ct)	M56E (Ct)
P 100	15.59	16.31
P 90	16.66	17.45
P 80	17.06	17.84
P 70	17.35	18.13
P 60	17.60	18.37
P 50	**17.84**	**18.62**
P 40	18.09	18.84
P 30	18.35	19.10
P 20	18.68	19.43
P 10	19.07	19.87
P 0	20.13	21.02
Statistics	**M56D (Ct)**	**M56E (Ct)**
Trials	2000	2000
Minimum	15.59	16.31
Maximum	20.13	21.02
Mean	17.86	18.63
Median	17.85	18.62
Mean Std. Error	0.02	0.02

Table 4: Total compressibility uncertainty range (percentiles) and statistics (Initial Conditions)

4

1. Gray, K. E: Approximating Well-to Fault Distance From Pressure Build-up Tests, J. Pet. Tech, 761-67 (July 1965).
2. William D. McCain, The Properties of Petroleum Fluids, 2nd Edition tn870.5.m386, 453-54 (1989).
3. R. Zimmerman Expert Report
4. Weatherford Measurements
5. R. Zimmerman Expert Report

APPENDIX C

Definition and computation of the pressure derivative

The derivative of the pressure is defined as:

$$\Delta p'(\Delta t) = \frac{dp(\Delta t)}{dS(\Delta t)}$$ (A-1)

In the case of a multirate test, where $S(\Delta t)$ is the superposition function:

$$S(\Delta t) = \sum_{i=1}^{n-1} \frac{q_i - q_{i-1}}{q_{n-1} - q_n} \ln\left(\sum_{j=i}^{n-1} \Delta t_j + \Delta t\right) - \ln(\Delta t)$$ (A-2)

In Eq. A-1, q_i represent the ith rate in the multirate test, which has a duration Δt_i. In Fig. 3.3 for instance, odd values of i correspond to drawdowns, whereas even values of i correspond to build ups. n is the total number of periods with different rates up to and including the period being analysed. It is equal to 18 in Fig. 3.3 and q_{18} is equal to zero.

Eq. A-2 is used instead of the simpler definition:

$$\Delta p'(\Delta t) = \frac{dp(\Delta t)}{d \ln \Delta t}$$ (A-3)

which is only valid for the very first drawdown in a reservoir. If Eq. A-3 is used in a multirate test, the resulting derivative is sensitive to the production time and may not exhibit a stabilization during radial flow even if radial flow has developed.

The derivative is calculated, not measured, and is therefore affected by the algorithm used for the derivation. The most common algorithm used in commercial software is based on a moving window, as illustrated in Fig. A-1:
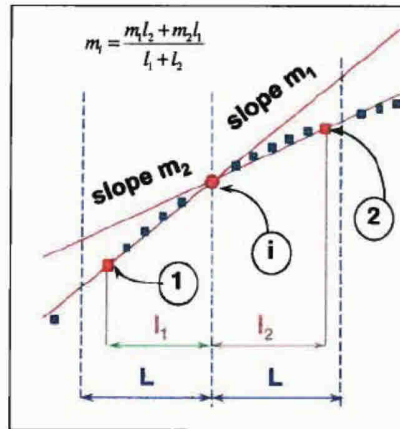
Time function

Figure A-1: Calculation of the derivative with a moving window. The derivative is the slope of a set of discrete points. To calculate the derivative at point i, a window of size L is selected on each side of point i. The last points of the set in each window are 1 and 2, at time distances from i equal to l_1 and l_2, respectively. The straight lines between 1 and i, and 2 and i have slopes m_1 and m_2. The slope is given by the formula in the figure. A noisy derivative can be smoothed by increasing L.

The derivative also depends on the pressure gauge resolution, and on the rate history as indicated in Eq. A-2.

APPENDIX D

DECONVOLUTION REFERENCES

Deconvolution transforms variable rate pressure data into a constant rate initial drawdown with the duration equal to the total duration of the test and yields directly the corresponding pressure derivative, normalised to a unit rate. Deconvolution provides additional information on the pressure transient, which cannot be obtained from conventional analysis, such as information over a greater radius of investigation and the adapted (corrected) rates. These corrected rates based on the available pressure history have become a very useful tool when rates are not correctly measured, reported inaccurately or are unavailable.

The deconvolution problem is based on Duhamel's principle:

$$p(t) - p_0 = \Delta p(t) = \int_0^T q(t - \tau) \frac{dp_u(\tau)}{dt} d\tau \qquad \text{Equation 1}$$

Where q(t) is the instantaneous flow rate in the well, p(t) is the bottomhole pressure, p_0 is the initial reservoir pressure and $p_u(\tau)$ is the pressure response to a constant unit production rate after stabilisation. It assumes that the reservoir is initially in equilibrium with a uniform pressure. Several authors (Hutchinson and Sikora, 1958; Jargon and van Poollen, 1965; Roumboutsos and Stewart, 1988; Thompson and Reynolds, 1986; Mendes et al. 1989; Kuchuck *et al.* 1990; Gilly and Horne, 1999; Levitan, 2003; Amudo et al. 2006) have proposed different spectral and time-domain techniques to the convolution integral (Eq. 1) in the literature. However, these solution algorithms proved to be unstable and could not tolerate errors normally present in actual well test data. von Schroeter *et al.* (2001) developed a new formulation "Nonlinear Total Least Squares" in terms of the logarithm of the response function, which does not require explicit sign constraints and incorporates an error model which accounts for errors in pressure and rate data. The authors solved Equation 1 for a new solution variable, $z(\sigma)$, instead of the constant rate pressure $p_u(\tau)$:

$$z(\sigma) = \ln\left(\frac{d\Delta p}{d(\ln \tau)}\right) = \ln\left(\tau \frac{dp_u(\tau)}{d\tau}\right) \qquad \text{Equation 2}$$

$\sigma = \ln(\tau)$.

In addition, a user defined regularisation parameter was introduced by von Schroeter *et al.* that imposes just enough smoothness to eliminate small-scale oscillations while preserving genuine reservoir features. This method was tested by von Schroeter *et al.* (2002) and Levitan (2005) on simulated pressure and rate data with different levels of noise, as well as by Gringarten *et al.* (2003) and Gringarten (2005) on actual data from different fields. In 2005, a deconvolution software (TLSD) was developed at Imperial College by von Schroeter and Gringarten that implemented their new algorithms.

Levitan et al. (2004) discussed specific issues to be aware of when deconvolving pressure and rate data. They provided practical considerations and recommendations on how to produce correct deconvolution results. The reliability of deconvolution was underlined by applying deconvolution to several simulated and real sets of oil and gas pressure and rate data. They concluded that deconvolution is a very useful tool for well test analysis but should not be a replacement of conventional well test techniques.

References

1

1. Aluko, O. A. and Gringarten, A.C. 2009: "Well Test Dynamics of Rich Gas Condensate Reservoirs under Gas Injection," Paper 121848 presented at 2009 SPE EUROPEC/EAGE Annual Conference and Exhibition held in Amsterdam, The Netherlands, 8-11 June.
2. Amudo C., Turner, J., Frewin J.; Kgogo, T., and Gringarten A. C., 2006:"Integration of Well Test Deconvolution Analysis and Detailed Reservoir Modelling in 3D Seismic Data Interpretation: A Case Study," paper SPE 100250 presented at the SPE Europec/EAGE Annual Conference and Exhibition, Vienna, Austria, 12–15 June
3. Bozorgzadeh, M. and Gringarten, A.C. 2005: "Application of Build-up Transient Pressure Analysis to Well deliverability Forecasting in Gas Condensate Reservoirs Using Single-Phase and Two Phase Pseudo-pressure," Paper SPE 94018, presented at the 14th SPE Europec Technical Conference and Exhibition held in Madrid, Spain, 13-16 June; "Estimating Productivity-Controlling Parameters in Gas/Condensate Wells From Transient Pressure Data", *SPEREE* (APR. 2007) 100-111.
4. Bozorgzadeh, M. and Gringarten, A.C. 2006. Condensate-Bank Characterization from Well-Test Data and Fluid PVT Properties. *SPEREE* 9 (5): 596-611
5. Gringarten, A.C., Ogunrewo, O. and Uxukbayev, G. 2011: "Assessment of Rate-Dependent Skin Factors in Gas Condensate and Volatile Oil Wells, SPE 143592, presented at SPE EUROPEC/EAGE Annual Conference Vienna, Austria, 23-26 May 2011
6. Gringarten, A.C.: "Practical use of well test deconvolution", SPE paper 134534, September 2010
7. Gringarten A. C., 2006:" From Straight lines to Deconvolution: the Evolution of the State of the art in Well Test Analysis," paper SPE 102079, presented at the 2006 SPE Annual Technical Conference and Exhibition, San Antonio, Texas, U.S.A., 24–27 September 2006; SPEREE (Feb. 2008) 11-1 pp. 41-62.
8. Gringarten, A. C., Bozorgzadeh, M., Daungkaew, S. and Hashemi, A. 2006:" Well Test Analysis in Lean Gas Condensate Reservoirs: "Theory and Practice," Paper SPE 100993 presented at the 2006 SPE Russian Oil and Gas Technical Conference and Exhibition, Moscow, 3-6 October.
9. Gringarten, A.C., T. von Schroeter, Rolfsvaag, T., Bruner, J. 2003. "Use of Downhole Permanent Pressure Gauge Data to Diagnose Production Problems in a North Sea Horizontal Well", SPE paper 84470, October
10. Gringarten, A.C. 2008. "Additional Well Test Analysis of Well E-M02Pa for PetroSA", Consulting report for PetroSA, May
11. Kuchuck, F.J., Carter, R.G., and Ayestaran, L.: "Deconvolution of Wellbore Pressure and Flow Rate," SPEFE 53, March, 1990.
12. Levitan, M. M., 2003:"Practical Application of Pressure-Rate Deconvolution to Analysis of Real Well Tests", paper SPE 84290, presented at the 2003 SPE Annual Technical Conference and Exhibition, Denver, CO, Oct. 5 – Oct. 8.
13. Levitan, M. M., Crawford, G. E., and Hardwick, A., 2004:" Practical Considerations for Pressure-Rate Deconvolution of Well Test Data," paper SPE 90680 presented at the SPE Annual Technical Conference and Exhibition held in Houston, Texas, U.S.A., 26–29 September.
14. Levitan, M.M. and Wilson, M.R., 2010:" Deconvolution of Pressure and Rate Data From Gas Reservoirs With Significant Pressure Depletion," paper SPE 134261 presented at the 2010 Annual Conference and Exhibition held in Florence, Italy, 19-22 September
15. Mendes, L.C.C., Tygel, M., and Correa, A.C.F.: "A Deconvolution Algorithm for Analysis of Variable Rate Well Test Pressure Data," paper SPE 19815, presented at the SPE ATCE, San Antonio, Texas, 1989.
16. Meunier, D.F., Kabir, C.S., and Wittmann, M.J. 1987:"Gas Well Test Analysis: Use of Normalized Pressure and Time Functions", *SPEFE* 2 (4): 629–636. SPE-13082-PA. DOI: 10.2118/13082-PA.
17. Ogunrewo, O. 2013. "Well test analysis of gas condensate and volatile oil below saturation pressure", an unpublished PhD thesis, Imperial College London.
18. Roumboutsos, A., and Stewart, G.: "A Direct Deconvolution or Convolution Algorithm for Well Test Analysis," paper SPE 18157, presented at the SPE ATCE, Houston, 2-5 October, 1988.
19. Sanni, M. and Gringarten, A.C., 2008: "Well Test Analysis in Volatile Oil Reservoirs," Paper SPE 116239 presented at the 2008 SPE Annual Technical Conference and Exhibition, Denver, 21-24 September.
20. von Schroeter, T., Hollaender, F., and Gringarten, A. C., 2001: "Deconvolution ofWell Test Data as a Nonlinear Total Least Squares Problem," paper SPE 71574 presented at the 2001 SPE Annual Technical Conference and Exhibition, New Orleans, Louisiana, 30 September – 3 October; SPEJ (Dec. 2004) pp. 375-390.
21. Thompson, L. and Reynolds, A.: "Analysis of Variable-Rate Well-Test Pressure Data using Duhamels Principle", Society of Petroleum Engineers Formation Evaluation, (October 1986), pp. 453-469.
22. von Schroeter, T., Hollaender, F., and Gringarten, A. C., 2001: "Deconvolution ofWell Test Data as a Nonlinear Total Least Squares Problem," paper SPE 71574 presented at the 2001 SPE Annual Technical Conference and Exhibition, New Orleans, Louisiana, 30 September – 3 October; SPEJ (Dec. 2004) pp. 375-390.
23. von Schroeter, T., Hollaender, F., Gringarten, A., 2002:"Analysis of Well Test Data From Permanent Downhole Gauges by Deconvolution," paper SPE 77688, presented at the 2002 SPE Annual Technical Conference and Exhibition, San Antonio, TX, Sept. 29 –Oct. 2.
24. Evgeny Pimonov, SPE and Cosan Ayan, SPE, Schlumberger, Mustafa Onur, SPE, Istanbul Technical University and Fikri Kuchuk, SPE, Schlumberger. A New Pressure/Rate-Deconvolution Algorithm to Analyse Wireline Formation-Tester and Well Test data. SPE 123982-PA-P1, August 2010 SPE Reservoir Evaluation and Engineering.

APPENDIX E

1 DETERMINATION OF FORMATION PERMEABILITY FROM WIRELINE FORMATION TESTERS (MDT)

1.1 Introduction to MDT Pretests and Sampling

The Deepwater Horizon incident involved flow of fluids from the Macondo reservoir. The flow rates from the Macondo reservoir can be determined from the reservoir's mobility (k*h/μ). Where k is the reservoir permeability; h is the net thickness of the reservoir and μ is the viscosity of the formation fluid.

$$Mobility = \frac{k*h}{\mu} \qquad \text{Eq. 1.1}$$

The net reservoir thickness (h) in the near wellbore has been determined from downhole petrophysical log analysis and the formation viscosity (μ) from fluid analysis based on downhole samples. The only information available from the Macondo Well for determining the reservoir permeability under downhole and flowing conditions is from the Wireline formation tester (WFT) measurements (pressures and rates) during formation pressure measurements 'pretests' and fluid 'sampling' periods. The Wireline formation tester used for data acquisition in the Macondo well was Schlumberger's Modular Dynamics Formation Tester (MDT). A schematic of a typical Wireline formation tester is shown in Figure 1.
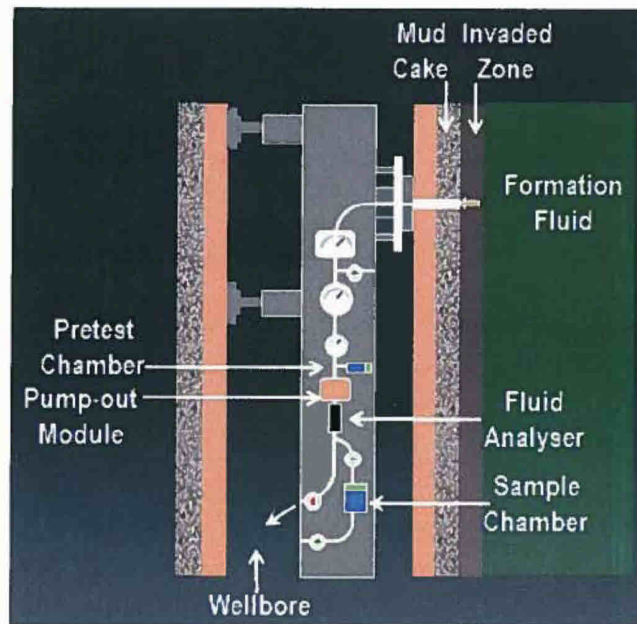
Figure 1: Schematic of a typical Wireline formation tester

A 'pretest' is when formation pressure is obtained by withdrawing a small amount of fluid (typically less than 20 cc) from the formation to generate a short transient test[1]. The response (pressure and rate) is then recorded during shut-in until it stabilises (Figure 2). Pretests are performed at different depths. A total of 33 MDT pretests were taken with 22 good measurements, 3 fair measurements and 8 bad measurements[2].
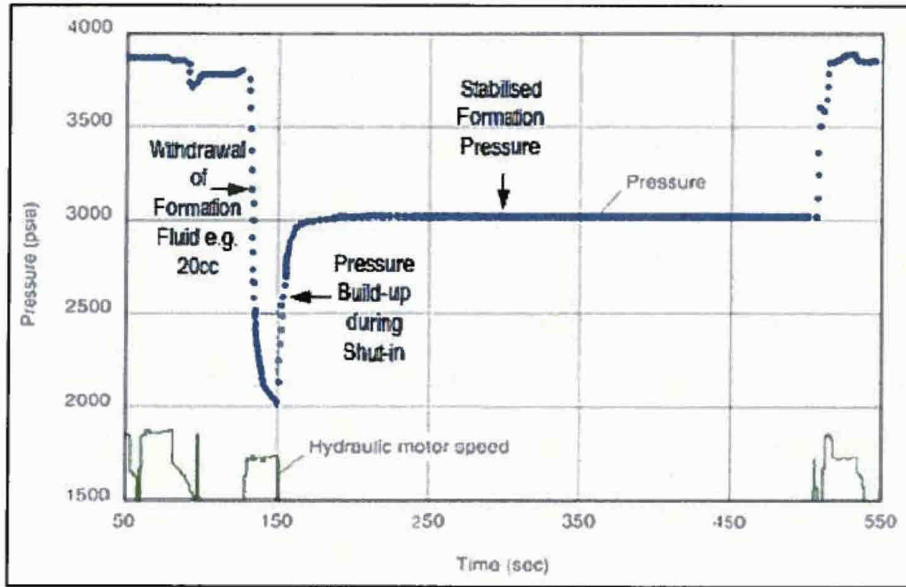
Figure 2: Typical pressure versus time plot of a Pretest

The two main challenges facing the analysis of pretest data from the MDT are:

- Very limited production (<20cc) during a pretest, which limits the depth of investigation.
- The near-wellbore fluid is likely to be predominantly mud filtrate, and its viscosity (required for permeability determination) at reservoir conditions are unknown for the Macondo Well.

However, pressure and rate data are available from the three samplings periods (one sample from the M56D and two samples from the M56E formations) as shown in Figure 3 below.
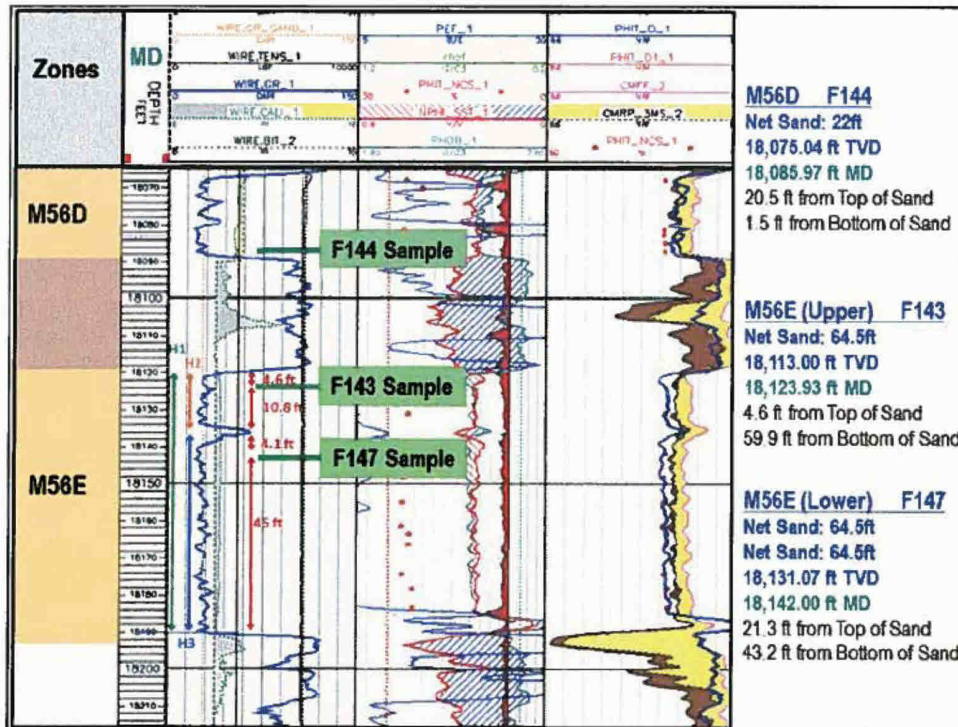
Figure 3: MDT Sample Points

2

The MDT tool has been designed to overcome contamination problems during sampling by use of pump-out and fluid analyser (LFA) modules. The pump-outs allow fluid from the formation to be pumped through the MDT tool string and dumped into the well bore whilst the LFA monitors the fluid passing through the tool string and can distinguish between the invaded fluid (mud filtrate) and the formation fluid (oil). When the LFA detects the fluid flowing through the tool has changed from mud filtrate to predominantly formation fluid, the fluid through the tool is diverted from being dumped into the wellbore and into a sample chamber within the MDT tool string. The pressure within the tool builds up to the formation pressure as the sample chamber is filled. Two pump-outs and LFA modules were connected to the MDT string used in the Macondo Well and readings from these modules were available for well test analysis.

During the transients generated during pretests or sampling, the pressure disturbance propagates spherically (Figure 4) and continues in this manner until one impermeable barrier is reached. At this stage, the spherical flow pattern is altered and becomes hemispherical. Eventually, if a second vertical barrier is detected, the hemispherical flow becomes radial[1]. If a radial flow regime develops, the formations mobility (kh/μ) can be determined using conventional well test analysis methods.
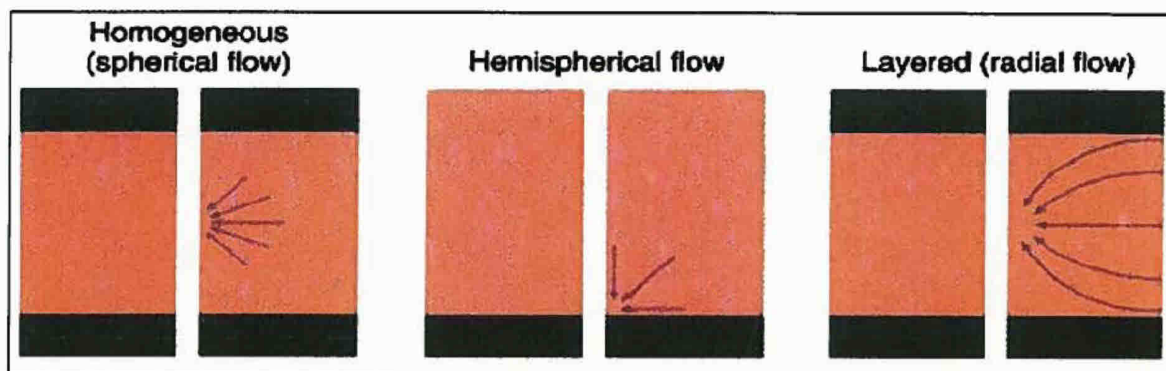
Figure 4: Examples of flow geometries experienced in the vicinity of a Wireline formation tester (Goode et al., 1991)

The sampling duration for the three samples typically lasted 4-6 hours, compared to the pretests that were all less than 5 minutes Applying deconvolution to the multi-rate pressure transient data recorded during the MDT sampling allows for the generation of the pressure derivative that provides significant additional data (about two log cycles) and allows for better understanding, identification and diagnosis of the reservoir features.

1.2 Determination of Formation Permeability from MDT Measurements

Determining permeability using well test analysis requires input parameters about the reservoir, well, completion, MDT tool specifications, measured rates, and measured pressures. Table 1 shows the acronyms for the rate and pressure measurements from the MDT.

Acronym	Description	Units
BRD1	QUARTZDYNE PRES MDT	PSI
PQRD2	PROBE 2 QUARTZDYNE PRES MRPQ	PSI
POTFR	TOTAL FLOW RATE MRPO	C3/S
POFR	FLOW RATE MRPO	C3/S
POCV	CONTINUOUS VOLUME MRPO	C3
POTCV	CONTINUOUS TOTAL CORRECTED VOLUME MRPO	C3
POFR2	FLOW RATE MRPO	C3/S

Table 1: Pressure, Rate and Volume Acronyms for the MDT

3

1.2.1 *Macondo M56D Permeability Determination*

1.2.1.1 M56D – Pressure and Rate Data

Shown in Figure 5 is the rate data from the MDT measured by the pump-out module (MRPO) prior to sample collection. The MPRO reported erroneous rates from about 13.2 to 13.8 hrs which was corrected prior to analysis by using the average rate during the preceding period. This is consistent with the corresponding pressure information. The total production period lasted for about 4.2 hrs. The pressure measurement during the entire sampling process is shown in Figure 6.
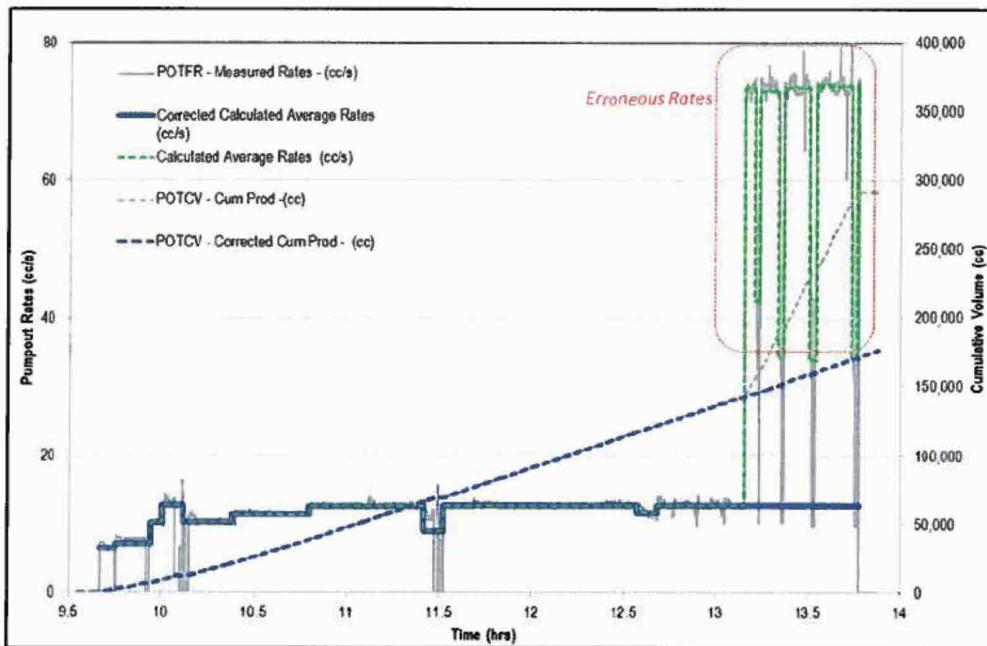
Figure 5: M56D Rate Data from MDT (F144)

4
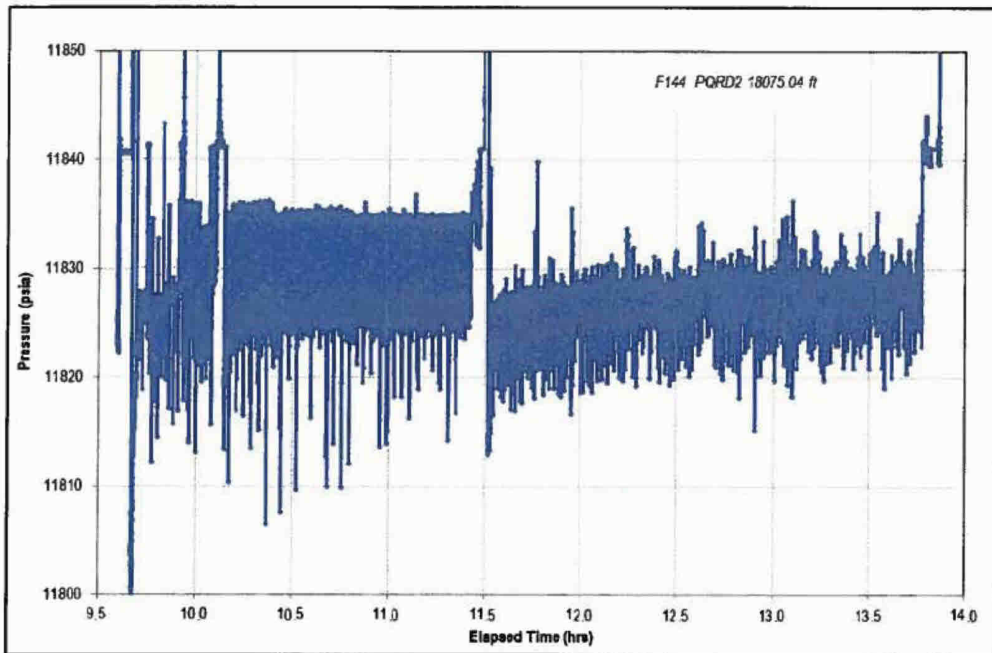
Figure 6: M56D Pressure Data from MDT (F144)

The pressure gauge resolution for the measurement quartz gauge is about 0.02 psi. Shown in Figure 7 is the pressure data during the final build-up. The data appears noisy due to gauge resolution effects. The 0.01 psi jumps in the data are not rapid fluctuations in pressure; they are a limitation of the gauge's ability to measure changes smaller than 0.02 psi. Under the conditions, the actual pressure trend lies between the jumps or along the extremes of the jumps. These two possible pressure trends were extracted from the data and are shown in Figure 7. The 'Main Trend' follows the exact data trend while the 'Average Trend' uses the averages of the data.
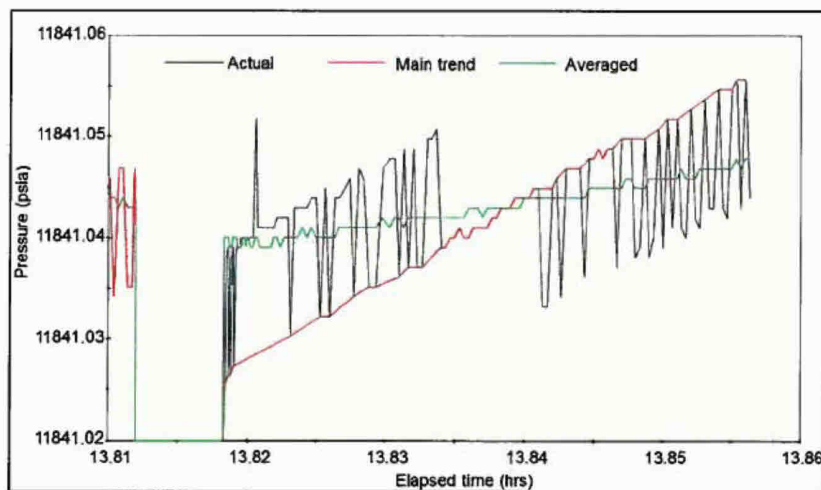
Figure 7: M56D Pressure Comparison for various smoothings of the Final BU (FP175)

1.2.1.2   M56D – Deconvolution

Using deconvolution, the entire production rate history and the final build-up is converted to a unit rate drawdown corresponding to the entire duration of the test. The range of initial pressures (11,841.12 psia

5

TREX-011696R.086

and 11841.24 psia) is used to constrain the deconvolution and generate two unit rate pressure responses (Figure 8). The initial pressures of 11,841.12 psia and 11841.24 psia correspond to the initial pressures based on the well test analysis of the 'average' and 'main' trends respectively.
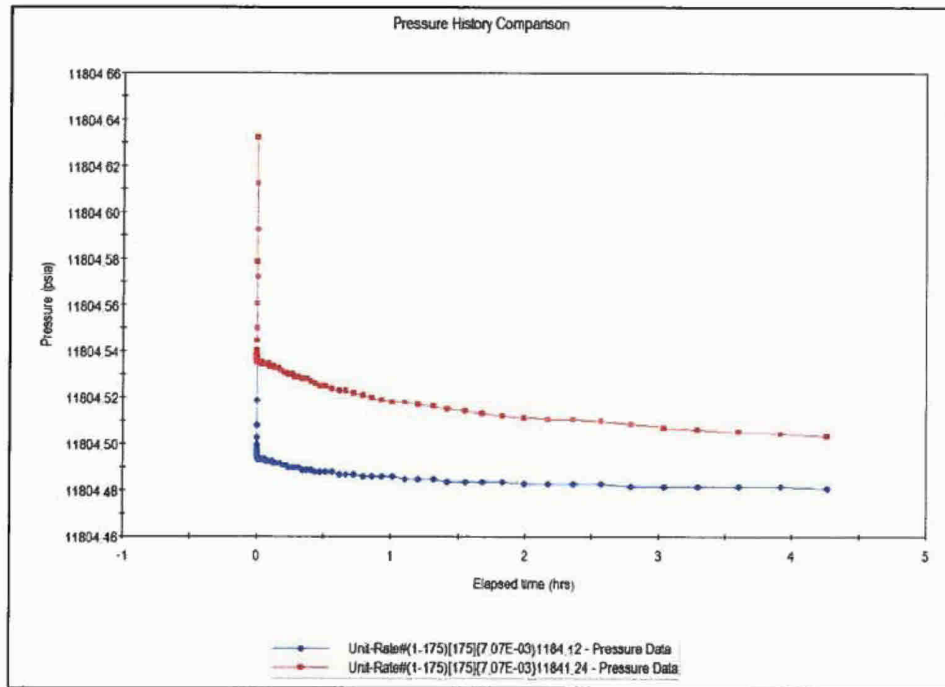
Figure 8: M56D Unit Rate Pressure Responses from Deconvolution

The corresponding deconvolved derivatives corresponding to initial pressures of 11,841.12 psia and 11841.24 psia are compared with the actual build up derivative (Figure 9). The deconvolved derivative extends the analysable data by an additional 2 log cycles i.e. from 0.04 hrs to over 4hrs. The diagnosis of the actual buildup and both deconvolved derivatives indicate two possible radial flow stabilisation levels. The range of radial flow stabilisation levels are considered in the well test interpretation.

6
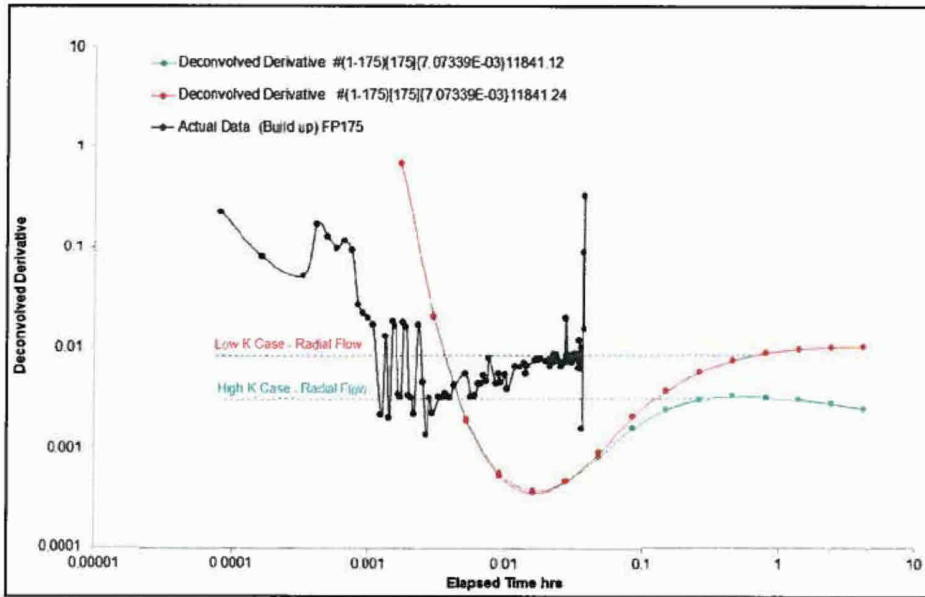
Figure 9: M56D Comparison of Deconvolved Derivative and Actual Buildup Derivative

Figure 10 shows a good pressure match of the convolved pressures from the deconvolved derivative and the actual build up data within the limits of the gauge resolution.
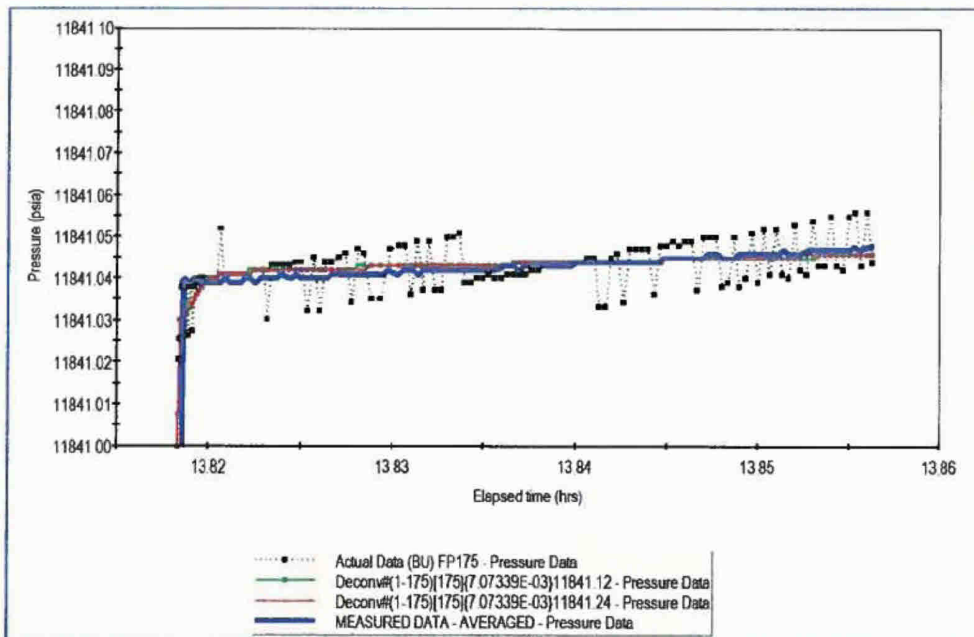
Figure 10: M56D Deconvolution Pressure Match (FP175)

1.2.1.3   M56D – Model Diagnosis and Selection of Interpretation Model

Based on the MDT probe dimensions, the actual build up data and deconvolution analysis, the interpretation model is selected as: Partial Penetration with Wellbore Storage and Skin; Homogenous; and Infinite Acting as shown in Figure 11. Partial Penetration with Wellbore Storage and wellbore storage

7

is selected at early times because only 0.04 ft (probe diameter) is open to flow and wellbore storage effects will occur because of the volume of the flow lines within the MDT tool. A Homogenous reservoir is selected at middle times based on the radial flow stabilisation and no diagnosed heterogeneities. No boundaries are observed at late times during the test duration and so the reservoir is still infinite acting.
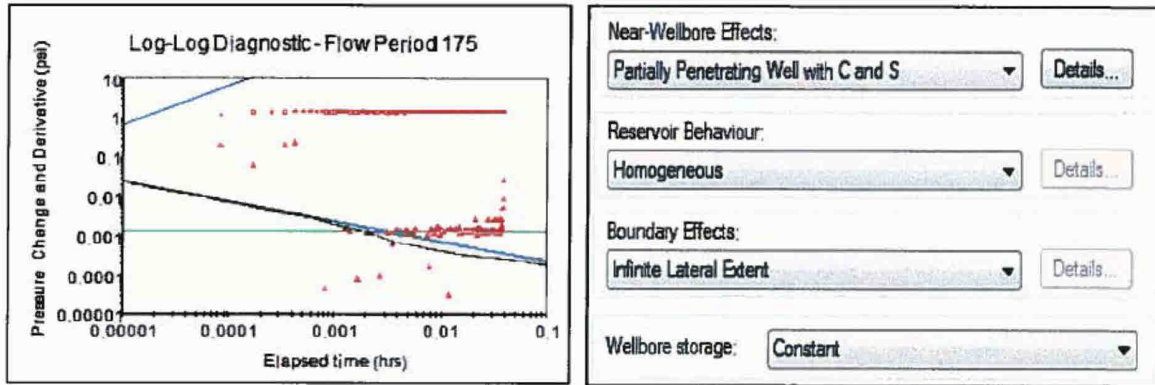
Figure 11: M56D Model Diagnosis and Selection of Interpretation Model

Shown in Table 2 are the input parameters for the M56D analysis.

M56D Sand Thickness: 22ft	Standard Probe Diameter: 0.433 inches	Probe Distance to Base of Sand: 1. 5 ft	Wellbore Radius: 0.412 ft
Oil Viscosity: 0.243 cP	Total Compressibility: 17.8 microsips	Porosity: 0.207	Reservoir Pressure: 11,841 psia

Table 2: M56D Input Parameters for MDT Sampling Well Test Analysis

1.2.1.4 M56D – Main Trend Analysis

The Main Trend data is analysed primarily to determine the reservoir permeability and skin. The model match and analysis results are shown in Figure 12. The green continuous lines show the model match to the actual data (blue points).

Top Left – (Log-Log Match): Shows the match of the interpretation model (green lines) to pressure change data [P(Δt) – P(Δt=0)] during the buildup period (top blue points) and to the pressure derivative data (bottom blue points) on a log-log plot.

Top Right – (Simulation – Variable Skin): This match of the simulated pressure based on the interpretation model using the input rates (with variable skin) with the input pressures

Bottom Left – (Skin vs. Time): This shows the required skin to match the pressure history based on the rates and interpretation model.

Bottom Left – (Horner Match): Shows the model match on the Horner plot.

9
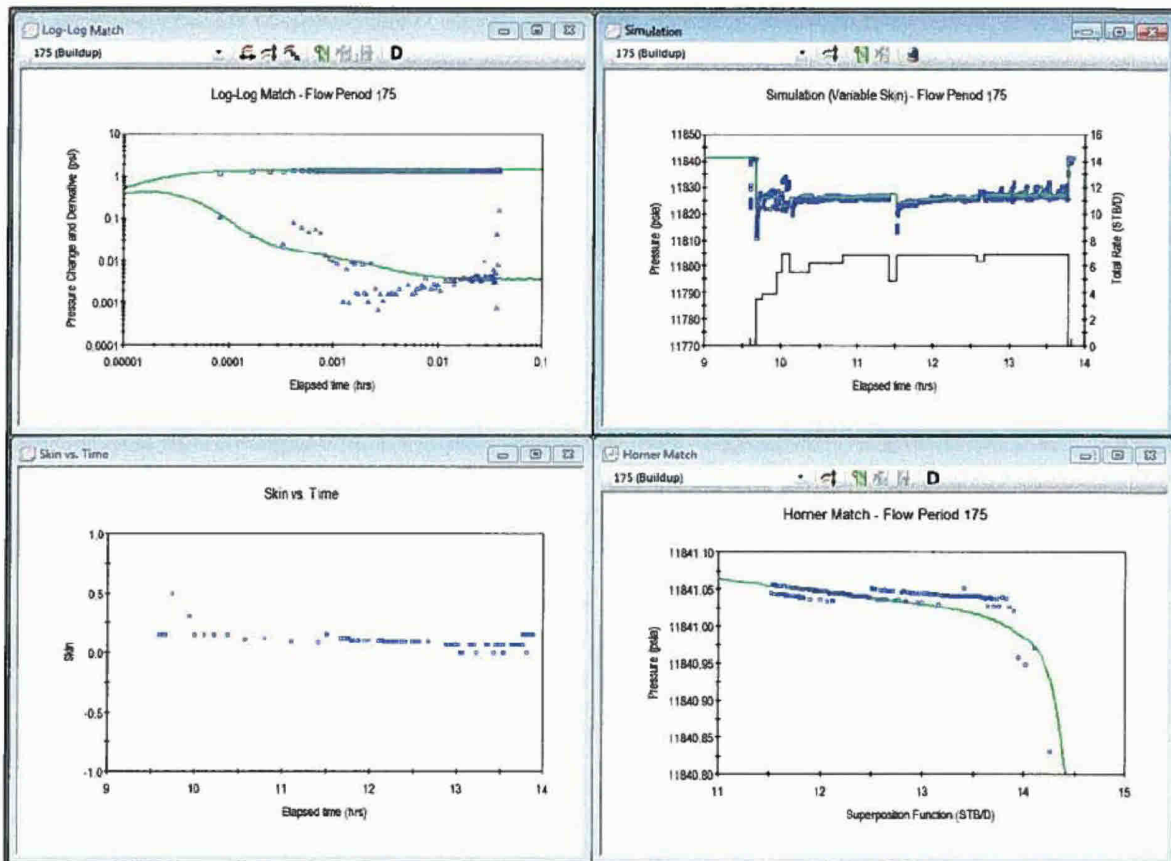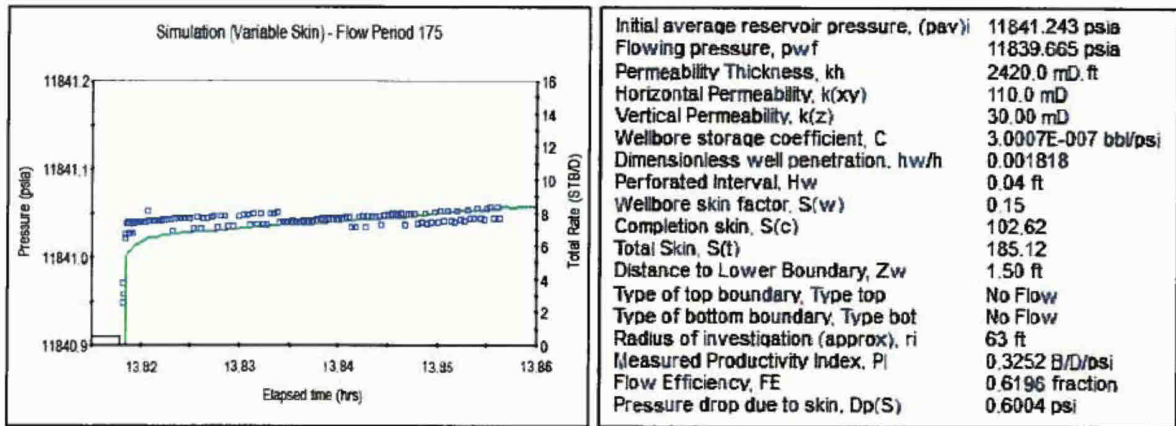
Figure 12: M56D Model Match and Analysis Results (Main Trend)

The Main Trend data results give a horizontal permeability of 110 mD with a skin ranging from 0 to 0.5.

TREX-011696R.091

1.2.1.5 M56D – Average Trend Analysis

The Average Trend data is analysed primarily to determine the reservoir permeability and skin.

The model match and analysis results are shown in Figure 13. The green continuous lines show the model match to the actual data (blue points).
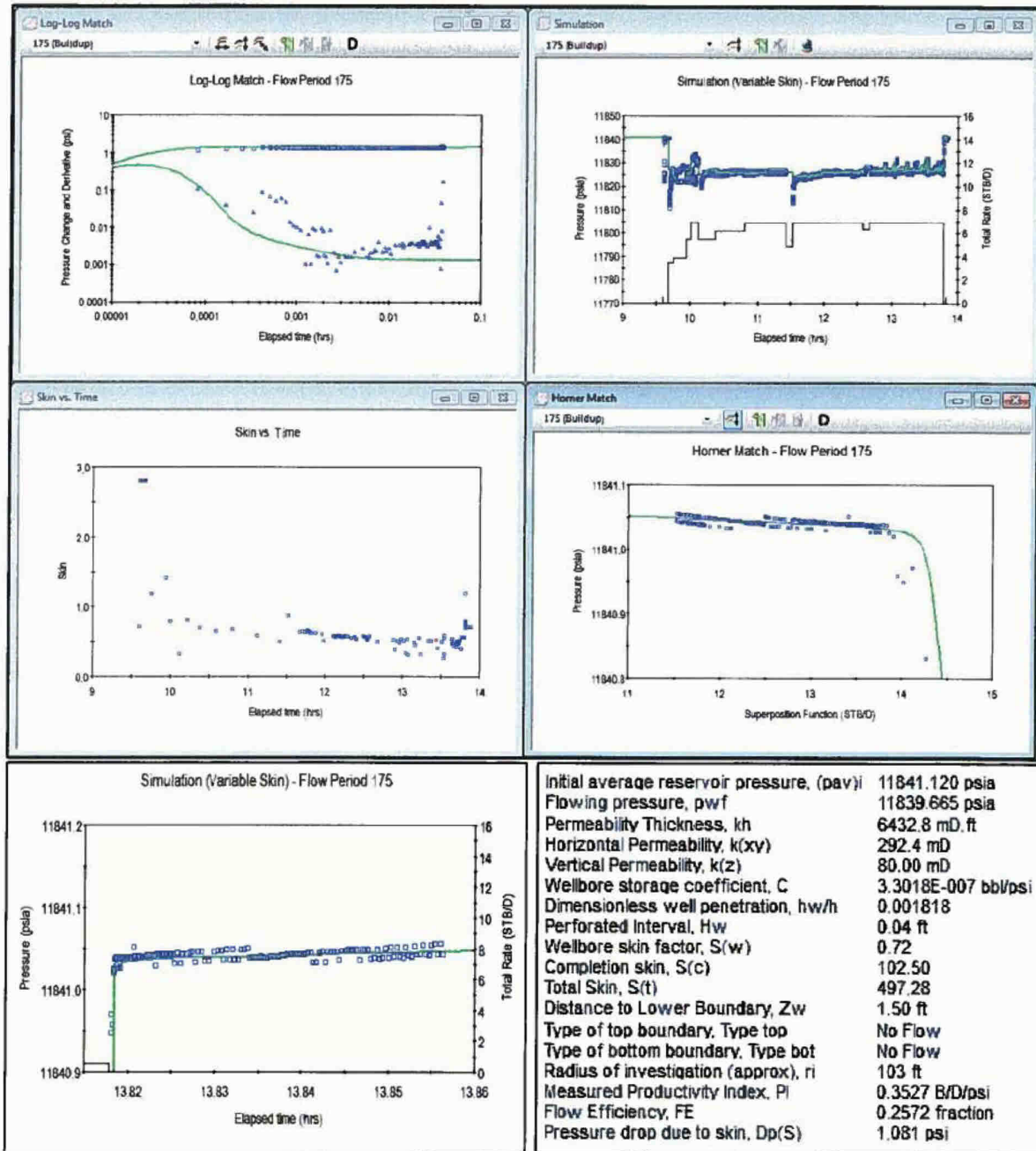
Figure 13: M56D Model Match and Analysis Results (Average Trend)

Initial average reservoir pressure, (pav)i	11841.120 psia
Flowing pressure, pwf	11839.665 psia
Permeability Thickness, kh	6432.8 mD.ft
Horizontal Permeability, k(xy)	292.4 mD
Vertical Permeability, k(z)	80.00 mD
Wellbore storage coefficient, C	3.3018E-007 bbl/psi
Dimensionless well penetration, hw/h	0.001818
Perforated Interval, Hw	0.04 ft
Wellbore skin factor, S(w)	0.72
Completion skin, S(c)	102.50
Total Skin, S(t)	497.28
Distance to Lower Boundary, Zw	1.50 ft
Type of top boundary, Type top	No Flow
Type of bottom boundary, Type bot	No Flow
Radius of investigation (approx), ri	103 ft
Measured Productivity Index, PI	0.3527 B/D/psi
Flow Efficiency, FE	0.2572 fraction
Pressure drop due to skin, Dp(S)	1.081 psi

The Average Trend data results give a horizontal permeability of 292 mD with a final skin of 0.7 and a range of skin's during the sampling period of 0 to 3. The initial high skin of 3 at the start of the sampling could be due to debris at the probe filter which was dislodged during the sampling process.

1.2.1.6 M56D – Comparison of Main and Average Trend Analysis

Figure 14 shows a comparison of the derivatives (models) for the main trend and average trend analysis models with the actual data. The range of horizontal permeabilities is 110 mD to 292 mD.

The both matches are reasonable as they provide a good match to the possible radial flow stabilisation levels and provide reasonable upper and bounds of the M56D permeability.
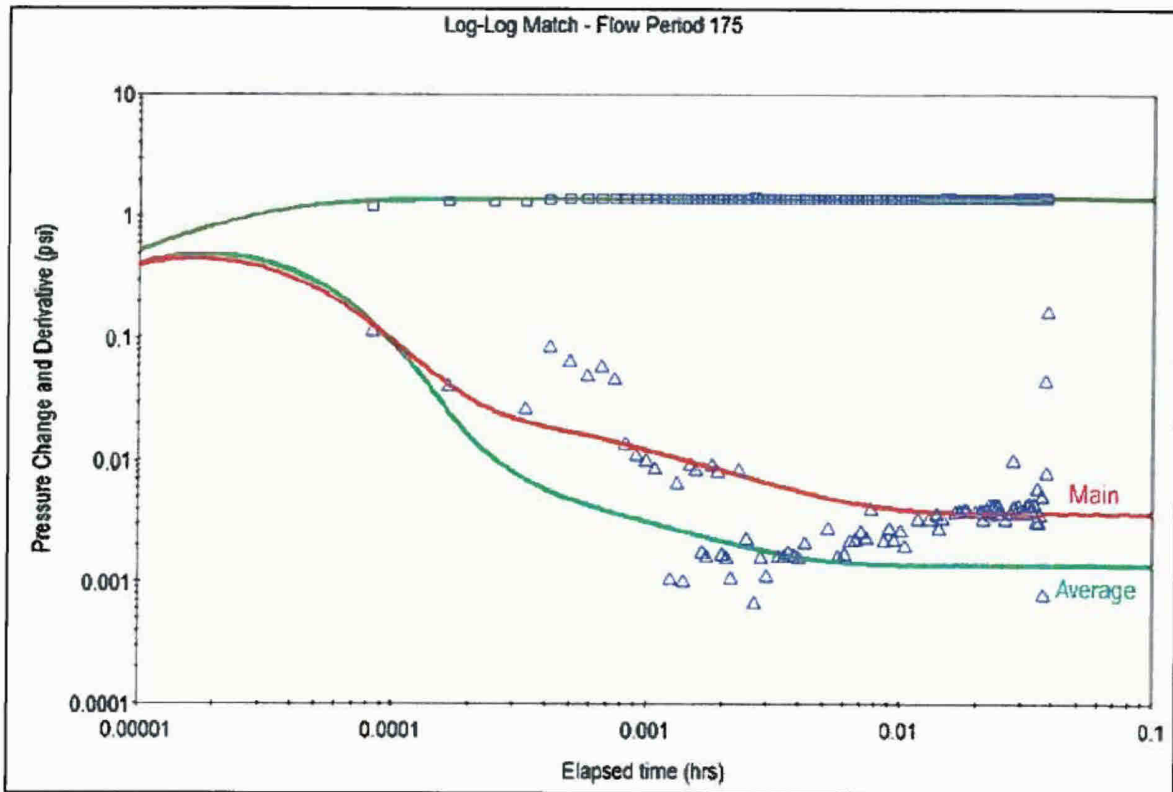
Figure 14: M56D Modes – Comparison of Derivatives (Main Trend vs. Average Trend)

12

1.2.2   Macondo M56E Permeability Determination

1.2.2.1   M56E (Upper) – Pressure and Rate Data

Shown in Figure 15 is the rate data from the MDT measured by the pump-out module (MRPO) prior to sample collection. The total production period lasted for about 4.2 hrs. The pressure measurement during the entire sampling process is shown in Figure 16.
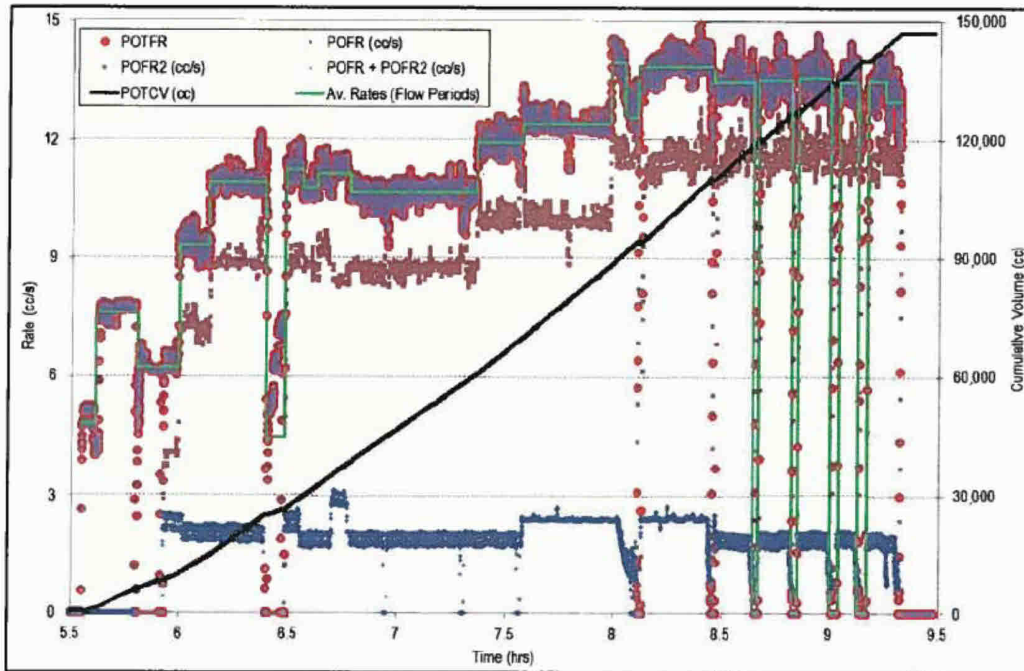
Figure 15: M56E (Upper) Rate Data from MDT (F143)
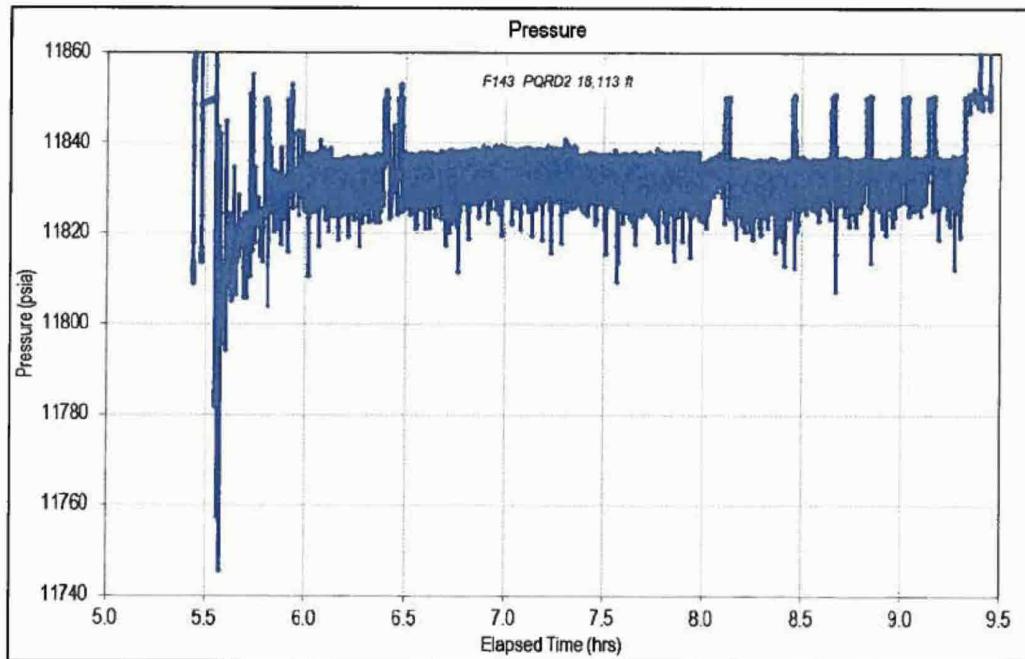
Figure 16: M56E (Upper) Rate Data from MDT (F143)

13

1.2.2.2 M56E (Upper) – Rate Validation

Rate validation analysis is conducted to determine if the measured flow rates are sufficiently reliable to be used in the well test analysis. Rate validation analysis is performed by comparing the radial flow stabilisation for each build-up we have. If the flow rates we have for each build-up are reliable, the normalised derivative of each build-up should have the same radial flow stabilisation. This is because radial flow stabilisation is a function of permeability and the permeability does not change between each build-ups. Thus, differences between radial flow stabilisation levels among the build-ups reflect a margin of error in the flow rate measurements. The pressure data indicates 7 shut-in periods (build ups) with slightly noisy data but of sufficient quality for rate validation analysis. The shut-in periods are obtained when the pump-out module is stopped for a short duration during the sampling, when the sample is being taken and when a pretest is conducted after the sample has been taken.

The rate validation plot is a log-log plot of the pressure change and normalised derivative against time (superposition time) which is used to compare the radial flow stabilisation level (the point on the y-axis where the plotted lines have a slope of 0 or are flat) from multiple flow periods. The derivative is normalised to a unit rate by dividing values of all points on the derivative by the rate of the preceding flow period. For a reservoir like the Macondo, where the test was entirely above the bubble point, the derivatives for each build-up should stabilise at the same level (if rates are correct), and the radial flow stabilisation level is proportional to the permeability.

The M56E upper rate validation plot (Figure 17) based on the 7 build-ups indicate the rates are consistent because all of the derivatives reach radial flow stabilization within a narrow range (band). The deterministic analysis will be done using the most likely radial flow stabilisation level for permeability determination and the band will be considered in uncertainty analysis. The most likely radial flow stabilisation level is determined from the consistent radial flow stabilisation of the deconvolved derivatives using a range of initial pressures (Figure 19). This level also coincides with the middle level of the band (Figure 17)
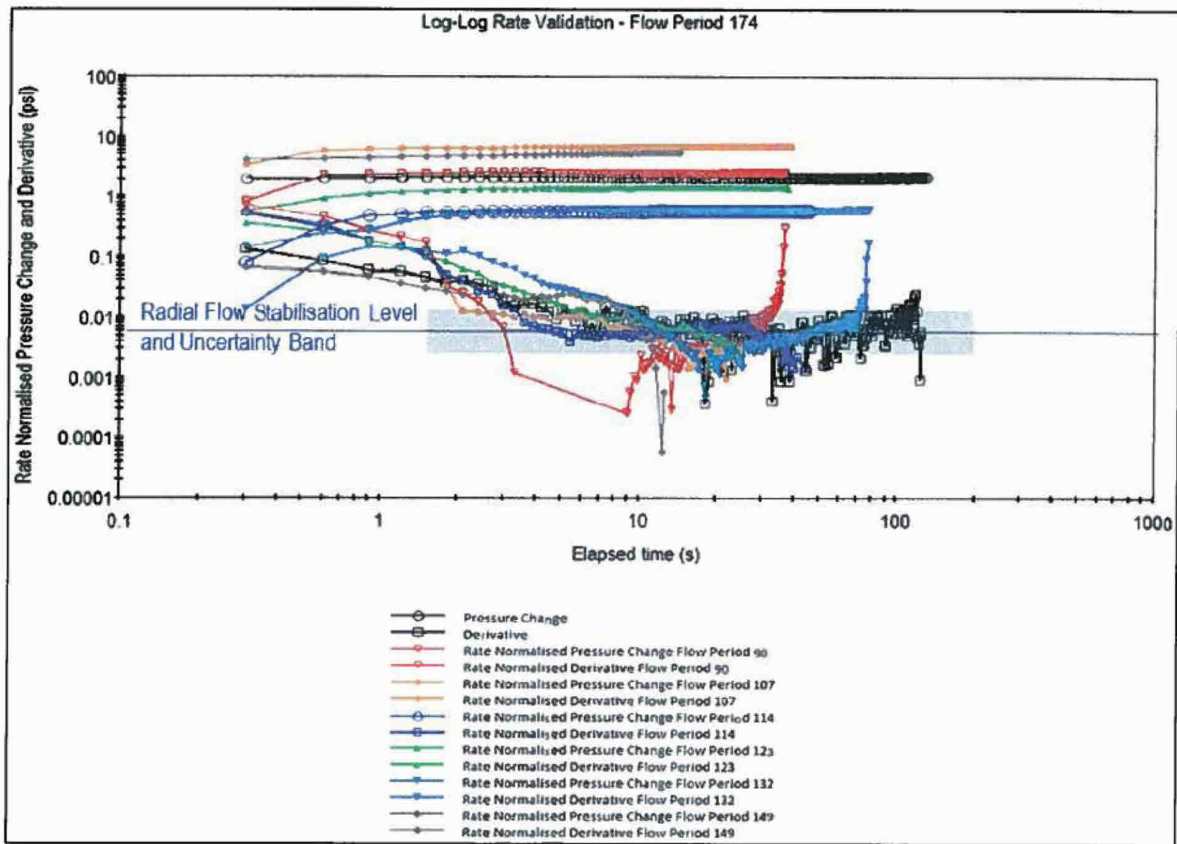
Figure 17: M56E (Upper) Rate Data from MDT (F143)

1.2.2.3 M56E (Upper) – Deconvolution

Using deconvolution, the entire production rate history and all build-ups is converted to a unit rate drawdown corresponding to the entire duration of the test. The analysis of the final buildup gives and initial pressure of 11,850.63 psia (Figure 23). The range of initial pressures (11,850.55, 11,850.60, 11,850.65 and 11,850.70 psia) is used to constrain the deconvolution and generate four unit rate pressure responses (Figure 18) to see the impact of initial pressure on the deconvolved derivative.

15
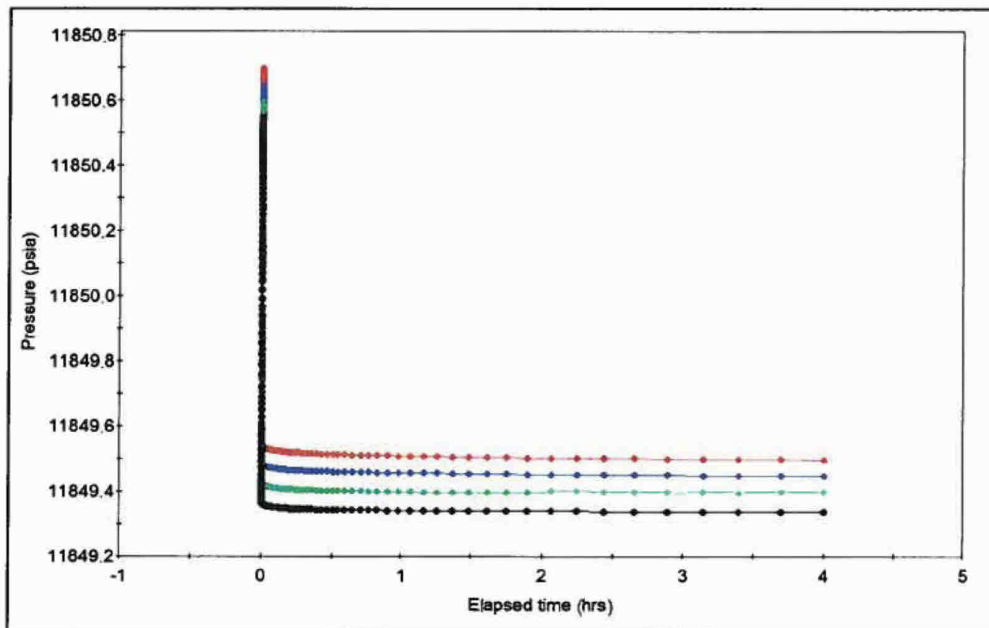
Figure 18: M56E (Upper) Unit Rate Pressure Responses from Deconvolution

The corresponding deconvolved derivatives corresponding to the range of initial pressures (plotted lines) are compared with the actual build up derivative (plotted boxes) (Figure 19). The deconvolved derivative extends the analysable data by an additional 2 log cycles i.e. from 0.04 hrs to over 4 hrs. The diagnosis of the actual buildup and deconvolved derivatives indicate a clear radial flow stabilisation level along the dashed blue line. The late-time behaviours differ for the derivatives based on the range of initial pressures. Initial pressures of 11850.55 to 11850.60 indicate increasing mobility at late times and could be a multi-layer effect i.e. communication with the lower part of the M56E sand. Initial pressures of 11850.61 to 11850.65 indicate are all generally flat and indicate an infinite acting behaviour (no boundaries or changing mobilities observed). Initial pressures of 11850.66to 11850.70 indicate slightly reducing mobilities at late times. However all the scenarios indicate a consistent initial radial stabilisation level and will give identical reservoir permeabilities.

16
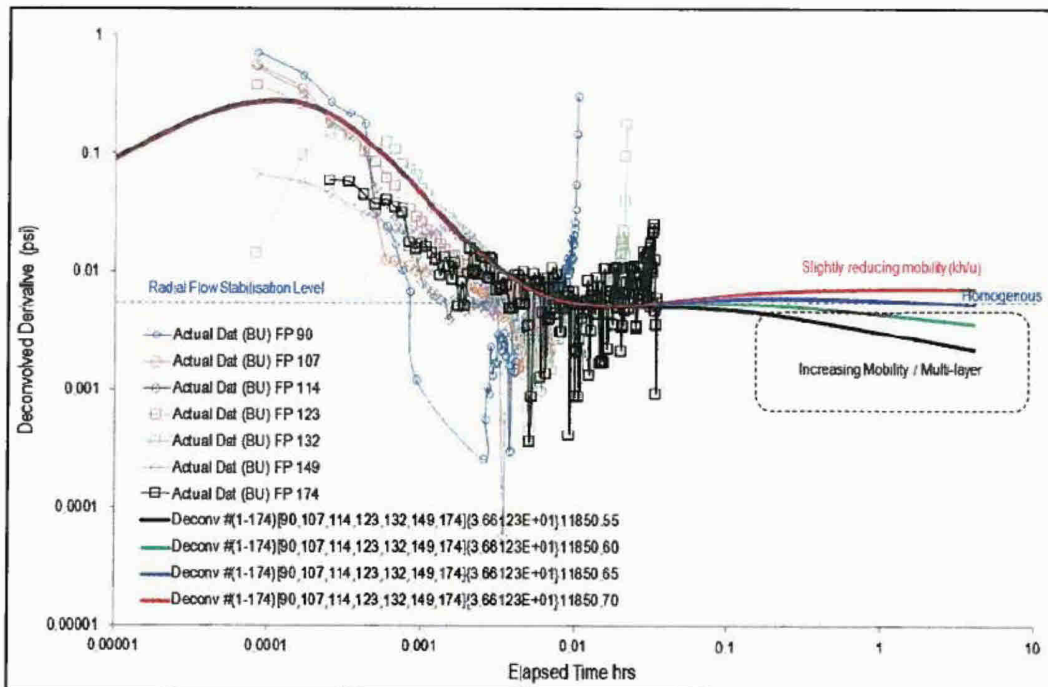
Figure 19: M56E (Upper) Comparison of Deconvolved Derivative and Actual Buildup Derivative

Figure 20 shows the pressure match of the convolved pressures from the deconvolved derivative and the actual build up data. A zoom into the pressure match of the final build up (Figure 21) shows the initial pressures of 11,850.60, 11,850.65 and 11,850.70 psia give a better match to the actual data. The actual data is affected by gauge resolution effects (limited to 0.01 psi).
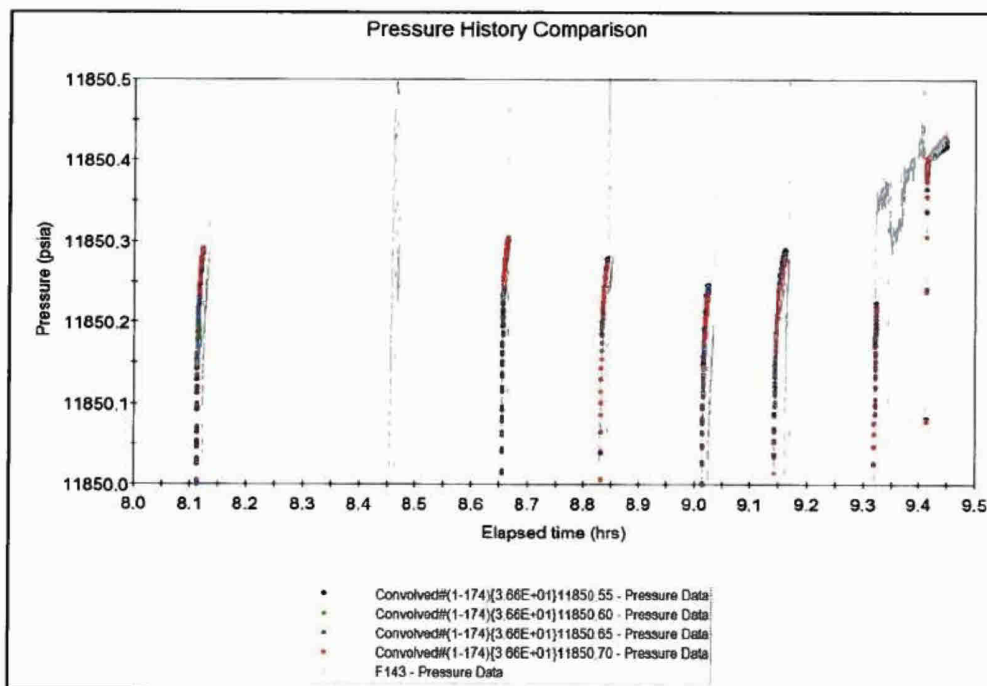
Figure 20: M56E (Upper) Deconvolution Pressure Match (Build ups)

17

TREX-011696R.098
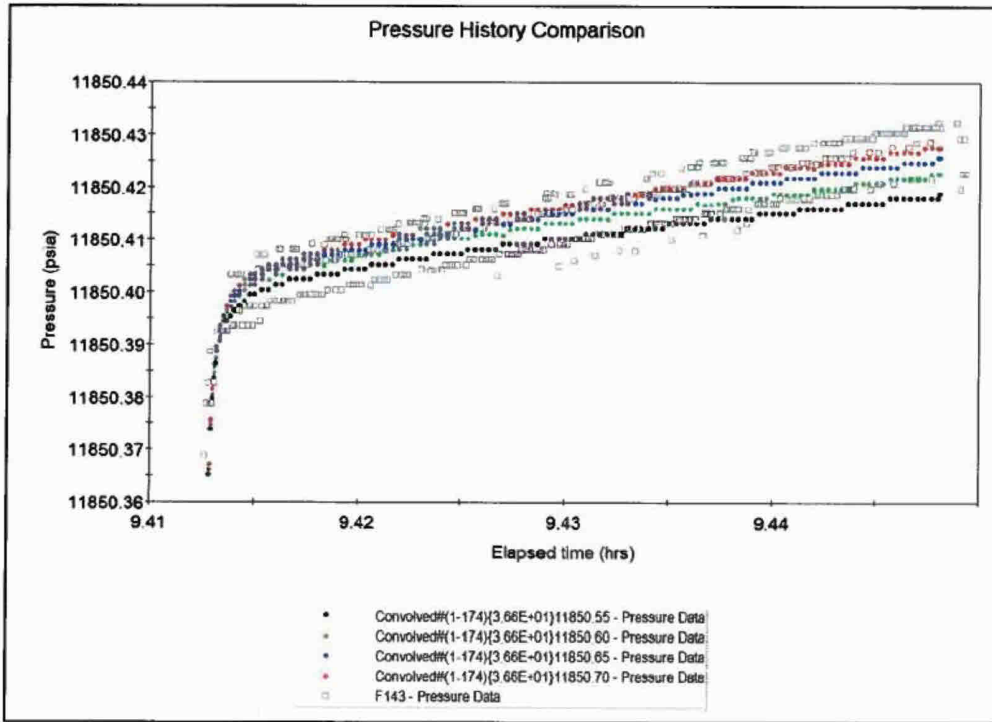
Figure 21: M56E (Upper) Deconvolution Pressure Match (Zoom in on Final Build up)

1.2.2.4   M56E (Upper) – Model Diagnosis and Selection of Interpretation Model

Based on the MDT probe dimensions, the actual build up data and deconvolution analysis, the interpretation model is selected as: Partial Penetration with Wellbore Storage and Skin; Homogenous; and Infinite Acting as shown in Figure 22.
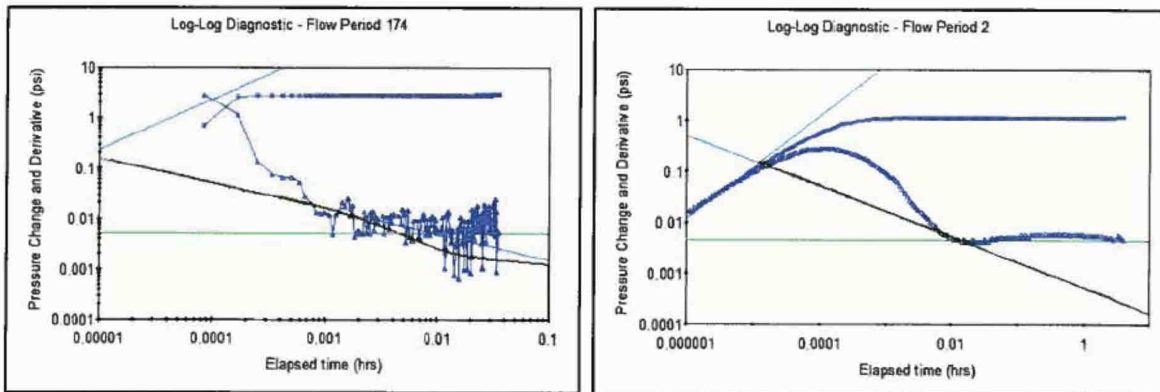
Figure 22: M56E (Upper) Model Diagnosis and Selection of Interpretation Model with Actual Buildup (Left) and Deconvolved Derivative with an Initial Pressure of 11,850.65 psia(Right)

Shown in Table 3 are the input parameters for the M56E (Upper) analysis.

18

M56E Upper Sand Thickness: 15.4 ft	Standard Probe Diameter: 0.433 inches	Probe Distance to Base of Sand: 10.8 ft	Wellbore Radius: 0.354 ft
Oil Viscosity: 0.243 cP	Total Compressibility: 18.6 microsips	Porosity: 0.221	Reservoir Pressure: 11,850.6 psia

Table 3: M56E (Upper) Input Parameters for MDT Sampling Well Test Analysis

1.2.2.5 M56E (Upper) – FP 174 (BU) Analysis

The model match and analysis results are shown in Figure 23.

TREX-011696R.100
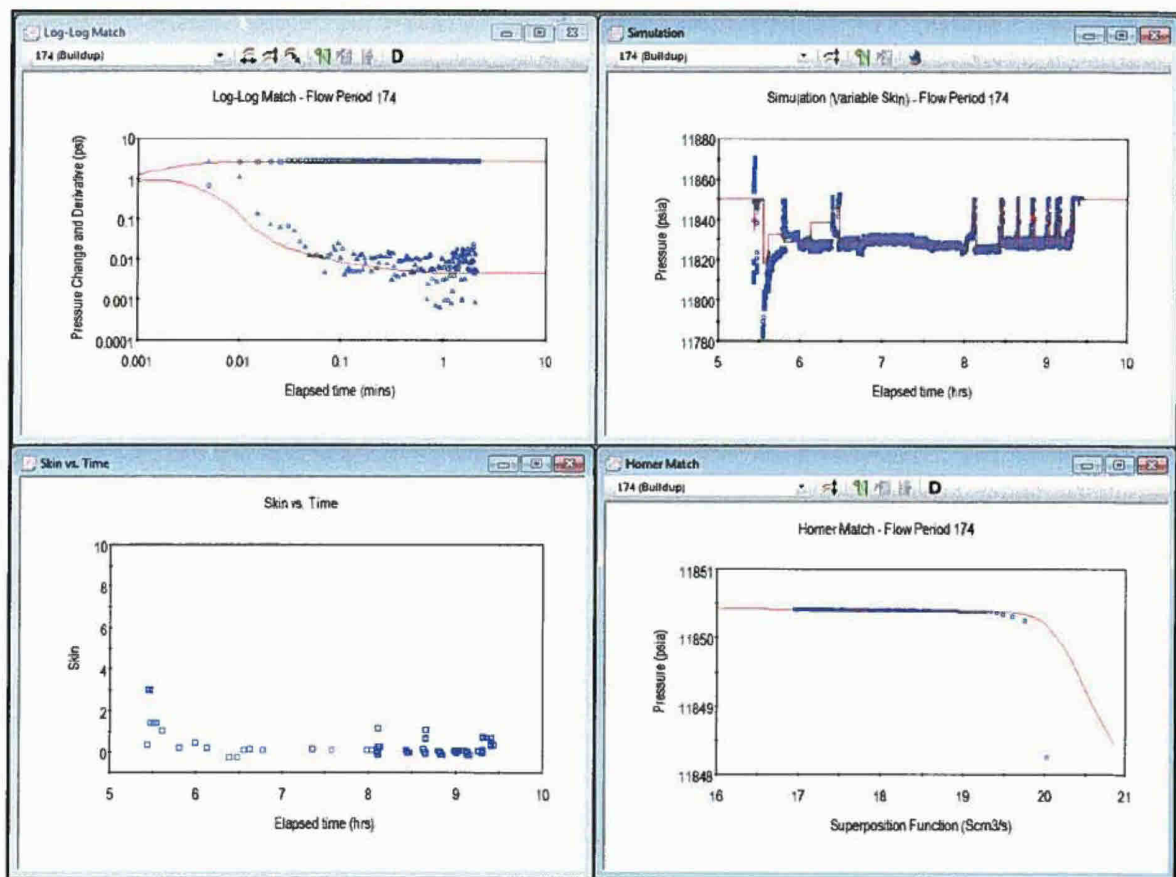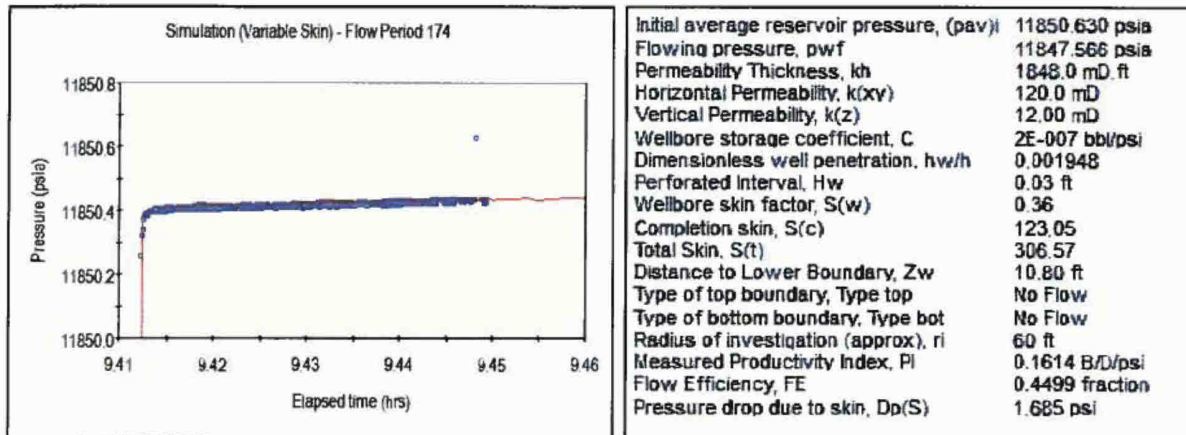
Figure 23: M56E (Upper) Model Match and Analysis Results (FP 174 - Buildup)

The table in the figure reads:

Initial average reservoir pressure, (pav)i	11850.630 psia
Flowing pressure, pwf	11847.566 psia
Permeability Thickness, kh	1848.0 mD.ft
Horizontal Permeability, k(xy)	120.0 mD
Vertical Permeability, k(z)	12.00 mD
Wellbore storage coefficient, C	2E-007 bbl/psi
Dimensionless well penetration, hw/h	0.001948
Perforated Interval, Hw	0.03 ft
Wellbore skin factor, S(w)	0.36
Completion skin, S(c)	123.05
Total Skin, S(t)	306.57
Distance to Lower Boundary, Zw	10.80 ft
Type of top boundary, Type top	No Flow
Type of bottom boundary, Type bot	No Flow
Radius of investigation (approx), ri	60 ft
Measured Productivity Index, PI	0.1614 B/D/psi
Flow Efficiency, FE	0.4499 fraction
Pressure drop due to skin, Dp(S)	1.685 psi

1.2.2.6 M56E (Upper) – Deconvolution Analysis (Initial Pressure: 11,850.65 psia)

The model match and analysis results are shown in Figure 24. The radius on investigation based on deconvolution is 657 ft, compared to the buildup (FP 174) data which is 60 ft.
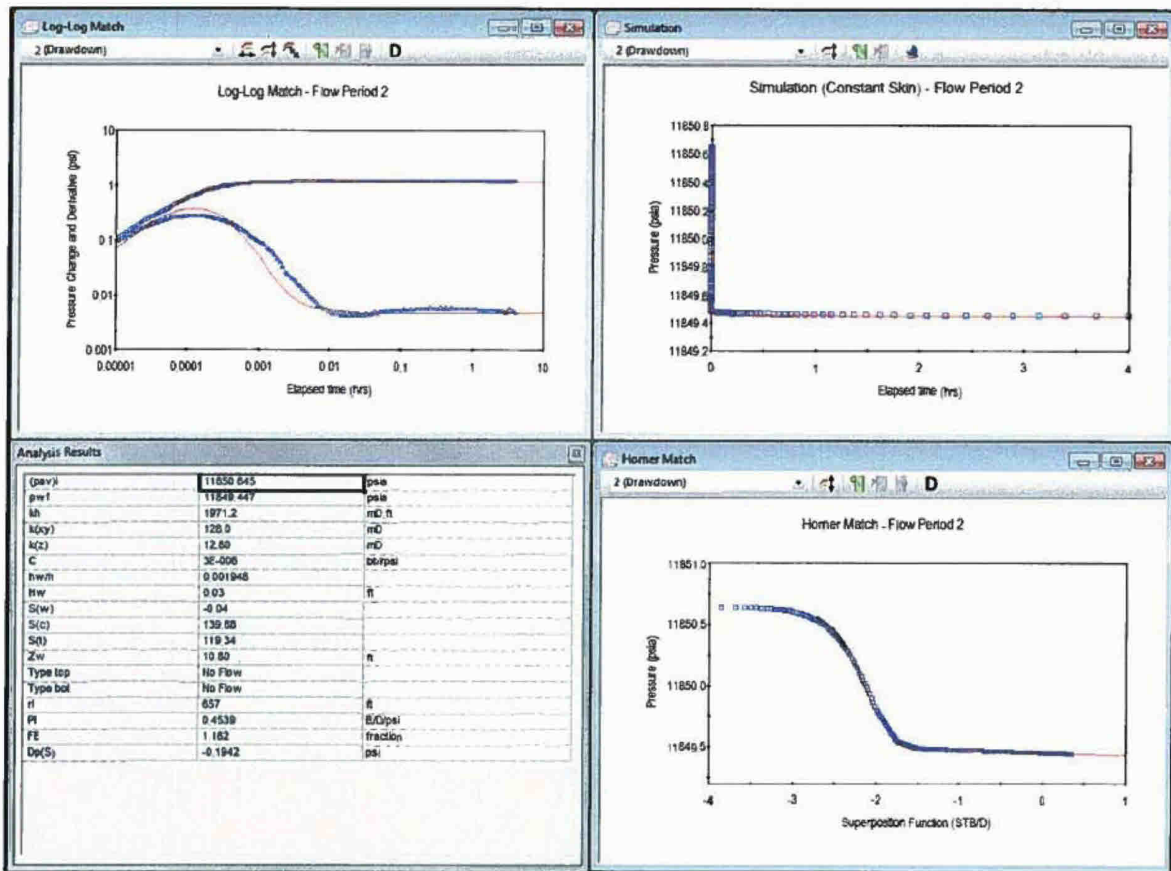
Figure 24: M56E (Upper) Deconvolution Model Match and Analysis Results

1.2.2.7 M56E (Lower) – Pressure and Rate Data

Shown in Figure 25 is the rate data from the MDT measured by the Pumpout module (MRPO) prior to sample collection. The total production period lasted for about 4.2 hrs. The pressure measurement during the entire sampling process is shown in Figure 26.

TREX-011696R.102
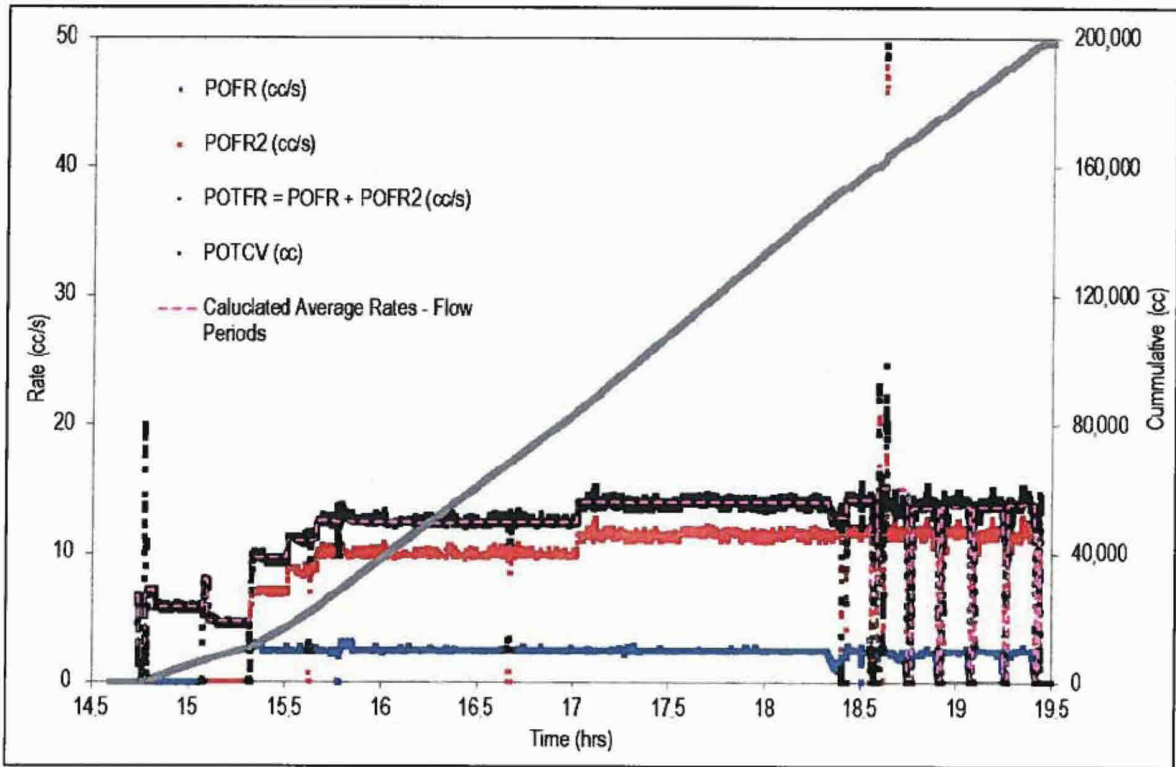
Figure 25: M56E (Lower) Rate Data from MDT (F147)
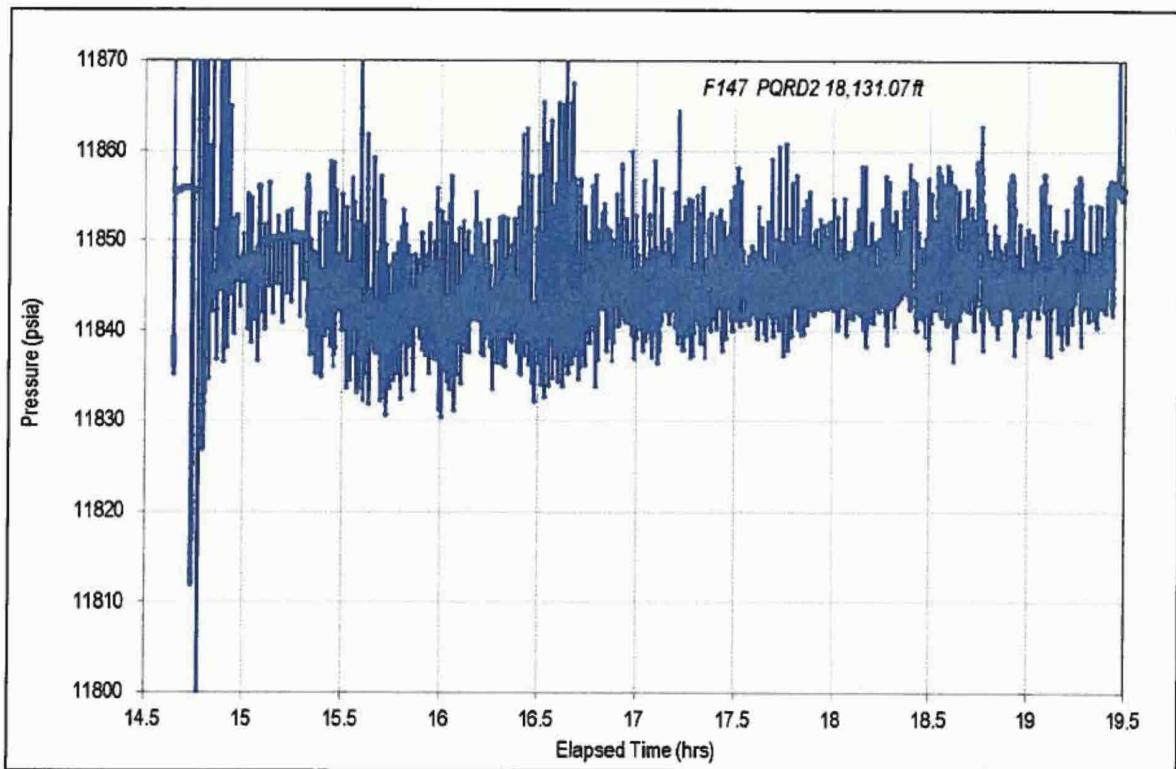
Figure 26: M56E (Lower) Pressure Data from MDT (F147)

22

TREX-011696R.103

1.2.2.8   M56E (Lower) – Rate Validation

The pressure data indicates 7 shut-in periods (build ups) with noisy data but of sufficient quality for analysis for an analysis range.

The M56E (lower) rate validation plot based on the 7 build-ups indicate the rates are consistent and the radial flow stabilisation levels lie with a wide range (band) based on the diagnosis of smoothed (Figure 27) and un-smoothed (Figure 28) pressure derivatives. The range of radial flow stabilisation levels will is considered for the deterministic permeability calculations and uncertainty analysis.
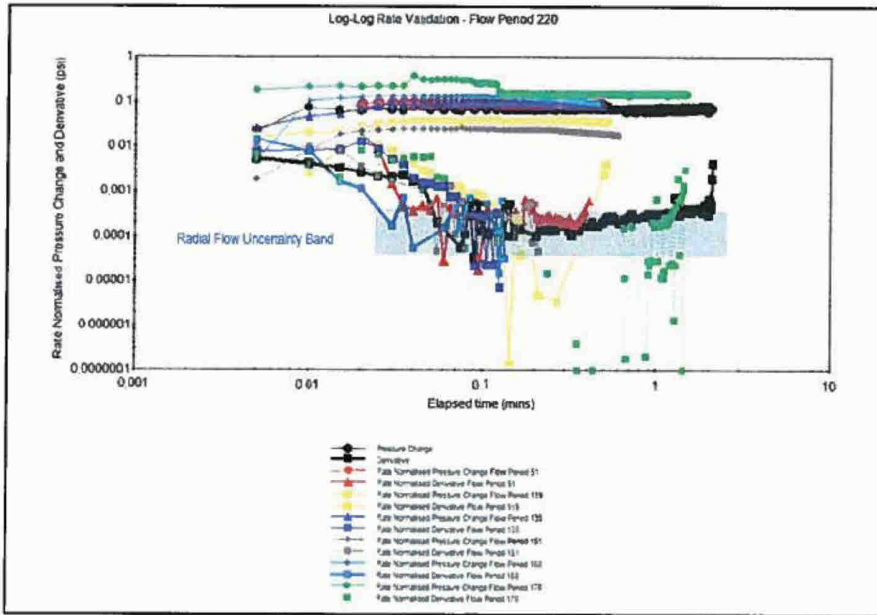
Figure 27: M56E (Lower) Rate Validation (F147) – Smoothed Derivatives
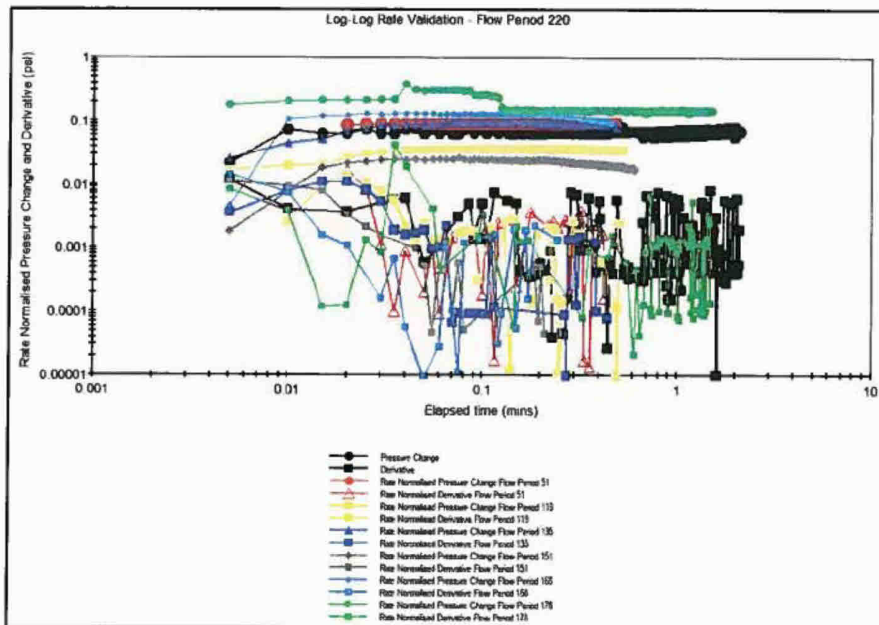
Figure 28: M56E (Lower) Rate Validation (F147) – Un-Smoothed Derivatives

23

1.2.2.9   M56E (Lower) – Deconvolution

Using deconvolution, the entire production rate history and all build-ups is converted to a unit rate drawdown corresponding to the entire duration of the test using an initial pressure of 11,855.87 psia (Figure 29).
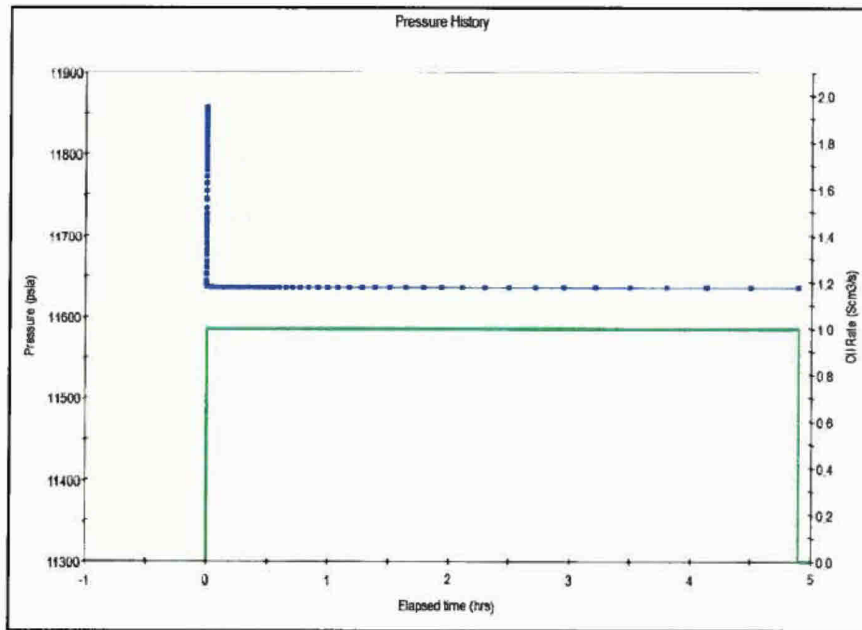
Figure 29: M56E (Lower) Unit Rate Pressure Response from Deconvolution

The corresponding deconvolved derivative is compared with the actual un-smoothed build up derivative (Figure 30). The deconvolved derivative extends the analysable data by an additional 2 log cycles i.e. from 0.05 hrs to about 5hrs. The diagnosis of the actual buildup derivatives and deconvolved derivative indicate a possible range of radial flow stabilisation levels.
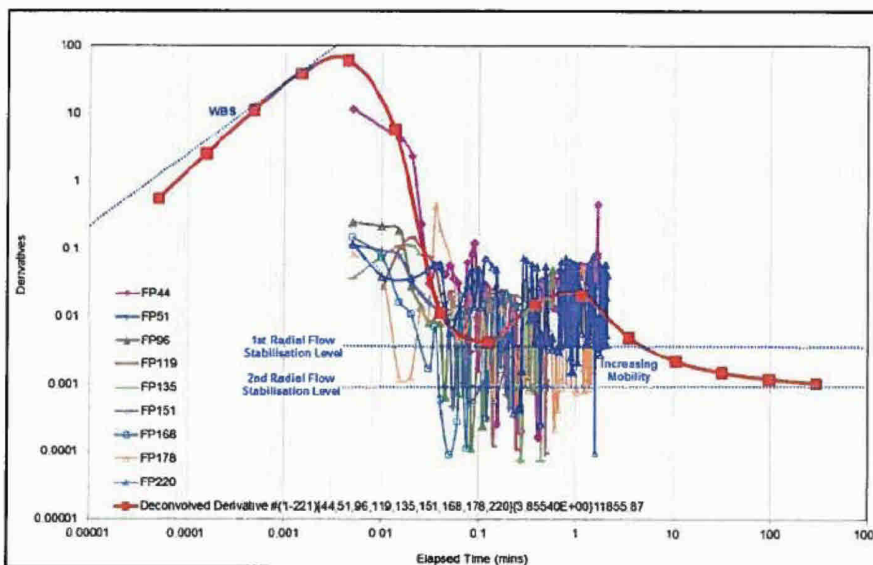
Figure 30: M56E (Lower) Comparison of Actual Buildup Derivatives and Deconvolved Derivative

24

Figure 31 shows the pressure match of the convolved pressures from the deconvolved derivative and the actual build up data. The match quality to the buildup data is fair and within about 0.04psi (maximum error) at the end of the build-up. As a result, a wide range (Figures 32 and 33) of radial flow stabilisation levels is considered in the analysis.
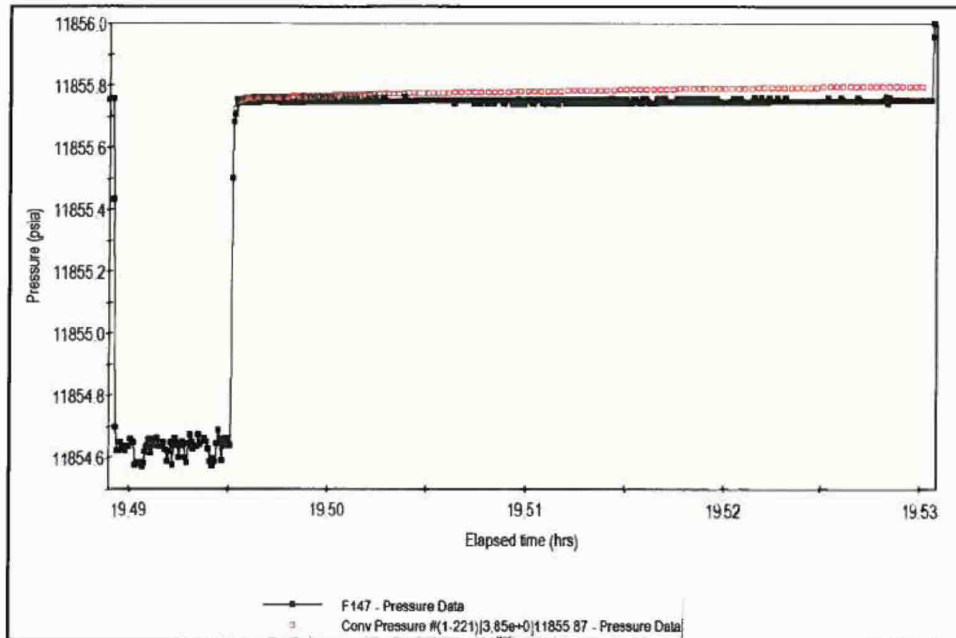
Figure 31: M56E (Lower) Deconvolution Pressure Match

1.2.2.10 M56E (Lower) – Model Diagnosis and Selection of Interpretation Model

Based on the MDT probe dimensions, the actual build up data and deconvolution analysis, the interpretation model is selected as: Partial Penetration with Wellbore Storage and Skin; Homogenous; and Infinite Acting as shown in Figure 32. Two options of radial flow stabilisations were considered for the homogenous and infinite acting model. Option 'A' considers a higher radial flow stabilisation level corresponding to a lower horizontal permeability and option 'B' considers a lower radial flow stabilisation level corresponding to a higher horizontal permeability.
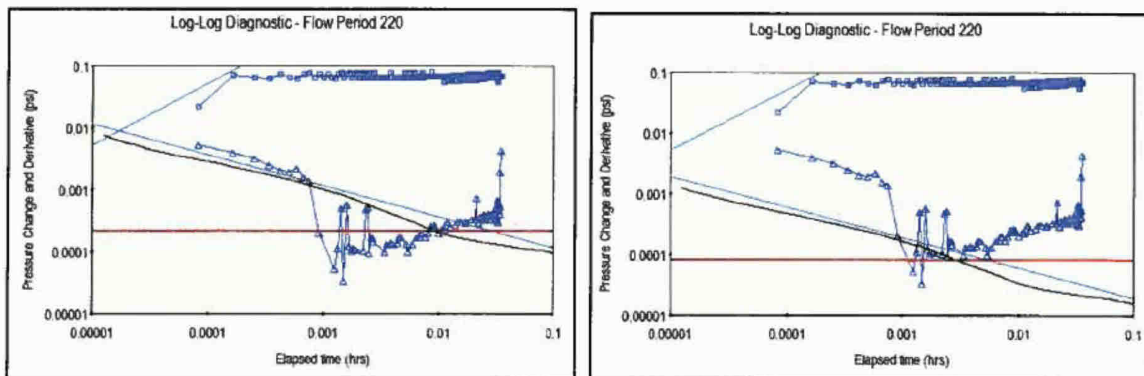
Figure 32: M56E (Lower) Model Diagnosis and Selection of Interpretation Model: Option A (left) and Option B (right)

25

A third option (C) was also considered (Figure 33), with boundaries diagnosed as the late time behaviour. This option shows the lowest possible radial flow stabilisation level and corresponds to the highest possible permeability.
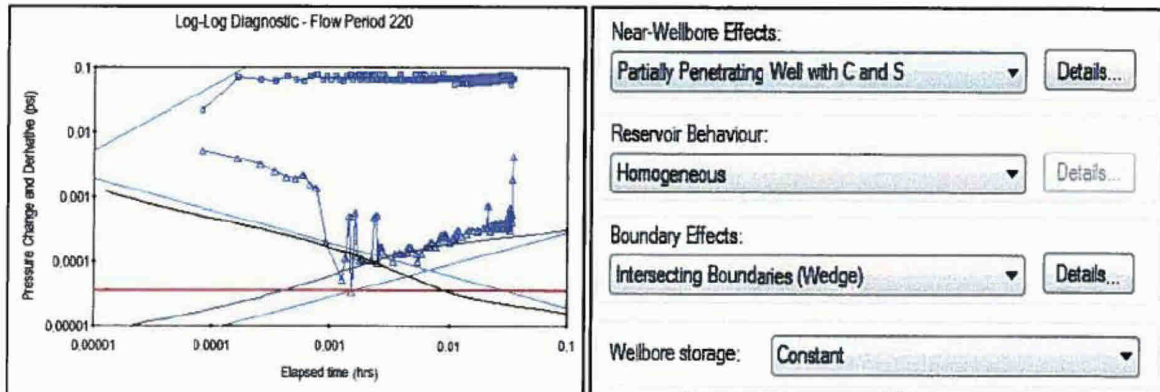
Figure 33: M56E (Lower) Model Diagnosis and Selection of Interpretation Model

Options A, B and C are considered for well test interpretation and uncertainty analysis.

Shown in Table 4 are the input parameters for the M56E (Lower) analysis.

M56E (Lower) Sand Thickness: 49.1 ft	Large Probe Diameter: 1.66 inches	Probe Distance to Base of Sand: 45 ft	Wellbore Radius: 0.354 ft
Oil Viscosity: 0.243 cP	Total Compressibility: 18.6 microsips	Porosity: 0.221	Reservoir Pressure: 11,855.9 psia

Table 4: M56E (Upper) Input Parameters for MDT Sampling Well Test Analysis

1.2.2.11 M56E (Lower) – FP 220 (BU) Analysis

The model matches for Option A, B and C is shown in Figure 34 and the corresponding analysis results are shown in Table 5 and 6.
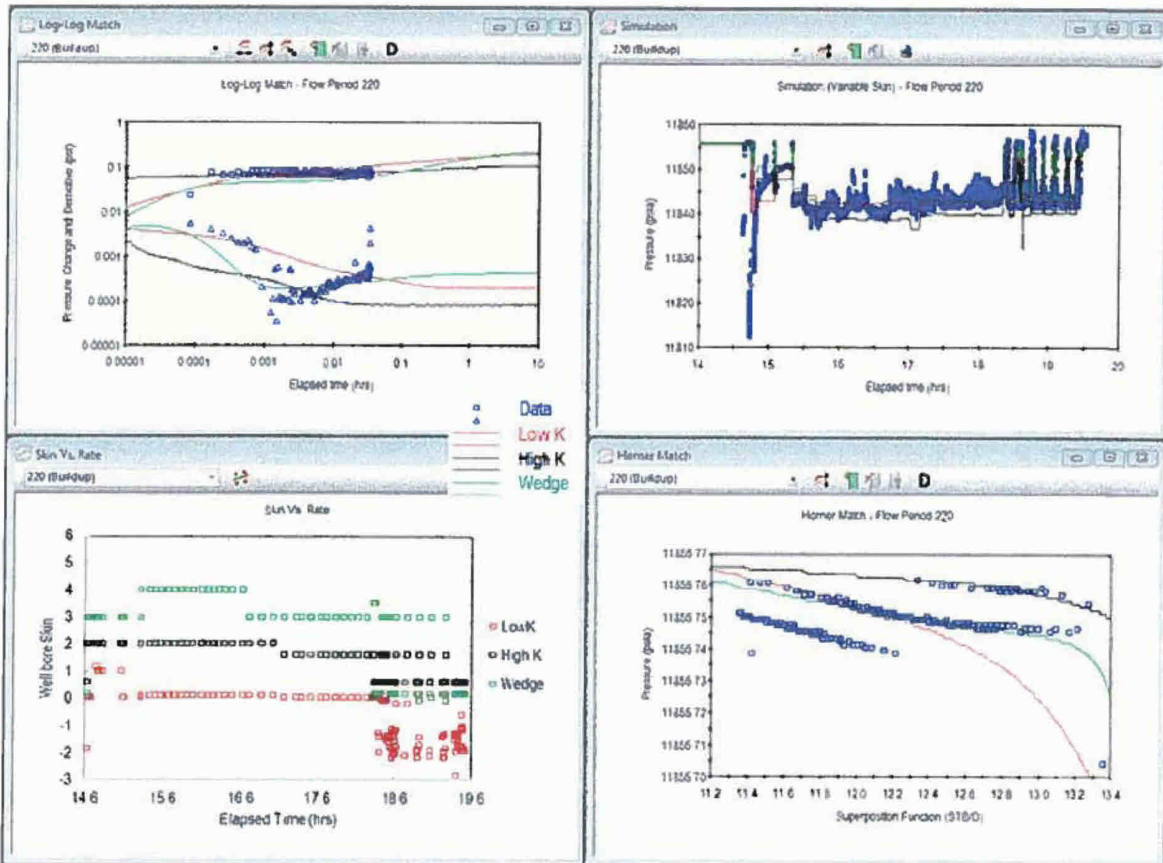
Figure 34: M56E (Lower) Model Match for Options A, B and C (FP 220 - Buildup)

Near Wellbore Effect:	Partially Penetrating Well with C and S		Near Wellbore Effect:	Partially Penetrating Well with C and S
Reservoir Behaviour:	Homogeneous		Reservoir Behaviour:	Homogeneous
Boundary Effect:	Infinite Lateral Extent		Boundary Effect:	Infinite Lateral Extent
Initial average reservoir pressure, (pav)i	11855.862 psia		Initial average reservoir pressure, (pav)i	11855.803 psia
Flowing pressure, pwf	11855.682 psia		Flowing pressure, pwf	11855.682 psia
Permeability Thickness, kh	4959.1 mD.ft		Permeability Thickness, kh	11784 mD.ft
Horizontal Permeability, k(xy)	101.0 mD		Horizontal Permeability, k(xy)	240.0 mD
Vertical Permeability, k(z)	10.00 mD		Vertical Permeability, k(z)	100.00 mD
Wellbore storage coefficient, C	7.8845E-007 bbl/psi		Wellbore storage coefficient, C	3E-008 bbl/psi
Dimensionless well penetration, hw/h	0.002851		Dimensionless well penetration, hw/h	0.002851
Perforated Interval, Hw	0.14 ft		Perforated Interval, Hw	0.14 ft
Wellbore skin factor, S(w)	-1.94		Wellbore skin factor, S(w)	0.59
Completion skin, S(c)	742.85		Completion skin, S(c)	153.44
Total Skin, S(t)	60.89		Total Skin, S(t)	360.36
Distance to Lower Boundary, Zw	45.00 ft		Distance to Lower Boundary, Zw	45.00 ft
Type of top boundary, Type top	No Flow		Type of top boundary, Type top	No Flow
Type of bottom boundary, Type bot	No Flow		Type of bottom boundary, Type bot	No Flow
Radius of investigation (approx), ri	55 ft		Radius of investigation (approx), ri	84 ft
Measured Productivity Index, PI	0.6373 B/D/psi		Measured Productivity Index, PI	0.9509 B/D/psi
Flow Efficiency, FE	4.007 fraction		Flow Efficiency, FE	0.4271 fraction
Pressure drop due to skin, Dp(S)	-0.2613 psi		Pressure drop due to skin, Dp(S)	0.03336 psi

Table 5: M56E (Lower) Analysis Results for Option A (left) and Option B (right)

Near Wellbore Effect:	Partially Penetrating Well with C and S
Reservoir Behaviour:	Homogeneous
Boundary Effect:	Intersecting Boundaries (Wedge)
Initial average reservoir pressure, (pav)i	11855.938 psia
Flowing pressure, pwf	11855.682 psia
Permeability Thickness, kh	27005 mD.ft
Horizontal Permeability, k(xy)	550.0 mD
Vertical Permeability, k(z)	55.00 mD
Wellbore storage coefficient, C	5E-006 bbl/psi
Dimensionless well penetration, hw/h	0.002851
Perforated Interval, Hw	0.14 ft
Wellbore skin factor, S(w)	0.15
Completion skin, S(c)	244.48
Total Skin, S(t)	298.11
Distance to Lower Boundary, Zw	45.00 ft
Type of top boundary, Type top	No Flow
Type of bottom boundary, Type bot	No Flow
Distance to first boundary, d1	25 ft
Distance to second boundary, d2	35 ft
Angle between Wedge Boundaries (Degrees), Wdg Angle	30
Type of first boundary, Type d1	No Flow
Type of second boundary, Type d2	No Flow
Distance investigated (approx), Dinv	33 m
Measured Productivity Index, PI	0.2156 B/D/psi
Flow Efficiency, FE	0.9853 fraction
Pressure drop due to skin, Dp(S)	0.003773 psi

Table 6: M56E (Lower) Analysis Results for Option C

1.3 Permeability Uncertainty Analysis from MDT Measurements

1.3.1 Uncertainty Parameters and Distributions

Tables 7, 8 and 9 show the uncertainty parameter inputs with their distributions for the M56D, M56E Upper and M56E Lower formations respectively.

Basic Parameters	Distribution	Dev.	F144		
			M56D		
Porosity	Normal	5%	0.21	0.0105	
Reservoir Thickness (ft)	Normal	15%	22	3.3	
Wellbore Radius (ft)	Single Value		0.412		
Oil Viscosity (cP)	Normal		0.236	0.243	0.249
Total Compressibility (10-6/psi)	Triangular		1.49E-05	1.78E-05	2.09E-05
Production Rate (stb/d)	Normal	10%	0.3044	0.03044	
Model					
Pressure Match (.PM) 1/psi	Rectangular		137.4	365.3	
Time Match (.TM) 1/hr	Rectangular		9.79E+06	2.37E+07	
CDe2s Match	Rectangular		-1.578	-1.043	
(hd2/Cd) match	Rectangular		5.35E+05	4.85E+05	
(hwd) match	Normal	10%	0.001818	0.0001818	
(Zwd) match	Normal	10%	0.06818	0.006818	

Table 7: M56D Uncertainty Parameter Inputs and Distributions

Basic Parameters	Distribution	Dev.	F143		
			M56E Upper		
Porosity	Normal	5%	0.22	0.011	
Reservoir Thickness (ft)	Normal	15%	15.4	2.31	
Wellbore Radius (ft)	Single Value		0.354		
Oil Viscosity (cP)	Normal		0.236	0.243	0.249
Total Compressibility (10-6/psi)	Triangular		1.56E-05	1.86E-05	2.17E-05
Production Rate (stb/d)	Normal	10%	0.49453	0.049453	
Model					
Pressure Match (.PM) 1/psi	Rectangular		108.9	105.7	
Time Match (.TM) 1/hr	Rectangular		1.12E+07	7.98E+05	
CDe2s Match	Rectangular		-1.337	-0.5063	
(hd2/Cd) match	Rectangular		8.40E+05	56003	
(hwd) match	Normal	10%	0.001948	0.0001948	
(Zwd) match	Normal	10%	0.7013	0.07013	

Table 8: M56E (Upper) Uncertainty Parameter Inputs and Distributions

TREX-011696R.110

Basic Parameters	Distribution	Dev.	F-147		
			M56E Lower		
Porosity	Normal	5%	**0.22**	0.011	
Reservoir Thickness (ft)	Normal	15%	**49.1**	7.365	
Wellbore Radius (ft)	Single Value		**0.354**		
Oil Viscosity (cP)	Normal	15%	0.236	**0.243**	0.249
Total Compressibility (10-6/psi)	Triangular		1.56E-05	**1.86E-05**	2.17E-05
Production Rate (stb/d)	Normal	10%	0.055366	0.0055366	
Model					
Pressure Match (.PM) 1/psi	Triangular		2610.4	6202.9	14215
Time Match (.TM) 1/hr	Triangular		7.64E+06	4.77E+08	6.56E+06
CDe2s Match	Triangular		-3.162	-2.463	-0.3798
(hd2/Cd) match	Triangular		6.98E+06	4.36E+07	1.09E+06
(hwd) match	Normal	10%	0.002851	0.0002851	
(Zwd) match	Normal	10%	0.9165	0.09165	

Table 9: M56E (Lower) Uncertainty Parameter Inputs and Distributions

1.3.2   Uncertainty Modelling

Most well test interpretation software programmes use non-linear regression to determine the reservoir parameters that provide the best match between actual rate and pressure data and a given interpretation model. The non-linear regression evaluates the match quality as a standard correlation between each parameter. This, however, only estimates the match errors, and does not incorporate the other errors that must be accounted for to understand the overall uncertainty on the analysis[3]. A methodology developed at Imperial College has been employed in this study to estimating the impact and uncertainty range on well test analysis results of errors in both well and reservoir input data, and match parameters. The software utilizes the Monte Carlo simulation for uncertainty analysis.

Figure 35: Well Test Uncertainty Modelling Software[3]

30

The resulting probability distribution functions based on the errors in the reservoir input data and match parameters for the M56D, M56E (Upper) and M56E (Lower) are shown in Figures 36 to 38.
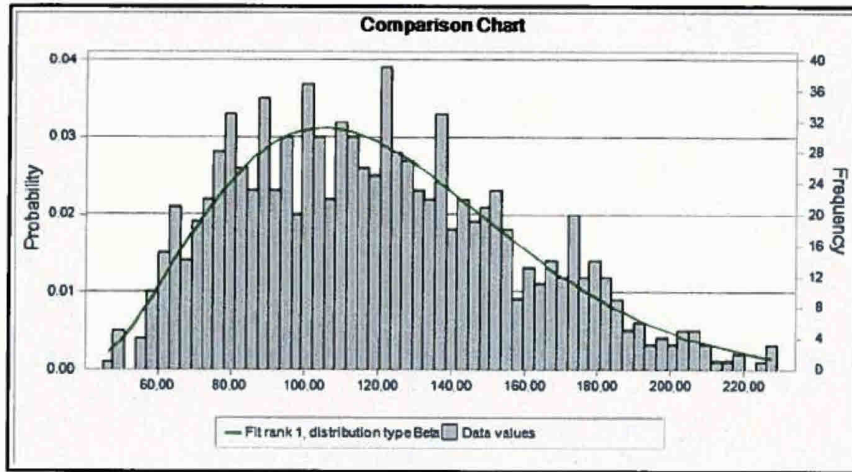
Figure 36: M56D Permeability – Probability Distribution Function
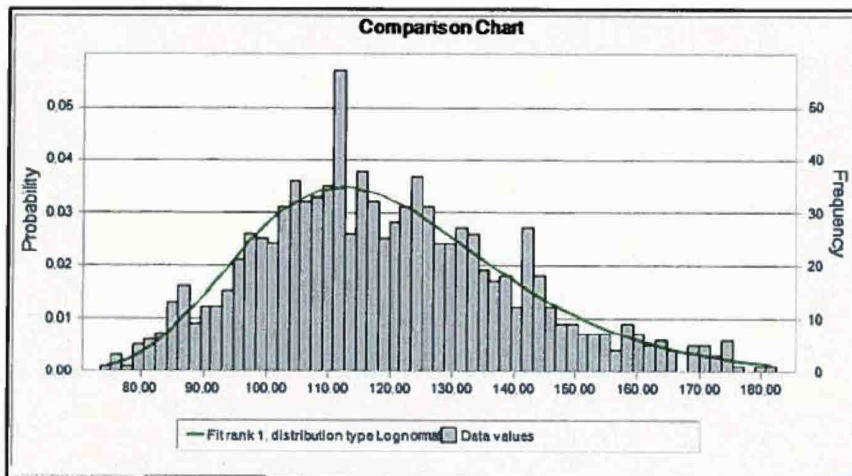
Figure 37: M56E (Upper) Permeability – Probability Distribution Function
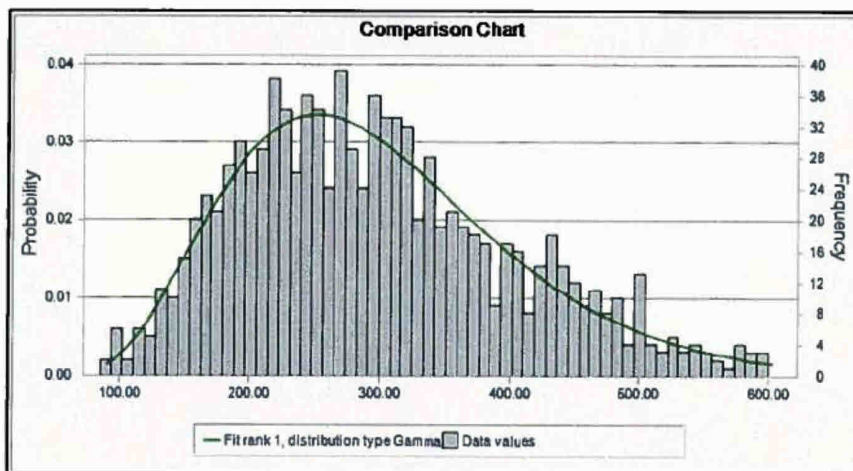
Figure 38: M56E (Lower) Permeability – Probability Distribution Function

31

Shown in Table 10 are the corresponding probability and statistical results.

Percentiles	M56D (144)	M56E (143 Upper)	M56E (147 Lower)
P100	45.0	73.4	85.3
P90	74.3	94.9	171.2
P80	84.5	102.6	202.8
P70	95.1	107.9	229.9
P60	105.9	112.3	256.7
P50	116.3	117.3	284.7
P40	126.9	123.6	311.6
P30	138.3	129.5	343.2
P20	152.9	137.4	390.2
P10	174.4	148.0	453.6
P0	281.9	233.4	725.9
	Horizontal permeability mD	Horizontal permeability mD	Horizontal permeability mD
Min	45.0	73.4	85.3
Max	281.9	233.4	725.9
Mean or Average	120.6	120.4	299.8
Median	116.3	117.3	284.7

Table 10: M56D, M56E (Upper) and M56E (Lower) Probability and Statistical Results

Monte Carlo simulation using Oracle's Crystal Ball was used to quantify the uncertainty for the overall average Macondo's permeability using an arithmetic averaging of the permeability ranges for the M56D, M56E (Upper), M56E (Lower) and the M56F formations.

Monte Carlo simulation is a computerized mathematical technique that allows people to account for uncertainty in quantitative analysis. The technique is used by professionals in many industries including the oil and gas industry. Monte Carlo simulation performs risk or uncertainty analysis by building models of possible results by substituting a range of values (a probability distribution) for any factor that has inherent uncertainty. It then calculates results over and over, each time using a different set of random values from the probability functions. Monte Carlo simulation produces distributions of possible outcome values.

The input permeability range and distribution for the M56D, M56E (Upper) and M56E (Lower) where determined from the best fit match to their determined probability density functions shown in Figures 36 to 38. The M56F did not have any MDT sampling, and its range of permeabilities was based on various averaging methods.[4] Arithmetic Air Perm 1440.6mD; Geometric Air Perm 129.9 mD; Geometric Oil Perm K_{eff} 110.4 mD respectively are used as the low, peak and high numbers in a triangular distribution. The M56F net thickness is 6.5ft (less than 7% of the total net thickness at the well) and its impact on the overall arithmetic average permeability is expected to be small to negligible. Figures 39 – 42 show the probability distribution for all the sands expected to contribute to flow.
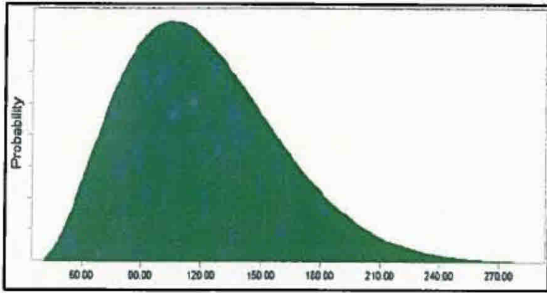
Figure 39: M56D Probability Distribution
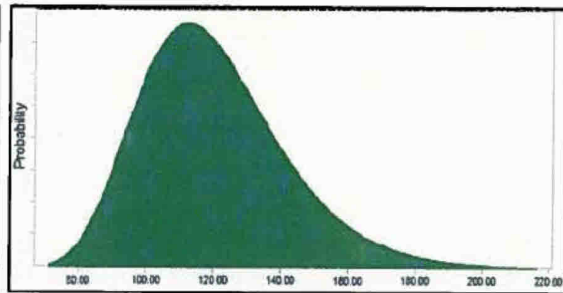
Figure 40: M56E (Upper) Probability Distribution
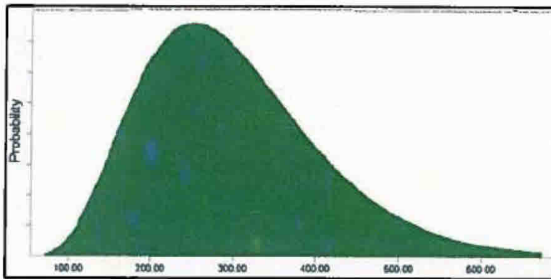
Figure 41: M56E (Lower) Probability Distribution
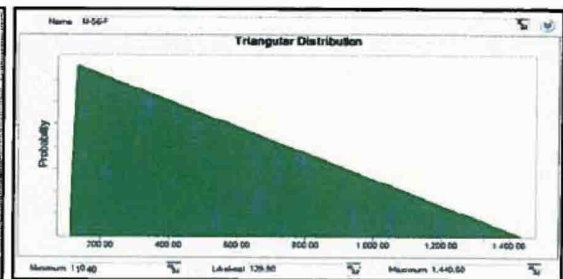
Figure 42: M56F Probability Distribution

The Probability Distribution and Cumulative Probability Distribution charts are shown in Figures 43 and 44 respectively and the corresponding statistical results and percentiles is shown in Table 11.

The results indicate the following permeabilities: P90 170 mD; P50 238 mD; P10 329 mD; and an average permeability of 245 mD.
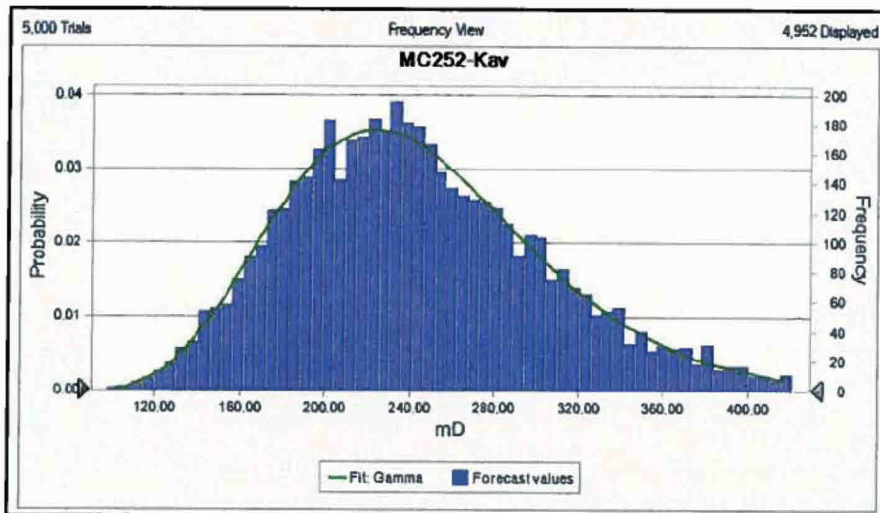
Figure 43: Macondo Permeability – Probability Distribution

33
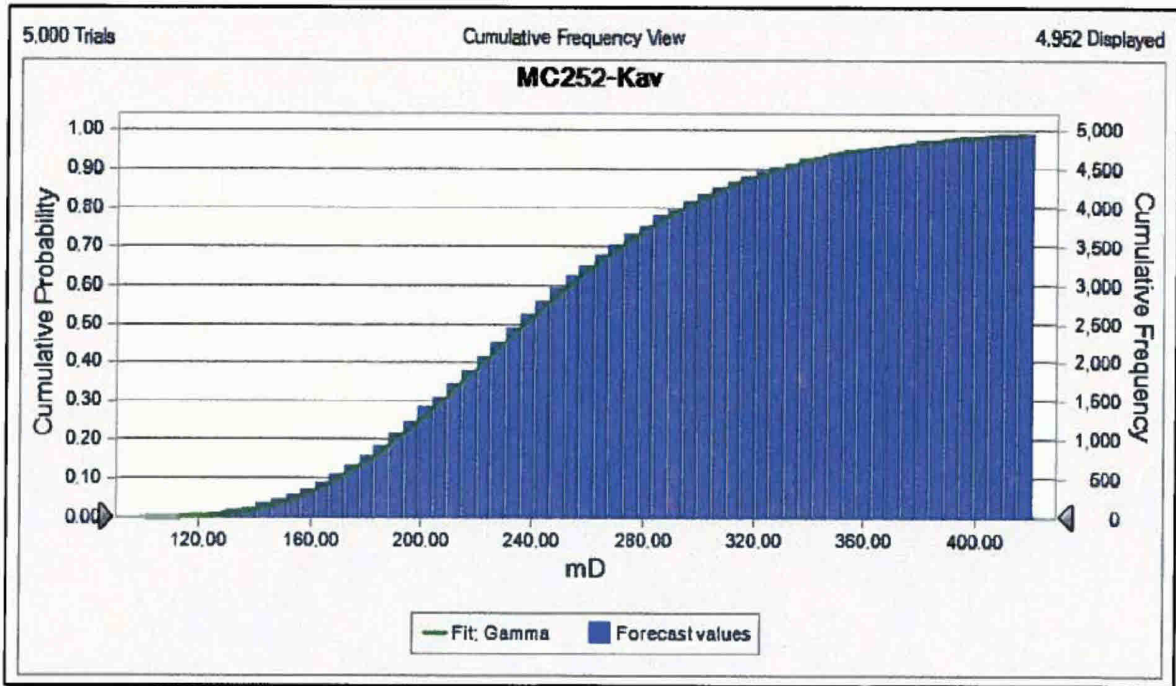
Figure 44: Macondo Permeability – Cumulative Probability Distribution

Percentiles	MC252-Kav
P 100	99
P 90	170
P 80	192
P 70	207
P 60	223
P 50	**238**
P 40	253
P 30	272
P 20	295
P 10	329
P 0	519
Statistics	**MC252-Kav**
Trials	5000
Mean	**245**
Median	**238**
Minimum	99
Maximum	519
Mean Std. Error	0.89

Table 11: Macondo Permeability - Probability and Statistical Results

APPENDIX F

Table of Contents

TABLE OF FIGURES

TREX-011696R.118

1   MACONDO PRESSURE TRANSIENT ANALYSIS

The objective of this study is to use pressure transient analysis and deconvolution methods to estimate entire flow rate histories during the flowing period of the BP Macondo well and determine ranges of the various well and reservoir parameters with the available data.

1.1   DATA AVAILABILITY, REVIEW & UNCERTAINTY

This section reviews the available data (and associated uncertainties) required for the well test and deconvolution analysis of the BP01 MC252 well.

1.1.1   Basic and General Data

Well Deviation: Vertical Well through the reservoir section

Well Bore Radius: 9-7/8" Hole (17,168 to 18,126 ft MD)

                          8-1/2" Hole (18,126 to 18,360 ft MD)

Start Date of Incident: 20th April 2010

Start Time of Incident: 21:38hrs (Estimated time of hydrocarbons in riser - 2010-09-08 BP Deepwater Horizon Accident Investigation Report.pdf Page 108)

1.1.2   Completion
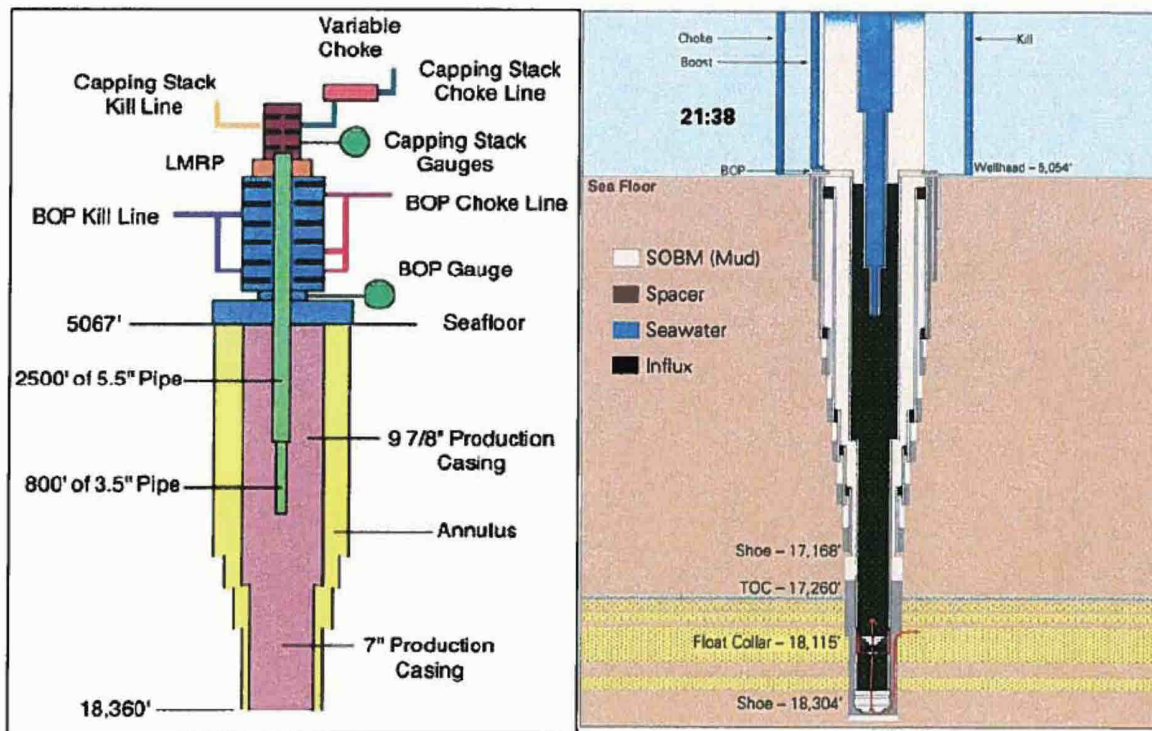
The pressure gauges located in the BOP (PT-B), Choke line (PT-C) and Kill line (PT-K). The Mud line was at 4,992 ft below sea level (bsl) or 5067 ft below Horizon Rotary Table. The Horizon Rotary was 75 ft above sea level.

The depths of the pressure gauges used in the Macondo analysis are:

- PT-B: 4,972 ft TVDss
- PT-3K-2: 4,912 TVDss[i]

1.1.3   *Pressure and Production Data*

1.1.3.1 Pressure Data

All the pressure data presented in this study were analysed in a systematic way. Pressure data was provided by Dr. Trusler.[ii] Pressure data were, where necessary, first converted to the consistent formats, units and datum levels for the entire available pressure history and merged into data sets.
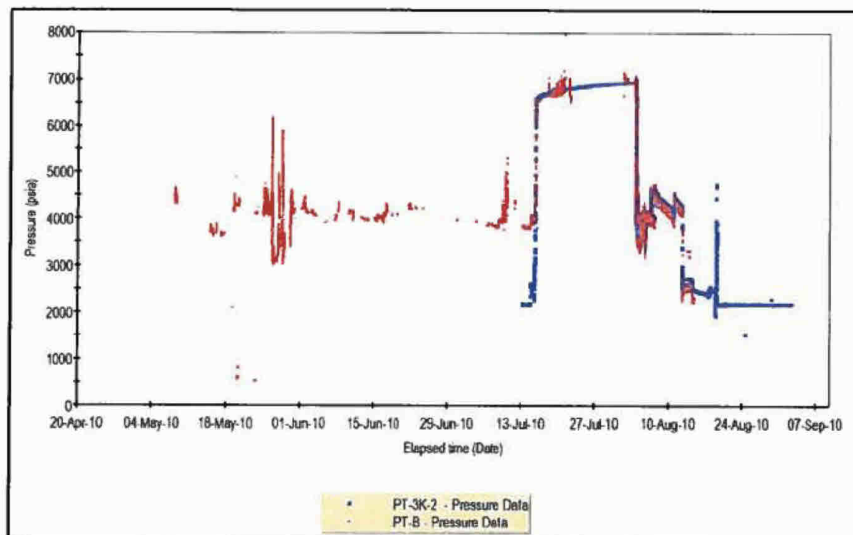
Figure 3: Available Pressure Data for Analysis

The PT-B data after the well was completely closed (after the shut-in from 15 July 2010 14:19) was noisy and could not be used for analysis. As part of quality control on the PT-B data, it was compared to PT-3K-2 during the days (14th – 15th July, 2010) just prior to shut-in (Figure-2) and their pressure difference computed.

TREX-011696R.124
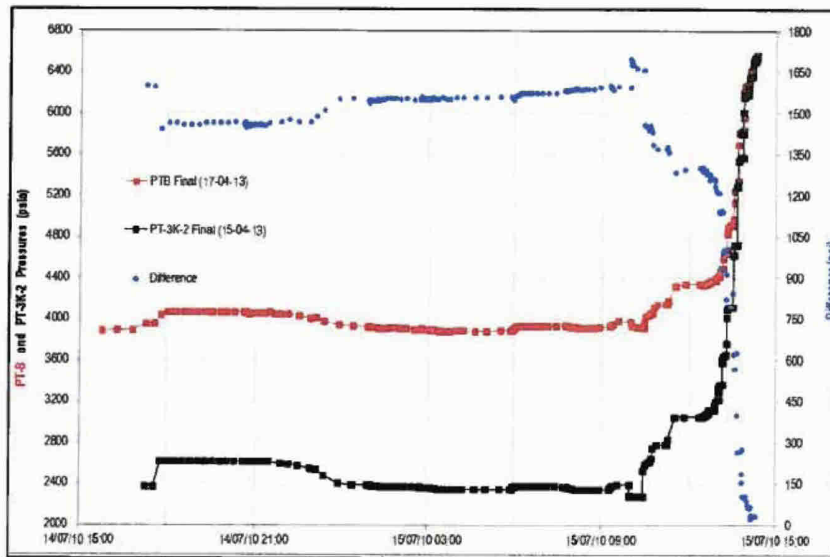
Figure 4: PT-B and PT-3K Data Quality Control

PT-B pressures were utilised during the flowing period (05/08/2010 02:12:00 to 07/15/2010 14:19:03) and PT-3K-2 pressures used during the shut-in period (07/15/2010 14:21:37 to 08/03/2010 13:03:00). PT-3K2 shut-in data was translated to the PT-B datum depth (4,972 ft TVDss) by adding 15psi (based on the vertical depth difference of 60 ft and fluid gradient of approximately 0.25 psi/ft) prior to merging data from both gauges into one data set (Figure 6).[iii]
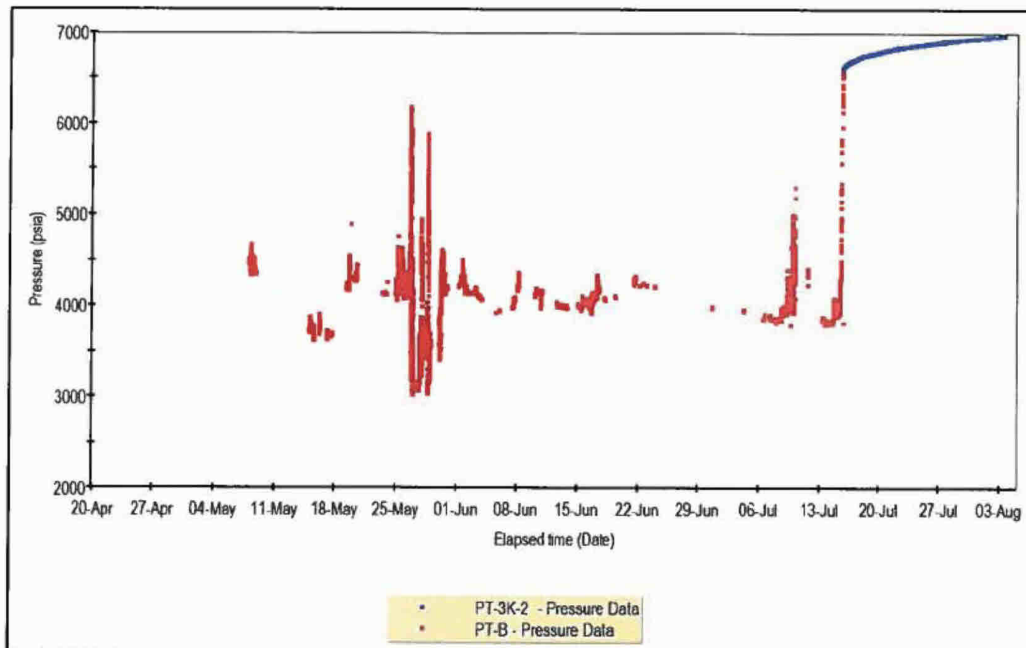
Figure 5: PT-B and PT-3K Merged Data Set.

9

1.1.3.2 Calculated Initial Shut-in Pressures at Seabed (BOP, PT-B gauge, 4,972ft TVDss)

The sample and MDT points show very slight different gradients between the sands. The difference was explained because the measurements were taken with different probes.[iv] The Differential Liberation experiment (at 243 °F) conducted during the Reservoir Fluid Study by CoreLab reports the oil density as 0.587 g/cc at 11,856 psia.[v] This is converted to a fluid gradient by multiplying with a constant of 0.433 to give a fluid gradient of 0.254 psi/ft.[vi] An average initial gradient of 0.251 psi/ft is calculated based on the average of data considered.

Taking into consideration the shut-in pressures are above the bubble point, the static pressure difference between the PT-B sensor and reservoir depth is calculated as 3,286 psi, assuming the fluid column was at 243 degrees, and the initial reservoir pressure at the PT-B depth of 8,570 psia.

| MDT Depth: 18,056.0ft TVDss	Depth for CS gauge (PT-B): 4,972.0 ft
Reservoir Pressure: 11,856.0 psia	Delta-P Depth (Reservoir minus PT-B): 13,084.0 ft
2 Delta-P Pressure 3,286 psi	3 Initial Pressure at PT-B: 8570 psia

Table 1: Initial Reservoir Pressure at BOP (4,972 ft TVDss) depth

3.1.1.1 Petrophysical and Fluid Properties

Shown in Tables 2 and 3 below are the Macondo fluid and petrophysical properties used in the study.

Initial Reservoir Pressure: 11,856 psia	Average Porosity 0.217	Average Oil Saturation 0.877
Reservoir Temperature 243 °F	Net Sand Thickness: 93 ft	Average Water Saturation 0.877

Table 2: Petrophysical Properties (a171636bbcf06977e2637c7c13737b5f.ppt, BP-HZN-2179MDL03290054.pdf)

Reference Av. Property Values	Pressure, psia	Oil Formation Volume Factor, RB/STB	Oil Viscosity, cp	Oil Compressibility (/psi)
Initial Reservoir Pressure	11856	2.316	0.243	1.321E-05

10

Final Reservoir Pressure	10400	2.366	0.212	1.462E-05

Table 3: Fluid Properties (Averages from ECL Black Oil Tables - T=243F-SSF-ALL.xls)

3.2 DECONVOLUTION BASED ON PRESSURES AT PT-B DEPTH (WHP)

Deconvolution transforms variable rate pressure data into a constant rate initial drawdown with the duration equal to the total duration of the test and yields directly the corresponding pressure derivative, normalized to a unit rate. Deconvolution provides additional information on the pressure transient, which cannot be obtained from conventional analysis, such as the larger radius of investigation and adapted rates. These are corrected rates based on the available pressure history which has become a very useful tool when rates are not measured, reported inaccurately or are unavailable. Additional information on deconvolution and references are shown in Appendix D.

Deconvolution is used at this stage to determine a first approximation of rate history to enable the pressures at the BOP datum depth to be converted (translated) to the reservoir depth. This is to enable the well test interpretation to be done with pressures at reservoir conditions as is the case with conventional well testing e.g. drill stem tests (DST) or production tests.

The key steps used in the deconvolution process for the Macondo well include:

- Identify the pressures to be used in the deconvolution

- Linearly interpolate flowing pressures in periods where there are gaps of pressure data

- Calculate and input the initial pressure at the correct datum depth

- Assume an initial rate history

- Apply deconvolution to the entire pressure and rate history

- Quality check the results which includes:

  - Check Input assumptions

  - Compare the deconvolved derivative (drawdown) with the actual build up derivative from the Macondo shut-in

  - Check that the convolved pressures from the deconvolved derivative closely matches the actual (input) pressure history, with a percentage error difference of less than 1% and 10% during the buildup and flowing periods respectively.

  - Depending on the quality of the pressure match (convolved pressure versus actual pressures), revise the deconvolution through an iterative process. This involves using the output rates (adapted or sometimes called corrected rates) from the deconvolution as the initial rate assumption in the subsequent deconvolution stage. The pressure match quality is re-evaluated. The iterative process leads to a convergence of the rates and is completed when the match quality is acceptable.

- The results of the process include:

  - The production rate history required for well test analysis and pressure translation

  - The deconvolved derivative which provides additional information on the pressure transient and is used for diagnosis and selection of the correct interpretation model.

TREX-011696R.128

3.2.1 Pressure History

The pressure data described in Section 1.2.3 is used in this stage. In order to apply deconvolution, it was linearly interpolated where there are gaps in the pressure history. Shown in Figure 7 is the input pressure history (with linear interpolation) compared with the actual pressure measurements.
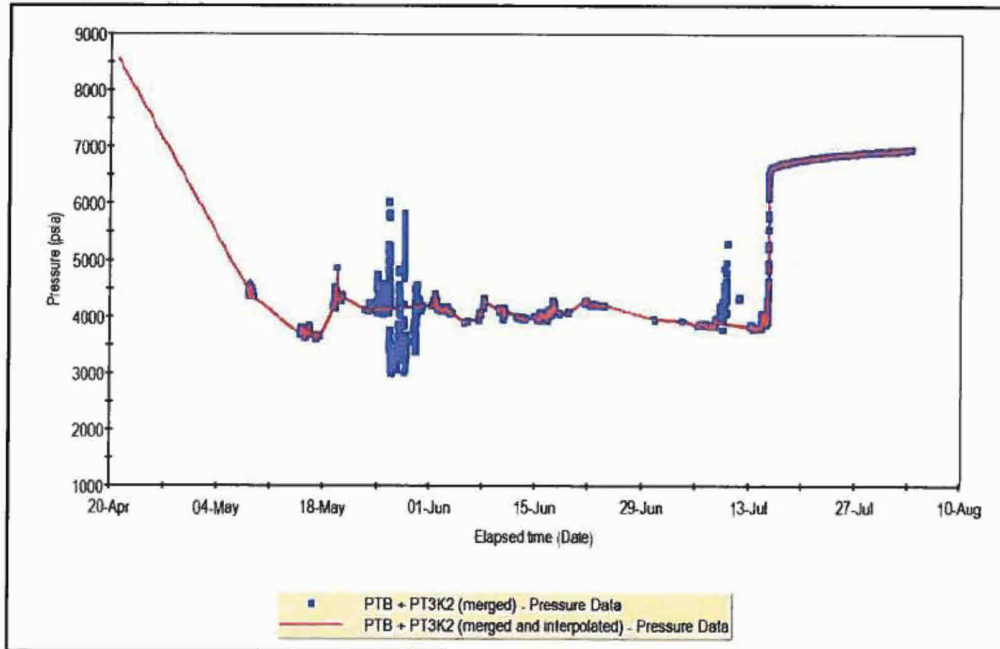

Figure 6: Comparison of BOP Datum Pressure from PTB and PT3K2 with Linearly Interpolated Pressures

3.2.2 Well Head Pressure (WHP) Deconvolution – Constant Rate Initial Assumption (Option-1)

I assume a constant rate of 45,000stb/d for the starting point in the analysis, which is then adjusted through deconvolution. Figures 8 – 14 below show the input pressures and rates, successive iterations of pressure rate histories, the final deconvolved derivative, the pressure match and quality of the pressure match. The quality (error difference) indicates a very good match and hence a reliable deconvolved derivative and adapted rates.

Figure 8 below shows the constant rate used as the starting point in the analysis with the corresponding input pressures as a function of time. All time axes (x-axes) are in hours unless otherwise stated on the x-axis and are the elapsed time from the start of the blow-out.

Figure 9 shows the corrected (adapted, step-1) rates from the deconvolution process and the corresponding percentage difference with respect to the starting constant rate. The percentage difference is the ratio of the input rate to the output (adapted rate). The trend in Figure 9 indicates that based on the pressure response, the rates need to be significantly corrected. Over the first 300 hrs, the error difference gradually decreased from 70% in the 1st hour to about 0% after 300 hrs. From 300 hrs to 600 hrs, the correction went from about 0% to -35%, after which the corrections generally hovered around +/-20%. This indicates relatively lower production rates at the start of the blow-out.

The quality of the deconvolution process is assessed by checking how convolved pressure based on the adapted rates match the input pressures as shown in Figures 12 and 13. A second iteration was done to further improve the match quality. This was done by using the output rates from step-1, with the same

13

input pressures and repeating the deconvolution (Figure 10). This showed the rates in the first 200 hrs had to be further reduced (by 60% in the first hour and gradually decreasing to 0% at about 200 hrs). The corrections from 200 to 2000 hrs were generally with 5%. The resulting deconvolved derivative is shown in Figure 11 and error difference between the convolved pressure and input pressure is shown in Figure 14. The match quality of the convolved pressure to the Macondo shut-in data from the 15th of July 2010 to 03rd August 2010 is less than 1% and indicative of a good pressure match.

This indicates a deconvolved derivative consistent with the rate and pressure history.
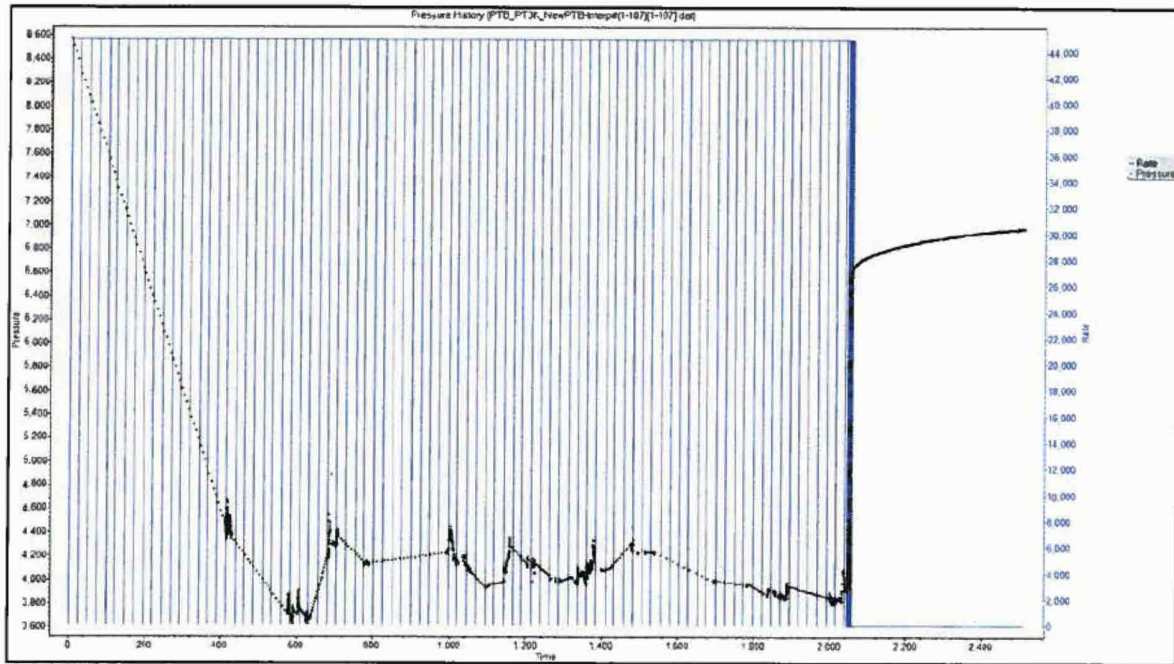
Figure 7: Input Pressure and Rate (Constant Rate of 45,000stb/day)

Figure 8: Comparison of Input and Adapted Rates (Iteration 1)

Figure 9: Comparison of Input and Adapted Rates (Iteration 2)

15

Figure 10: Deconvolved Derivative (Iteration 2)

PTB + PT3K2 (merged) - Pressure Data
PTB + PT3K2 (merged and interpolated) - Pressure Data
CP(1-107)[1-107](1.1933E+09)8570 - Pressure Data

Figure 11: Pressure Match (Iteration 2) – CP (Convolved Pressure)

16

Figure 12: Pressure Match (Iteration 2) – CP (Convolved Pressure) – Zoom into Shut-in period

Figure 13: Quality Check on Error Difference (Convolved Pressure)

TREX-011696R.133

3.2.3 Well Head Pressure (WHP) Deconvolution – Step Rate Initial Assumption (Option-2)

The step rate assumption of 30,000stb/d from 20th April 2010 to 31st May 2010 and 45,000stb/d from 1st June 2010 to 15th July, 2010 was made. Figures 15 – 25 below show the input pressures and rates, successive iterations of pressure rate histories, the final deconvolved derivative, the pressure match and quality of the pressure match. The quality (error difference) indicates a very good match.
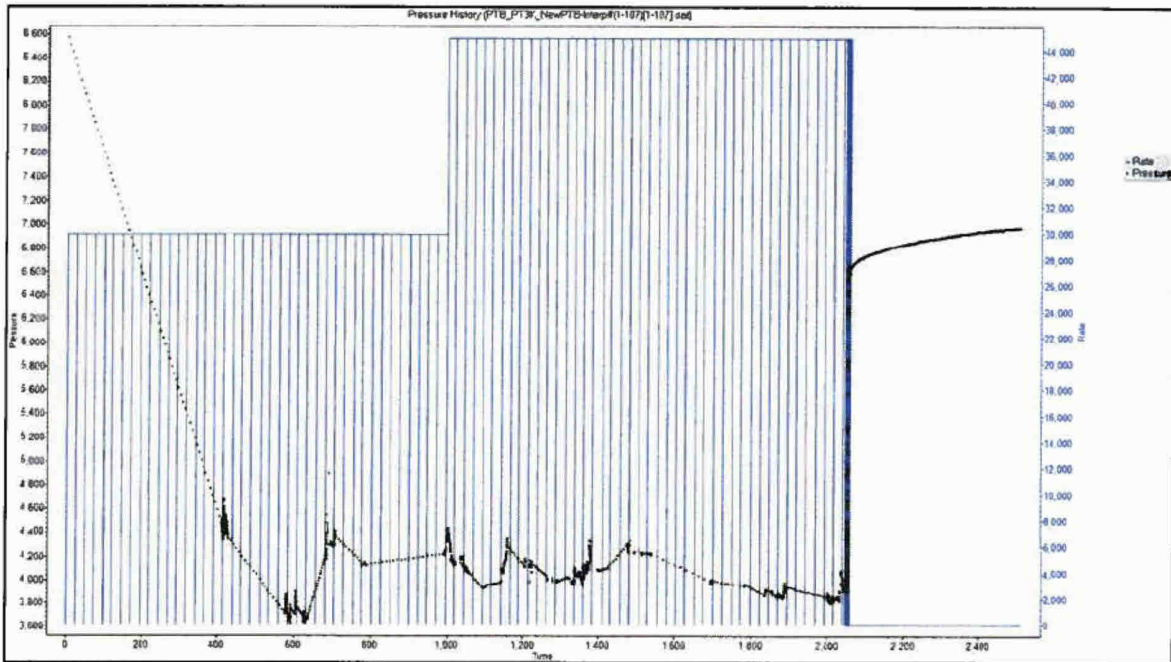
Figure 14: Input Pressure and Rate (Step Rate of 30,000stb/d to 45,000stb/day)
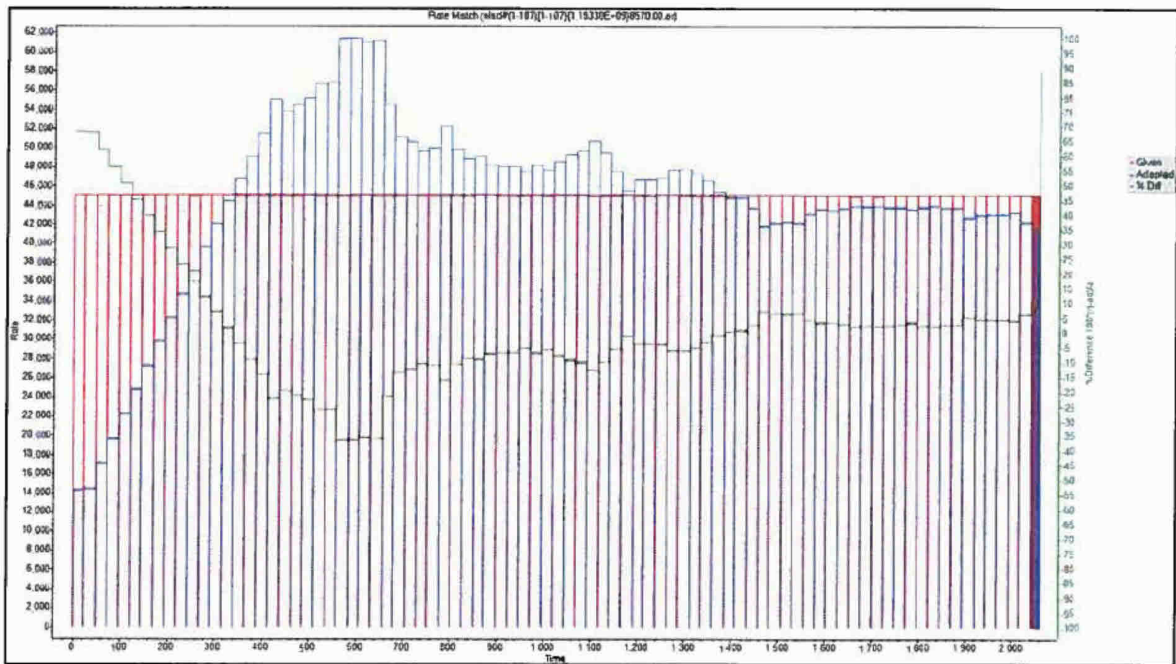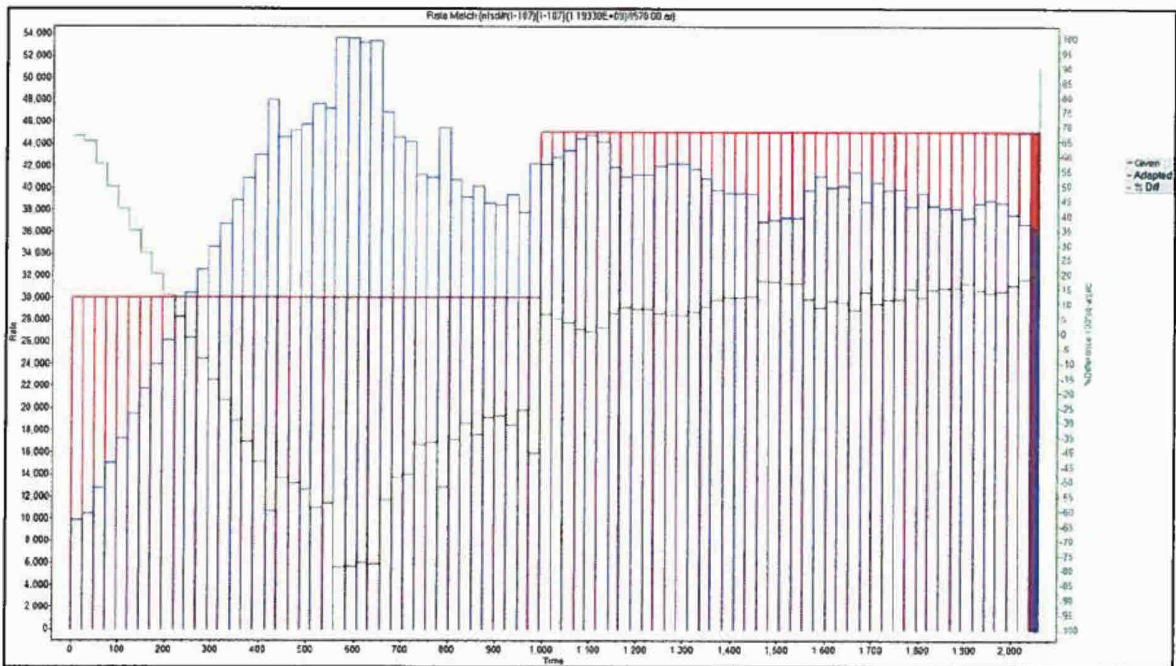

Figure 15: Comparison of Input and Adapted Rates (Iteration 1)
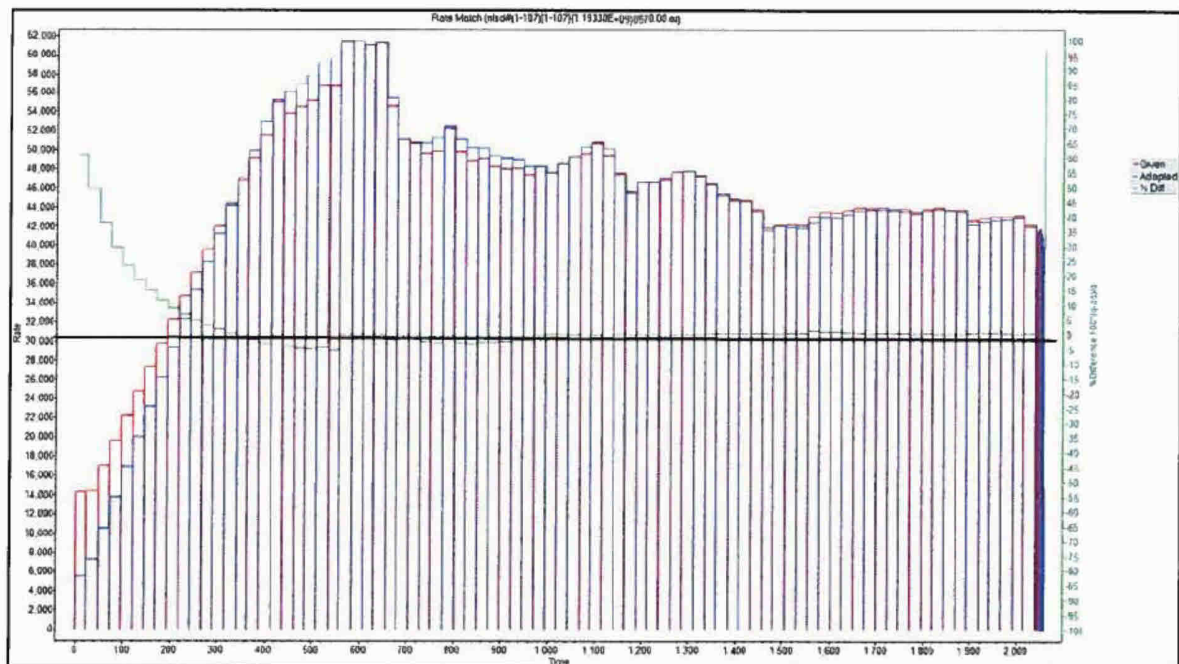
18
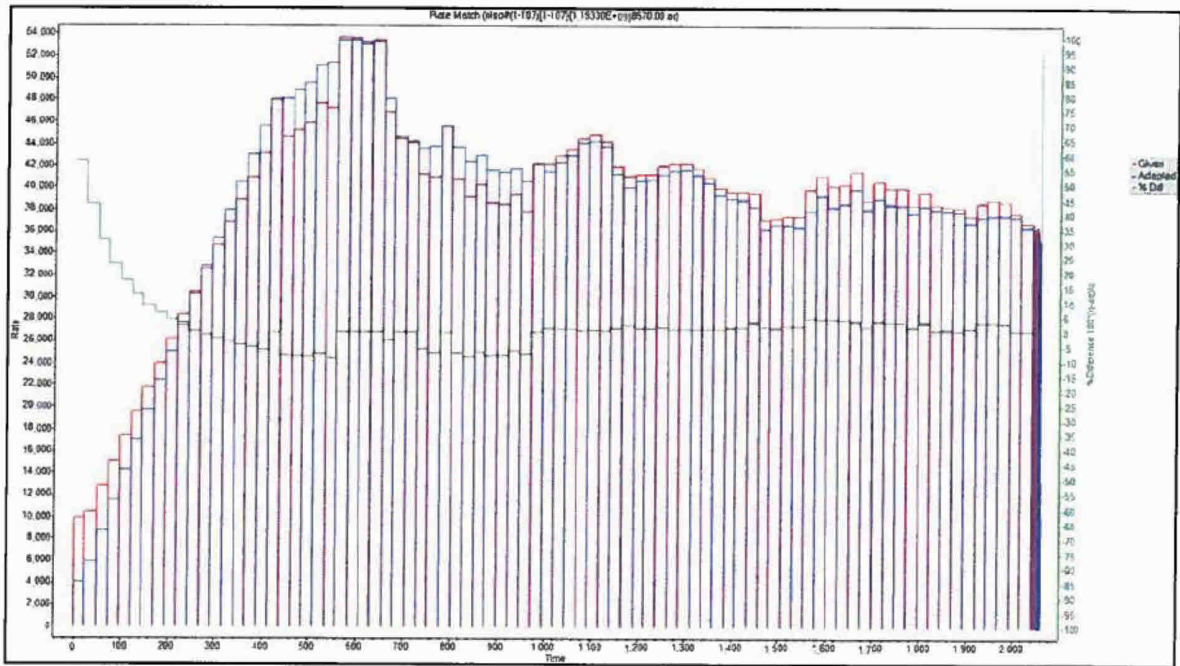
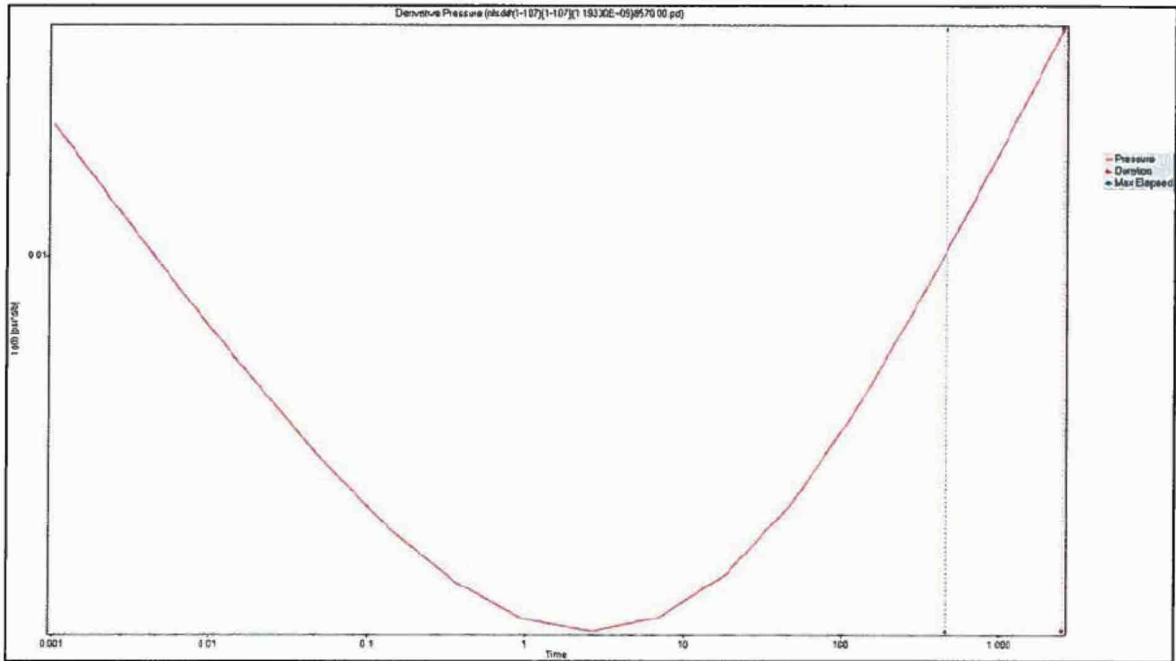**Figure 16: Comparison of Input and Adapted Rates (Iteration 2)**
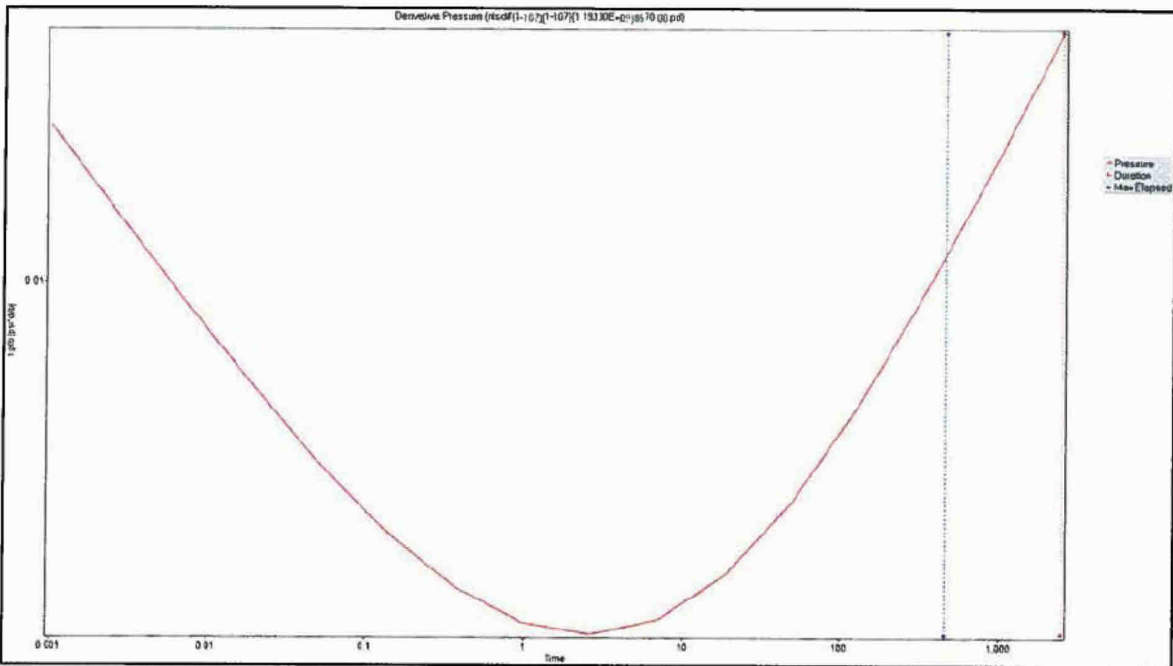
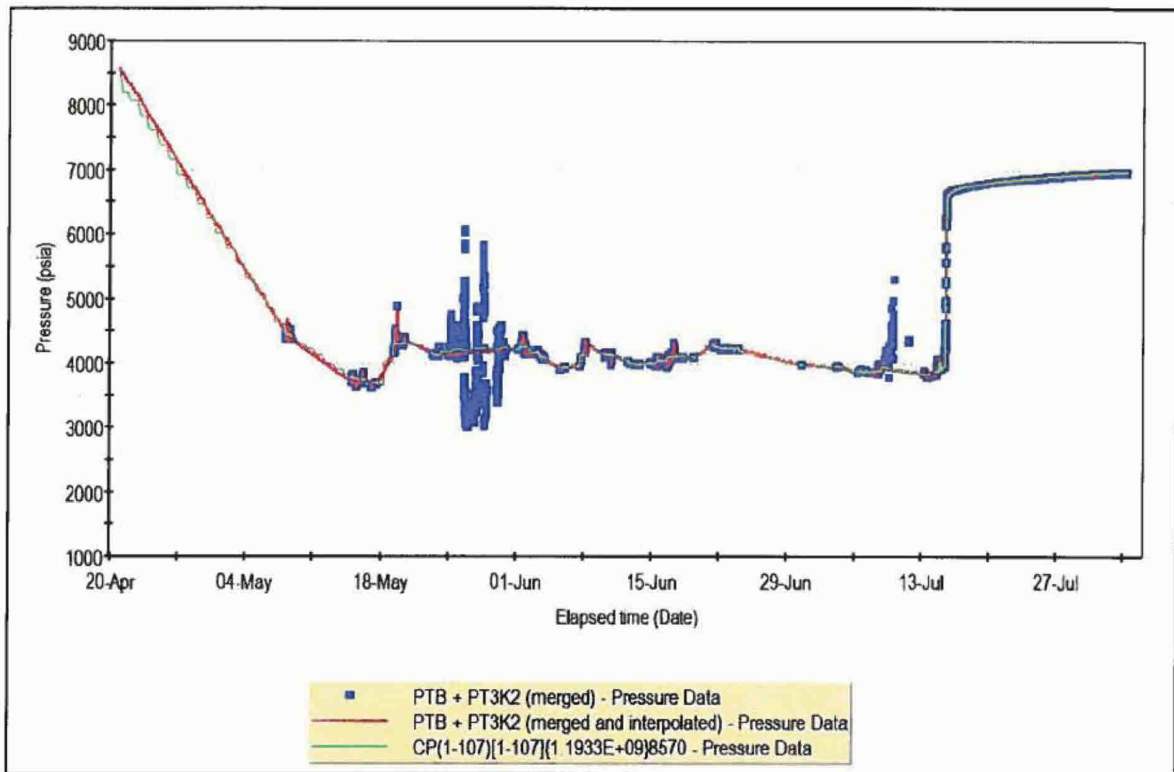**Figure 17: Deconvolved Derivative (Iteration 2)**

19
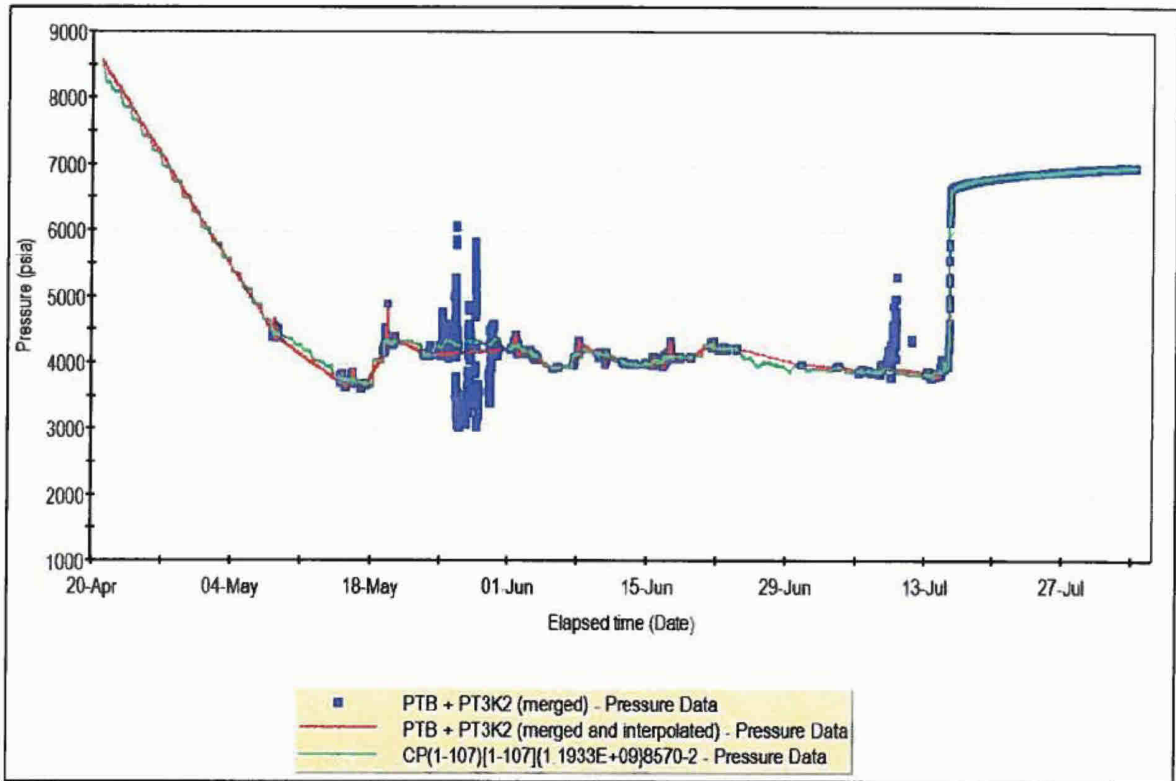
Figure 18: Pressure Match (Iteration 2) – CP (Convolved Pressure)
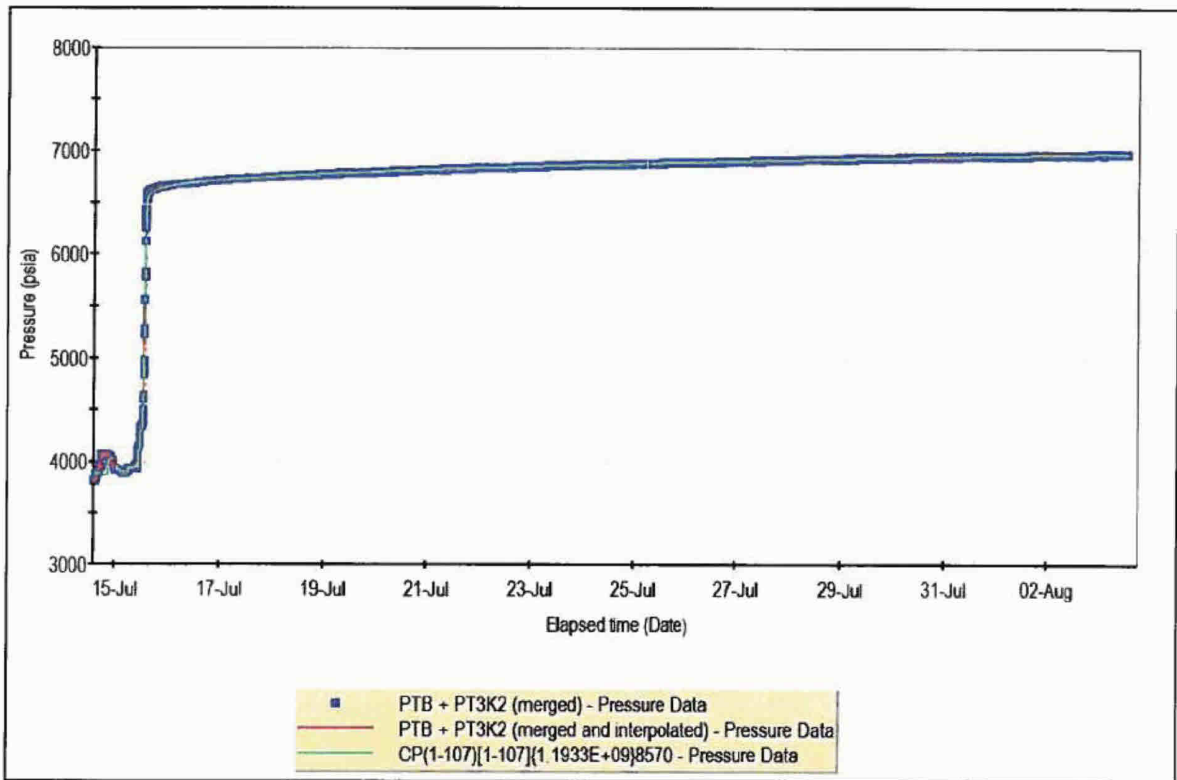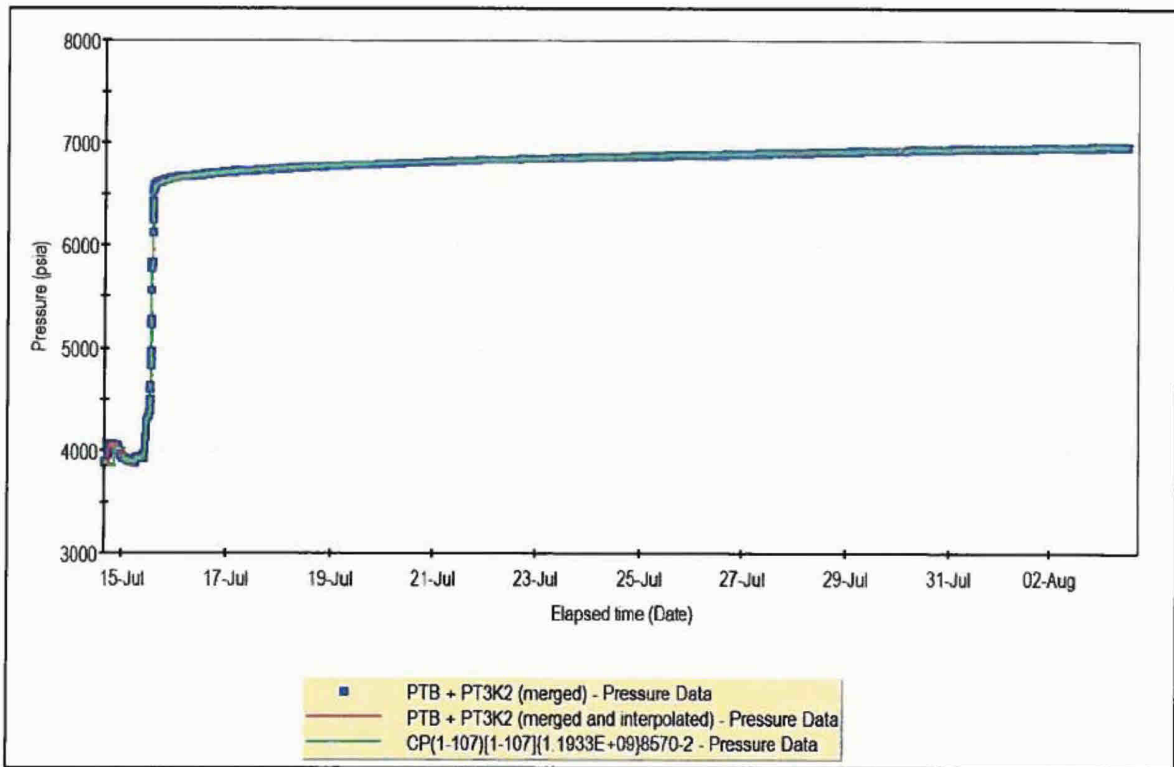

Figure 19: Pressure Match (Iteration 2) – CP (Convolved Pressure) – Zoom into Shut-in period
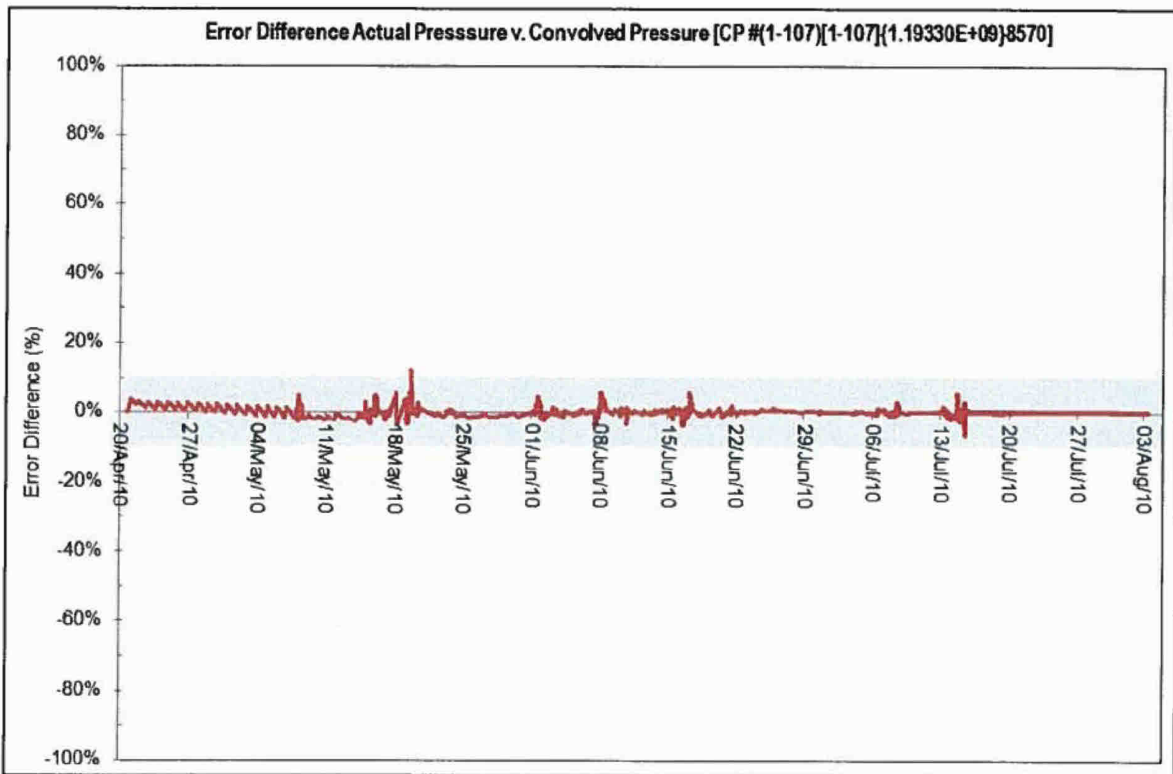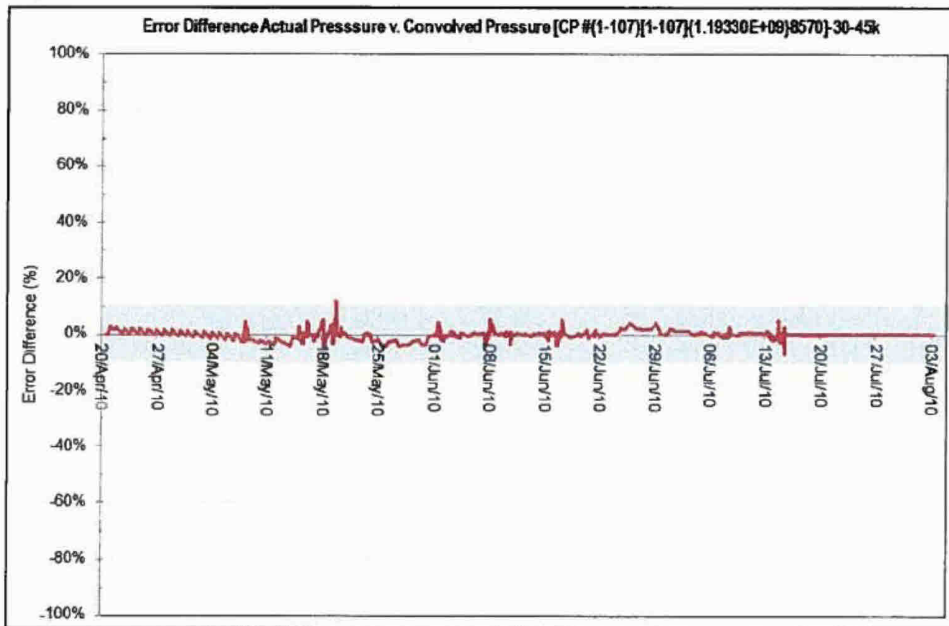
Figure 20: Quality Check on Error Difference (Convolved Pressure)

3.2.4 Discussions and Comparison on Resulting Production Rate Histories

A comparison of Option-1 and Option-2 indicate that the calculated rate histories for both assumed input (starting) rate profiles yield similar production rate trends and displaced by a ratio of about 15%. This indicates the relative rate profile from deconvolution is a function of the input pressures and is less affected by the assumed initial rate history. Both rates are used to translate the well head pressures (BOP datum, 4,972 ft TVDss) to the reservoir depth (18,056 ft TVDss) and are scaled proportionally to match the permeabilities from the MDT during the well test interpretation process.
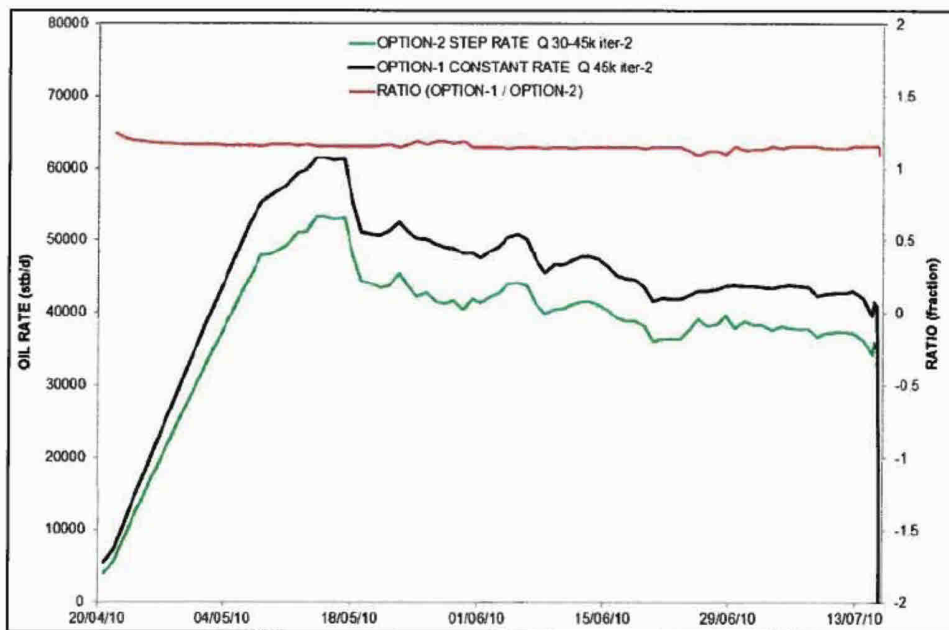
Figure 21: Rate Comparison (Option-1 vs. Option-2)

21

3.3 PRESSURE TRANSLATION TO RESERVOIR DEPTH

The shut-in pressures were translated from the BOP datum depth to the reservoir depth by Professor. Martin Blunt and take into account the pressure changes, including those caused by cooling of the fluid in wellbore during the shut-in.[vii] Three scenarios were generated based off fluid properties for CoreLab, Schlumberger and Intertek.

The flowing pressures up to the time of shut-in were translated using Schlumberger fluid properties.[viii] Two drill pipe scenarios were considered:

- Drill Pipe Low
- Drill Pipe High

The drill pipe high scenario assumes 2513 feet of 5.5 inch drill pipe hung from the bottom of the BOP and the 5.5 inch drill pipe was connected to 800 feet of 3.5 inch drill pipe. The drill pipe low scenario assumes the top of the drill pipe was at a depth of 9318 ft TVDss and 163 ft of the 3.5 inch drill pipe was in the 7in Casing.
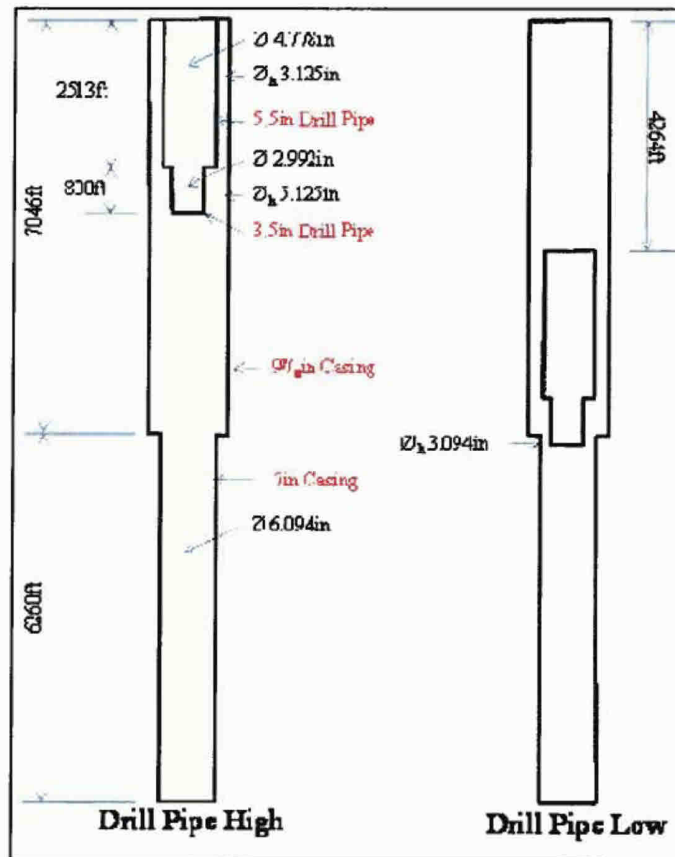
Figure 22: Drill Pipe Scenarios[2]

Shown in Figure 24 to 25 are plots of the translated pressures to reservoir depth for the following options:

- Option1 – Drill Pipe High
- Option2 – Drill Pipe High
- Option1 – Drill Pipe Low

22

- Option2 – Drill Pipe Low

Where Option-1 refers to the deconvolution generated rates with an initial constant rate assumption and Option-2 with the step rate assumption.
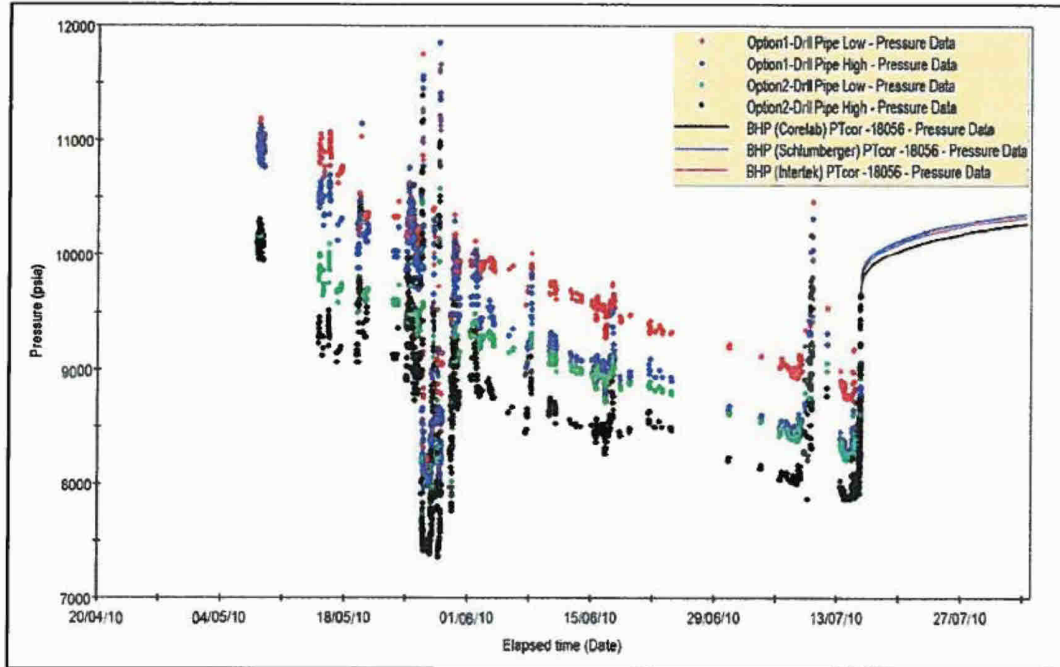
Figure 23: Translated Bottomhole Pressures
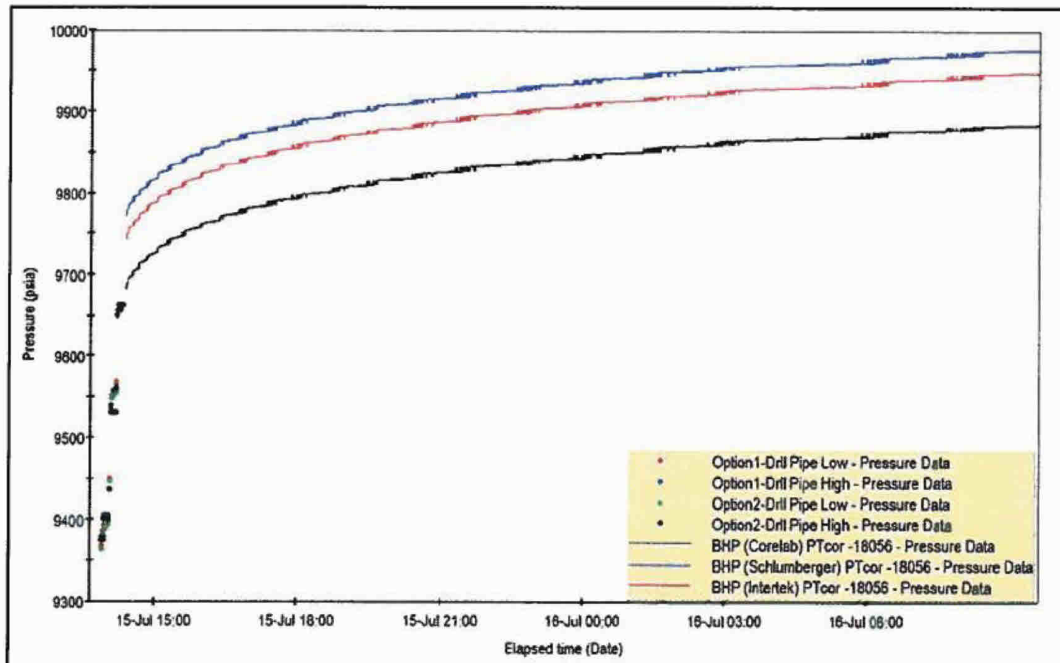
Figure 24: Translated Bottomhole Pressures – Zoom into Shut-in

23

A close look at the zoom pressures (Figure 25) reveals that the shut-in pressure data converted with CoreLab fluid properties synchronises well with the all the translated flowing pressure data. As a result, four data sets are generated by merging the four flowing bottomhole pressures with the shut-in pressure translated using CoreLab fluid properties (Figure 26). The shut-in pressures based on CoreLab fluid is the lowest pressure data of the three sets. The CoreLab pressure data results in a greater depletion calculation than if the Intertek or Schlumberger pressure data was used. We also ran one case using Schlumberger-translated shut-in pressures.
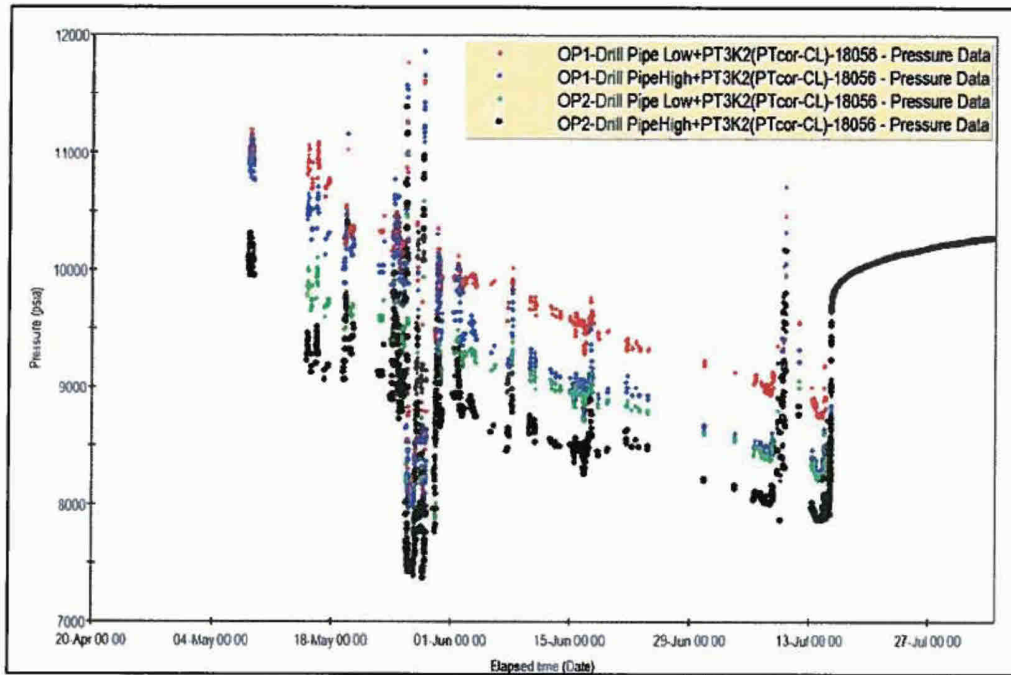
Figure 25: Translated Bottomhole Pressures (Merged)

Linear interpolation is used to fill in the gaps with missing flowing bottomhole pressure in order to generate a continuous pressure history (Figure 27) prior to deconvolution. The noisy data during the top kill (26th May 2010 to 29 May 2010) and noisy data during interventions (9th July 2010 to 12th July 2012) are excluded.

24
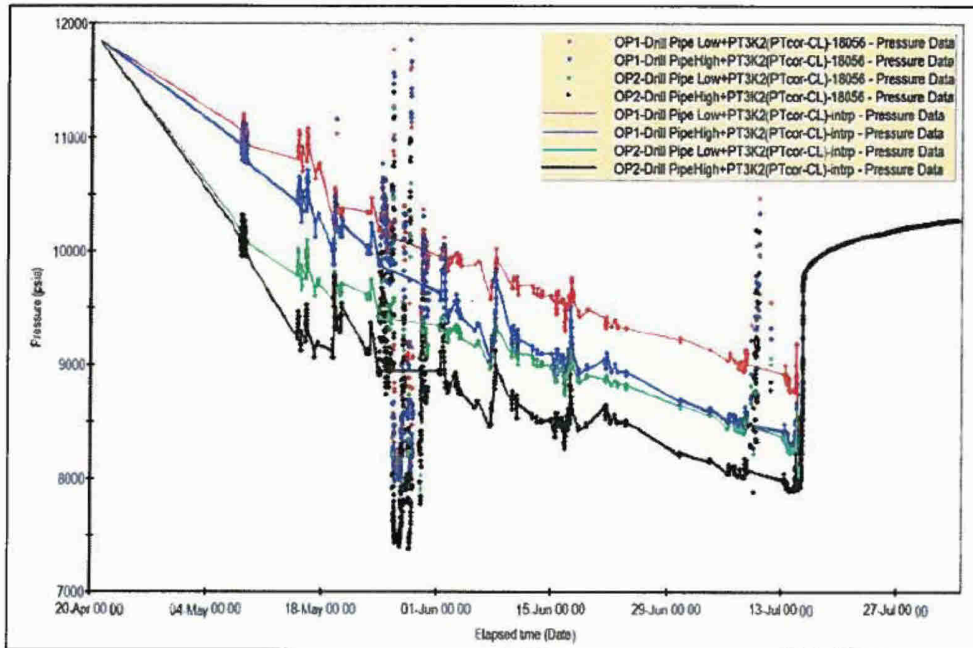
Figure 26: Translated Bottomhole Pressures (Merged with Linear Interpolation)

3.4 WELL TEST ANALYSIS (Pressures Translated To Reservoir Depth)

3.4.1 OPTION-1 DRILL PIPE HIGH

3.4.1.1 Flow Period Selection

A total of 107 flow periods were used to represent rate variations during the entire production and pressure history. A flow period signifies a period of changing pressures due to a rate change. The period when the Macondo well is fully shut-in is flow period 107.
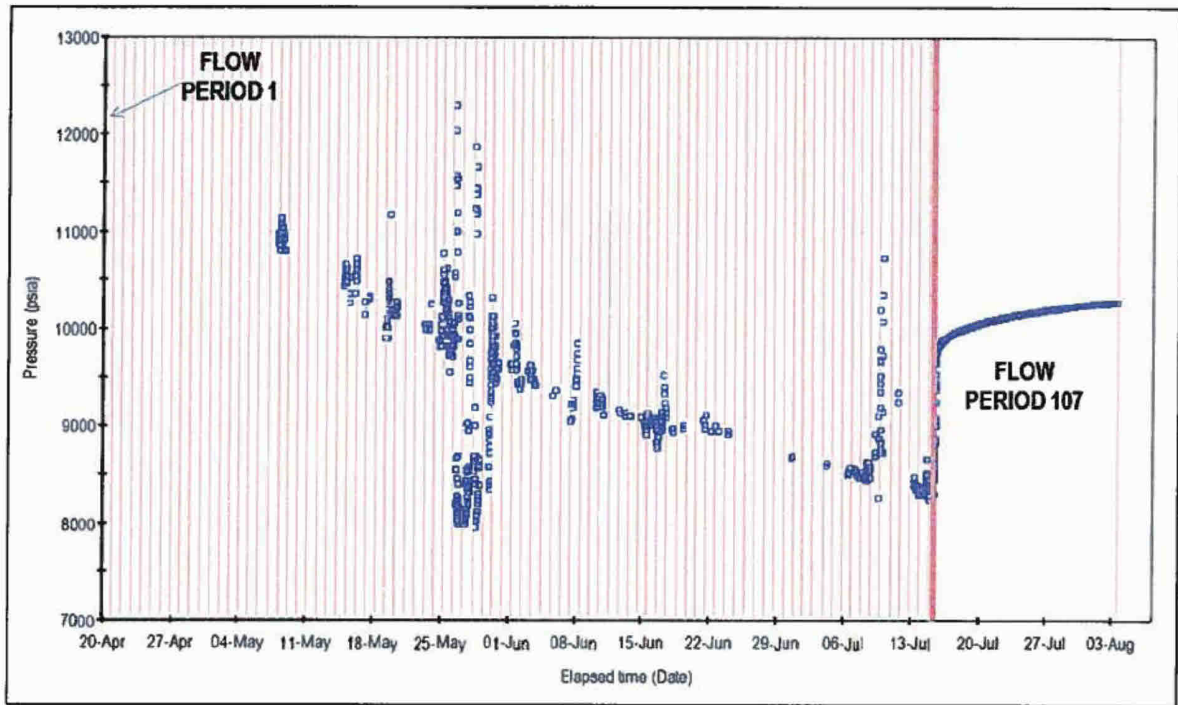
Figure 27: Flow Period Selection

3.4.1.2 Deconvolution

Figures 29 – 40 below show the input pressures and rates, successive iterations of pressure rate histories, the final deconvolved derivative, the pressure match and quality of the pressure match. The quality (error difference) indicates a very good match at the 4th iteration.
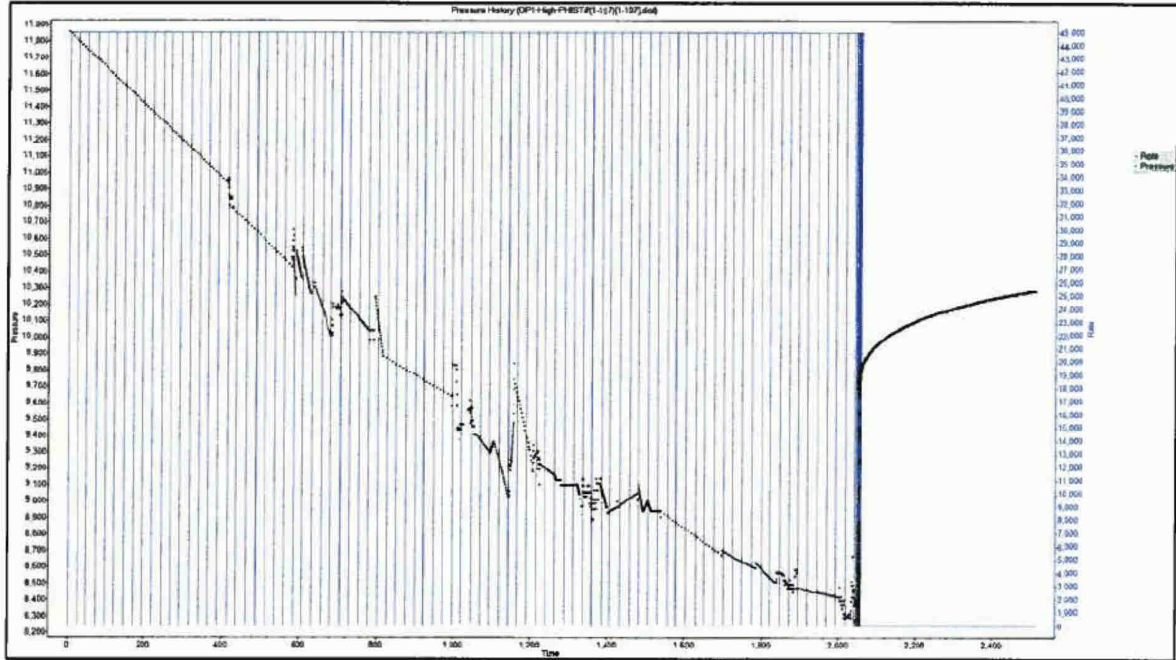
Figure 28: Input Pressure and Rate
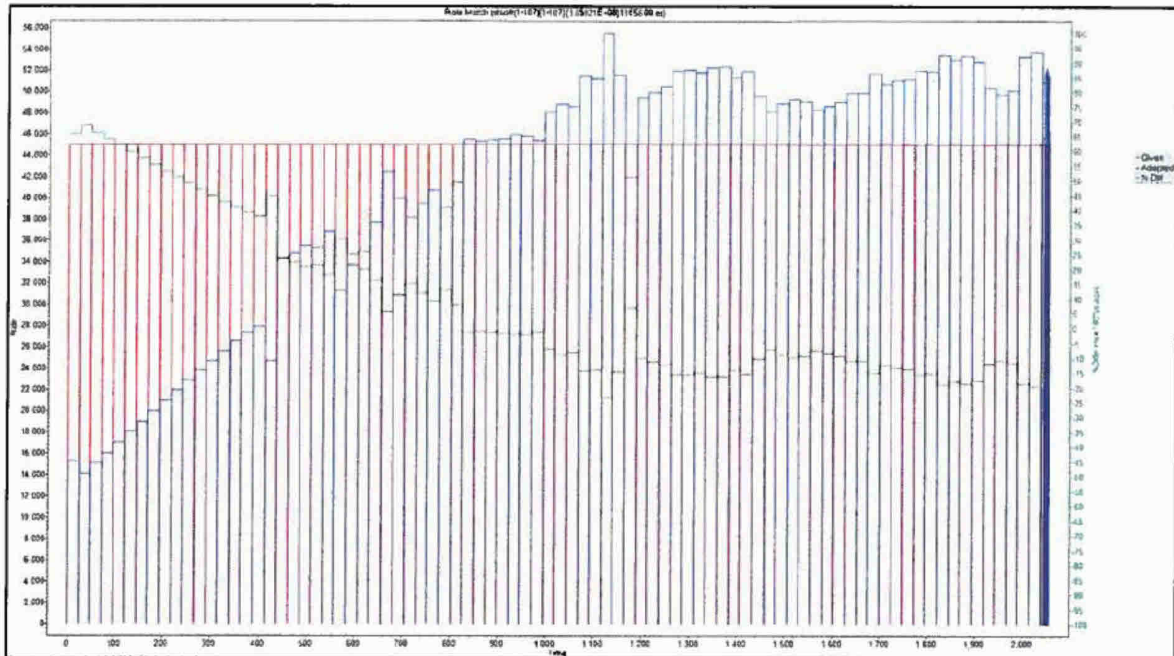
Figure 29: Adapted Rates (Iteration 1)

27
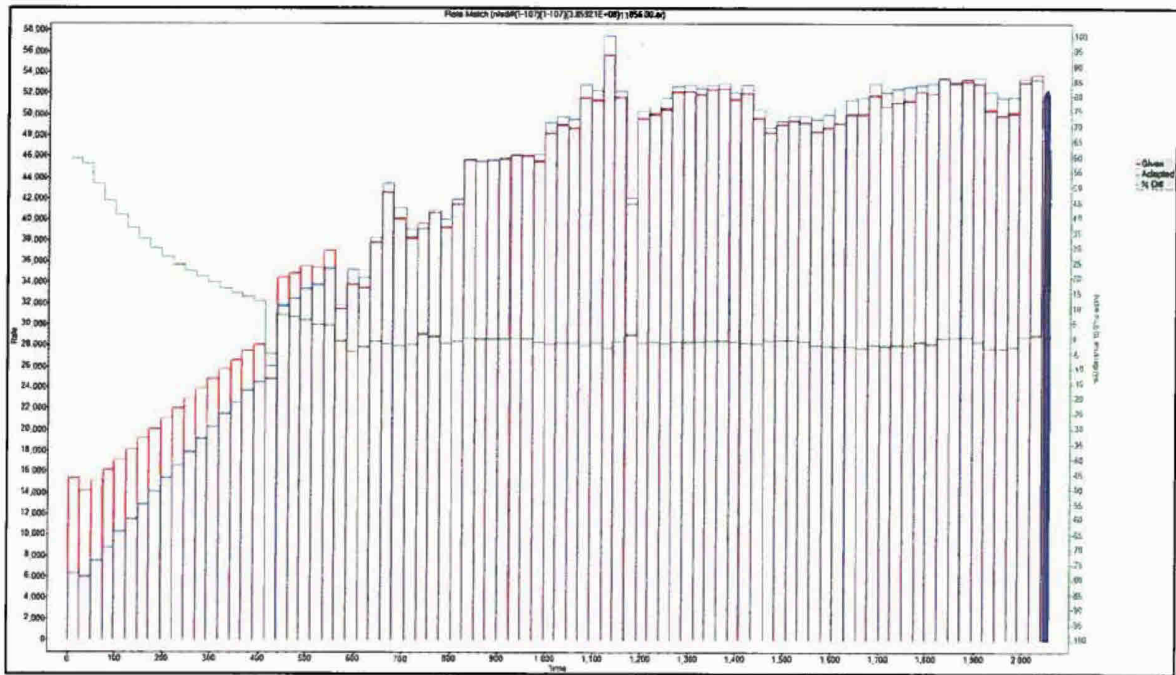
Figure 30: Adapted Rates (Iteration 2)
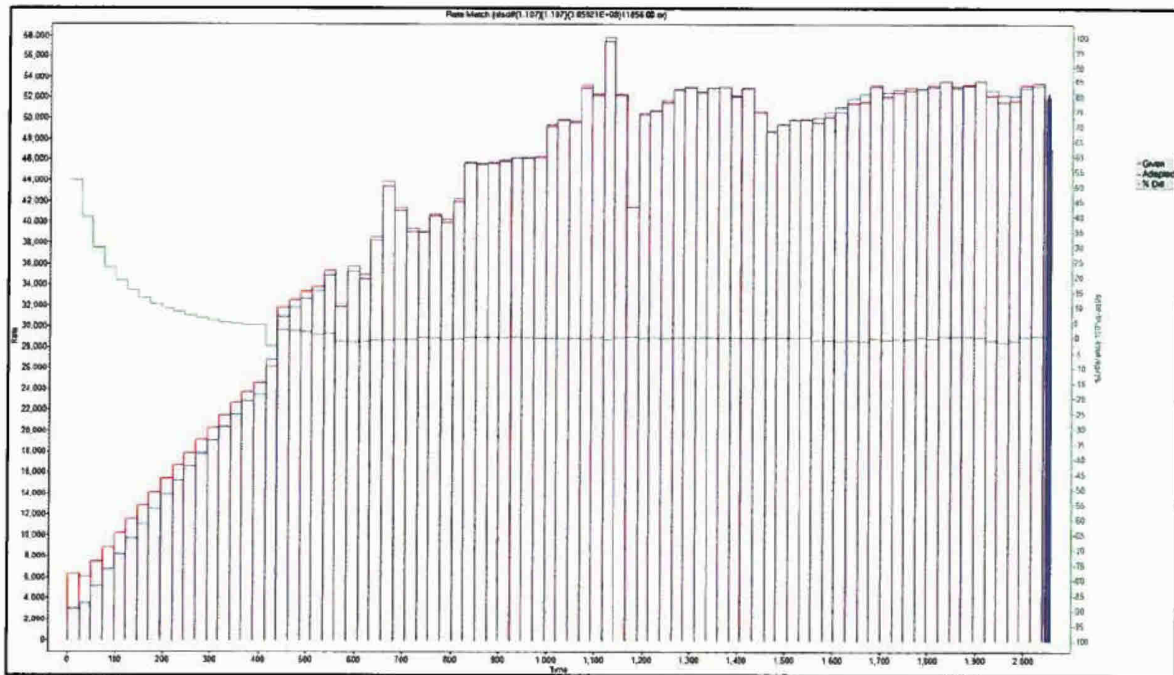
Figure 31: Adapted Rates (Iteration 3)

28

TREX-011696R.144
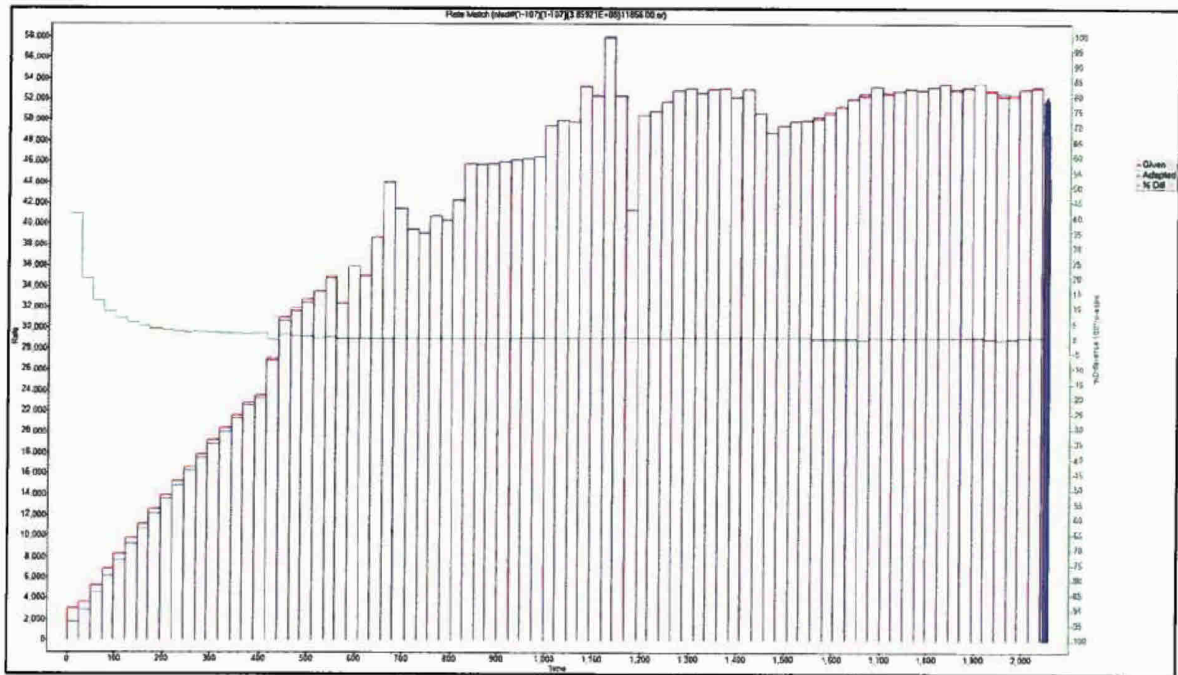
Figure 32: Adapted Rates (Iteration 4)
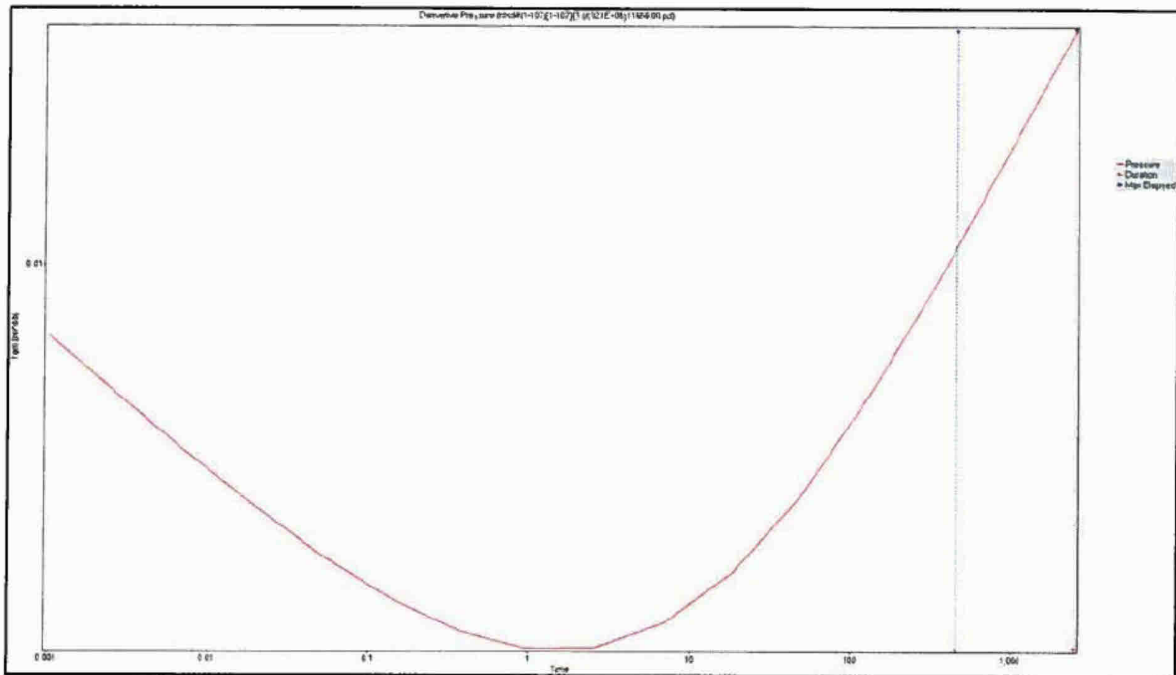
Figure 33: Deconvolved Derivative (Iteration 4)

29

TREX-011696R.145
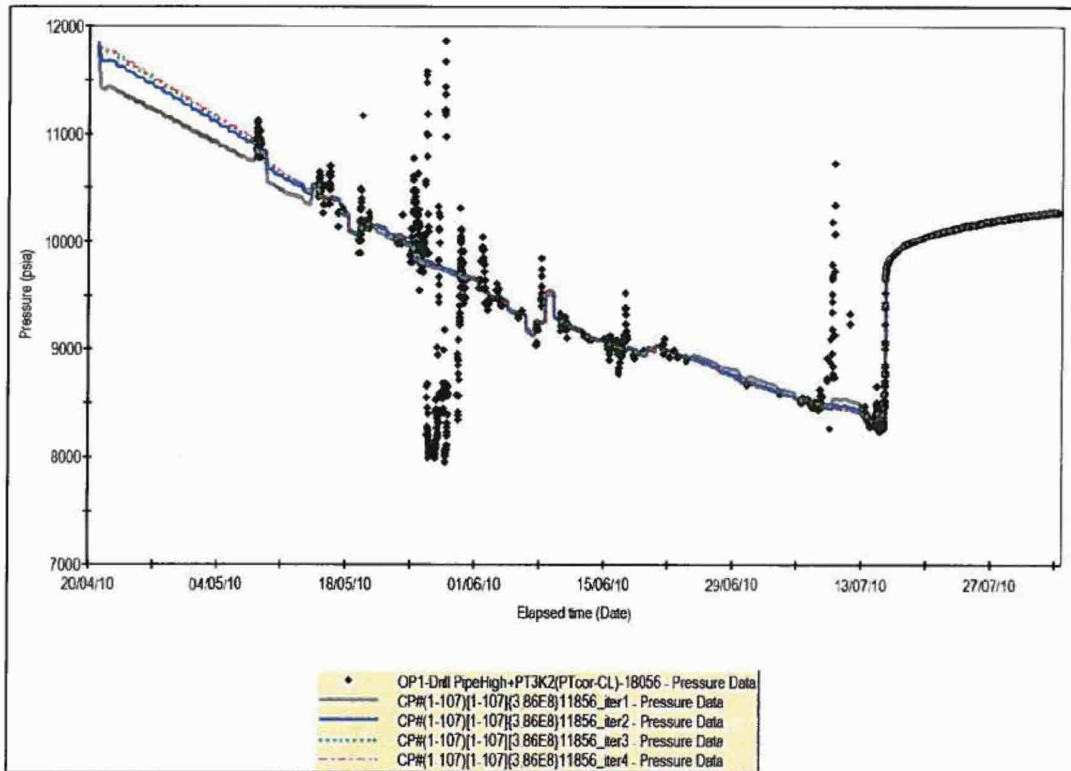
Figure 34: Pressure Match to Actual Translated Pressures (1)
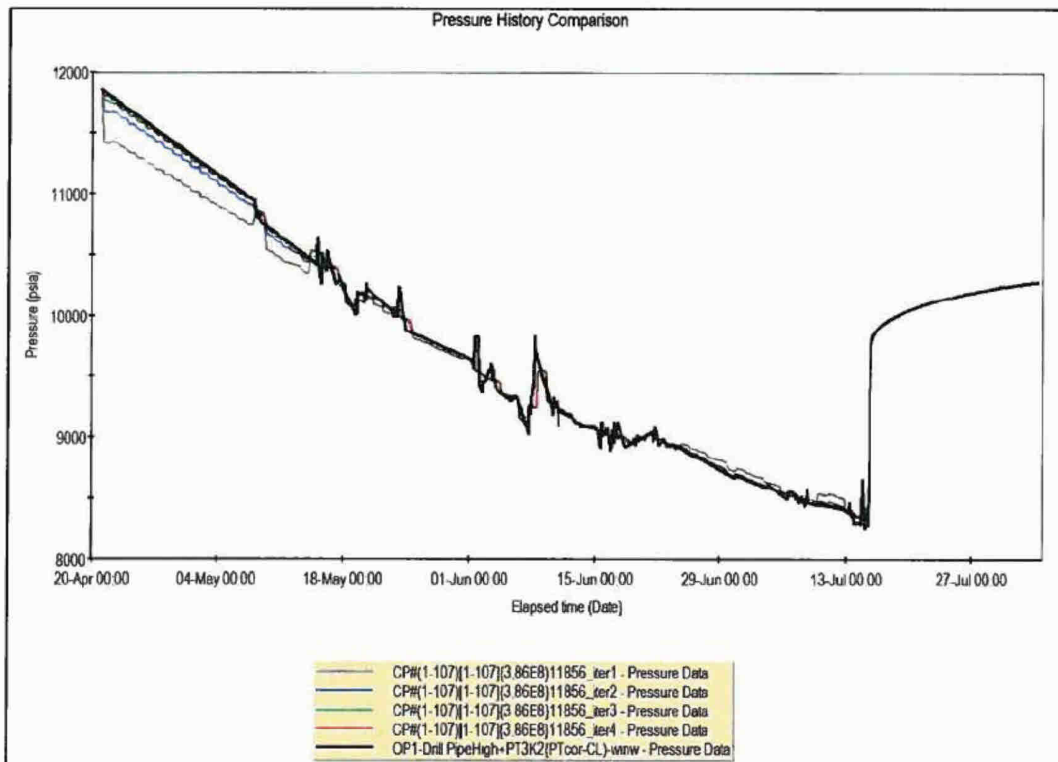
Figure 35: Pressure Match to Input Linearly Interpolated Pressures (1)

30
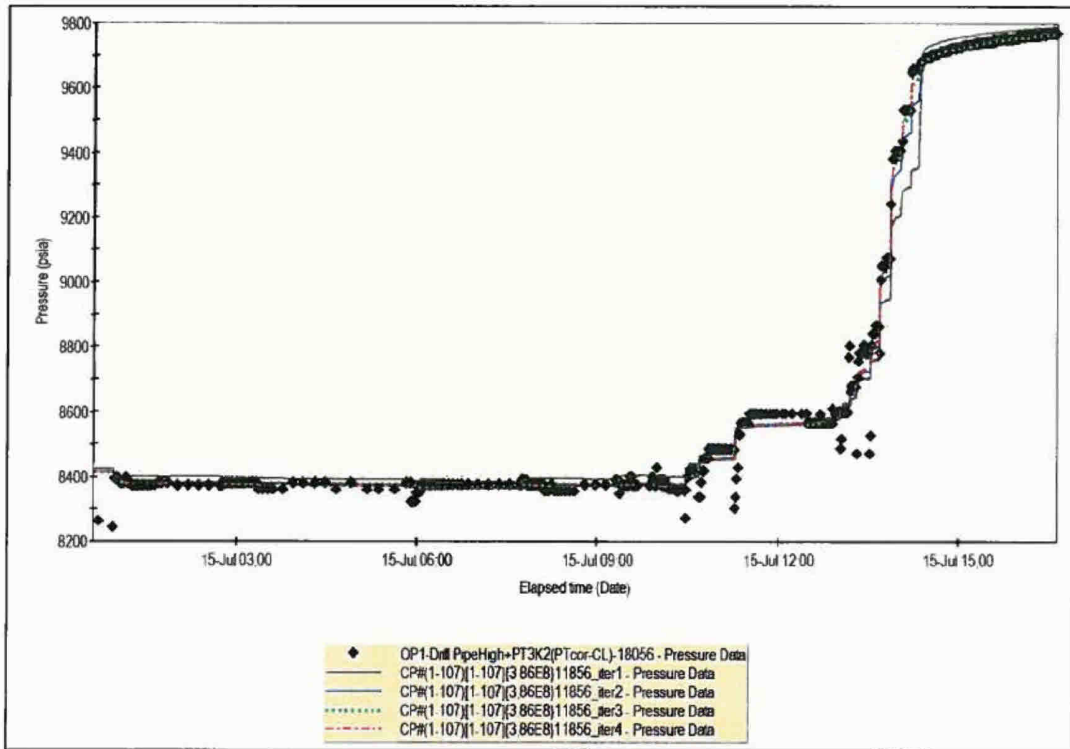
Figure 36: Pressure Match to Actual Translated Pressures (2)
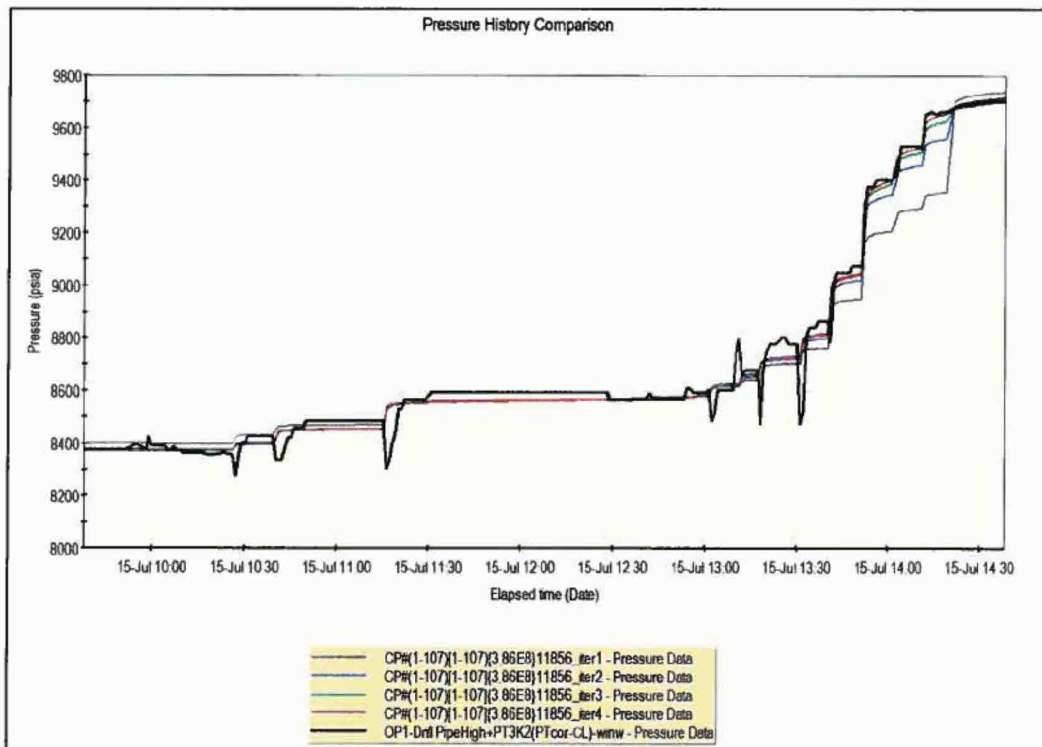
Figure 37: Pressure Match to Input Linearly Interpolated Pressures (2)

31

TREX-011696R.147
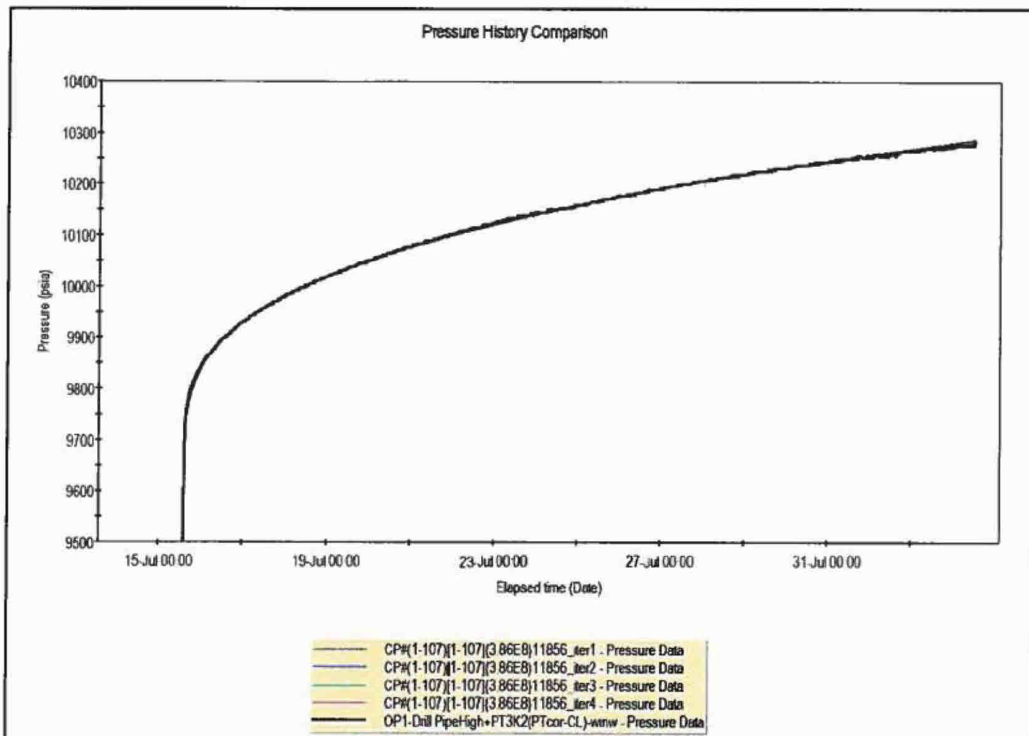
Figure 38: Pressure Match to Input Linearly Interpolated Pressures (3)
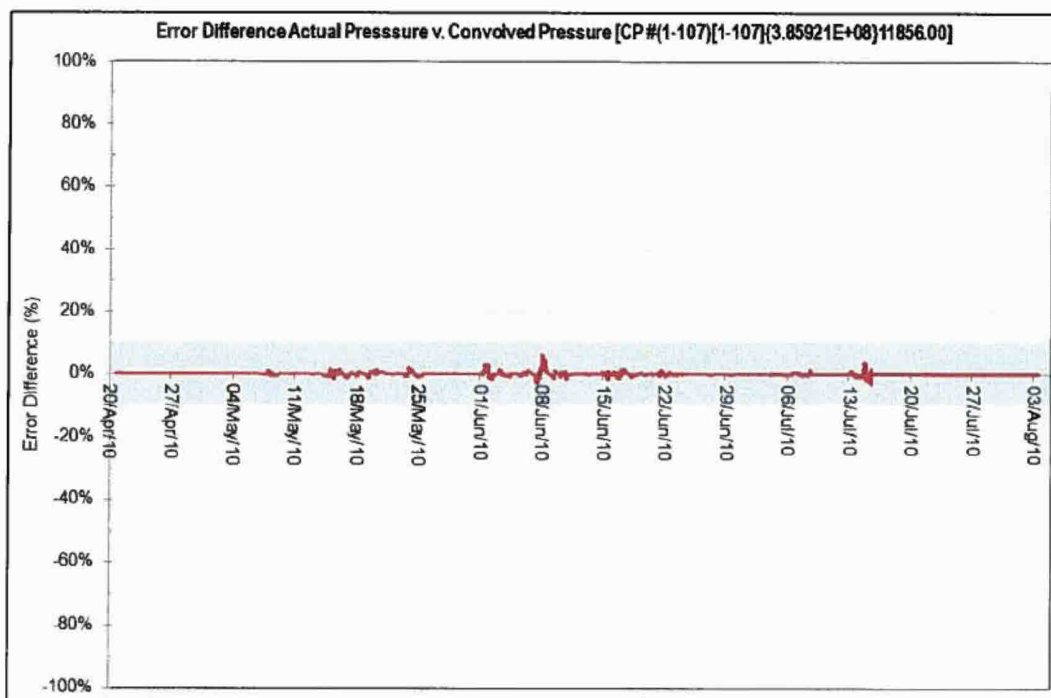
Figure 39: Quality Check on Error Difference (Convolved Pressure – iteration 4)

The convolved pressure match at the fourth iteration was near excellent and used as the rate profile in the well test analysis. The rates are scaled linearly to match the MDT uncertainty range of permeabilities (P50 238mD, P90 170mD, P10 329mD and Mean Permeability 245mD).

3.4.1.3 P50 Permeability Well Test Analysis

Shown in Figures 41 – 45 are the model diagnosis, interpretation model, model matches and analysis results which confirm a very good match to the pressure history, log-log pressure change and derivative, and the superposition (Horner) plot.

Brief description of the plots on Figure 41:

Top Left – (Log-Log Diagnostic Plot): Shows the pressure change data [P(Δt) – P(Δt=0)] during the Macondo Shut-in (top blue squares) and the pressure derivative data (bottom blue triangles) on a log-log plot. Superimposed on the pressure derivative data is a green line indicating where the radial flow stabilisation level has been picked on the pressure derivative data. The dark blue diagonal line has a slope of 0.5 and indicates linear flow due to the Macondo boundaries. The flow regime changes from radial flow to linear flow when the pressure response becomes affected by the impact of the channel boundaries. The diagnostic plot allows the selection of the interpretation model.

Top Right (Model) – This shows a description of the interpretation model used for the analysis

- Early time: Wellbore Storage and Skin
- Middle time: Homogenous reservoir
- Late time: Closed rectangular reservoir (A closed rectangular reservoir can be described as a channel with 'two parallel boundaries' with both ends closed. The closed system is verified using deconvoloution.)

Middle Left – (Horner Diagnostic Plot): Shows the position of the radial flow line on the Horner plot. This plot shows that the radial flow line from the derivative log-log plot corresponds to a straight line on the Horner plot and confirms the diagnosis of the radial flow interval.

Top Middle – (Log-Log Match): Shows the match of the interpretation model (red lines) to pressure change data [P(Δt) – P(Δt=0)] during the Macondo Shut-in (top blue squares) and to the pressure derivative data (bottom blue triangles) on a log-log plot.

Middle Middle – (Horner Match): Shows the model match (red lines) on the Horner plot and the extrapolation of the models to infinite times (x-axis = 0) to give the final reservoir pressure.

Bottom Left – (Skin vs. Time): This shows the required skin to match the pressure history based on the rates and interpretation model. An initial Skin of 19.7 was computed based on a partial penetration skin, which assumes flow from 16.5ft from 93ft of net reservoir with a Kv/Kh of 0.1.

Bottom Middle – (Simulation – Variable Skin): This match of the simulated pressure based on the interpretation model using the input rates with the input pressures.

Middle Right – (Results): This shows the results of the well test analysis and is based on the interpretation model and model parameters

33
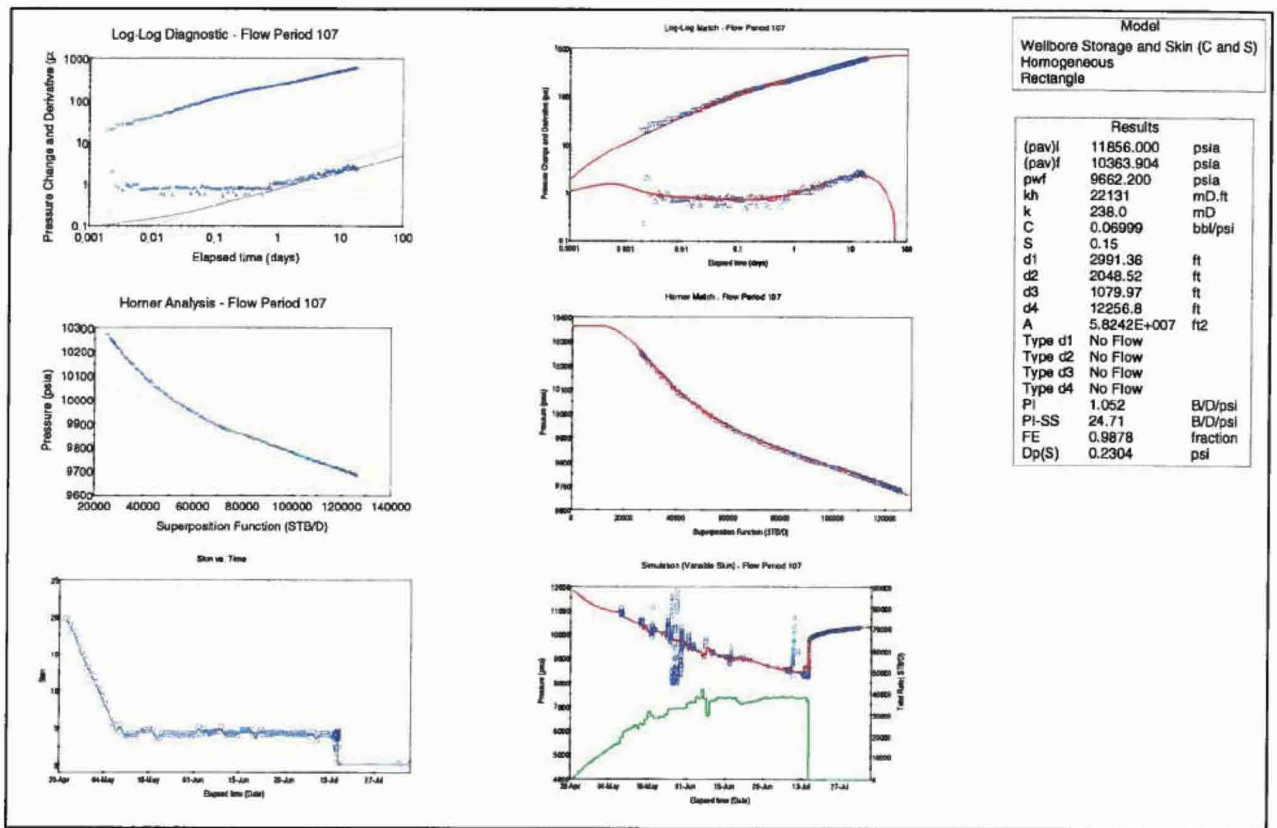
Figure 40: Diagnosis, Interpretation Model, Model Match and Analysis Results

The match to the pressure history at various scales, further confirm a good match giving more validity to the analysis results and higher confidence predicting the Macondo well and reservoir properties using the matched interpretation model.

Below are additional plots (Figures 42-45) showing the model match at various scales. The formats of the plots below are:

- Top Left: Analysis results
- Bottom Left: Interpretation model
- Top Middle – Log-Log plot of pressure change and pressure derivative
- Bottom Middle – Skin versus Time
- Top Right – Simulation Pressure History Match using Variable Skin
- Bottom Right – Horner Match
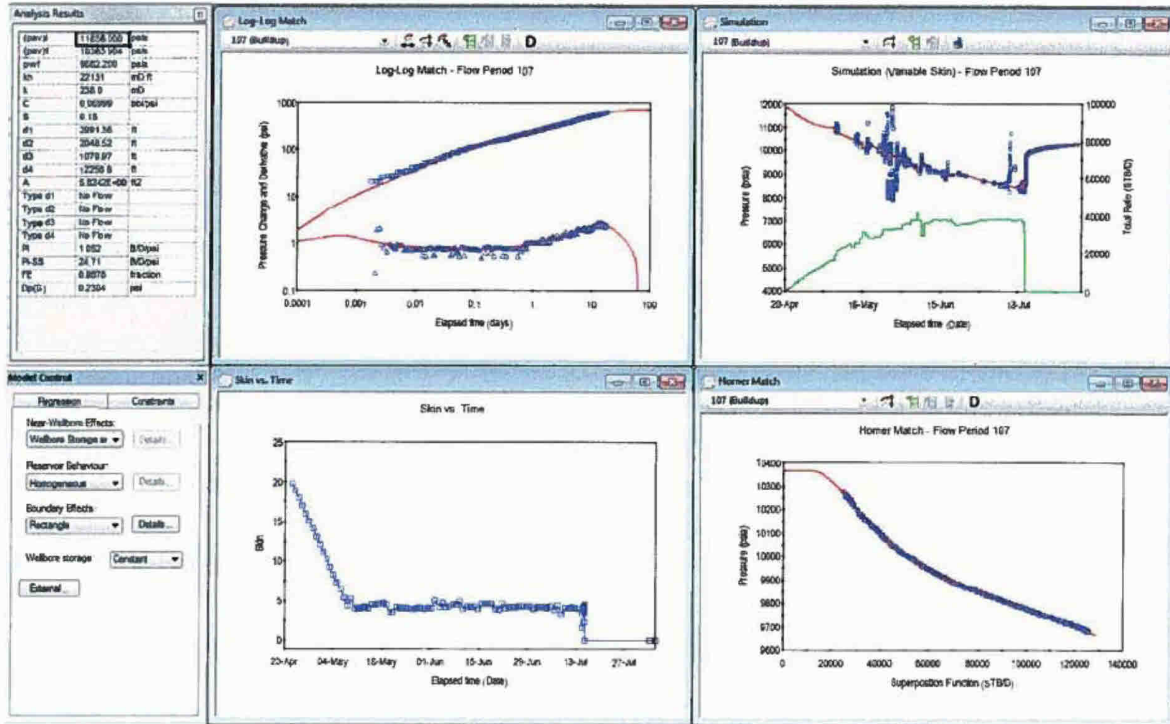
Figure 41: Interpretation Model, Model Match and Analysis Results

Figure 42: Interpretation Model, Model Match and Analysis Results (Zoom on Simulation – top left)

Figure 43: Interpretation Model, Model Match and Analysis Results (Further Zoom on Simulation – top left)

Analysis Model - Flow Period 107

Near Wellbore Effect: Wellbore Storage and Skin (C and S)
Reservoir Behaviour: Homogeneous
Boundary Effect: Rectangle

Initial average reservoir pressure, (pav)i	11856.000 psia
Final average reservoir pressure, (pav)f	10363.904 psia
Flowing pressure, pwf	9662.200 psia
Permeability Thickness, kh	22131 mD.ft
Permeability, k	238.0 mD
Wellbore storage coefficient, C	0.06999 bbl/psi
Wellbore skin factor, S	0.15
Distance to first boundary, d1	2991.36 ft
Distance to second boundary, d2	2048.52 ft
Distance to third boundary, d3	1079.97 ft
Distance to fourth boundary, d4	12256.8 ft
Drainage area, A	5.8242E+007 ft2
Type of first boundary, Type d1	No Flow
Type of second boundary, Type d2	No Flow
Type of third boundary, Type d3	No Flow
Type of fourth boundary, Type d4	No Flow
Measured Productivity Index, PI	1.052 B/D/psi
Steady State Productivity Index, PI-SS	24.71 B/D/psi
Flow Efficiency, FE	0.9878 fraction
Pressure drop due to skin, Dp(S)	0.2304 psi

Figure 44: P50 Model (Option-1 Drill Pipe High) – Summary of Results

36

TREX-011696R.152

3.4.1.4 P90 Permeability Well Test Analysis

Shown in Figures 46 – 50 are the model diagnosis, interpretation model, model matches and analysis results which confirm a very good match to the pressure history, log-log pressure change and derivative, and the superposition (Horner) plot.

The match to the pressure history at various scales, further confirm a good match giving more validity to the analysis results and higher confidence predicting the Macondo well and reservoir properties using the matched interpretation model.

Figure 45: Diagnosis, Interpretation Model, Model Match and Analysis Results

Below are additional plots (Figures 47-50) showing the model match at various scales.

Figure 46: Interpretation Model, Model Match and Analysis Results

Figure 47: Interpretation Model, Model Match and Analysis Results (Zoom on Simulation – top left)

Figure 48: Interpretation Model, Model Match and Analysis Results (Further Zoom on Simulation – top left)

Analysis Model - Flow Period 107

Near Wellbore Effect: Wellbore Storage and Skin (C and S)
Reservoir Behaviour: Homogeneous
Boundary Effect: Rectangle

Initial average reservoir pressure, (pav)i	11856.000 psia
Final average reservoir pressure, (pav)f	10363.904 psia
Flowing pressure, pwf	9662.200 psia
Permeability Thickness, kh	15808 mD.ft
Permeability, k	170.0 mD
Wellbore storage coefficient, C	0.04999 bbl/psi
Wellbore skin factor, S	0.32
Distance to first boundary, d1	2528.16 ft
Distance to second boundary, d2	1731.32 ft
Distance to third boundary, d3	912.745 ft
Distance to fourth boundary, d4	10358.9 ft
Drainage area, A	4.1601E+007 ft2
Type of first boundary, Type d1	No Flow
Type of second boundary, Type d2	No Flow
Type of third boundary, Type d3	No Flow
Type of fourth boundary, Type d4	No Flow
Measured Productivity Index, PI	1.052 B/D/psi
Steady State Productivity Index, PI-SS	17.66 B/D/psi
Flow Efficiency, FE	0.9745 fraction
Pressure drop due to skin, Dp(S)	0.4818 psi

Figure 49: P90 Model (Option-1 Drill Pipe High) – Summary of Results

39

TREX-011696R.155

3.4.1.5 P10 Permeability Well Test Analysis

Shown in Figures 51 – 55 are the model diagnosis, interpretation model, model matches and analysis results which confirm a very good match to the pressure history, log-log pressure change and derivative, and the superposition (Horner) plot.

The match to the pressure history at various scales, further confirm a good match giving more validity to the analysis results and higher confidence predicting the Macondo well and reservoir properties using the matched interpretation model.

Figure 50: Diagnosis, Interpretation Model, Model Match and Analysis Results

Below are additional plots (Figures 52-55) showing the model match at various scales.

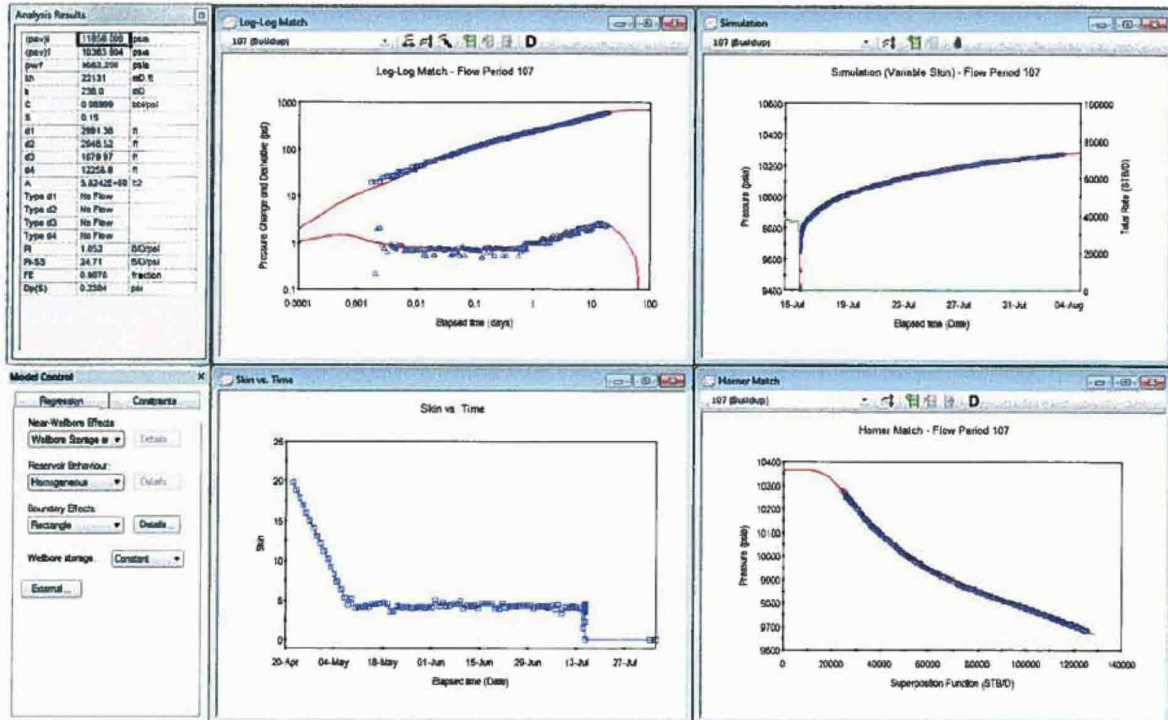Figure 51: Interpretation Model, Model Match and Analysis Results

Figure 52: Interpretation Model, Model Match and Analysis Results (Zoom on Simulation – top left)
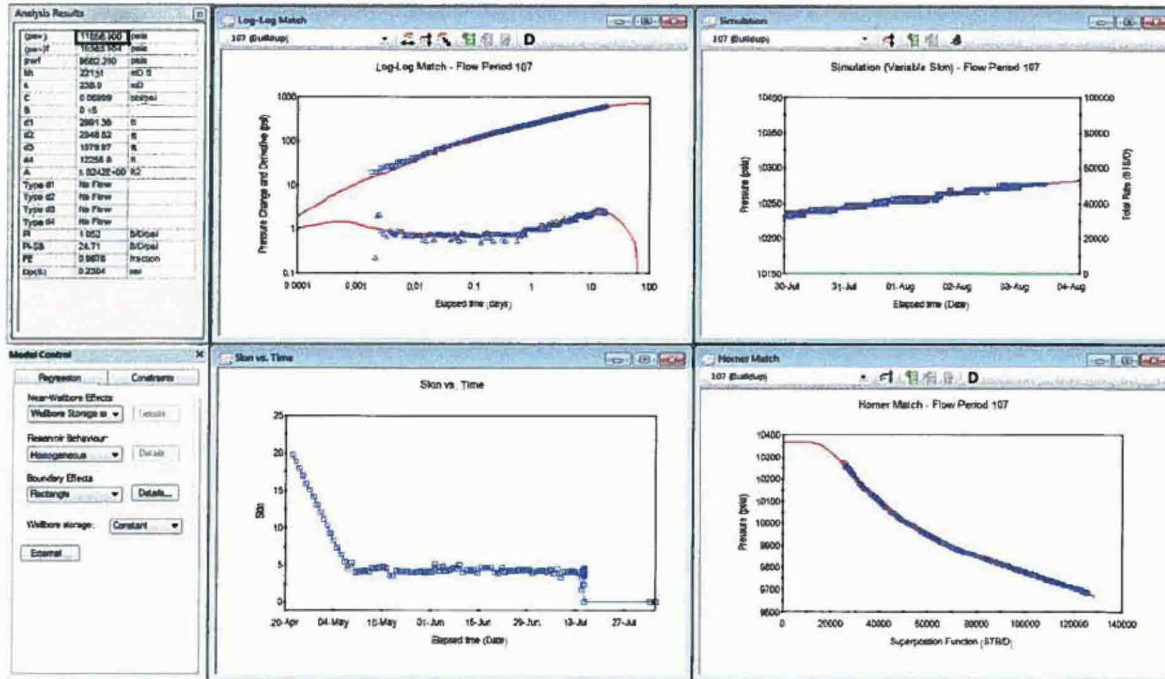
41

TREX-011696R.157

Figure 53: Interpretation Model, Model Match and Analysis Results (Further Zoom on Simulation – top left)

Analysis Model - Flow Period 107

Near Wellbore Effect: Wellbore Storage and Skin (C and S)
Reservoir Behaviour: Homogeneous
Boundary Effect: Rectangle

Initial average reservoir pressure, (pav)i	11856.000 psia
Final average reservoir pressure, (pav)f	10364.088 psia
Flowing pressure, pwf	9662.200 psia
Permeability Thickness, kh	30597 mD.ft
Permeability, k	329.0 mD
Wellbore storage coefficient, C	0.09676 bbl/psi
Wellbore skin factor, S	-0.01
Distance to first boundary, d1	3517.26 ft
Distance to second boundary, d2	2408.67 ft
Distance to third boundary, d3	1269.84 ft
Distance to fourth boundary, d4	14411.7 ft
Drainage area, A	8.0521E+007 ft2
Type of first boundary, Type d1	No Flow
Type of second boundary, Type d2	No Flow
Type of third boundary, Type d3	No Flow
Type of fourth boundary, Type d4	No Flow
Measured Productivity Index, PI	1.052 B/D/psi
Steady State Productivity Index, PI-SS	34.15 B/D/psi
Flow Efficiency, FE	1.001 fraction
Pressure drop due to skin, Dp(S)	-0.01162 psi

Figure 54: P10 Model (Option-1 Drill Pipe High) – Summary of Results

42

TREX-011696R.158

3.4.1.6 K mean (245mD) Permeability Well Test Analysis

Shown in Figures 56 – 60 are the model diagnosis, interpretation model, model matches and analysis results which confirm a very good match to the pressure history, log-log pressure change and derivative, and the superposition (Horner) plot.

The match to the pressure history at various scales, further confirms a good match giving more validity to the analysis results and higher confidence predicting the Macondo well and reservoir properties using the matched interpretation model.
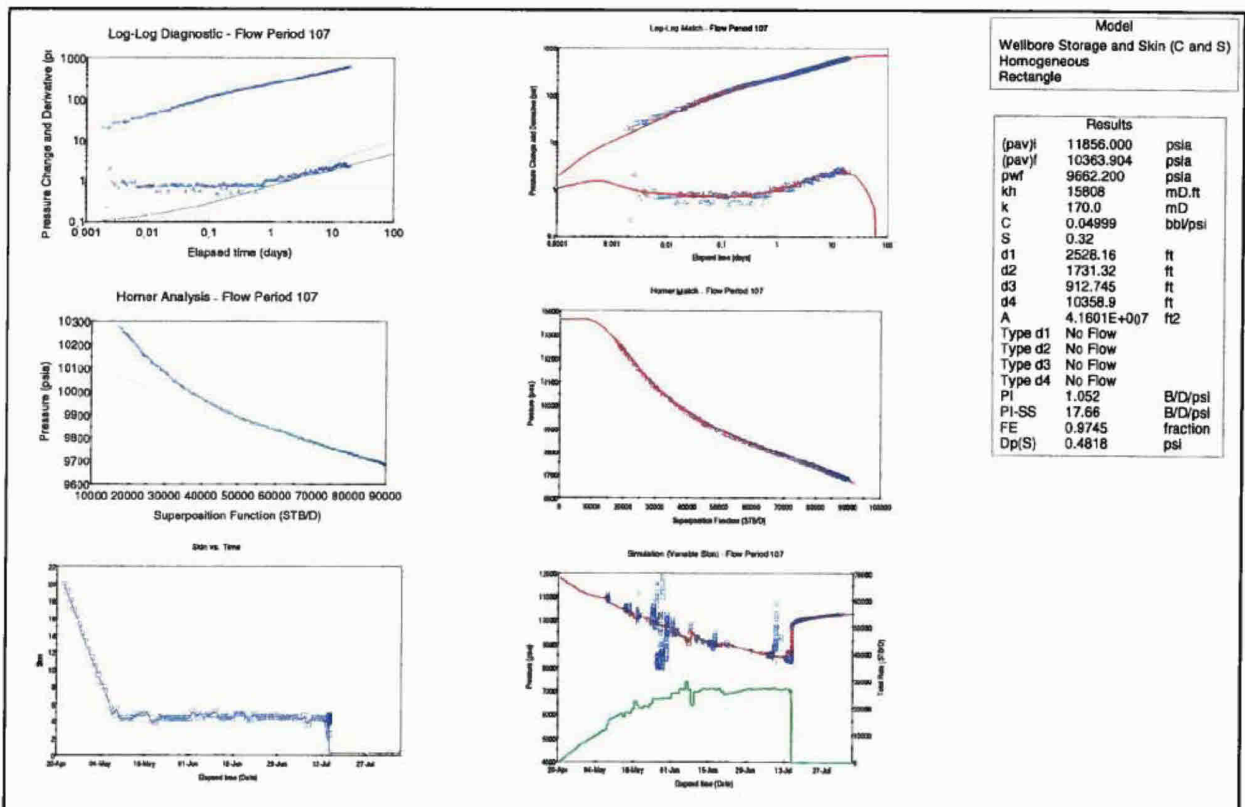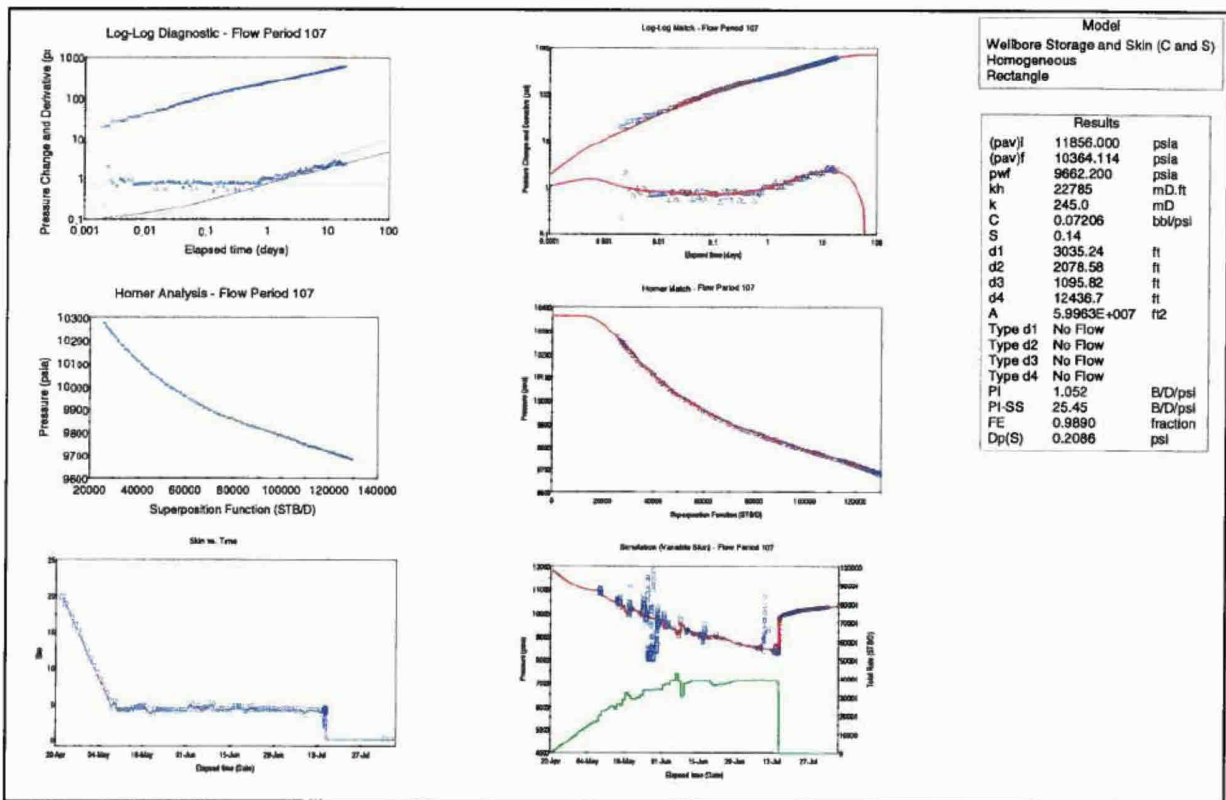

Figure 55: Diagnosis, Interpretation Model, Model Match and Analysis Results

Below are additional plots (Figures 57-60) showing the model match at various scales.
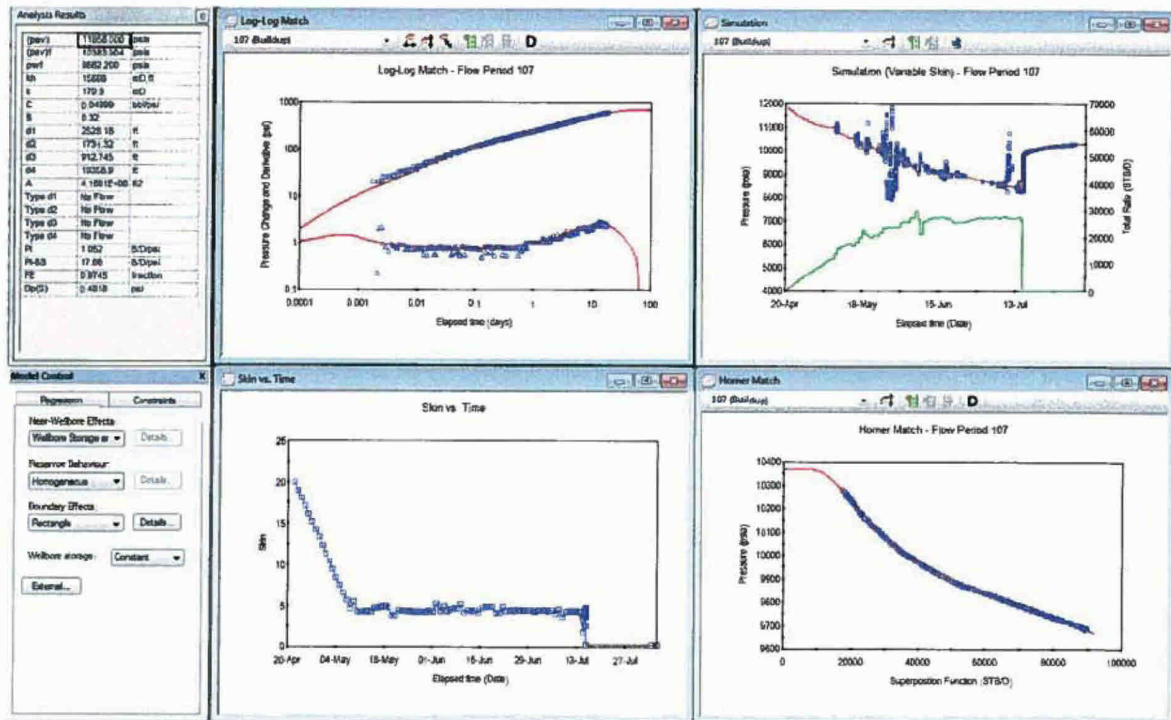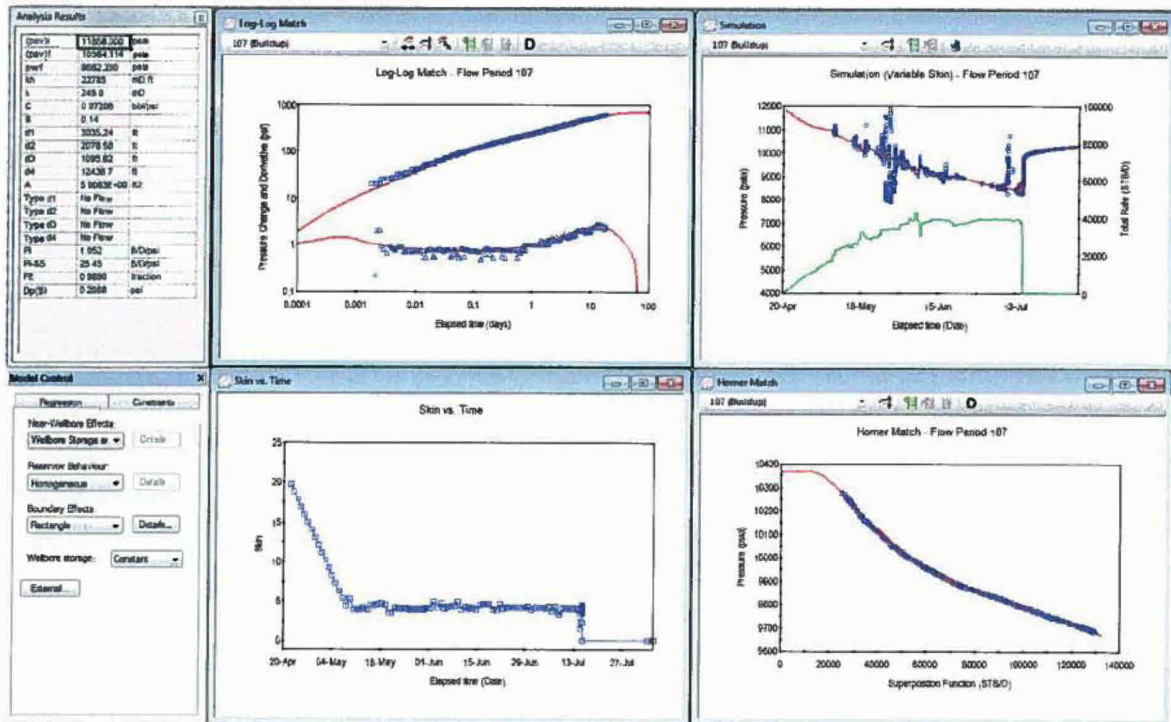
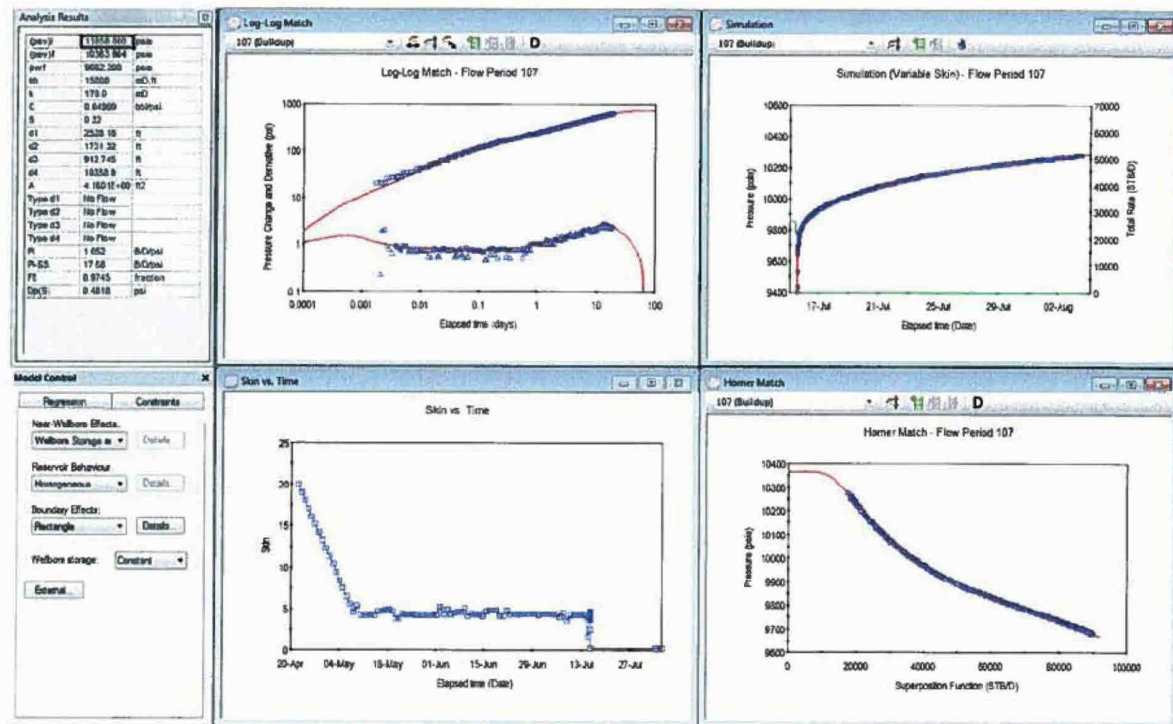Figure 56: Interpretation Model, Model Match and Analysis Results
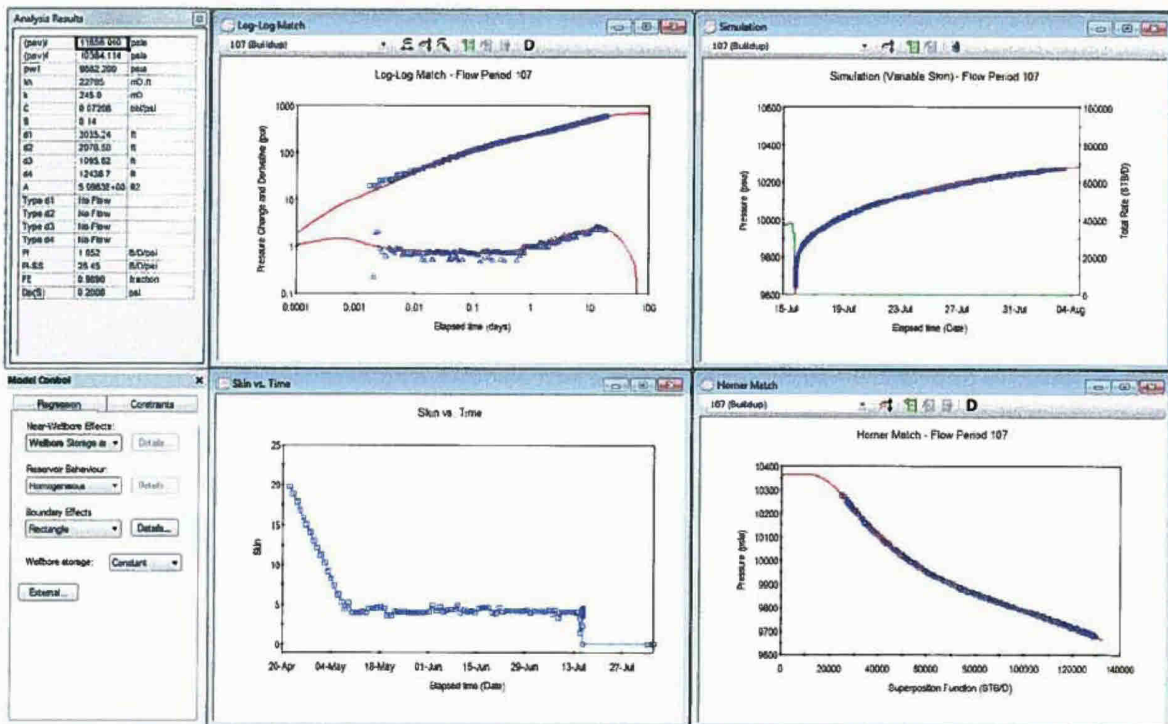
Figure 57: Interpretation Model, Model Match and Analysis Results (Zoom on Simulation – top left)
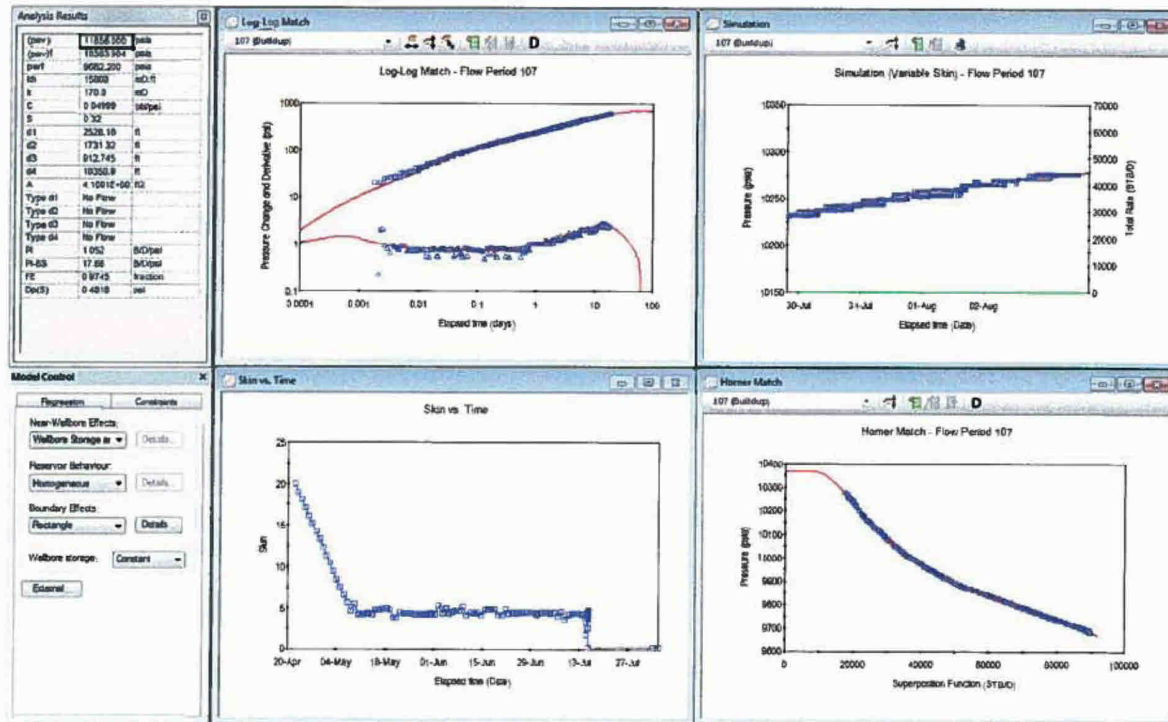
44
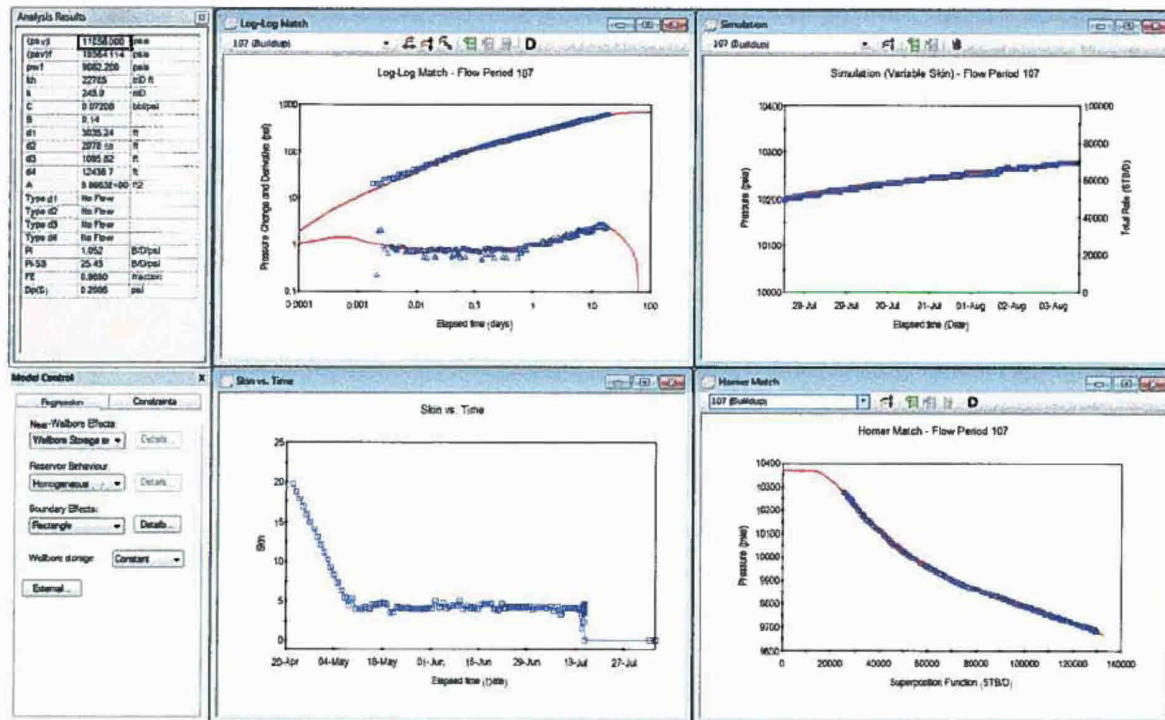
Figure 58: Interpretation Model, Model Match and Analysis Results (Further Zoom on Simulation – top left)

Analysis Model - Flow Period 107

Near Wellbore Effect:	Wellbore Storage and Skin (C and S)
Reservoir Behaviour:	Homogeneous
Boundary Effect:	Rectangle

Initial average reservoir pressure, (pav)i	11856.000 psia
Final average reservoir pressure, (pav)f	10364.114 psia
Flowing pressure, pwf	9662.200 psia
Permeability Thickness, kh	22785 mD.ft
Permeability, k	245.0 mD
Wellbore storage coefficient, C	0.07206 bbl/psi
Wellbore skin factor, S	0.14
Distance to first boundary, d1	3035.24 ft
Distance to second boundary, d2	2078.58 ft
Distance to third boundary, d3	1095.82 ft
Distance to fourth boundary, d4	12436.7 ft
Drainage area, A	5.9963E+007 ft2
Type of first boundary, Type d1	No Flow
Type of second boundary, Type d2	No Flow
Type of third boundary, Type d3	No Flow
Type of fourth boundary, Type d4	No Flow
Measured Productivity Index, PI	1.052 B/D/psi
Steady State Productivity Index, PI-SS	25.45 B/D/psi
Flow Efficiency, FE	0.9890 fraction
Pressure drop due to skin, Dp(S)	0.2086 psi

Figure 59: K-mean (245mD) Model (Option-1 Drill Pipe High) – Summary of Results

45

TREX-011696R.161

3.4.1.7 K=281mD Permeability Well Test Analysis

A sensitivity to 281mD was done by scaling the rates to match 45,000stb/d on the 14th of July, 2010.

Shown in Figures 61 – 65 are the model diagnosis, interpretation model, model matches and analysis results which confirm a very good match to the pressure history, log-log pressure change and derivative, and the superposition (Horner) plot.

The match to the pressure history at various scales, further confirm a good match giving more validity to the analysis results and higher confidence predicting the Macondo well and reservoir properties using the matched interpretation model.
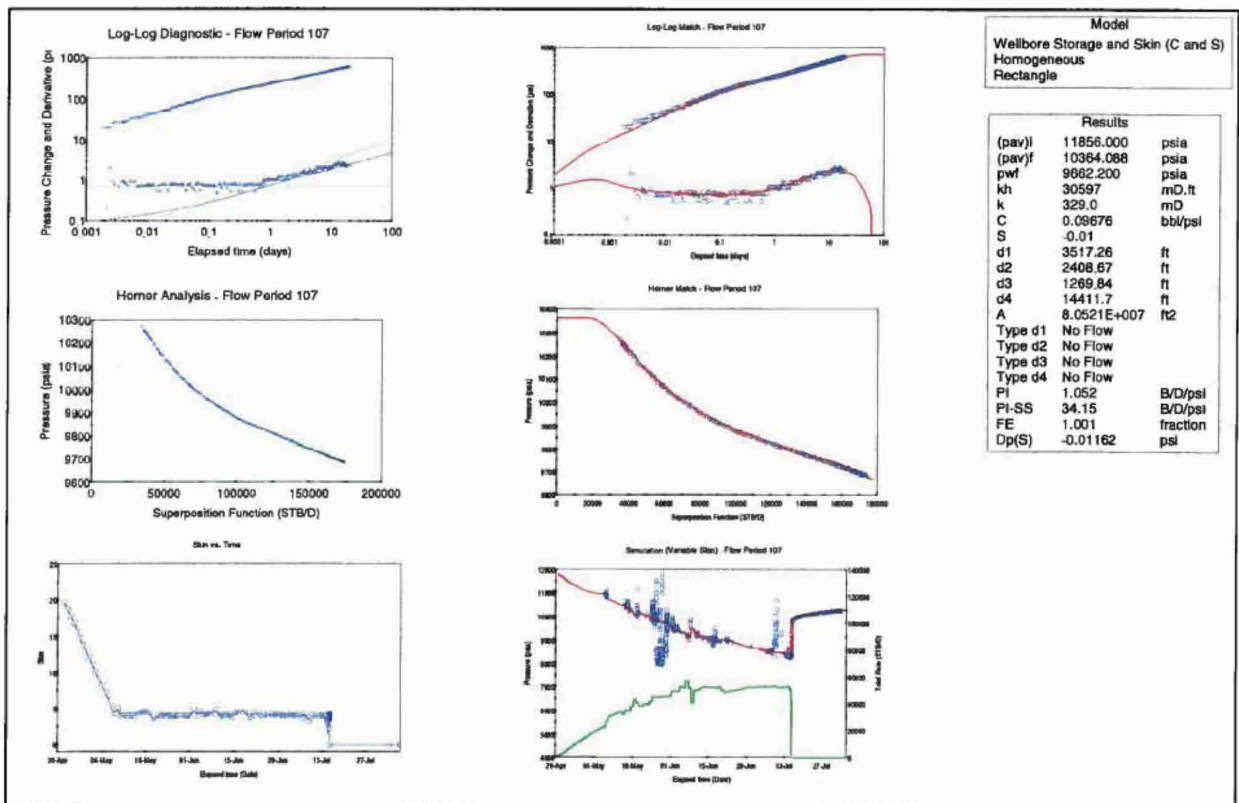

Figure 60: Diagnosis, Interpretation Model, Model Match and Analysis Results

Below are additional plots (Figures 62-65) showing the model match at various scales.
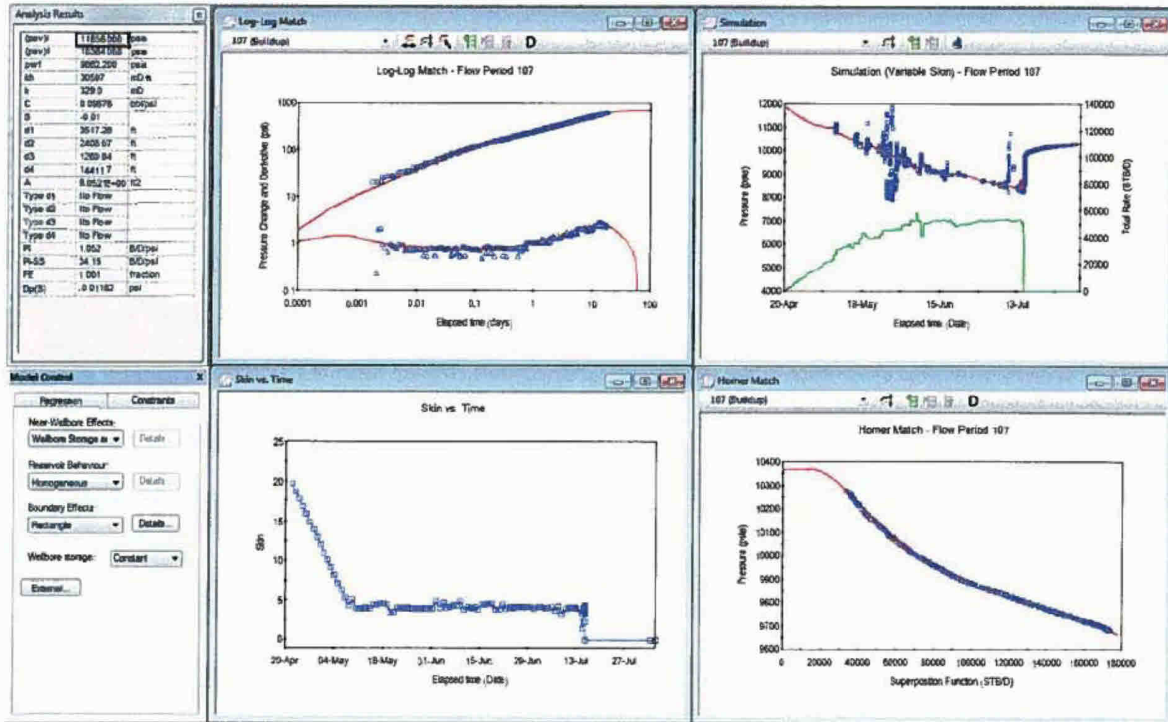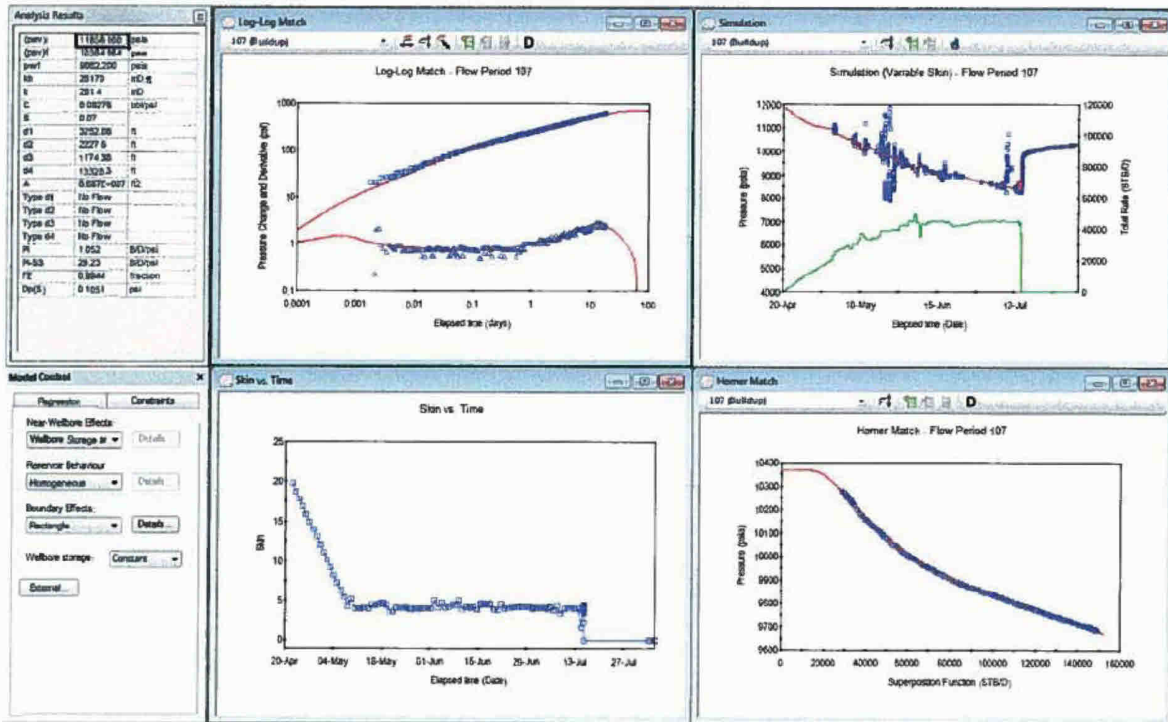
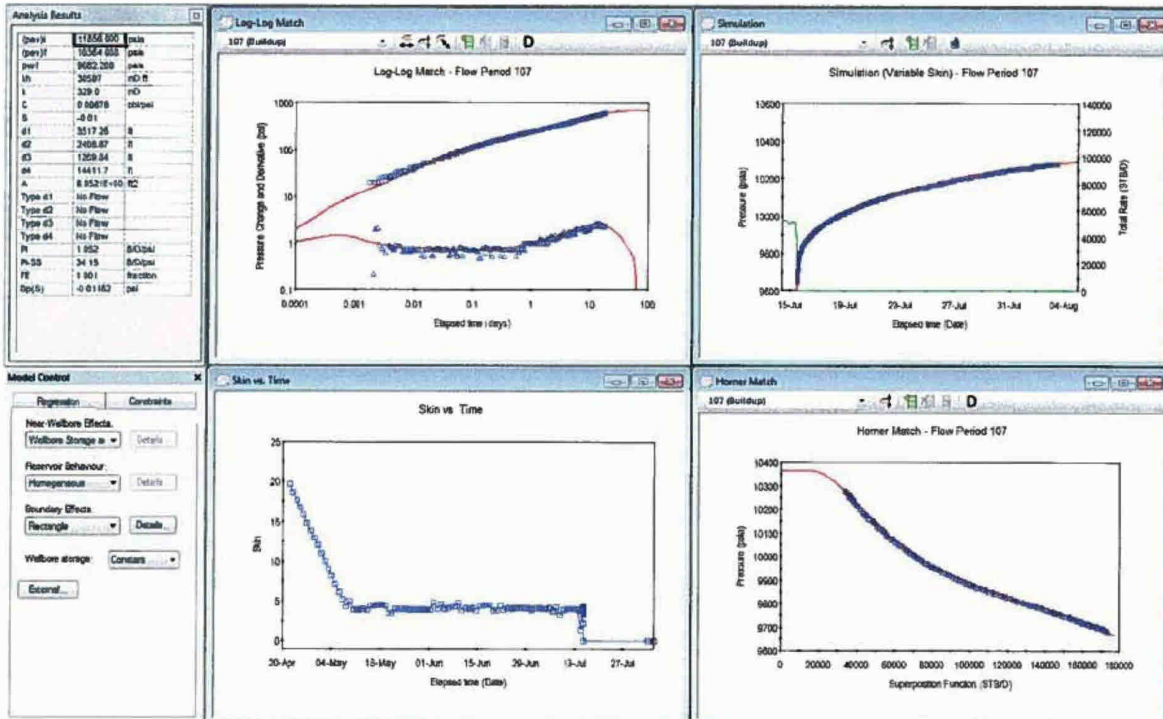Figure 61: Interpretation Model, Model Match and Analysis Results

Figure 62: Interpretation Model, Model Match and Analysis Results (Zoom on Simulation – top left)
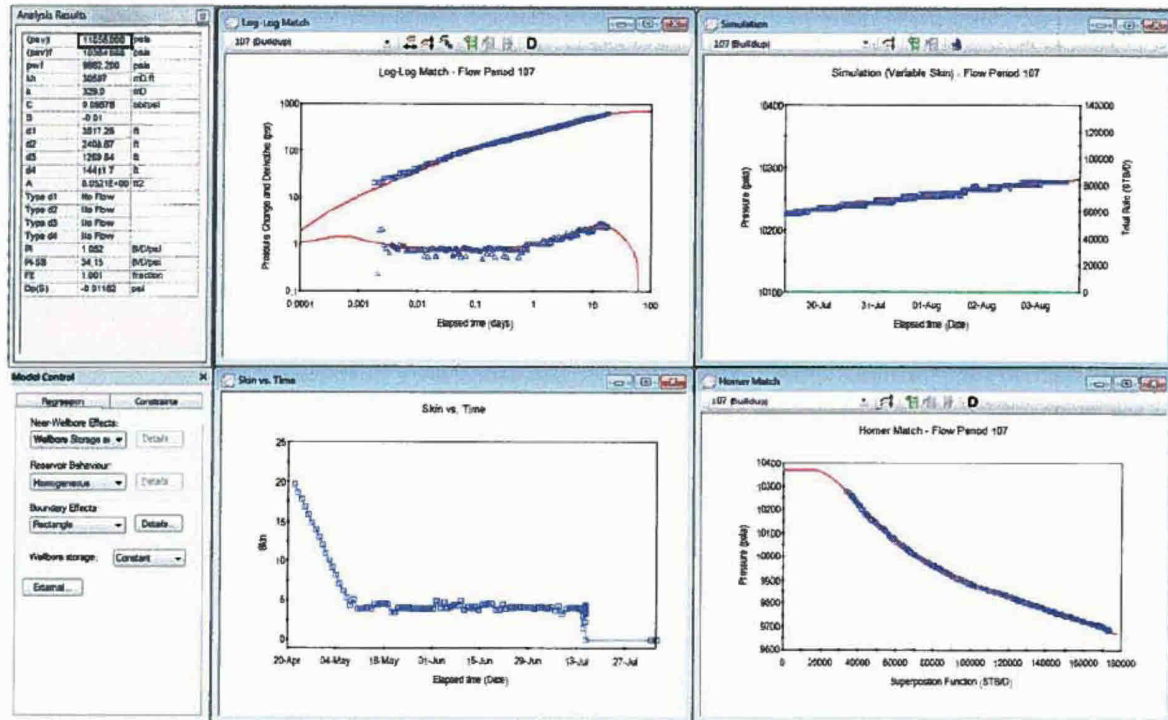
47

Figure 63: Interpretation Model, Model Match and Analysis Results (Further Zoom on Simulation – top left)

Analysis Model - Flow Period 107

Near Wellbore Effect: Wellbore Storage and Skin (C and S)
Reservoir Behaviour: Homogeneous
Boundary Effect: Rectangle

Initial average reservoir pressure, (pav)i	11856.000 psia
Final average reservoir pressure, (pav)f	10364.064 psia
Flowing pressure, pwf	9662.200 psia
Permeability Thickness, kh	26170 mD.ft
Permeability, k	281.4 mD
Wellbore storage coefficient, C	0.08276 bbl/psi
Wellbore skin factor, S	0.07
Distance to first boundary, d1	3252.86 ft
Distance to second boundary, d2	2227.6 ft
Distance to third boundary, d3	1174.38 ft
Distance to fourth boundary, d4	13328.3 ft
Drainage area, A	6.887E+007 ft2
Type of first boundary, Type d1	No Flow
Type of second boundary, Type d2	No Flow
Type of third boundary, Type d3	No Flow
Type of fourth boundary, Type d4	No Flow
Measured Productivity Index, PI	1.052 B/D/psi
Steady State Productivity Index, PI-SS	29.23 B/D/psi
Flow Efficiency, FE	0.9944 fraction
Pressure drop due to skin, Dp(S)	0.1051 psi

Figure 64: K (281mD) Model (Option-1 Drill Pipe High) – Summary of Results

48

TREX-011696R.164

3.4.1.8 OPTION-1 DRILL PIPE HIGH (SUMMARY AND RESULTS)

Parameters	P 90	P 50	P 10	Mean K	K-281
Initial Pressure @ Reservoir Depth (18,056 ft TVDss) psia	11,856	11,856	11,856	11,856	11,856
Final Pressure @ Reservoir Depth (18,056 ft TVDss) psia	10,364	10,364	10,364	10,364	10,364
Depletion (psi)	1,492.00	1,492.00	1,492.00	1,492.00	1,492.00
Reservoir Permeability (mD)	170	238	329	245	281
Skin	20 → 0	20 → 0	20 → 0	20 → 0	20 → 0
Boundary1 (d1) – ft	2,528	2,991	3,517	3,035	3,253
Boundary2 (d2) – ft	1,731	2,049	2,409	2,079	2,228
Boundary3 (d3) – ft	913	1,080	1,270	1,096	1,174
Boundary4 (d4) - ft	10,359	12,257	14,412	12,438	13,328
Reservoir Width - ft	3,441	4,071	4,787	4,131	4,427
Reservoir Length - ft	12,090	14,306	16,821	14,517	15,556
Area (MM ft²)	41.6	58.2	80.5	60.0	68.9
Area (Acres)	955	1,337	1,848	1,377	1,581
STOIIP (MMstb)	57	79	110	82	94
Cumulative Production (MMstb)	1.78	2.49	3.45	2.57	2.95

Figure 65: OPTION-1 DRILL PIPE HIGH – Summary of Results

49

TREX-011696R.165

3.4.2   OPTION-2 DRILL PIPE HIGH

3.4.2.1 Flow Period Selection

A total of 107 flow periods were also used to represent rate variations during the entire production and pressure history. The period when the Macondo well is full shut-in is flow period 107.

3.4.2.2 Deconvolution

Figures 67 – 77 below show the input pressures and rates, successive iterations of pressure rate histories, the final deconvolved derivative, the pressure match and quality of the pressure match. The quality (error difference) indicates a very good match at the 3rd and 4th iteration.
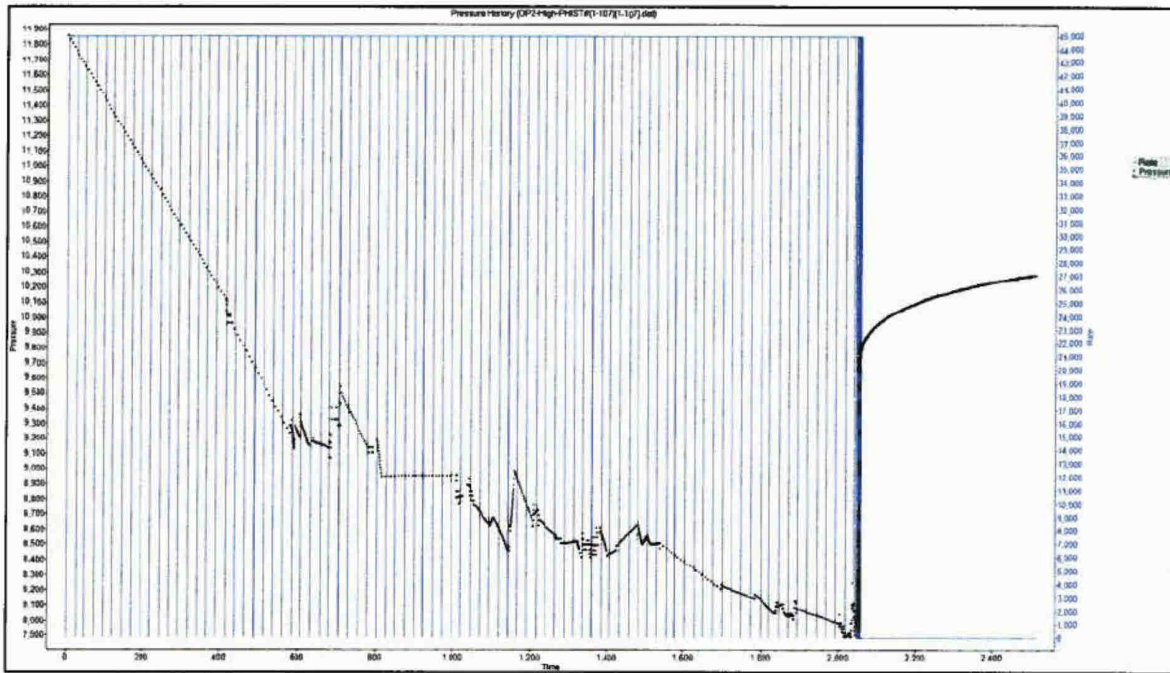
Figure 66: Input Pressure and Rate

50
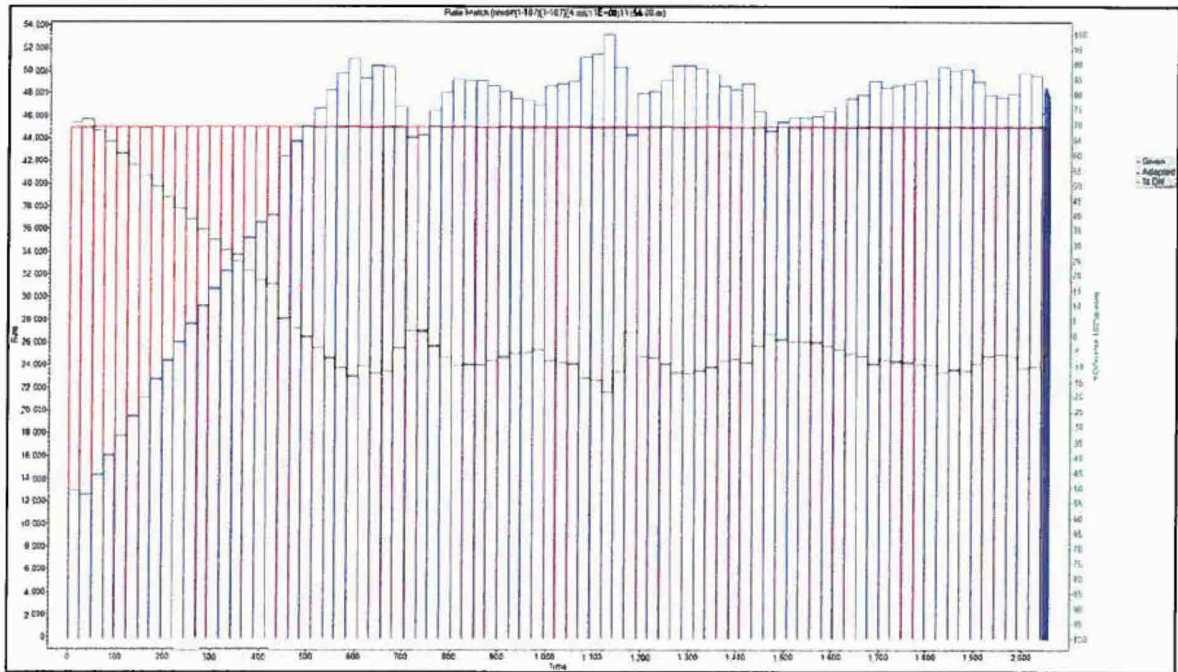
Figure 67: Adapted Rates (Iteration 1)
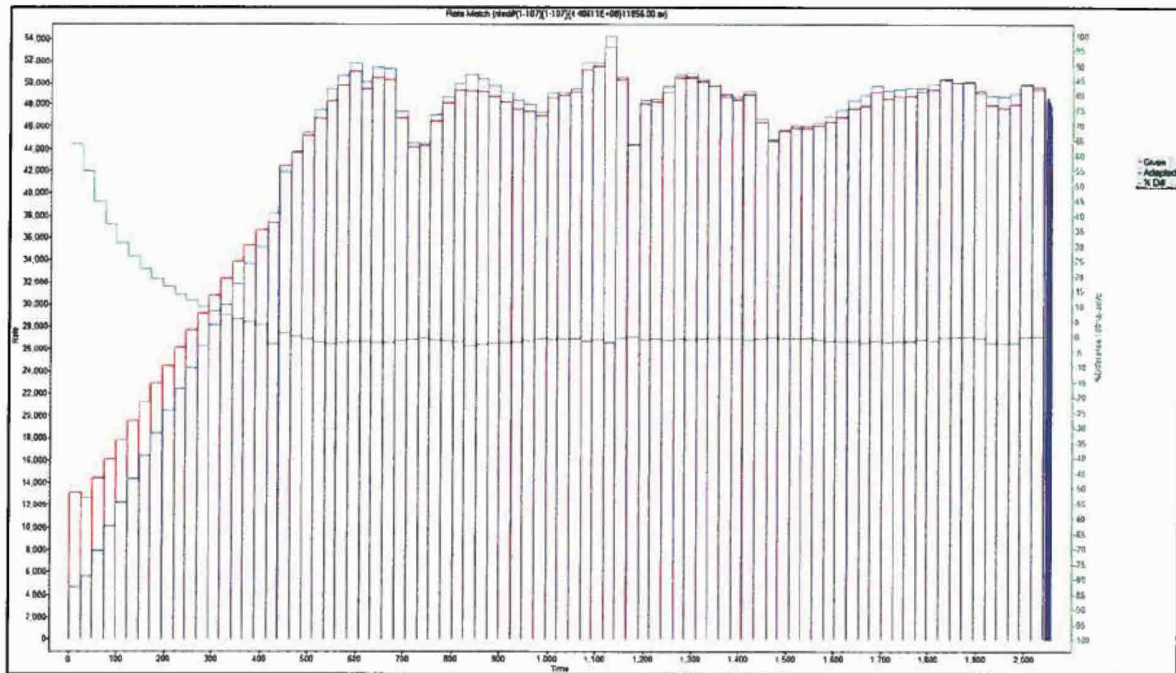
Figure 68: Adapted Rates (Iteration 2)

51
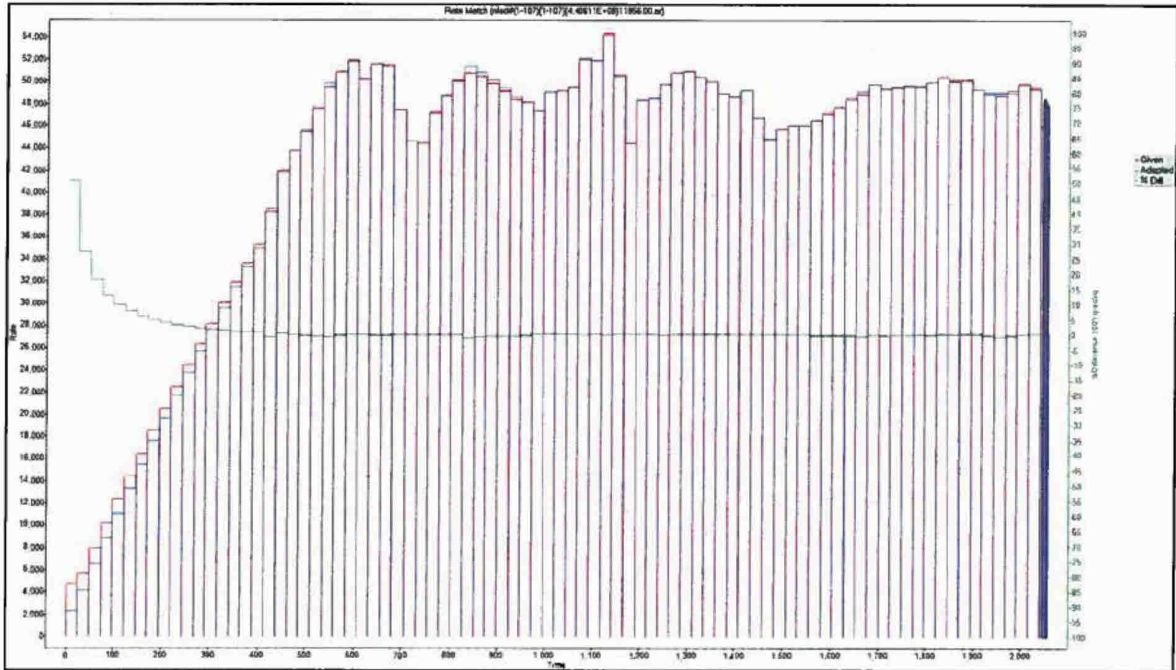
Figure 69: Adapted Rates (Iteration 3)
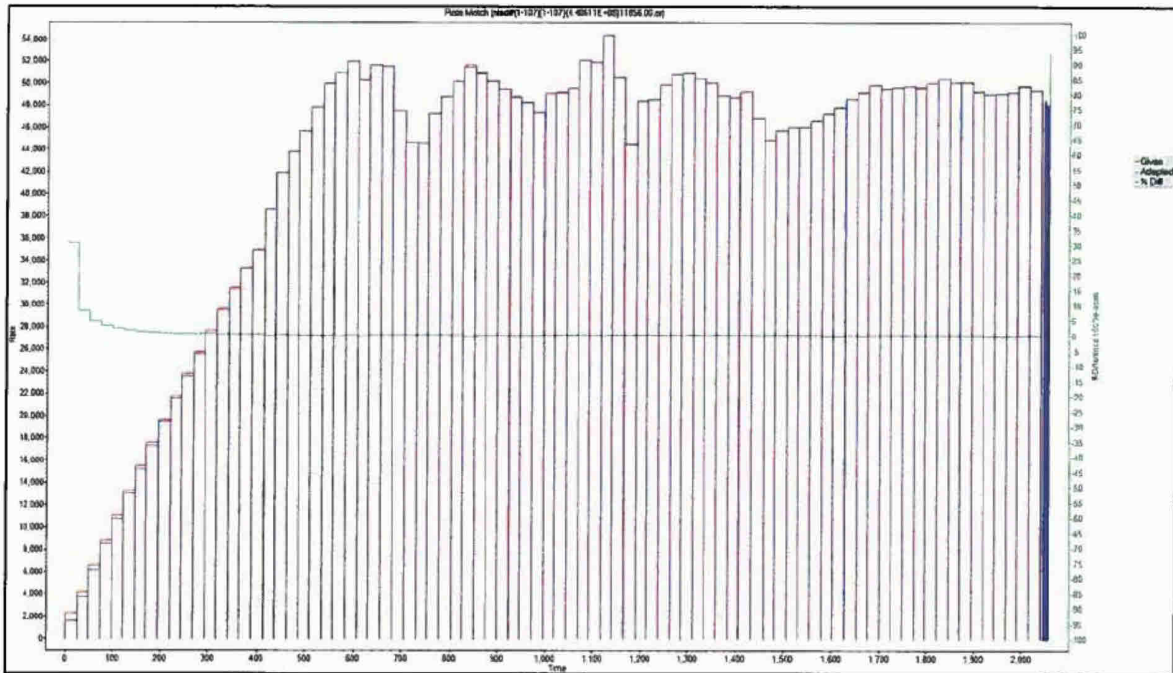
Figure 70: Adapted Rates (Iteration 4)

52
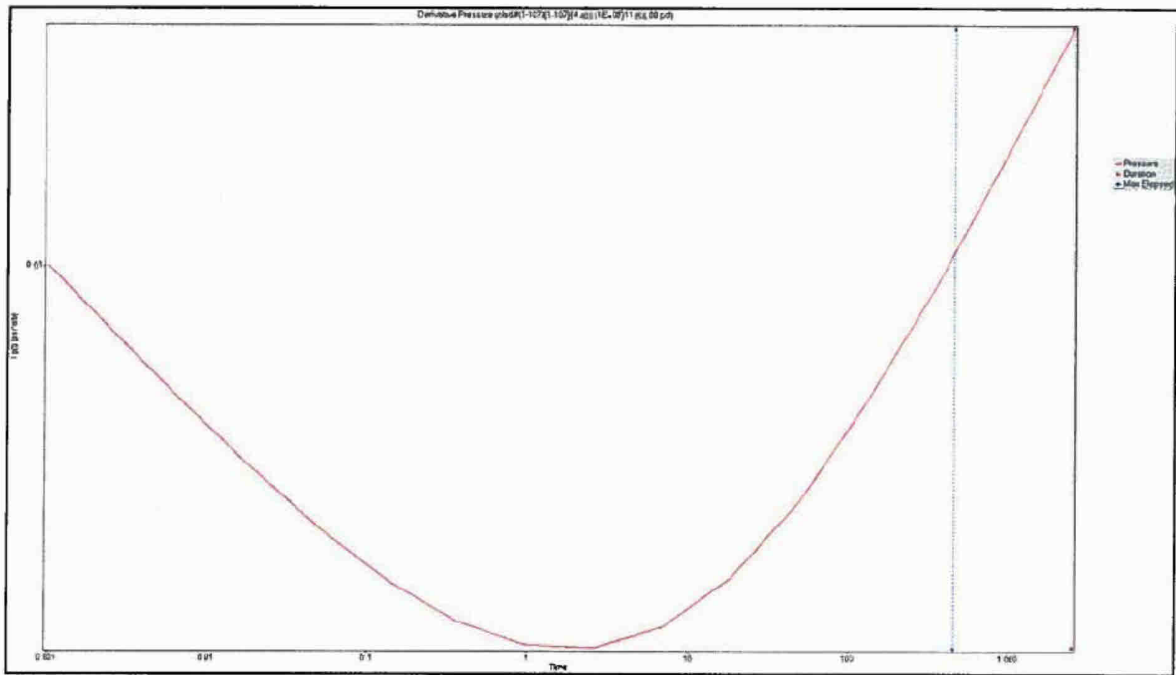
Figure 71: Deconvolved Derivative (Iteration 3)
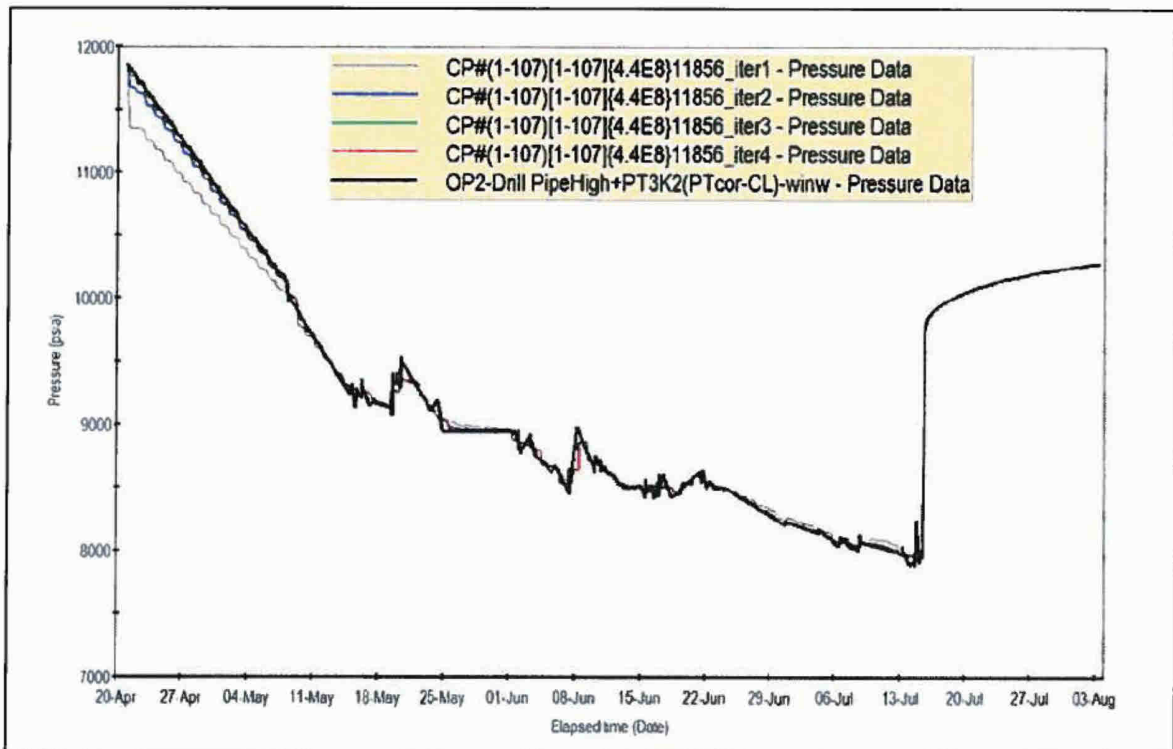
Figure 72: Pressure Match to Input Linearly Interpolated Pressures (1)

53
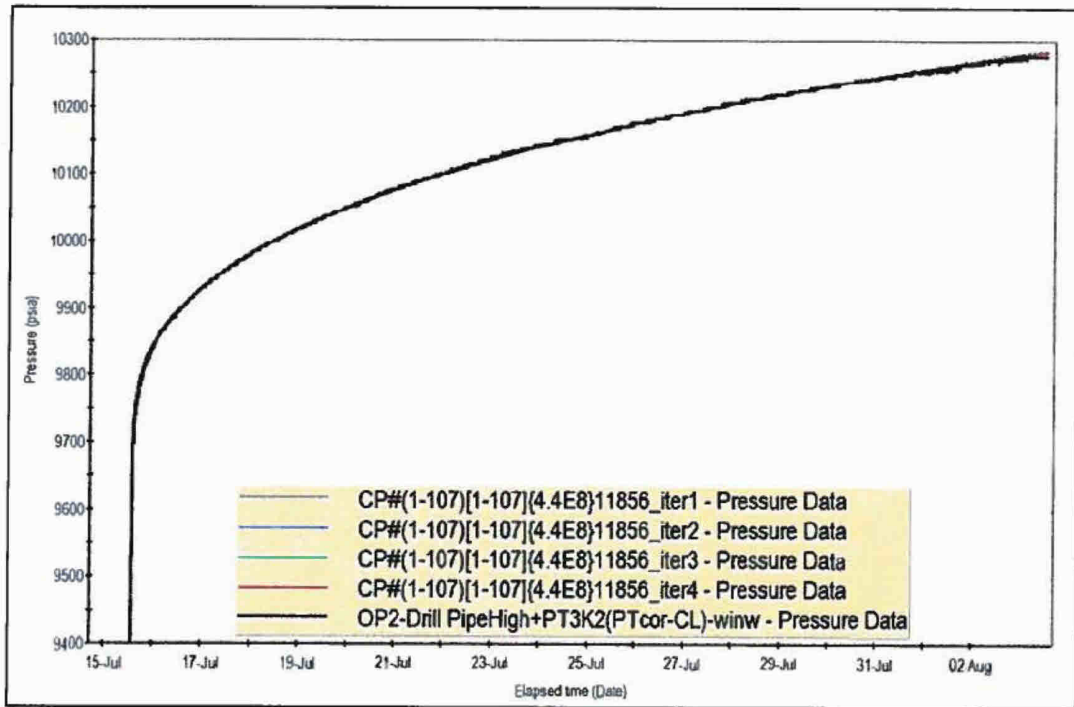
Figure 73: Pressure Match to Input Linearly Interpolated Pressures (2)
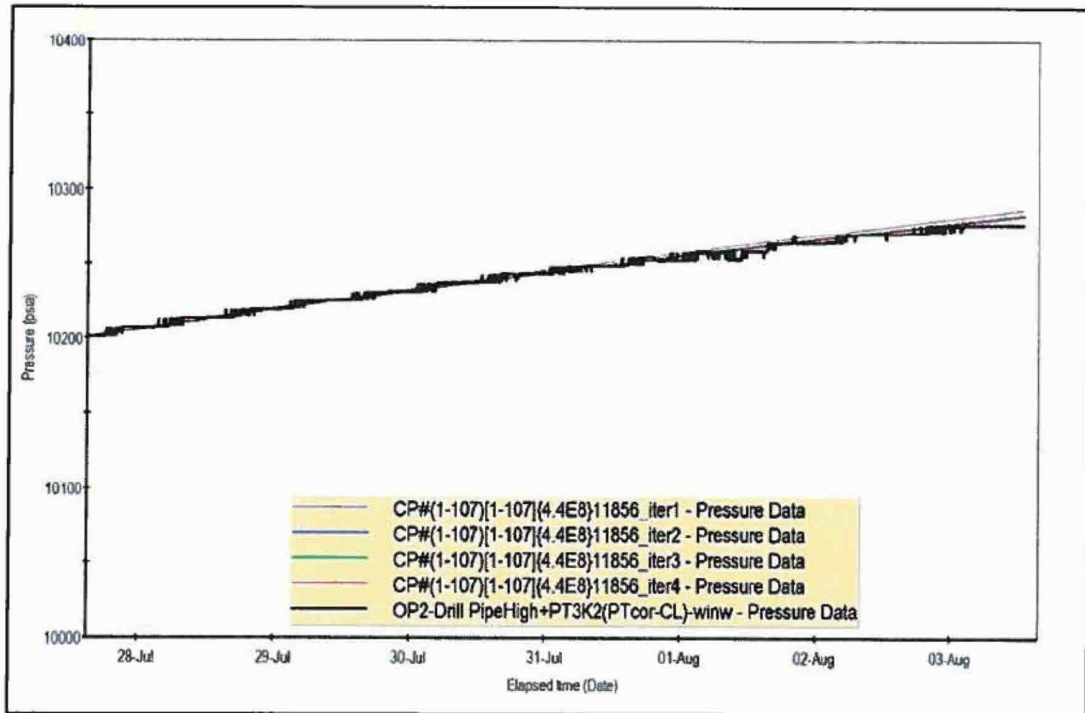
Figure 74: Pressure Match to Input Linearly Interpolated Pressures (3)

54
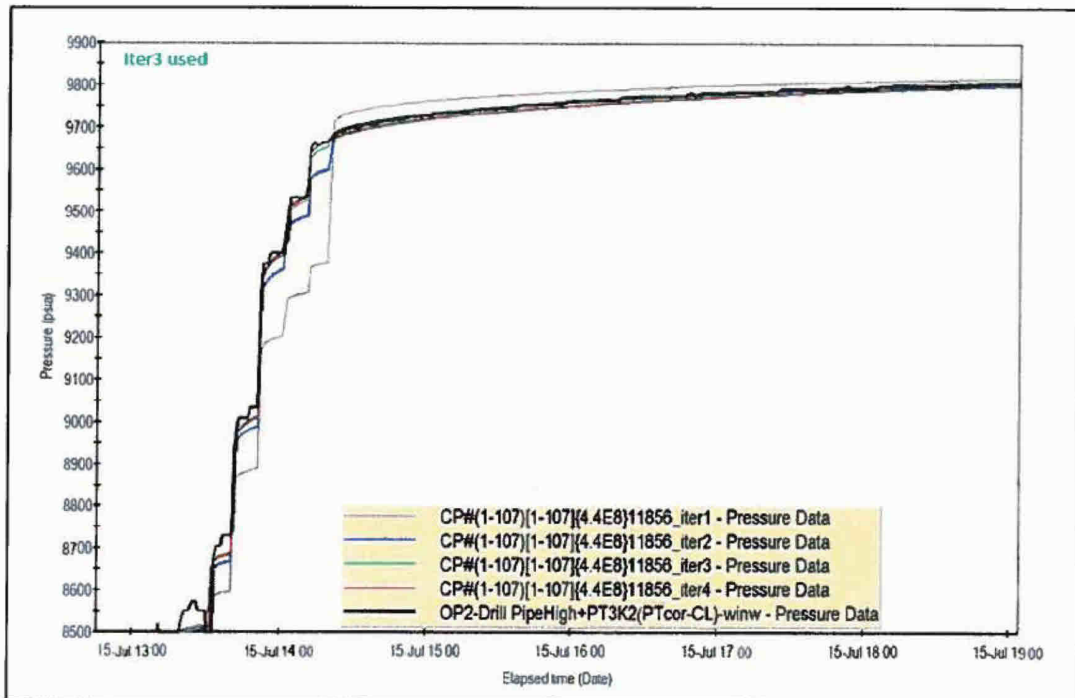
Figure 75: Pressure Match to Input Linearly Interpolated Pressures (4)
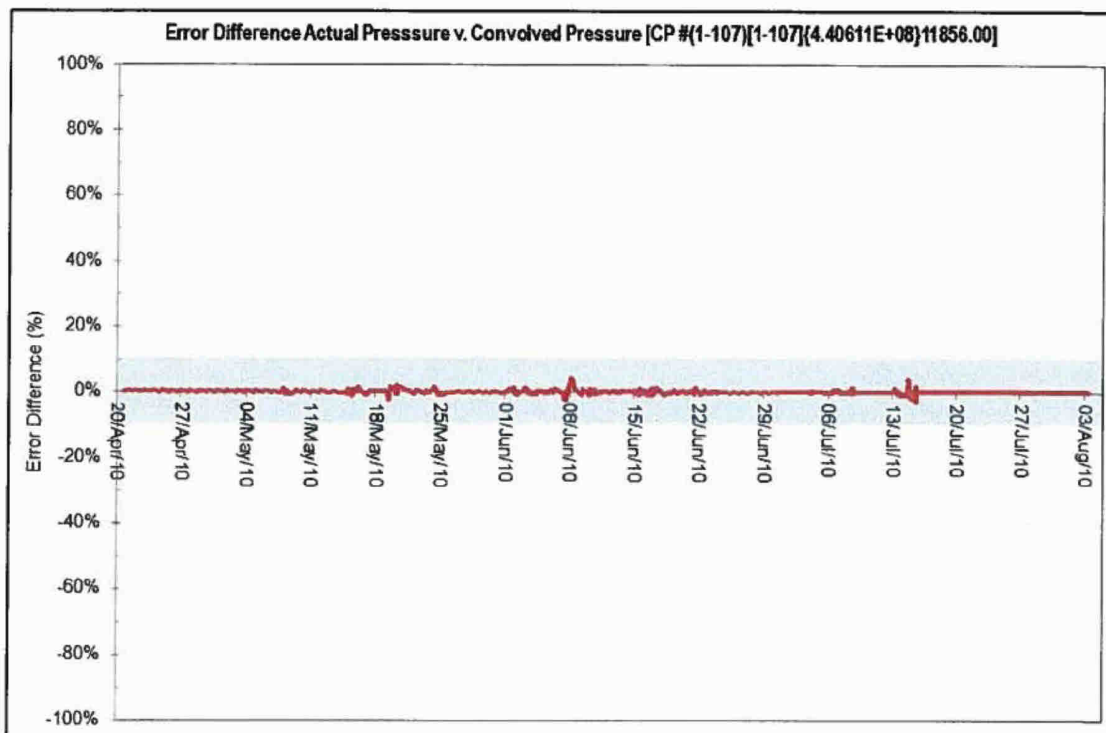
Figure 76: Quality Check on Error Difference (Convolved Pressure – iteration 3)

The convolved pressure match at the third iteration was near excellent and used as the rate profile for the well test analysis. The rates are scaled linearly to match the MDT uncertainty range of permeabilities (P50 238mD, P90 170mD, P10 329mD and Mean Permeability 245mD).

55

3.4.2.3 P50 Permeability Well Test Analysis

Shown in Figures 78 – 82 are the model diagnosis, interpretation model, model matches and analysis results which confirm a very good match to the pressure history, log-log pressure change and derivative, and the superposition (Horner) plot.

The match to the pressure history at various scales, further confirm a good match giving more validity to the analysis results and higher confidence predicting the Macondo well and reservoir properties using the matched interpretation model.
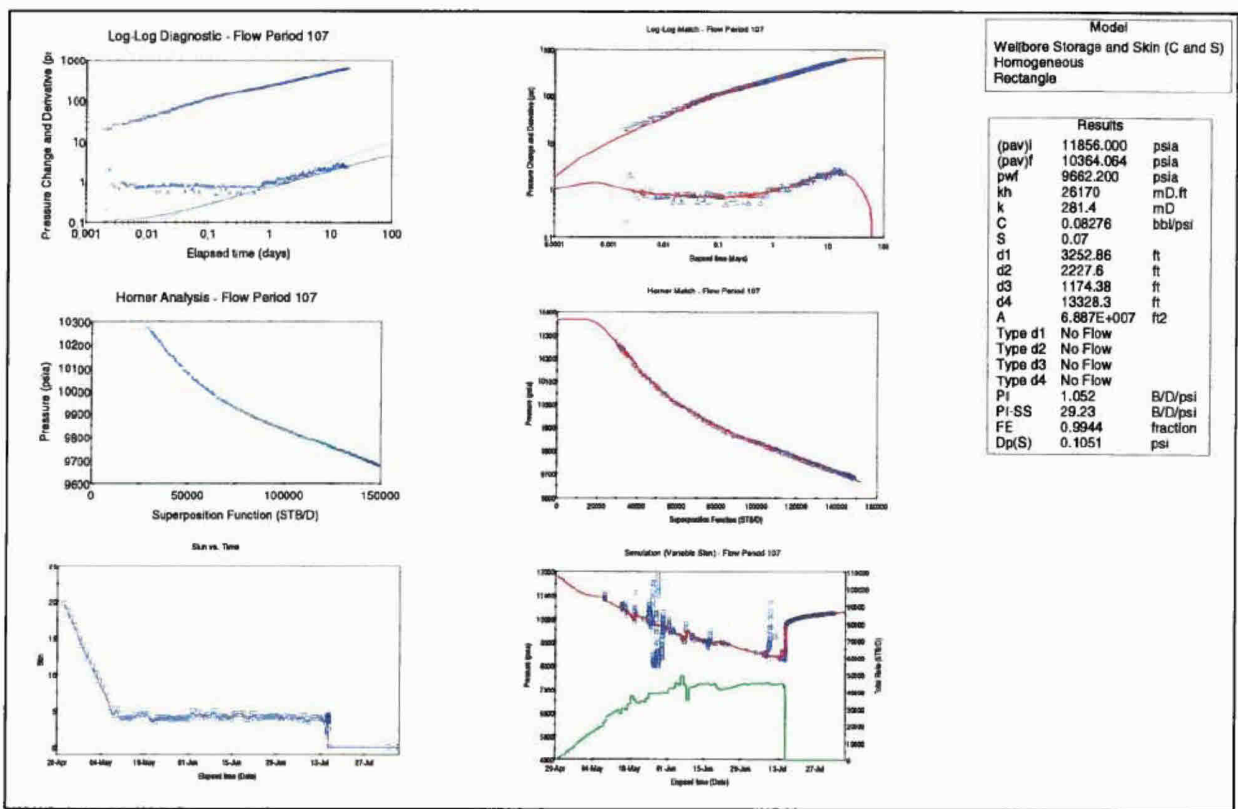

Figure 77: Diagnosis, Interpretation Model, Model Match and Analysis Results

Below are additional plots (Figures 79-82) showing the model match at various scales.

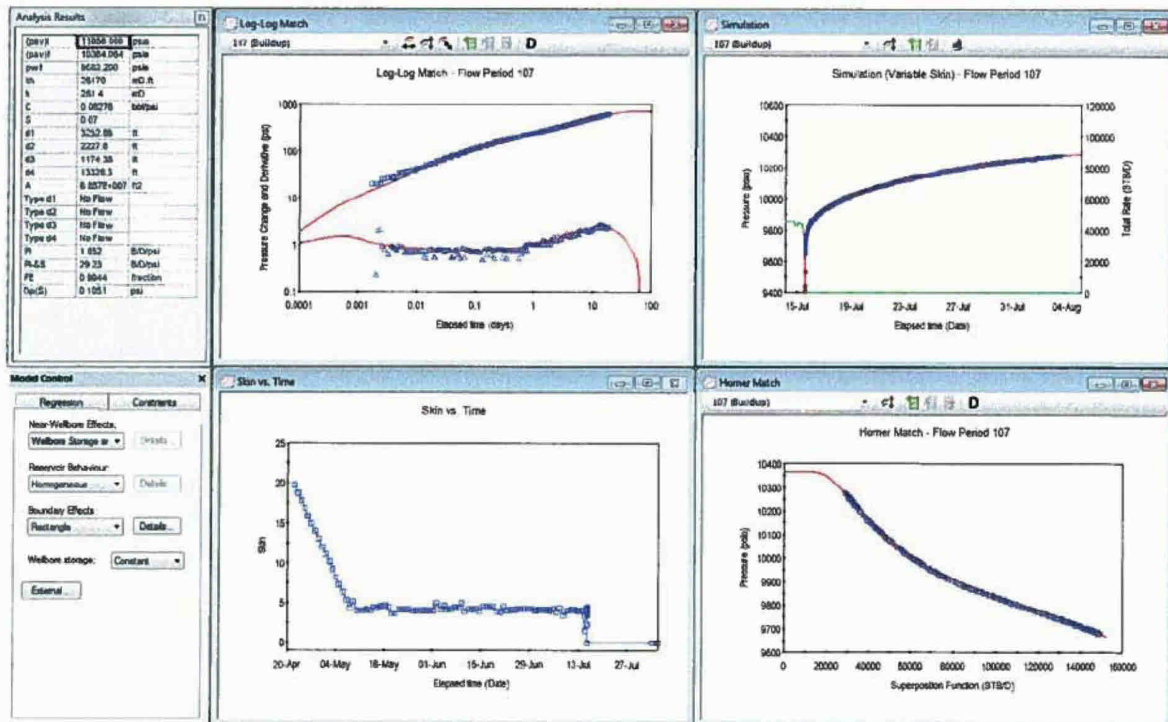Figure 78: Interpretation Model, Model Match and Analysis Results

Figure 79: Interpretation Model, Model Match and Analysis Results (Zoom on Simulation – top left)
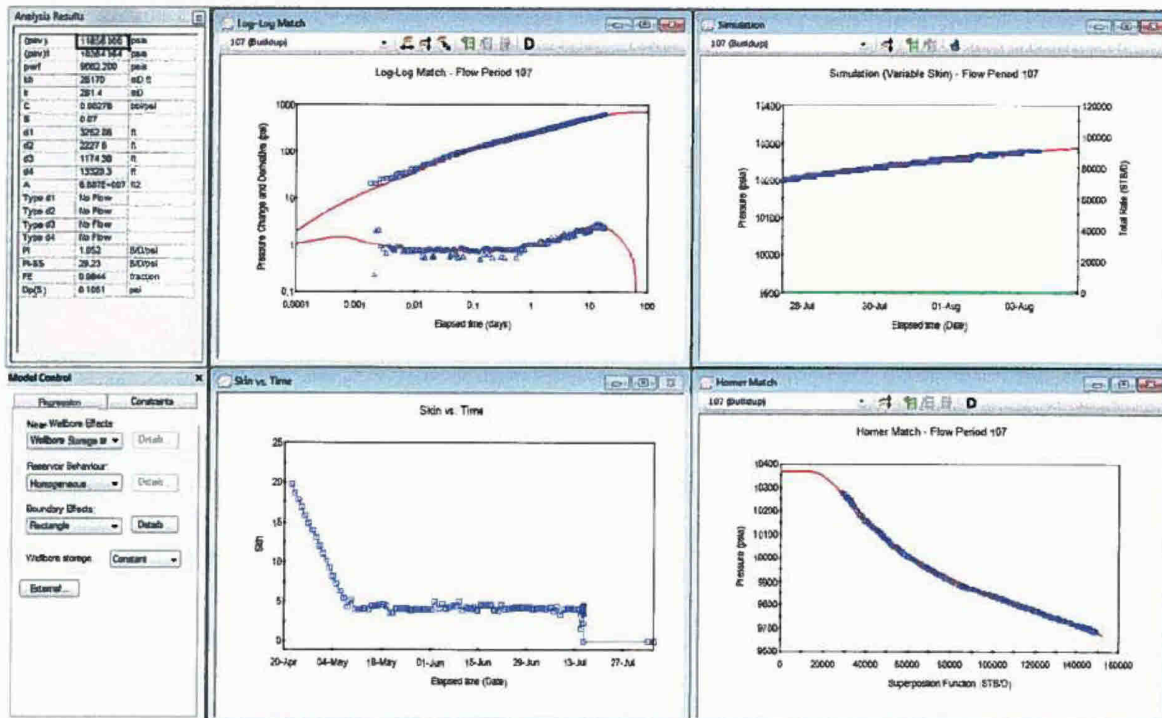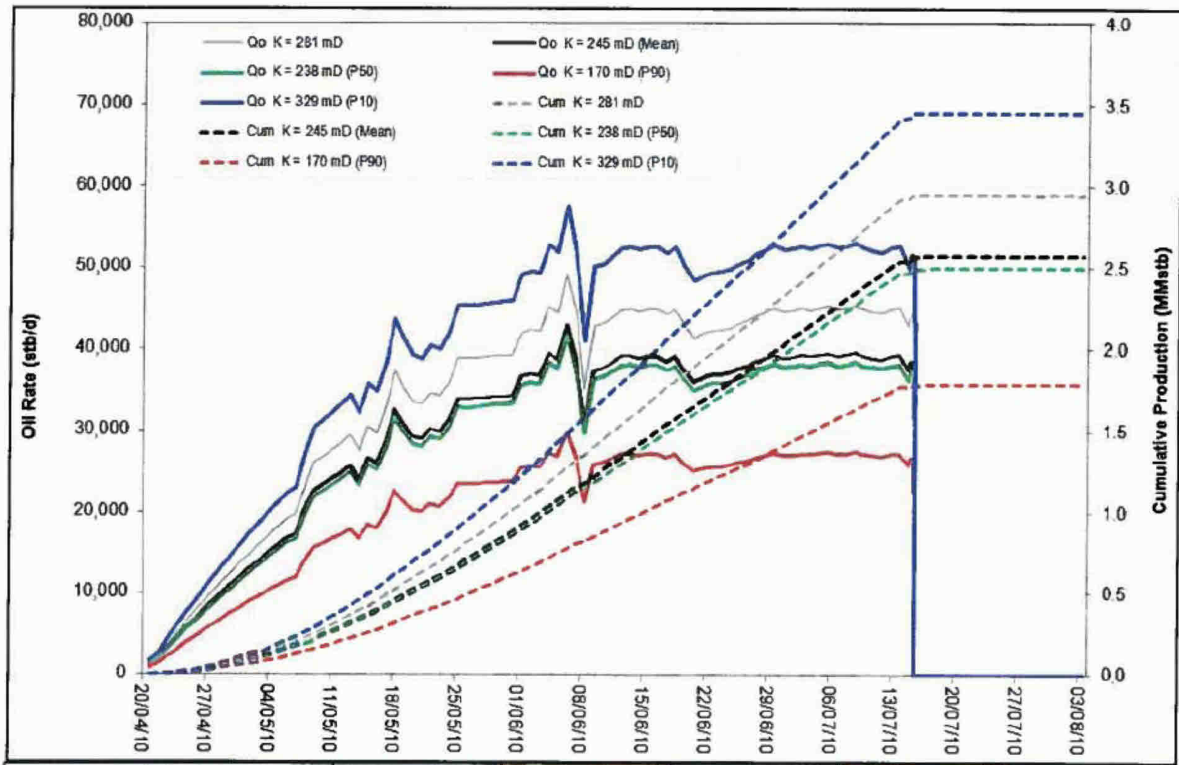
57

Figure 80: Interpretation Model, Model Match and Analysis Results (Further Zoom on Simulation – top left)

Analysis Model - Flow Period 107

Near Wellbore Effect: Wellbore Storage and Skin (C and S)
Reservoir Behaviour: Homogeneous
Boundary Effect: Rectangle

Initial average reservoir pressure, (pav)i	11856.000 psia
Final average reservoir pressure, (pav)f	10380.927 psia
Flowing pressure, pwf	9662.600 psia
Permeability Thickness, kh	22138 mD.ft
Permeability, k	238.0 mD
Wellbore storage coefficient, C	0.06783 bbl/psi
Wellbore skin factor, S	4.29
Distance to first boundary, d1	3342.24 ft
Distance to second boundary, d2	2046.96 ft
Distance to third boundary, d3	1345.75 ft
Distance to fourth boundary, d4	13085.7 ft
Drainage area, A	7.0942E+007 ft2
Type of first boundary, Type d1	No Flow
Type of second boundary, Type d2	No Flow
Type of third boundary, Type d3	No Flow
Type of fourth boundary, Type d4	No Flow
Measured Productivity Index, PI	1.028 B/D/psi
Steady State Productivity Index, PI-SS	18.83 B/D/psi
Flow Efficiency, FE	0.7417 fraction
Pressure drop due to skin, Dp(S)	6.806 psi

Figure 81: P50 Model (Option-2 Drill Pipe High) – Summary of Results

58

TREX-011696R.174

3.4.2.4 P90 Permeability Well Test Analysis

Shown in Figures 83 – 87 are the model diagnosis, interpretation model, model matches and analysis results which confirm a very good match to the pressure history, log-log pressure change and derivative, and the superposition (Horner) plot.

The match to the pressure history at various scales, further confirm a good match giving more validity to the analysis results and higher confidence predicting the Macondo well and reservoir properties using the matched interpretation model.

Figure 82: Diagnosis, Interpretation Model, Model Match and Analysis Results

Below are additional plots (Figures 84-87) showing the model match at various scales.

Figure 83: Interpretation Model, Model Match and Analysis Results

Figure 84: Interpretation Model, Model Match and Analysis Results (Zoom on Simulation – top left)

Figure 85: Interpretation Model, Model Match and Analysis Results (Further Zoom on Simulation – top left)

Analysis Model - Flow Period 107

Near Wellbore Effect: Wellbore Storage and Skin (C and S)
Reservoir Behaviour: Homogeneous
Boundary Effect: Rectangle

Initial average reservoir pressure, (pav)i	11856.000 psia
Final average reservoir pressure, (pav)f	10380.809 psia
Flowing pressure, pwf	9662.600 psia
Permeability Thickness, kh	15812 mD.ft
Permeability, k	170.0 mD
Wellbore storage coefficient, C	0.04845 bbl/psi
Wellbore skin factor, S	4.46
Distance to first boundary, d1	2824.6 ft
Distance to second boundary, d2	1729.93 ft
Distance to third boundary, d3	1137.32 ft
Distance to fourth boundary, d4	11059 ft
Drainage area, A	5.0669E+007 ft2
Type of first boundary, Type d1	No Flow
Type of second boundary, Type d2	No Flow
Type of third boundary, Type d3	No Flow
Type of fourth boundary, Type d4	No Flow
Measured Productivity Index, PI	1.028 B/D/psi
Steady State Productivity Index, PI-SS	13.45 B/D/psi
Flow Efficiency, FE	0.7315 fraction
Pressure drop due to skin, Dp(S)	7.073 psi

Figure 86: P90 Model (Option-2 Drill Pipe High) – Summary of Results

61

TREX-011696R.177

3.4.2.5 P10 Permeability Well Test Analysis

Shown in Figures 88 – 92 are the model diagnosis, interpretation model, model matches and analysis results which confirm a very good match to the pressure history, log-log pressure change and derivative, and the superposition (Horner) plot.

The match to the pressure history at various scales, further confirms a good match giving more validity to the analysis results and higher confidence predicting the Macondo well and reservoir properties using the matched interpretation model.
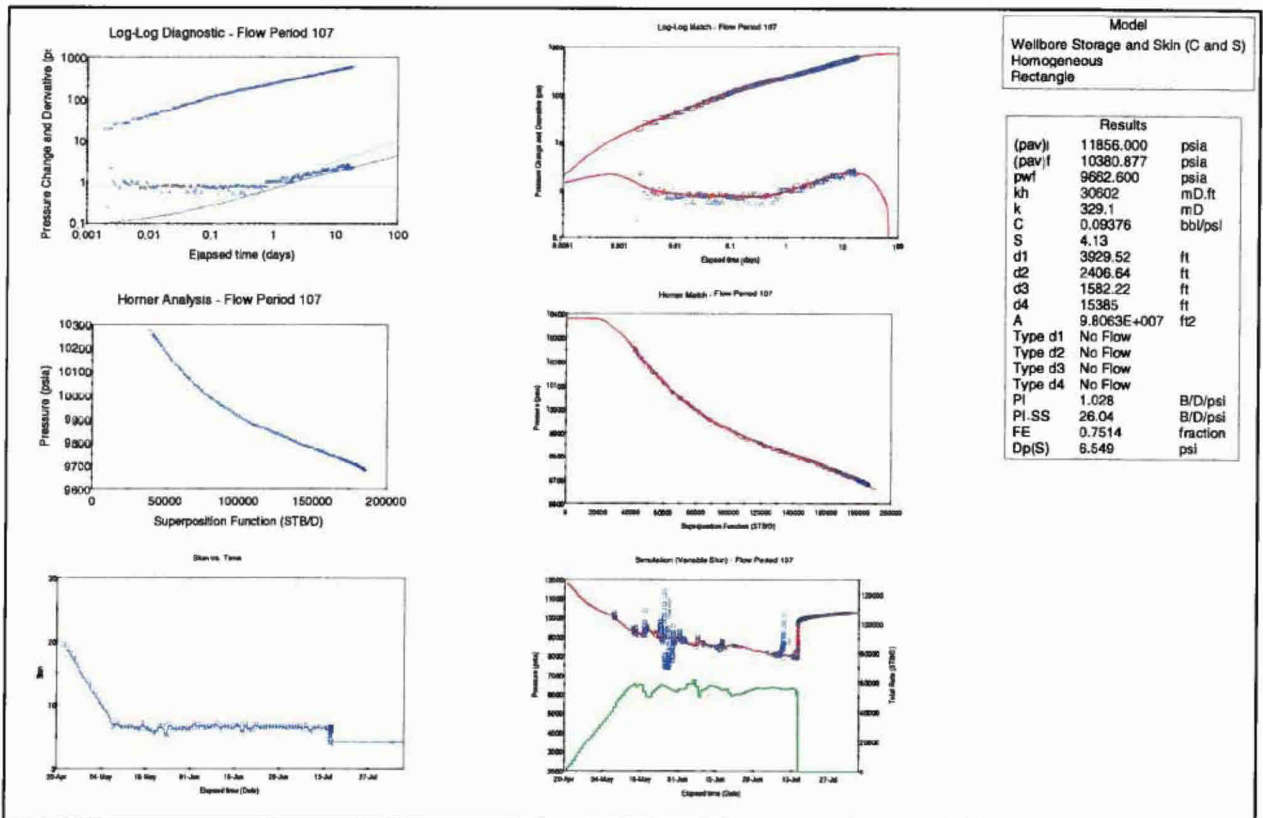
Figure 87: Diagnosis, Interpretation Model, Model Match and Analysis Results

Below are additional plots (Figures 89-92) showing the model match at various scales.
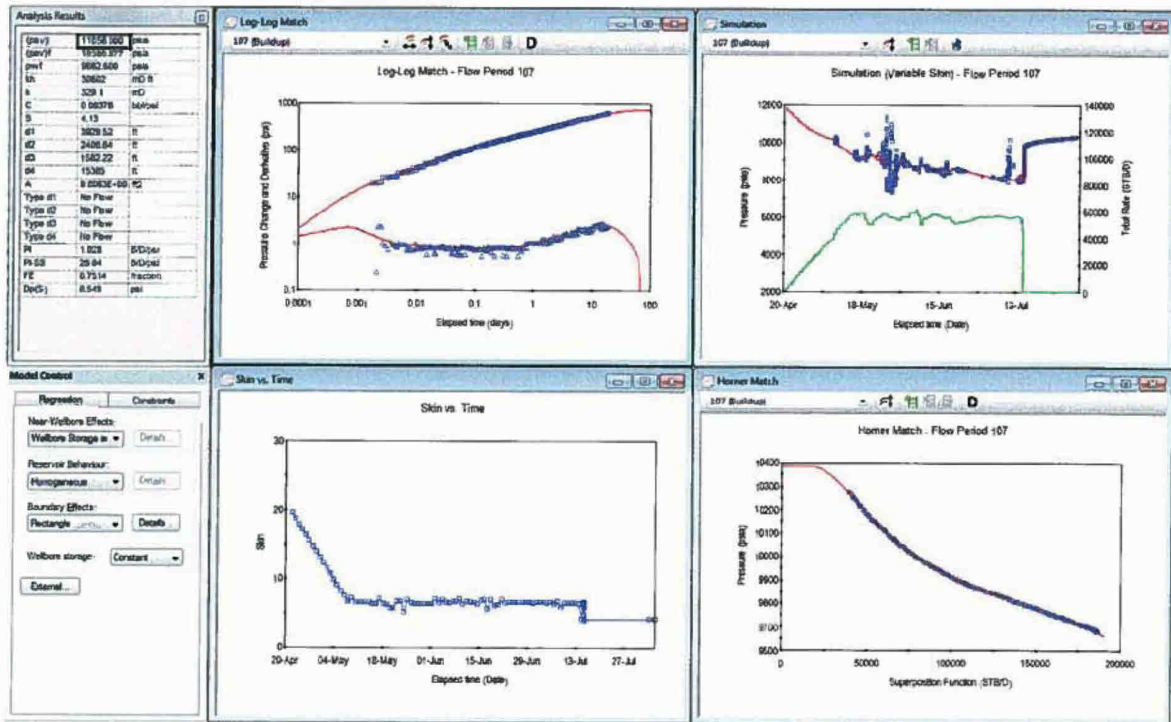
Figure 88: Interpretation Model, Model Match and Analysis Results
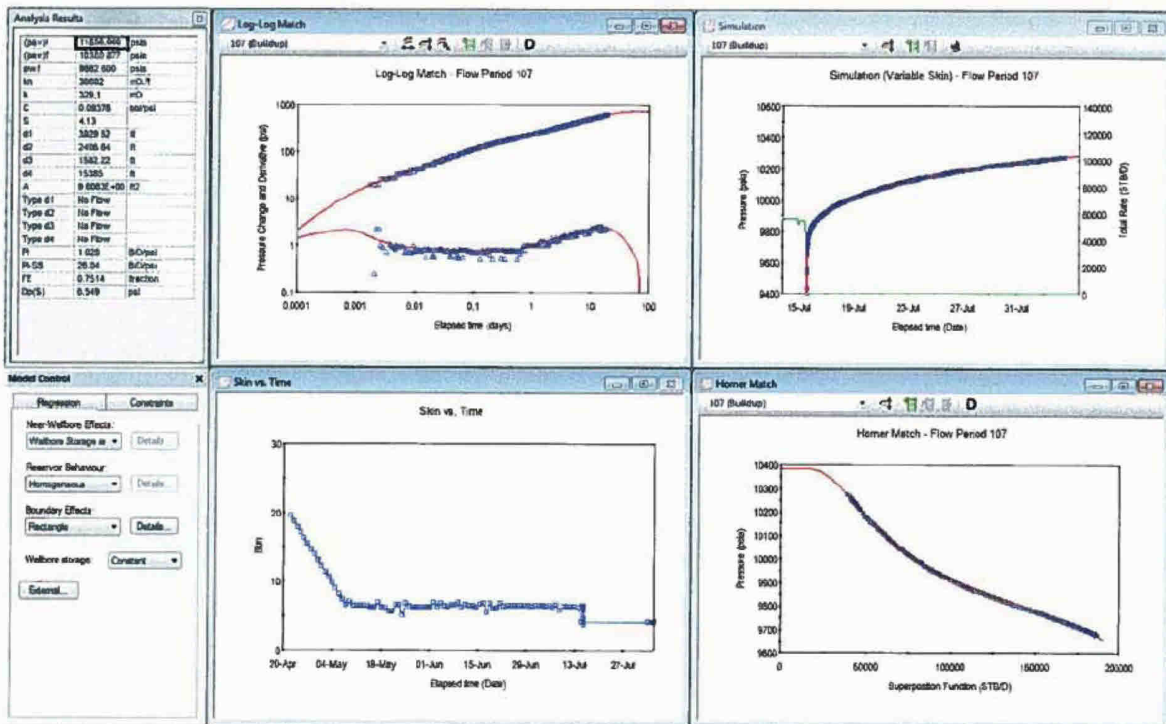
Figure 89: Interpretation Model, Model Match and Analysis Results (Zoom on Simulation – top left)

63
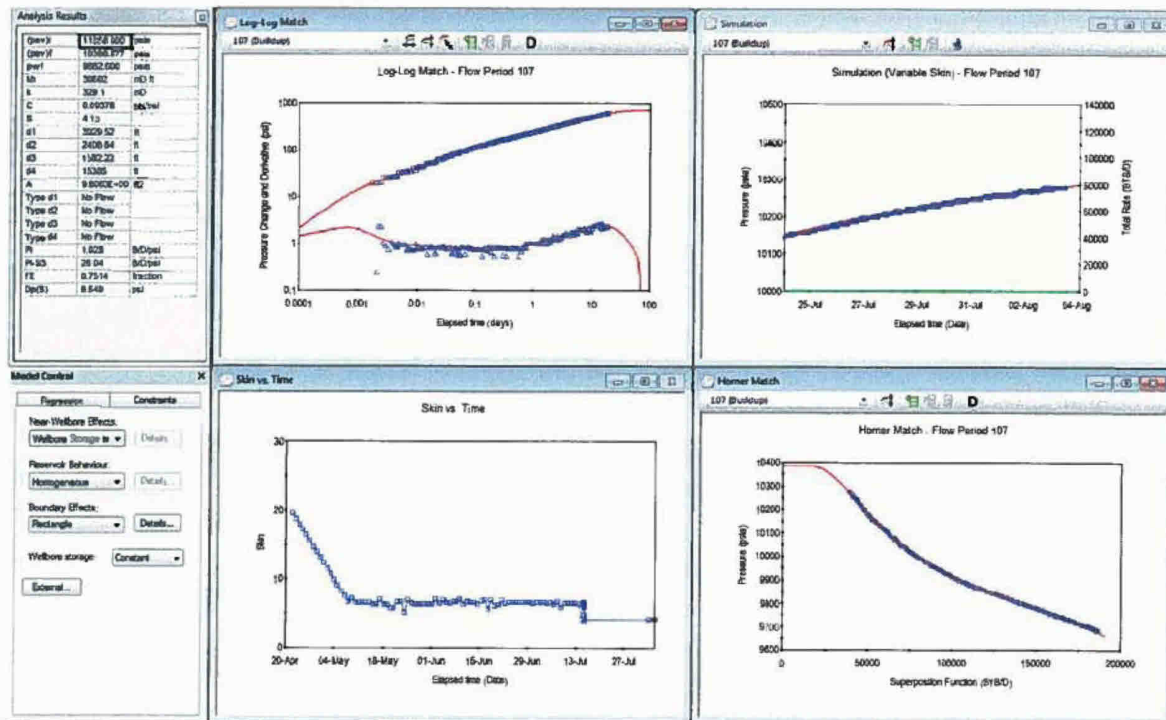
Figure 90: Interpretation Model, Model Match and Analysis Results (Further Zoom on Simulation – top left)

Analysis Model - Flow Period 107

Near Wellbore Effect: Wellbore Storage and Skin (C and S)
Reservoir Behaviour: Homogeneous
Boundary Effect: Rectangle

Initial average reservoir pressure, (pav)i	11856.000 psia
Final average reservoir pressure, (pav)f	10380.877 psia
Flowing pressure, pwf	9662.600 psia
Permeability Thickness, kh	30602 mD. ft
Permeability, k	329.1 mD
Wellbore storage coefficient, C	0.09376 bbl/psi
Wellbore skin factor, S	4.13
Distance to first boundary, d1	3929.52 ft
Distance to second boundary, d2	2406.64 ft
Distance to third boundary, d3	1582.22 ft
Distance to fourth boundary, d4	15385 ft
Drainage area, A	9.8063E+007 ft2
Type of first boundary, Type d1	No Flow
Type of second boundary, Type d2	No Flow
Type of third boundary, Type d3	No Flow
Type of fourth boundary, Type d4	No Flow
Measured Productivity Index, PI	1.028 B/D/psi
Steady State Productivity Index, PI-SS	26.04 B/D/psi
Flow Efficiency, FE	0.7514 fraction
Pressure drop due to skin, Dp(S)	6.549 psi

Figure 91: P10 Model (Option-2 Drill Pipe High) – Summary of Results

64

TREX-011696R.180

3.4.2.6 K mean (245mD) Permeability Well Test Analysis

Shown in Figures 93 – 97 are the model diagnosis, interpretation model, model matches and analysis results which confirm a very good match to the pressure history, log-log pressure change and derivative, and the superposition (Horner) plot.

The match to the pressure history at various scales, further confirms a good match giving more validity to the analysis results and higher confidence predicting the Macondo well and reservoir properties using the matched interpretation model.
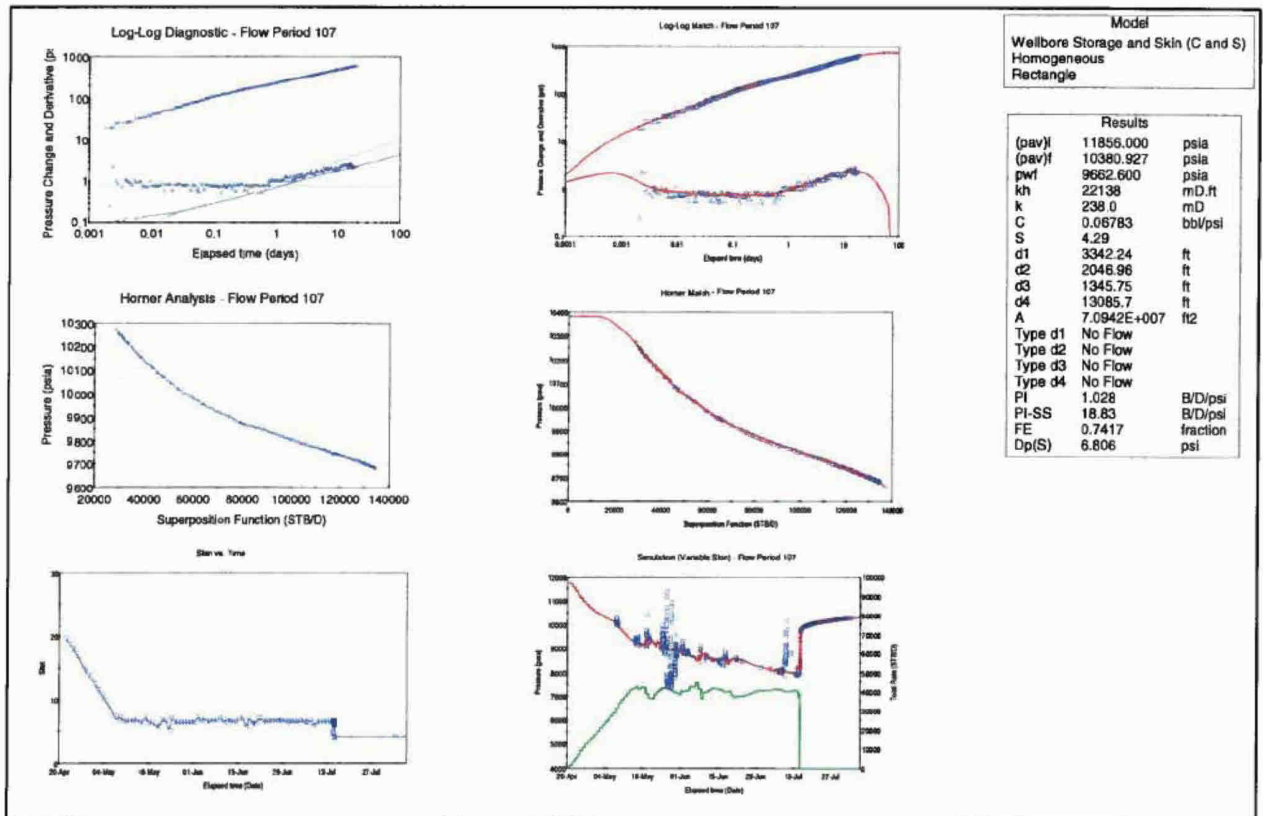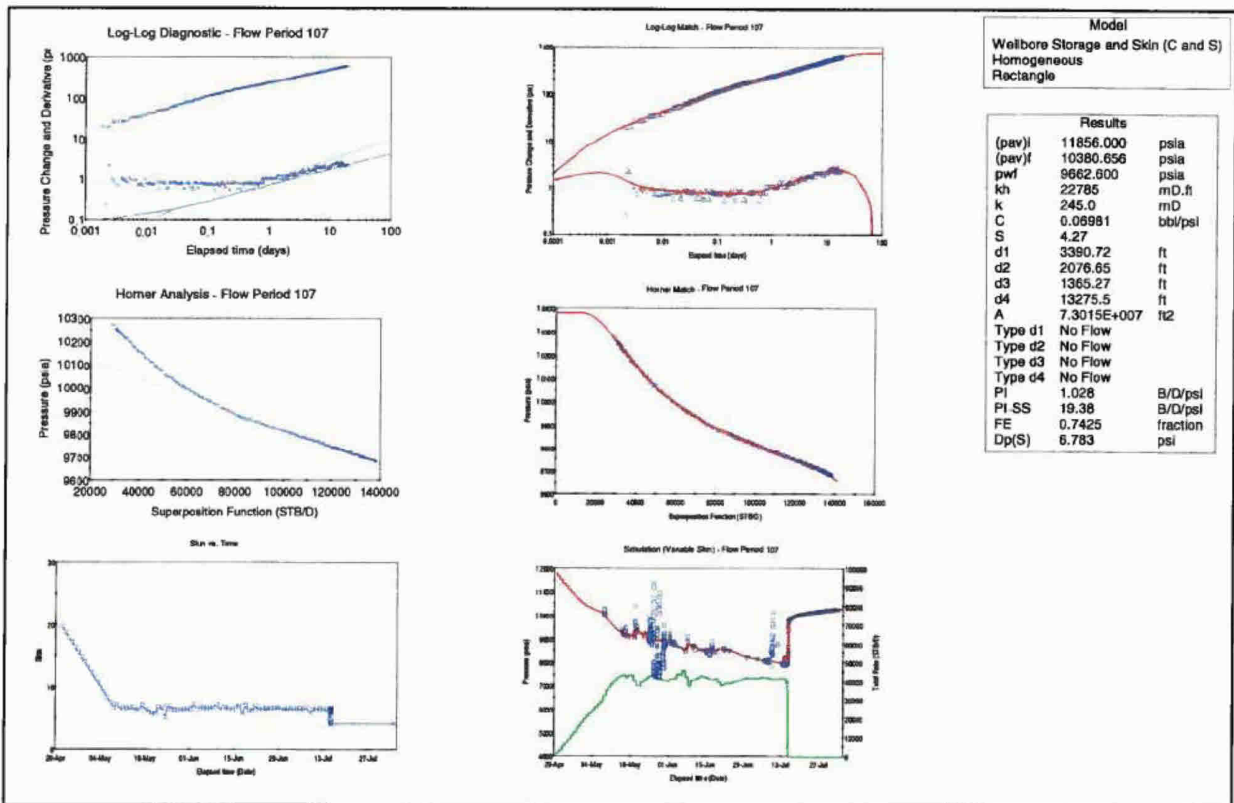

Figure 92: Diagnosis, Interpretation Model, Model Match and Analysis Results

Below are additional plots (Figures 94-97) showing the model match at various scales.
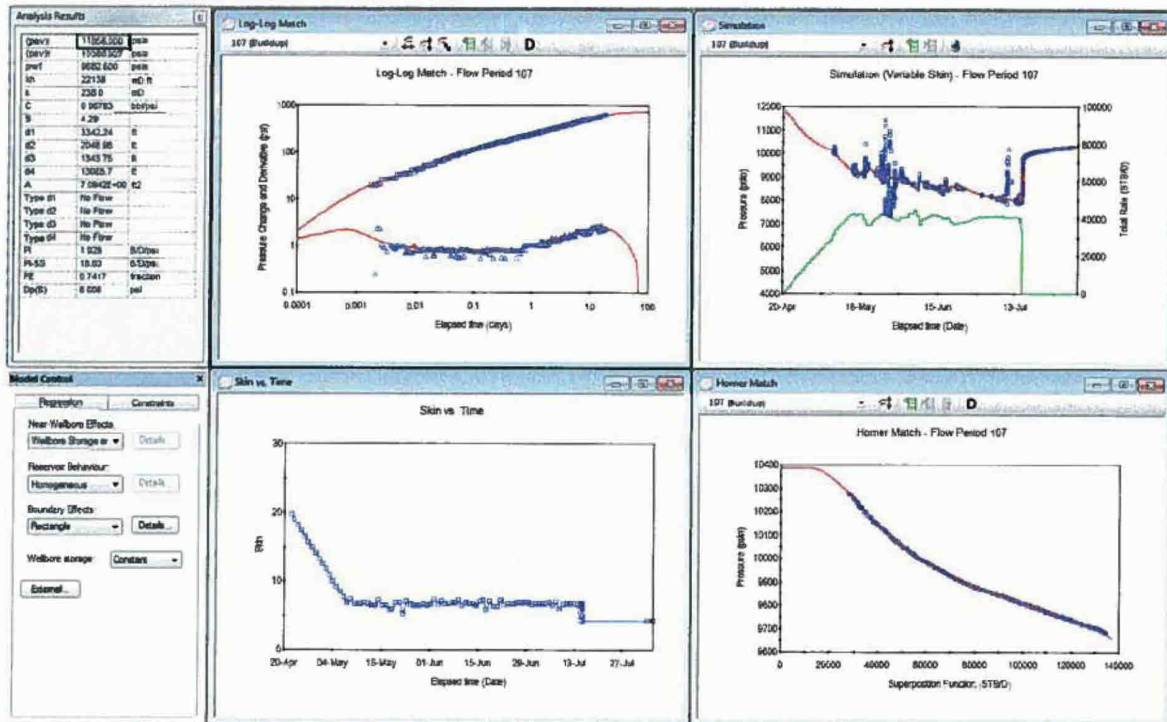
TREX-011696R.181
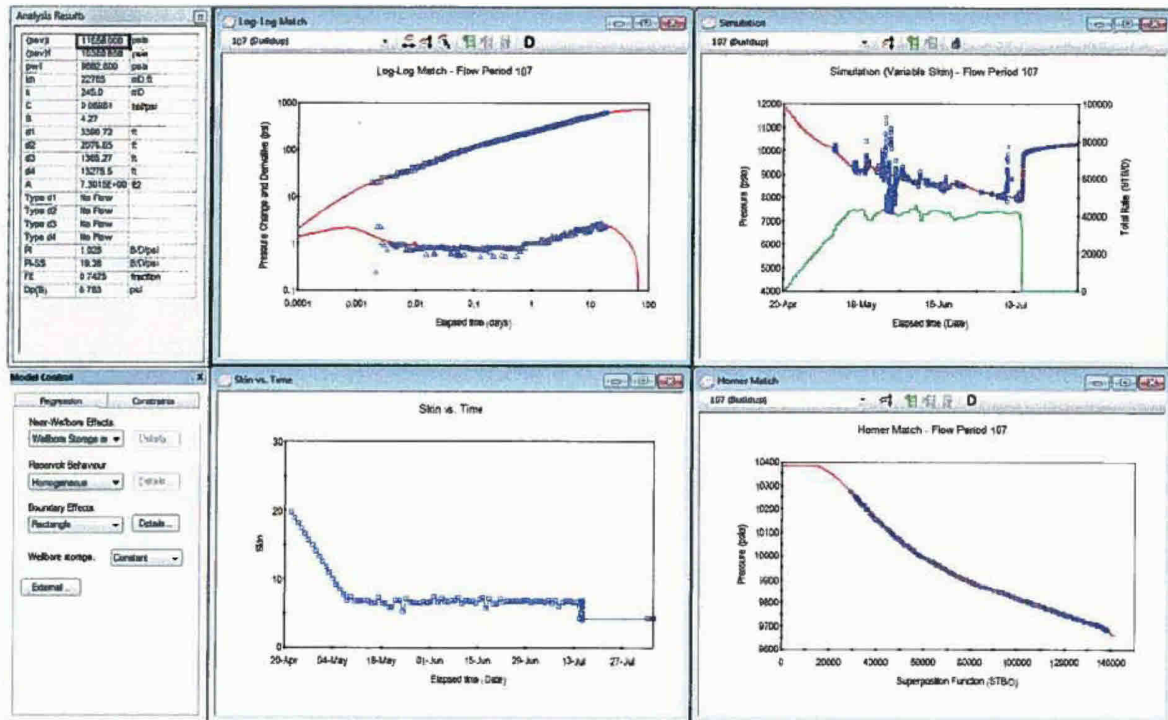
Figure 93: Interpretation Model, Model Match and Analysis Results
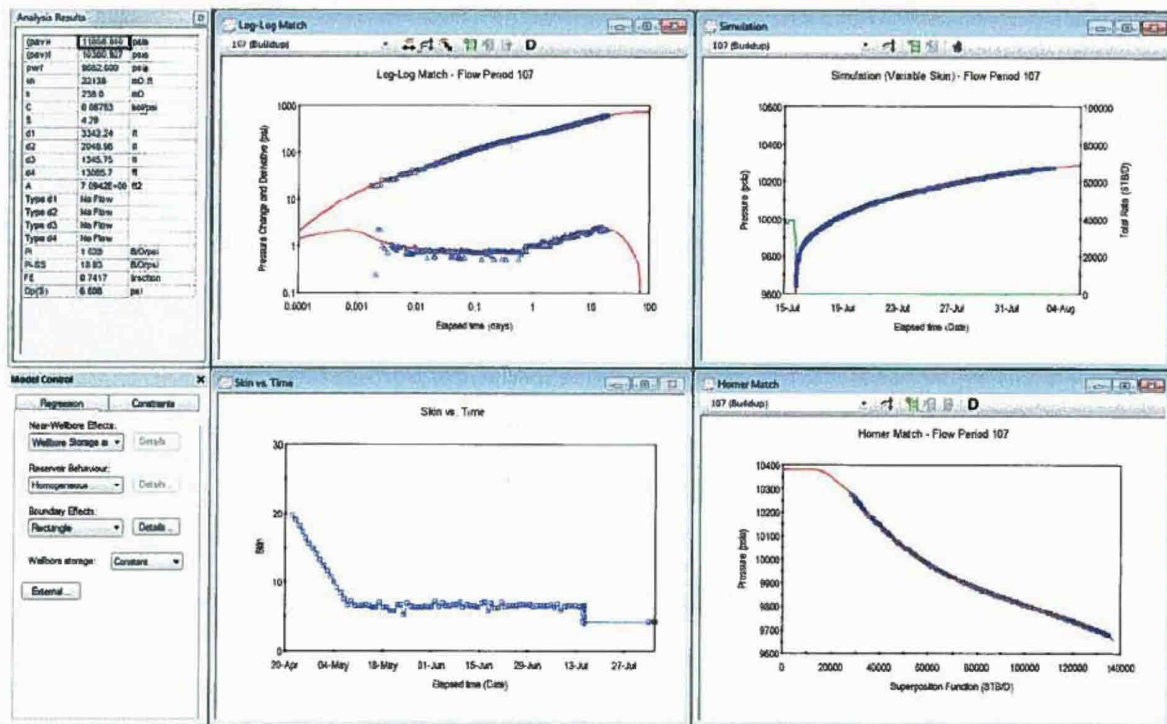

Figure 94: Interpretation Model, Model Match and Analysis Results (Zoom on Simulation – top left)
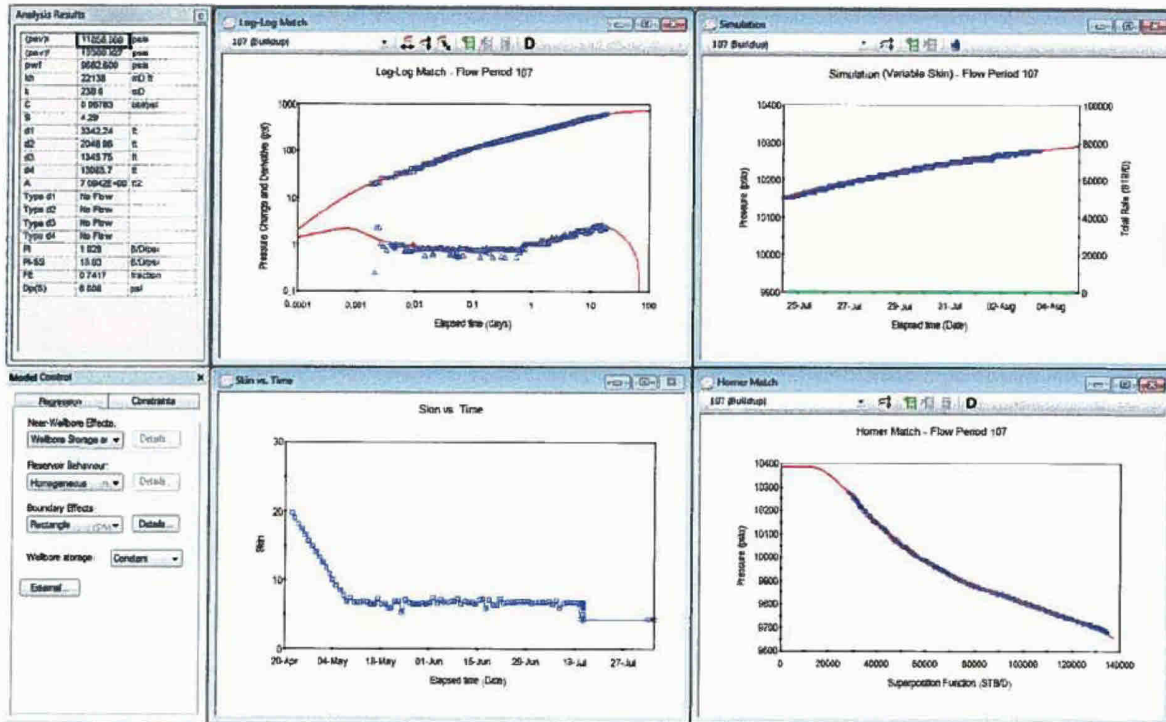
66

Figure 95: Interpretation Model, Model Match and Analysis Results (Further Zoom on Simulation – top left)

Analysis Model - Flow Period 107

Near Wellbore Effect: Wellbore Storage and Skin (C and S)
Reservoir Behaviour: Homogeneous
Boundary Effect: Rectangle

Initial average reservoir pressure, (pav)i	11856.000 psia
Final average reservoir pressure, (pav)f	10380.656 psia
Flowing pressure, pwf	9662.600 psia
Permeability Thickness, kh	22785 mD.ft
Permeability, k	245.0 mD
Wellbore storage coefficient, C	0.06981 bbl/psi
Wellbore skin factor, S	4.27
Distance to first boundary, d1	3390.72 ft
Distance to second boundary, d2	2076.65 ft
Distance to third boundary, d3	1365.27 ft
Distance to fourth boundary, d4	13275.5 ft
Drainage area, A	7.3015E+007 ft2
Type of first boundary, Type d1	No Flow
Type of second boundary, Type d2	No Flow
Type of third boundary, Type d3	No Flow
Type of fourth boundary, Type d4	No Flow
Measured Productivity Index, PI	1.028 B/D/psi
Steady State Productivity Index, PI-SS	19.38 B/D/psi
Flow Efficiency, FE	0.7425 fraction
Pressure drop due to skin, Dp(S)	6.783 psi

Figure 96: K-mean (245mD) Option-2 Drill Pipe High – Summary of Results

67

TREX-011696R.183

3.4.2.7 K 264mD Permeability Well Test Analysis

A sensitivity to 264mD was done by scaling the rates to match 45,000stb/d on the 14th of July, 2010.

Shown in Figures 98 – 102 are the model diagnosis, interpretation model, model matches and analysis results which confirm a very good match to the pressure history, log-log pressure change and derivative, and the superposition (Horner) plot.

The match to the pressure history at various scales, further confirm a good match giving more validity to the analysis results and higher confidence predicting the Macondo well and reservoir properties using the matched interpretation model.
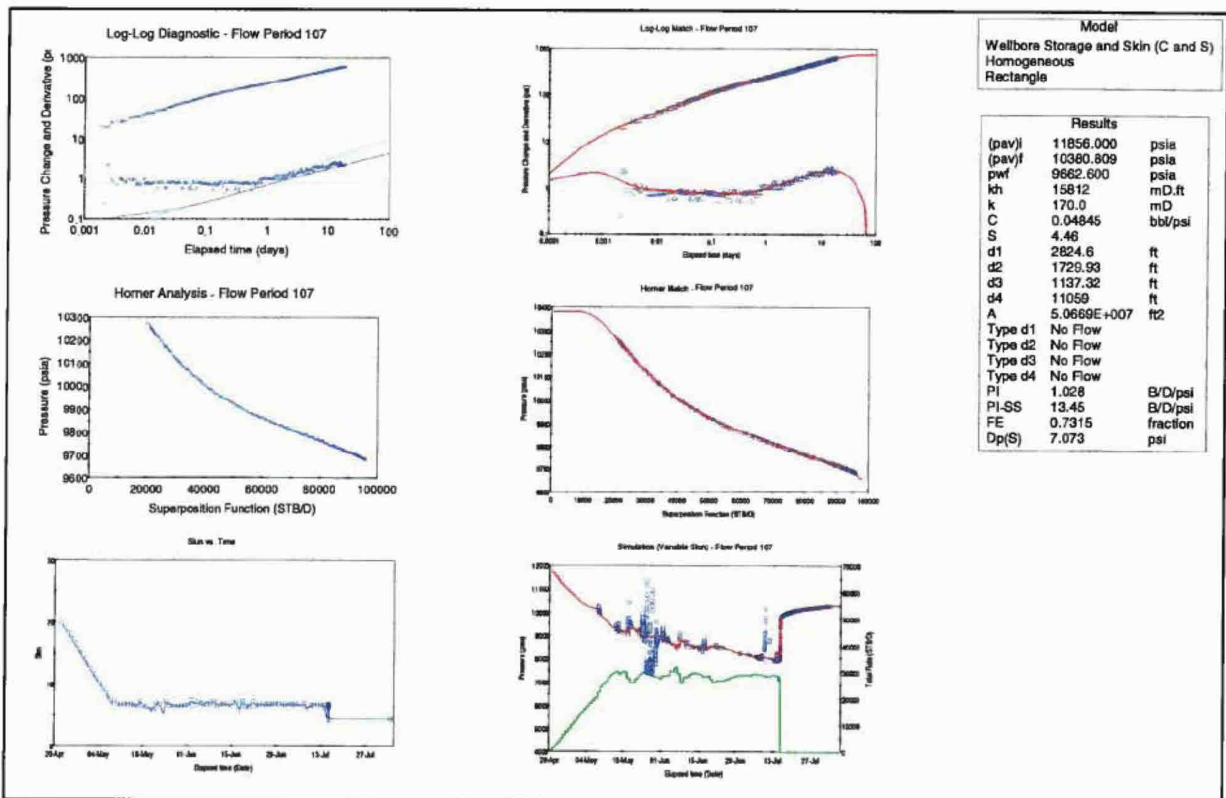

Figure 97: Diagnosis, Interpretation Model, Model Match and Analysis Results

Below are additional plots (Figures 99-102) showing the model match at various scales.
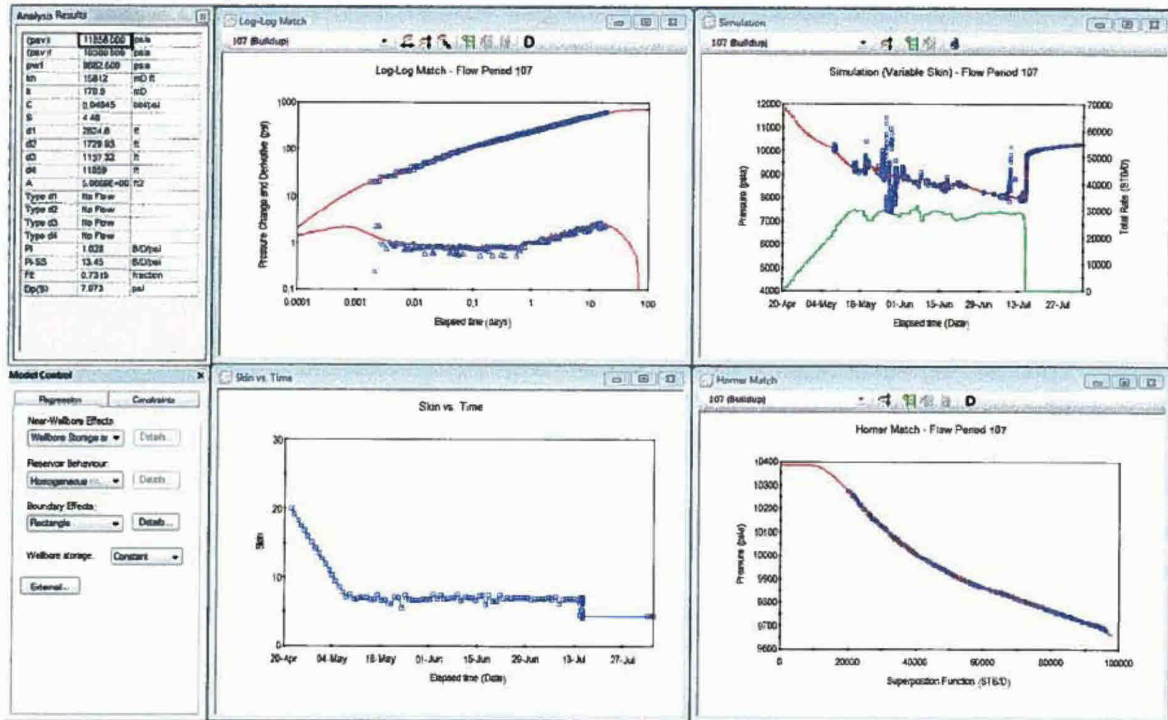
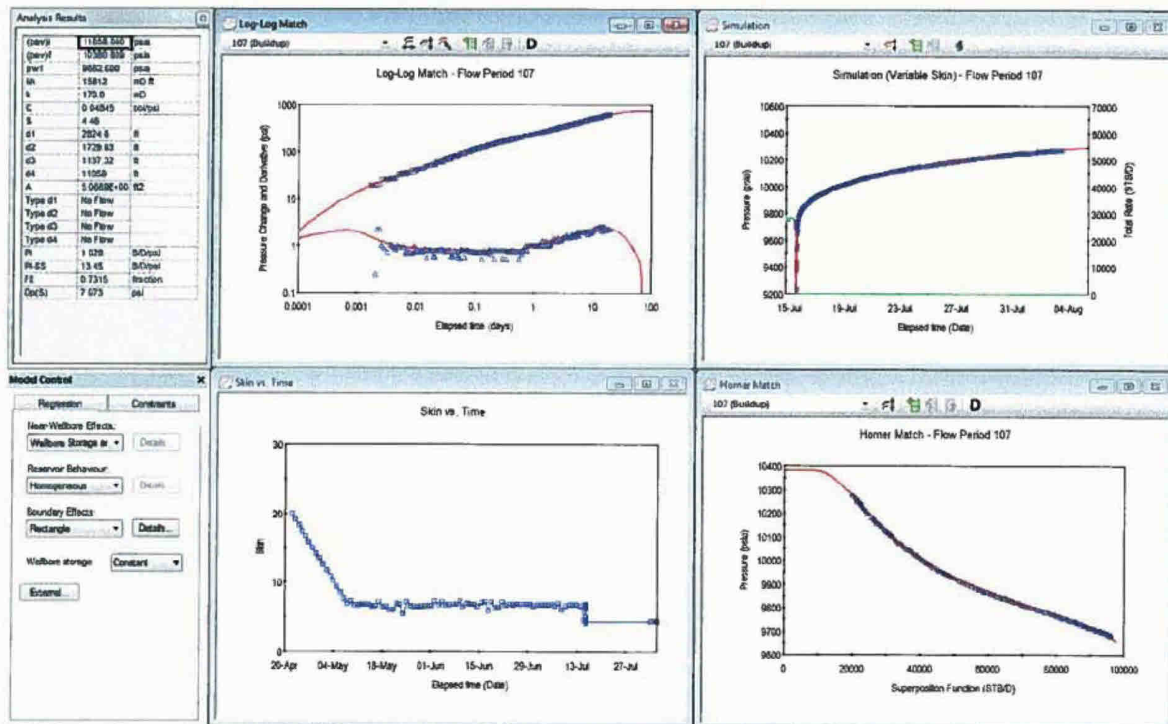**Figure 98: Interpretation Model, Model Match and Analysis Results**

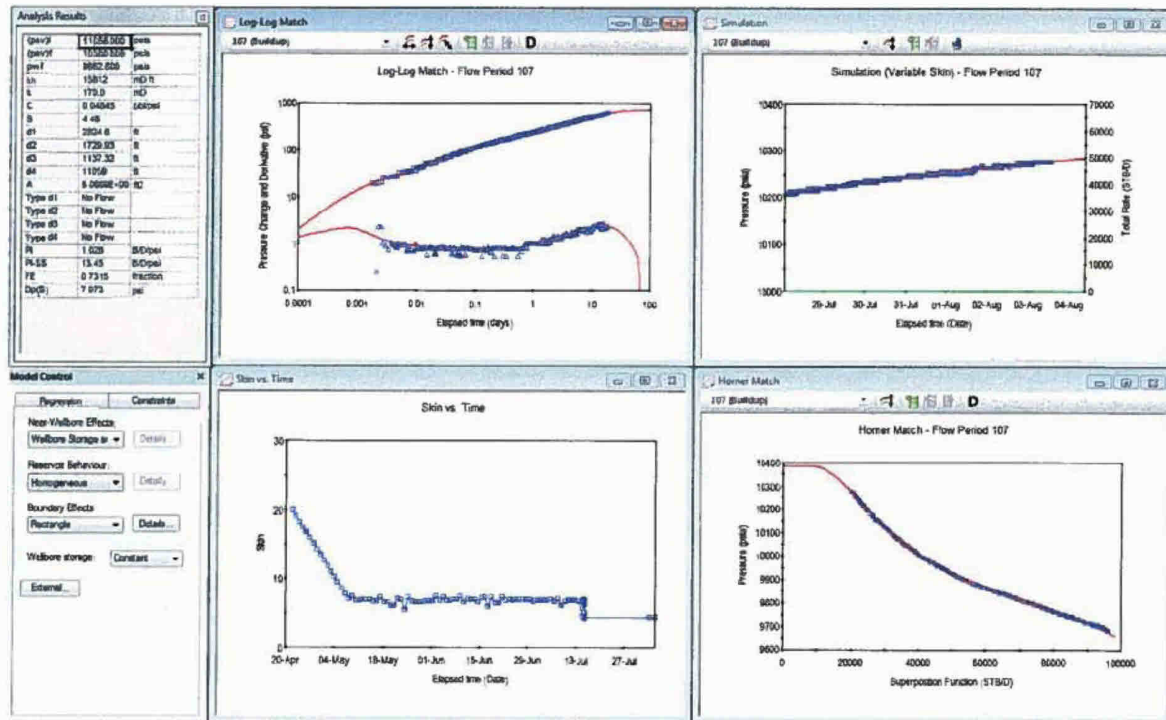**Figure 99: Interpretation Model, Model Match and Analysis Results (Zoom on Simulation – top left)**

69

Figure 100: Interpretation Model, Model Match and Analysis Results (Further Zoom on Simulation – top left)

Analysis Model - Flow Period 107

Near Wellbore Effect:	Wellbore Storage and Skin (C and S)
Reservoir Behaviour:	Homogeneous
Boundary Effect:	Rectangle

Initial average reservoir pressure, (pav)i	11856.000 psia
Final average reservoir pressure, (pav)f	10380.686 psia
Flowing pressure, pwf	9662.600 psia
Permeability Thickness, kh	24534 mD.ft
Permeability, k	263.8 mD
Wellbore storage coefficient, C	0.07517 bbl/psi
Wellbore skin factor, S	4.24
Distance to first boundary, d1	3518.45 ft
Distance to second boundary, d2	2154.88 ft
Distance to third boundary, d3	1416.7 ft
Distance to fourth boundary, d4	13775.6 ft
Drainage area, A	7.8619E+007 ft2
Type of first boundary, Type d1	No Flow
Type of second boundary, Type d2	No Flow
Type of third boundary, Type d3	No Flow
Type of fourth boundary, Type d4	No Flow
Measured Productivity Index, PI	1.028 B/D/psi
Steady State Productivity Index, PI-SS	20.87 B/D/psi
Flow Efficiency, FE	0.7448 fraction
Pressure drop due to skin, Dp(S)	6.725 psi

Figure 101: K 264mD (Option-2 Drill Pipe High) – Summary of Results

70

TREX-011696R.186

3.4.2.8 OPTION-2 DRILL PIPE HIGH (SUMMARY AND RESULTS)

Parameters	P 90	P 50	P 10	Mean K	K-264
Initial Pressure @ Reservoir Depth (18,056 ft TVDss) psia	11,856	11,856	11,856	11,856	11,856
Final Pressure @ Reservoir Depth (18,056 ft TVDss) psia	10,381	10,381	10,381	10,381	10,381
Depletion (psi)	1,475.00	1,475.00	1,475.00	1,475.00	1,475.00
Reservoir Permeability (mD)	170	238	329	245	264
Skin	20 → 4	20 → 4	20 → 4	20 → 4	20 → 4
Boundary1 (d1) – ft	2,825	3,342	3,930	3,391	3,518
Boundary2 (d2) – ft	1,730	2,047	2,407	2,077	2,155
Boundary3 (d3) – ft	1,137	1,346	1,582	1,365	1,417
Boundary4 (d4) - ft	11,059	13,086	15,385	13,276	13,776
Reservoir Width - ft	3,962	4,688	5,512	4,756	4,935
Reservoir Length - ft	12,789	15,133	17,792	15,353	15,931
Area (MM ft^2)	50.7	70.9	98.1	73.0	78.6
Area (Acres)	1,163	1,629	2,251	1,676	1,805
STOIIP (MMstb)	69	97	133	99	107
Cumulative Production (MMstb)	2.15	3.00	4.15	3.09	3.33

Figure 102: OPTION-2 DRILL PIPE HIGH – Summary of Results

71

3.4.3 OPTION-2 DRILL PIPE LOW

3.4.3.1 Flow Period Selection

A total of 107 flow periods were also used to represent rate variations during the entire production and pressure history. The period when the Macondo well is full shut-in is flow period 107.

3.4.3.2 Deconvolution

Figures 104 – 114 below show the input pressures and rates, successive iterations of pressure rate histories, the final deconvolved derivative, the pressure match and quality of the pressure match. The quality (error difference) indicates a very good match at the 3rd and 4th iteration.
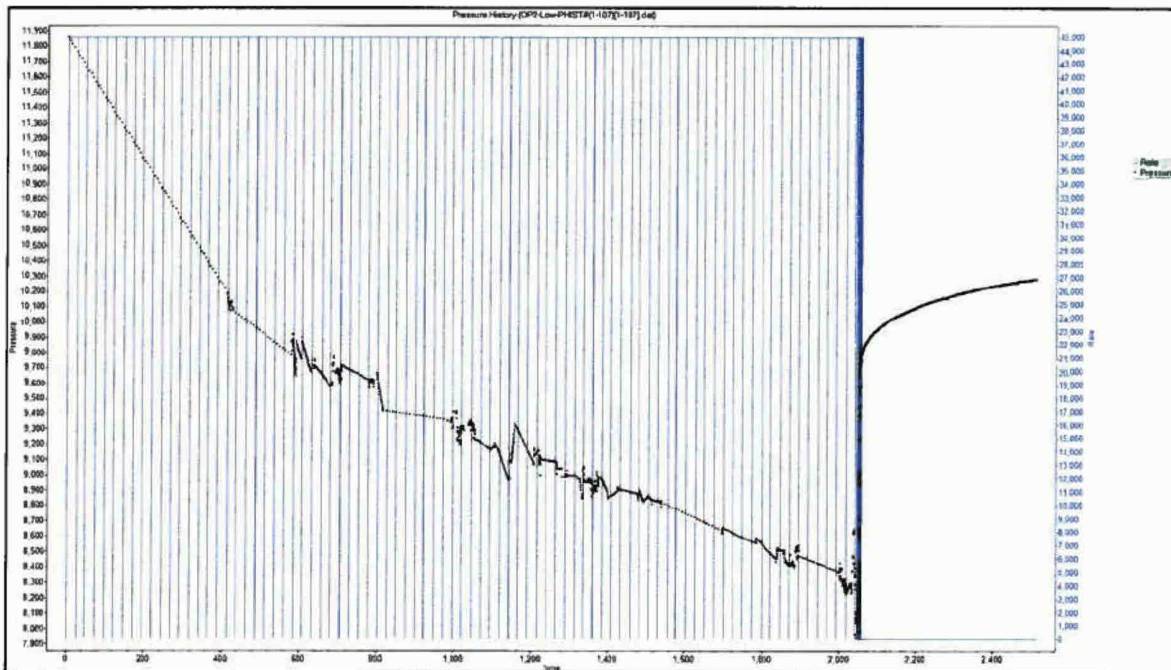
Figure 103: Input Pressure and Rate
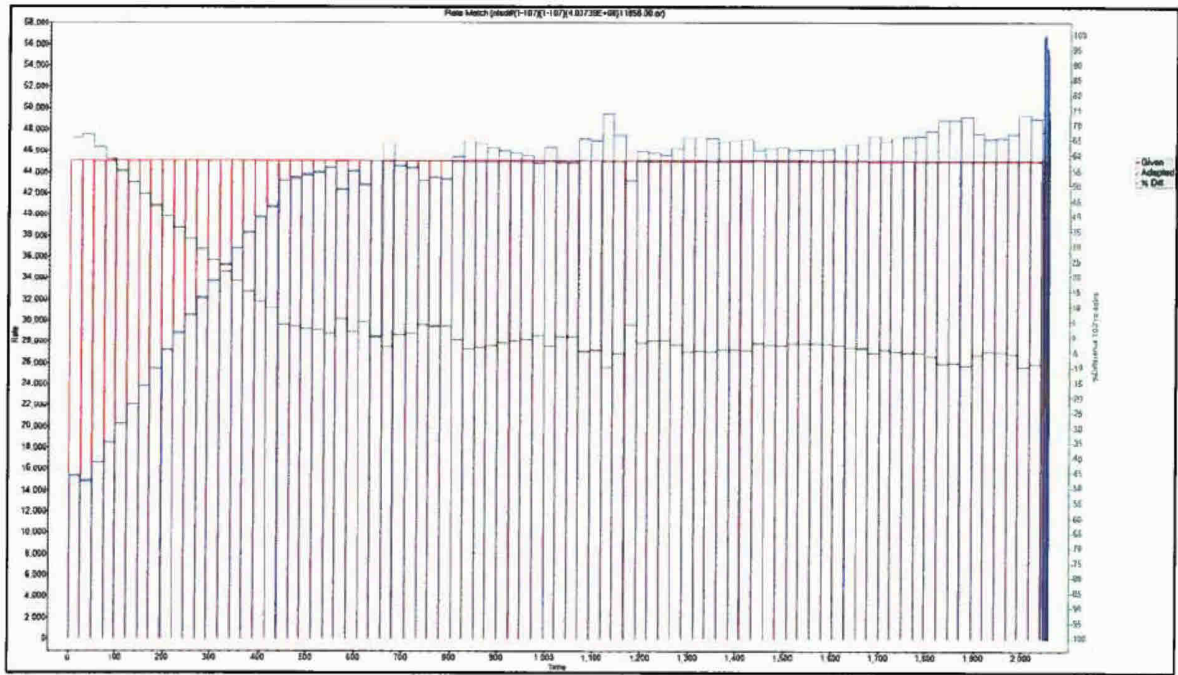
Figure 104: Adapted Rates (Iteration 1)
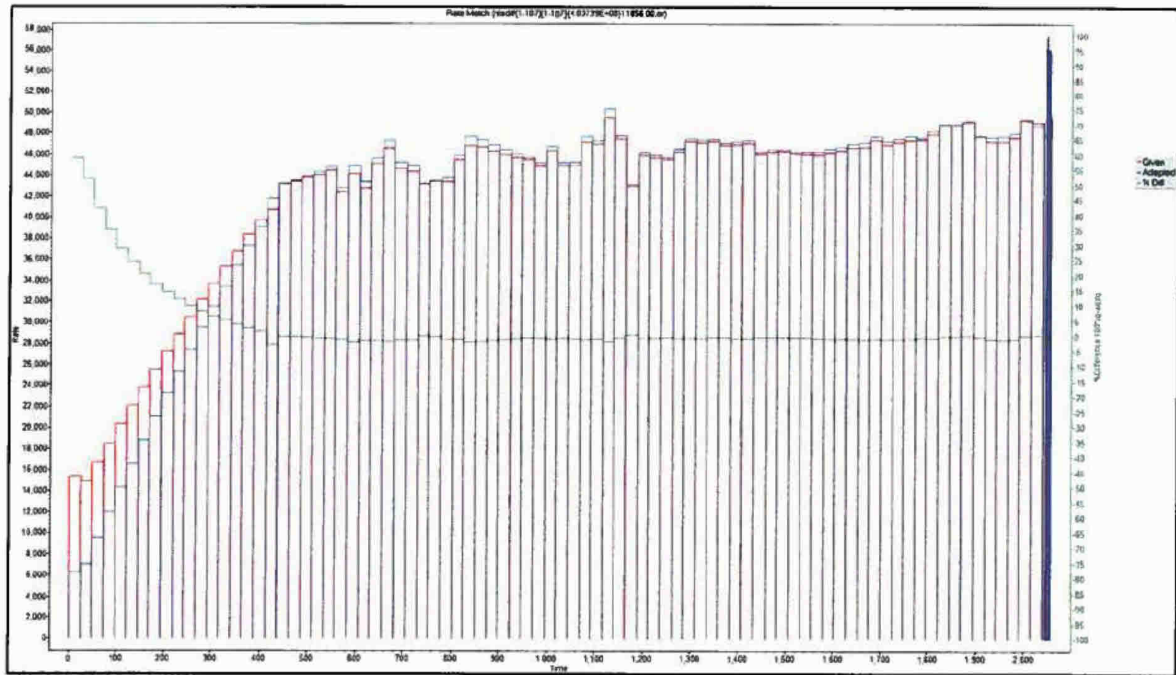
Figure 105: Adapted Rates (Iteration 2)

73
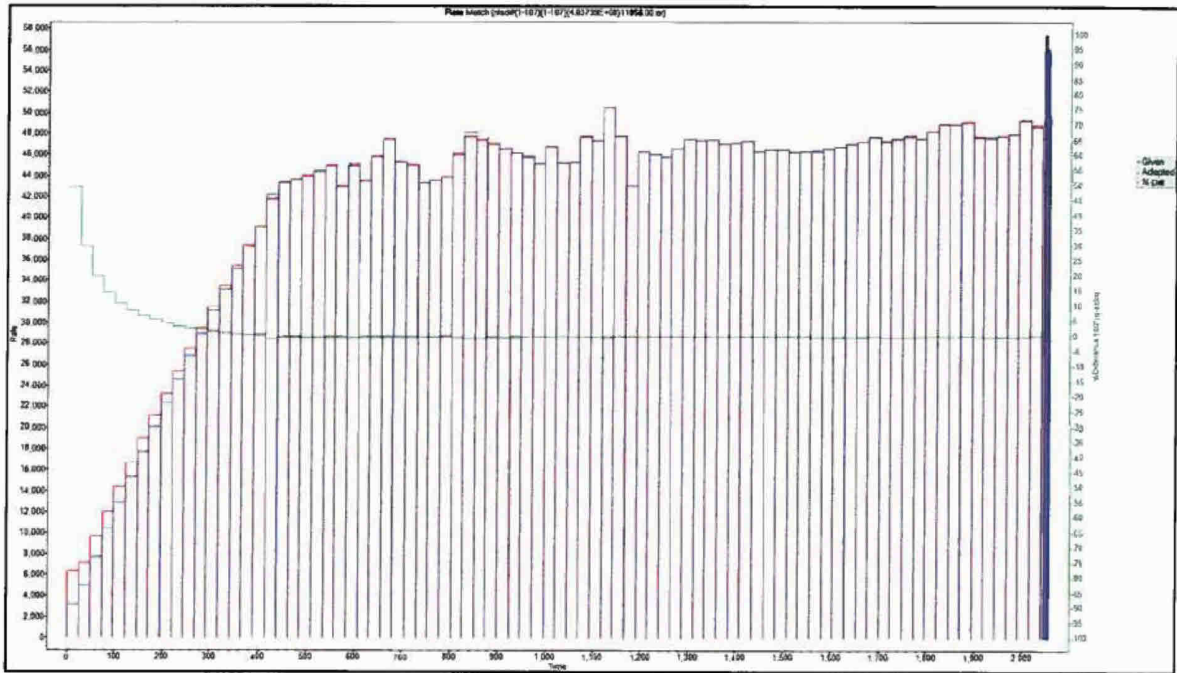
Figure 106: Adapted Rates (Iteration 3)
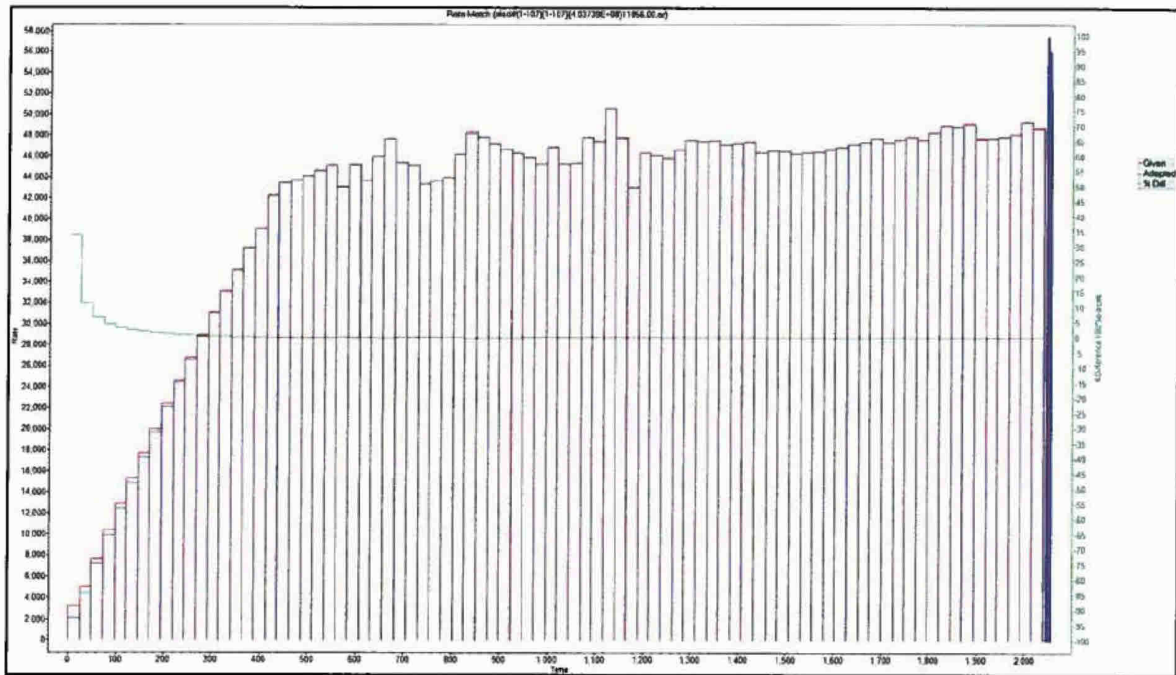
Figure 107: Adapted Rates (Iteration 4)

74
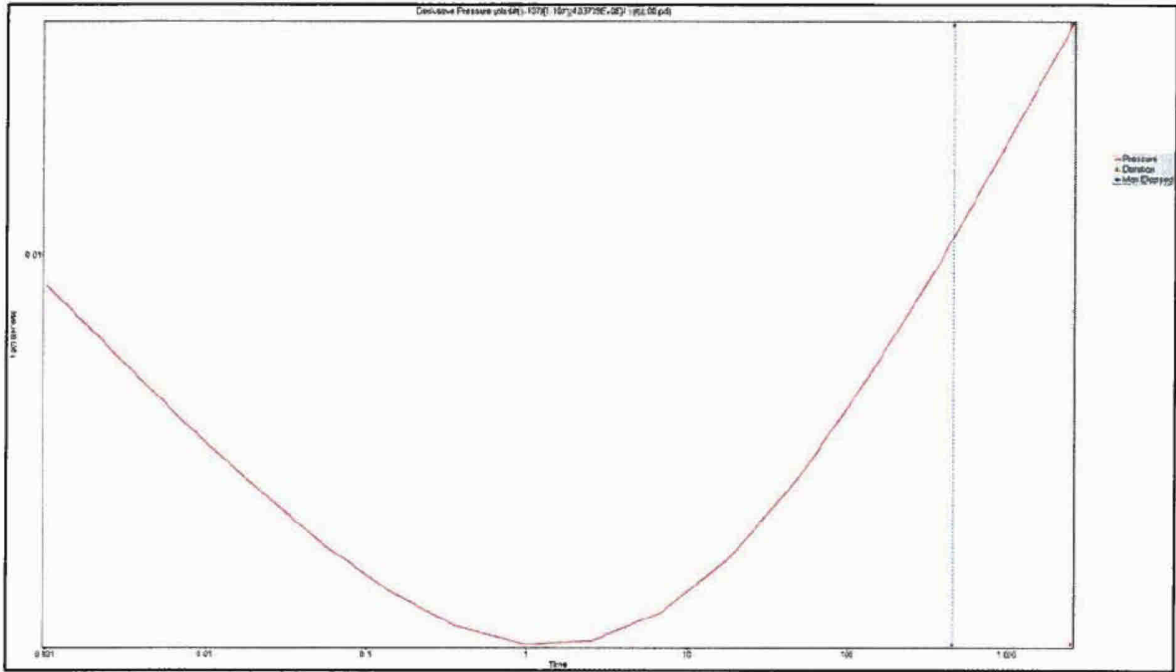
Figure 108: Deconvolved Derivative (Iteration 3)
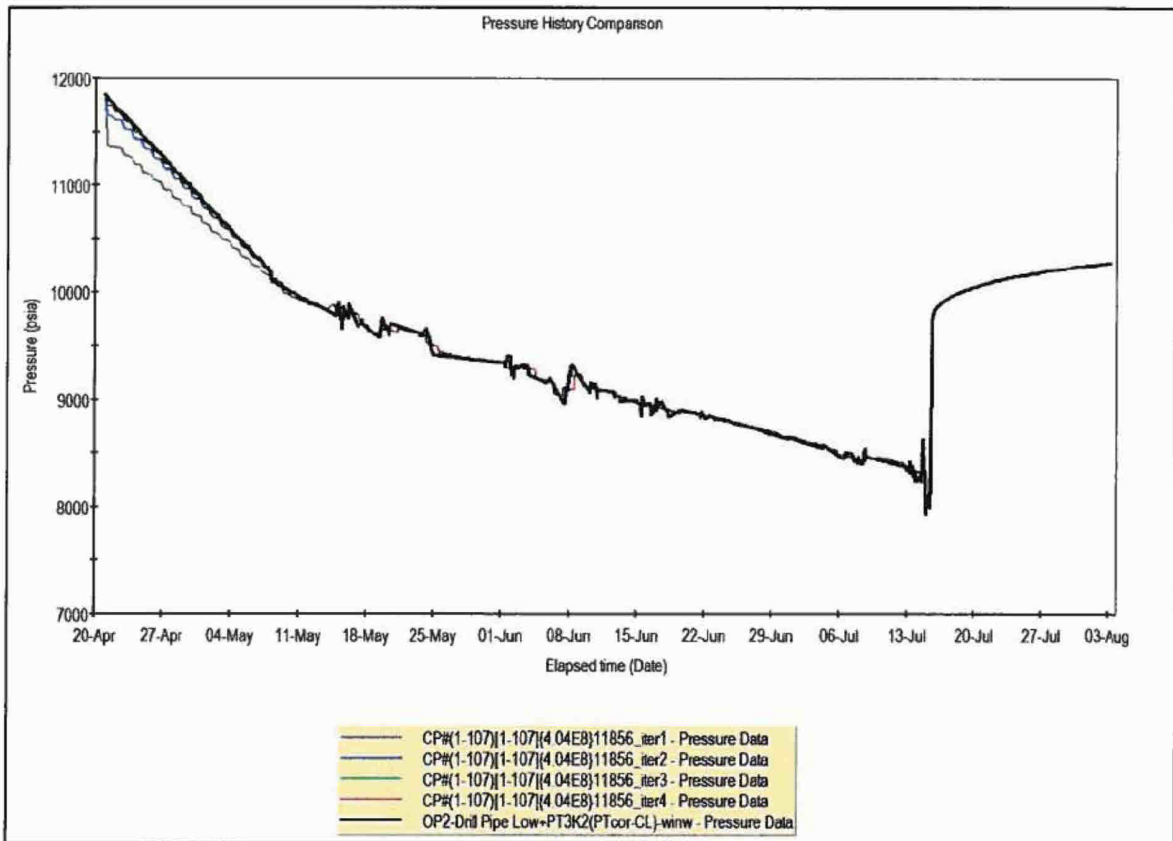
Figure 109: Pressure Match to Input Linearly Interpolated Pressures (1)

75
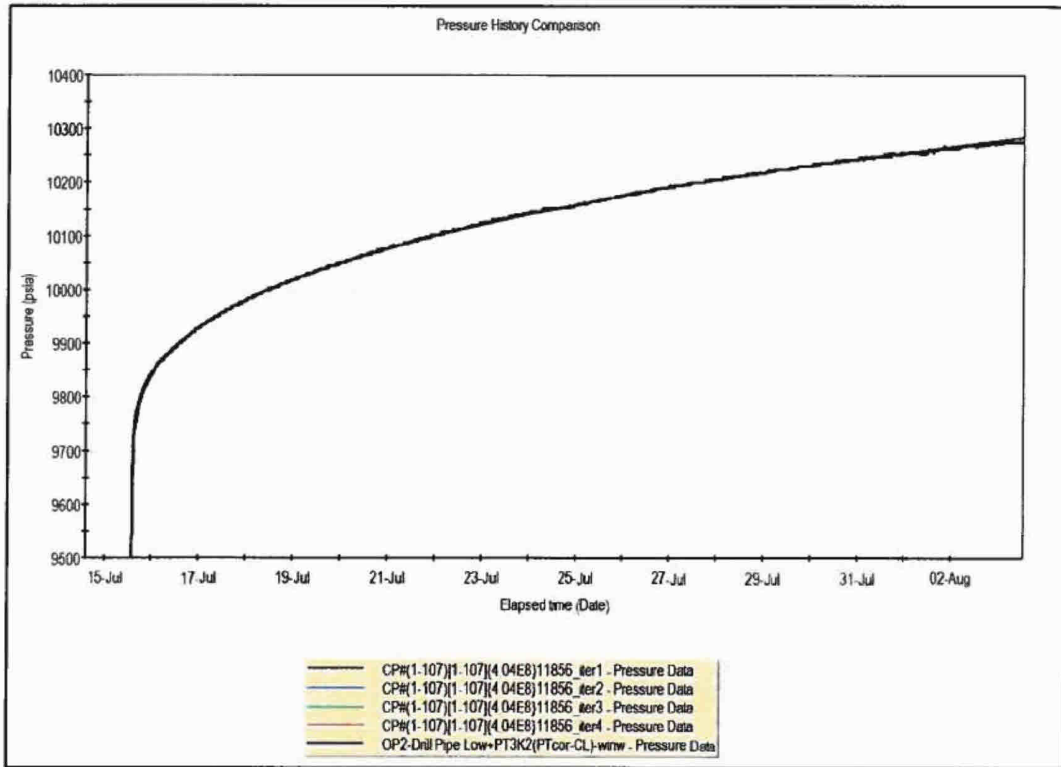
Figure 110: Pressure Match to Input Linearly Interpolated Pressures (2)
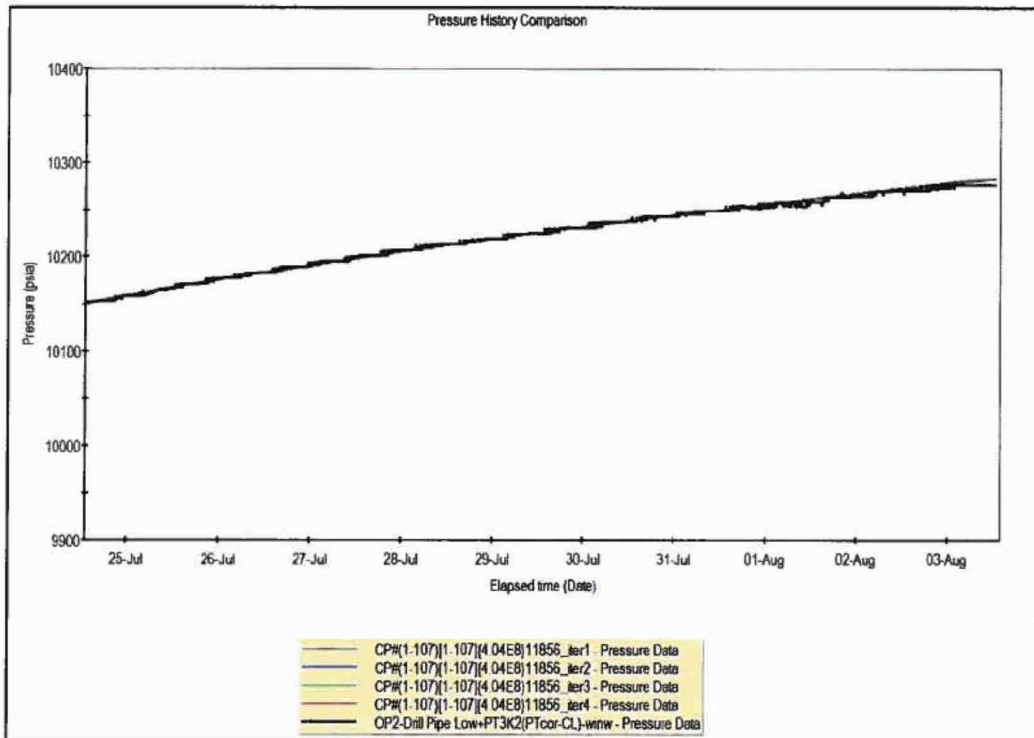
Figure 111: Pressure Match to Input Linearly Interpolated Pressures (3)

76
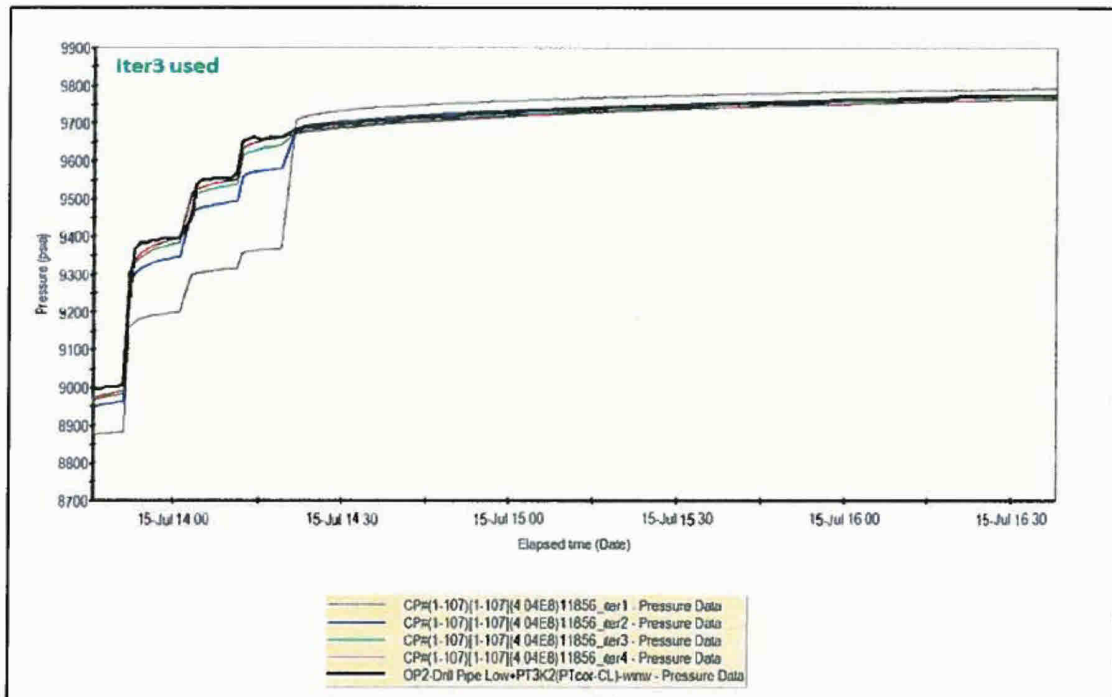
Figure 112: Pressure Match to Input Linearly Interpolated Pressures (4)
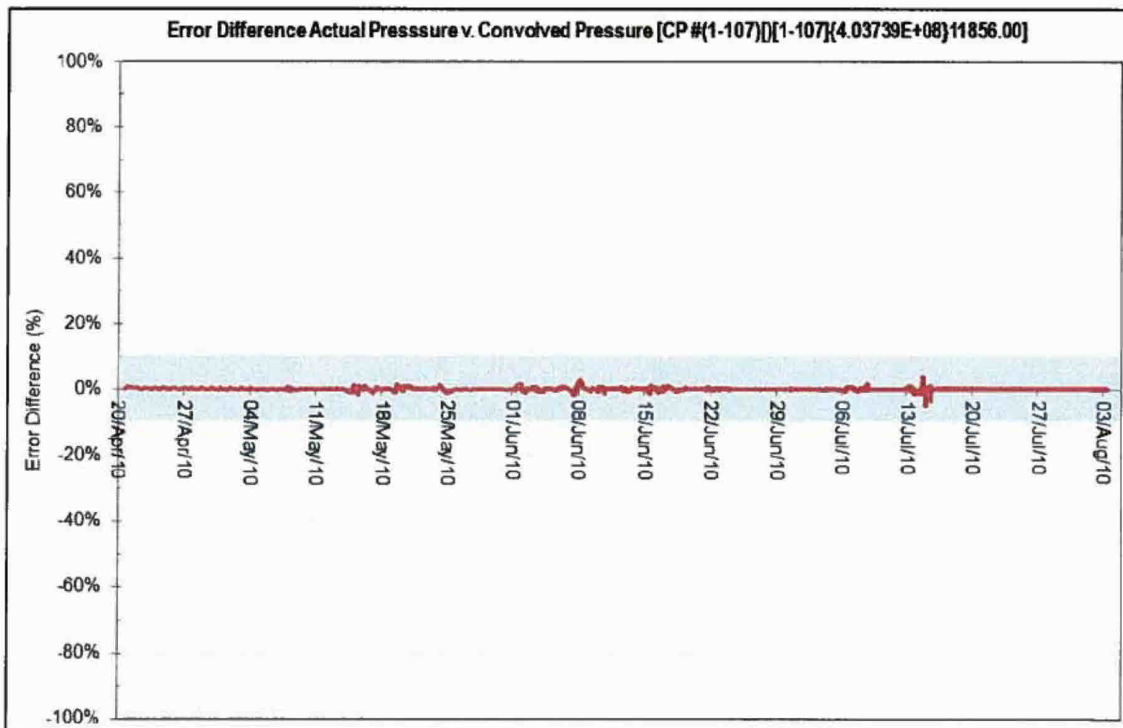
Figure 113: Quality Check on Error Difference (Convolved Pressure – iteration 3)

The convolved pressure match at the third iteration was near excellent and used as the rate profile for the well test analysis. The rates are scaled linearly to match the MDT uncertainty range of permeabilities (P50 238mD, P90 170mD, P10 329mD and Mean Permeability 245mD).

77

3.4.3.3 P50 Permeability Well Test Analysis

Shown in Figures 115 – 119 are the model diagnosis, interpretation model, model matches and analysis results which confirm a very good match to the pressure history, log-log pressure change and derivative, and the superposition (Horner) plot.

The match to the pressure history at various scales, further confirms a good match giving more validity to the analysis results and higher confidence predicting the Macondo well and reservoir properties using the matched interpretation model.

Figure 114: Diagnosis, Interpretation Model, Model Match and Analysis Results

Below are additional plots (Figures 116-119) showing the model match at various scales.

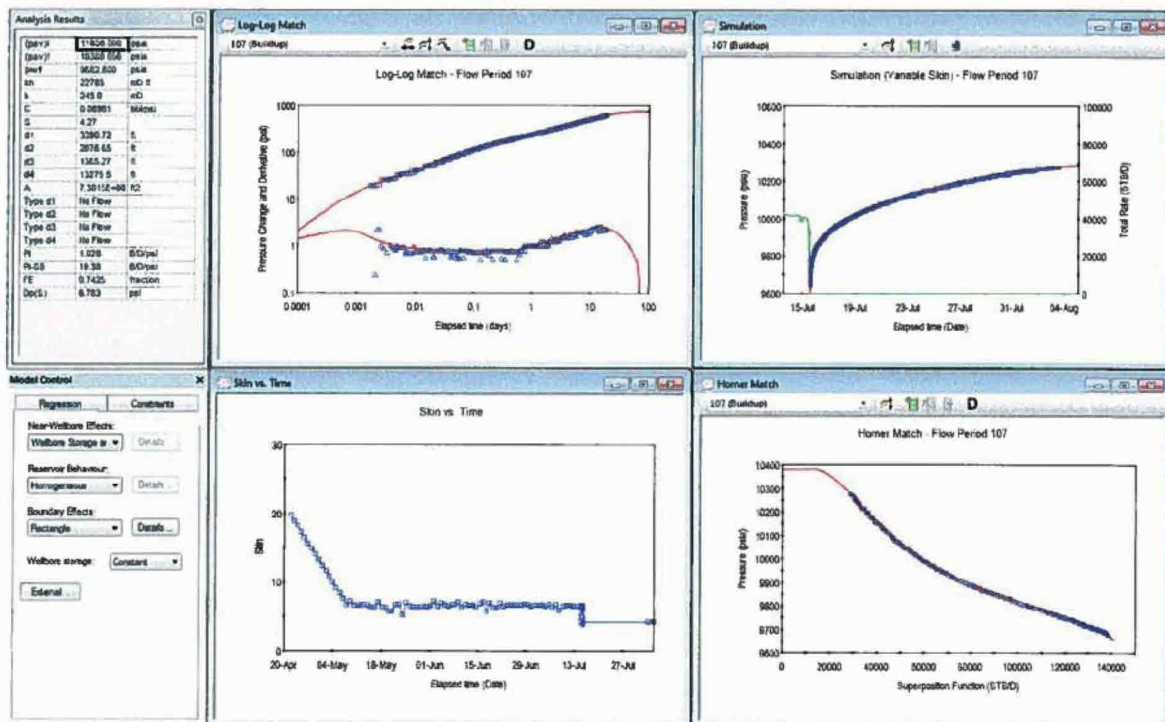**Figure 115: Interpretation Model, Model Match and Analysis Results**

Figure 116: Interpretation Model, Model Match and Analysis Results (Zoom on Simulation – top left)
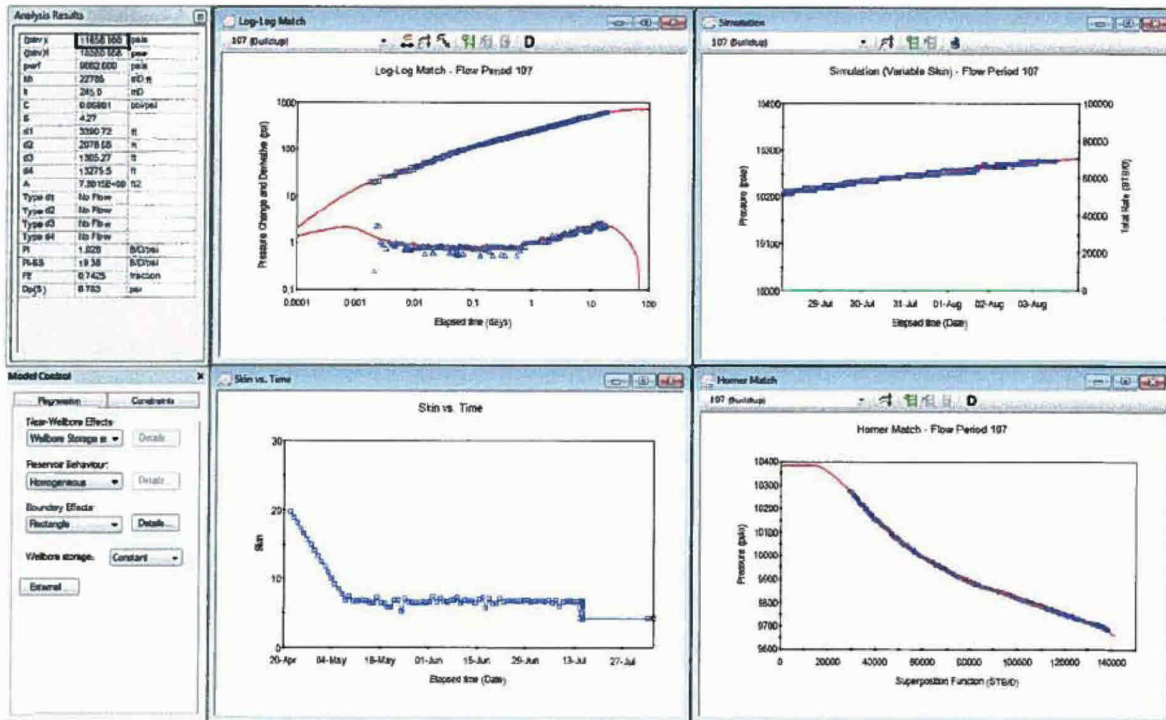
79

Figure 117: Interpretation Model, Model Match and Analysis Results (Further Zoom on Simulation – top left)

Analysis Model - Flow Period 107

Near Wellbore Effect: Wellbore Storage and Skin (C and S)
Reservoir Behaviour: Homogeneous
Boundary Effect: Rectangle

Initial average reservoir pressure, (pav)i	11856.000 psia
Final average reservoir pressure, (pav)f	10373.844 psia
Flowing pressure, pwf	9662.600 psia
Permeability Thickness, kh	22133 mD.ft
Permeability, k	238.0 mD
Wellbore storage coefficient, C	0.06142 bbl/psi
Wellbore skin factor, S	2.46
Distance to first boundary, d1	2842.26 ft
Distance to second boundary, d2	1862.72 ft
Distance to third boundary, d3	1027.71 ft
Distance to fourth boundary, d4	12898.5 ft
Drainage area, A	5.7126E+007 ft2
Type of first boundary, Type d1	No Flow
Type of second boundary, Type d2	No Flow
Type of third boundary, Type d3	No Flow
Type of fourth boundary, Type d4	No Flow
Measured Productivity Index, PI	1.038 B/D/psi
Steady State Productivity Index, PI-SS	20.02 B/D/psi
Flow Efficiency, FE	0.8421 fraction
Pressure drop due to skin, Dp(S)	6.249 psi

Figure 118: P50 Model (Option-2 Drill Pipe Low) – Summary of Results

80

3.4.3.4 P90 Permeability Well Test Analysis

Shown in Figures 120 – 124 are the model diagnosis, interpretation model, model matches and analysis results which confirm a very good match to the pressure history, log-log pressure change and derivative, and the superposition (Horner) plot.

The match to the pressure history at various scales, further confirms a good match giving more validity to the analysis results and higher confidence predicting the Macondo well and reservoir properties using the matched interpretation model.
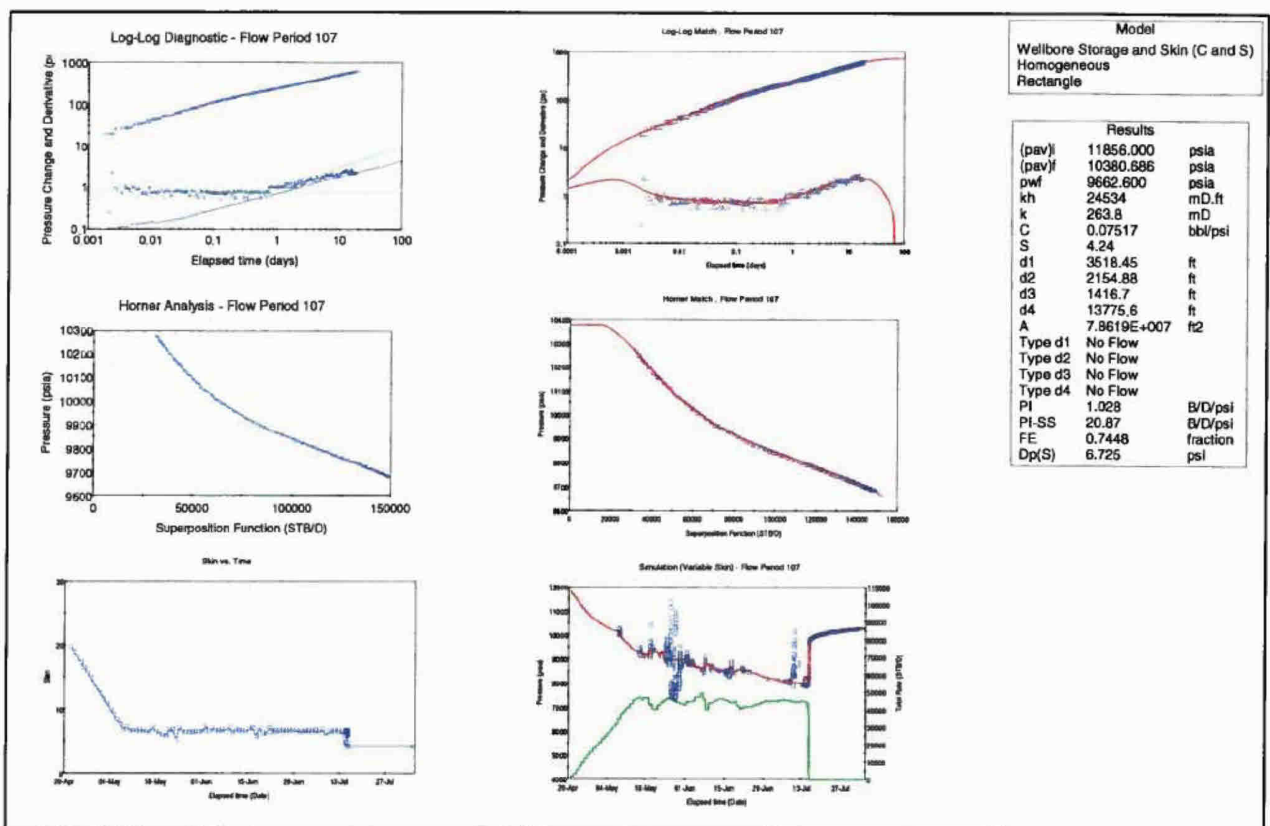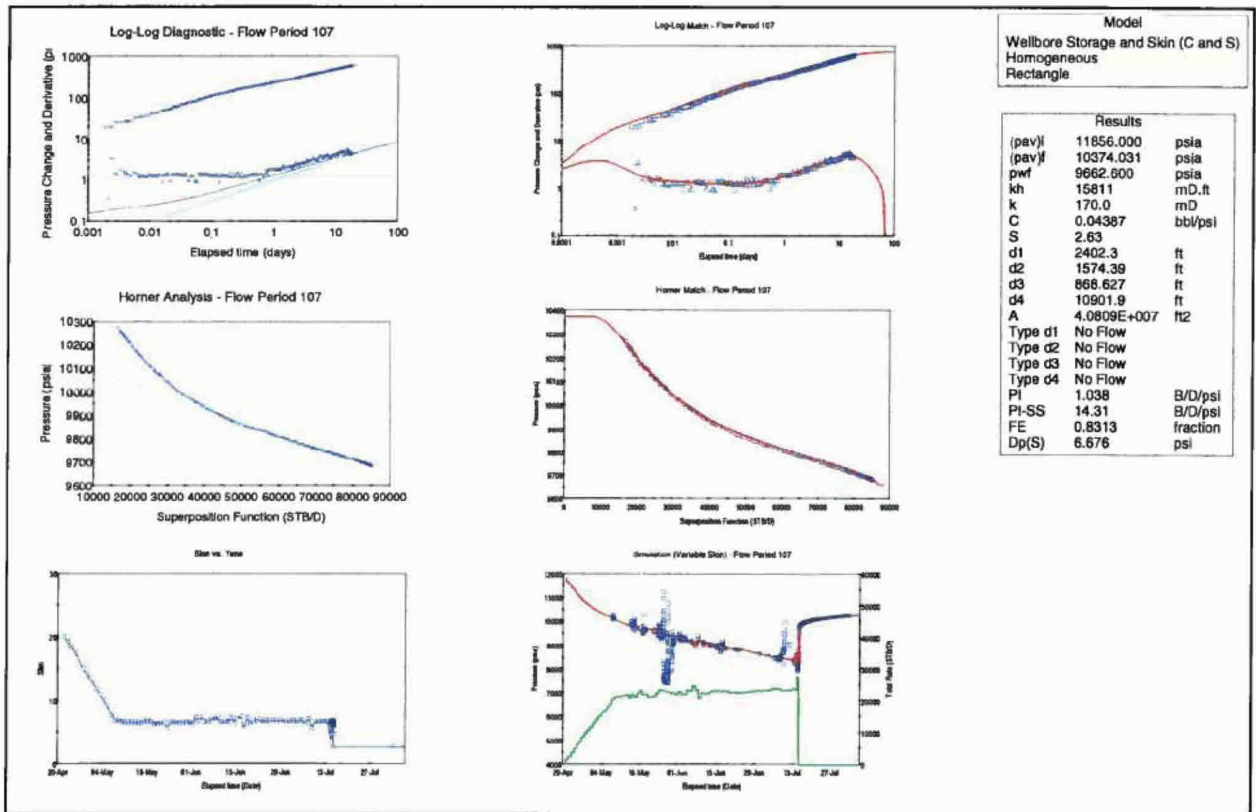

Figure 119: Diagnosis, Interpretation Model, Model Match and Analysis Results

Below are additional plots (Figures 121-124) showing the model match at various scales.
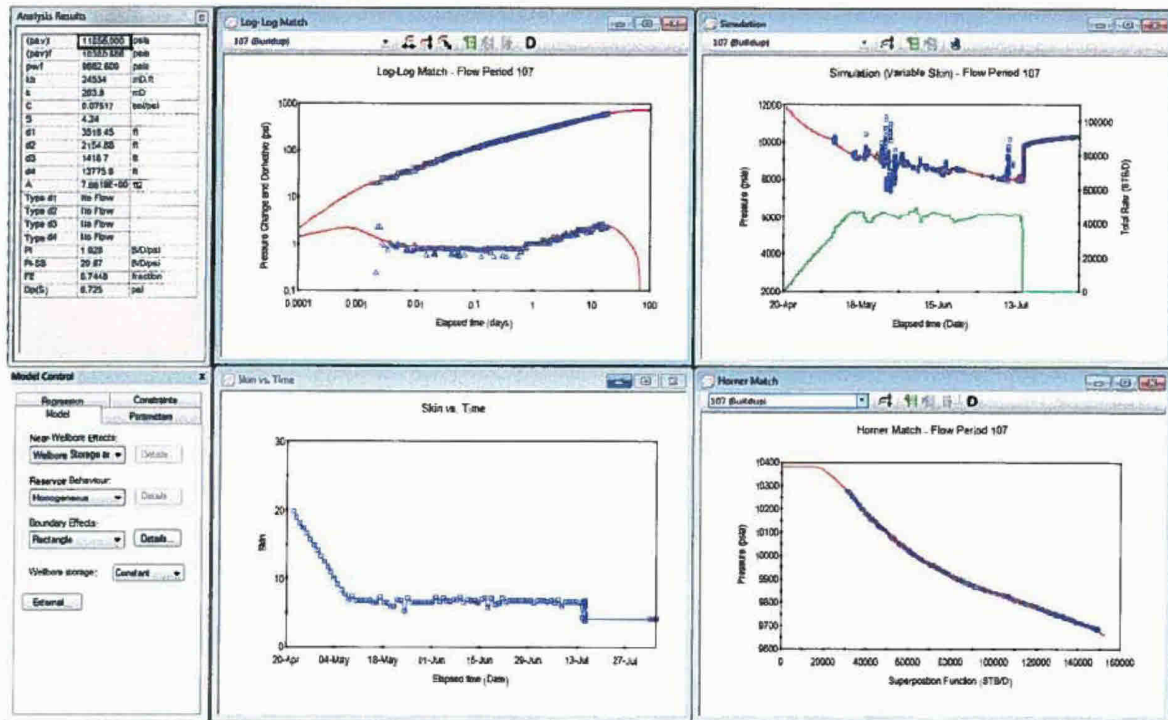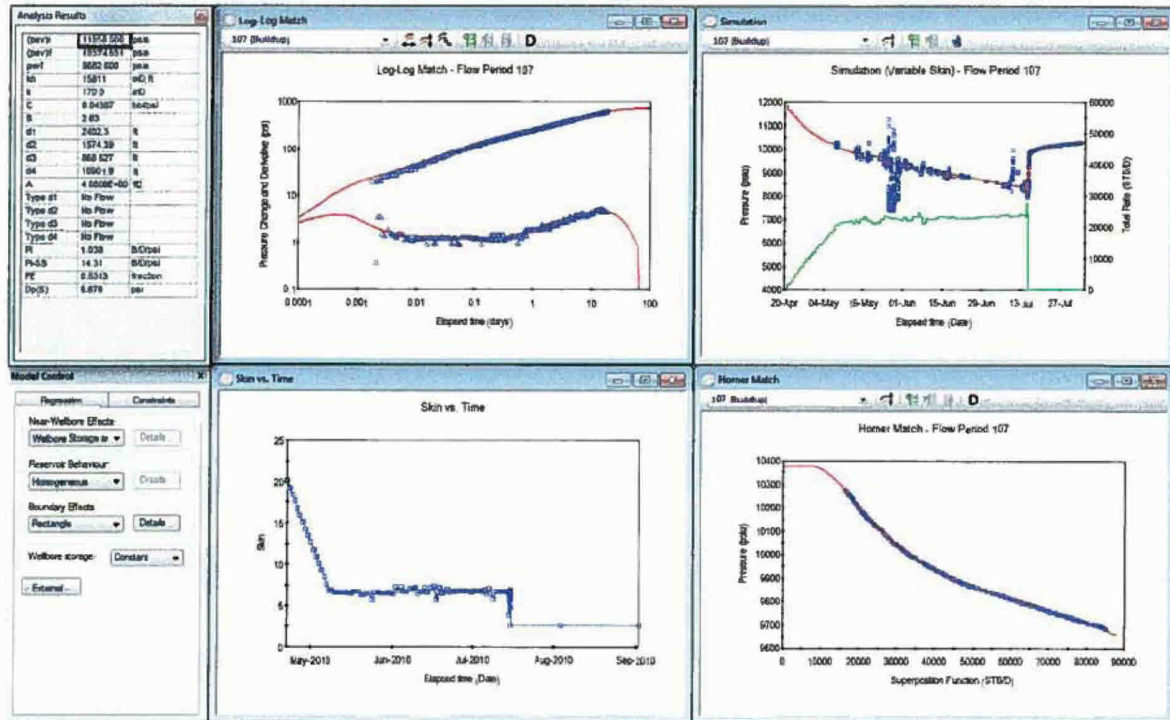
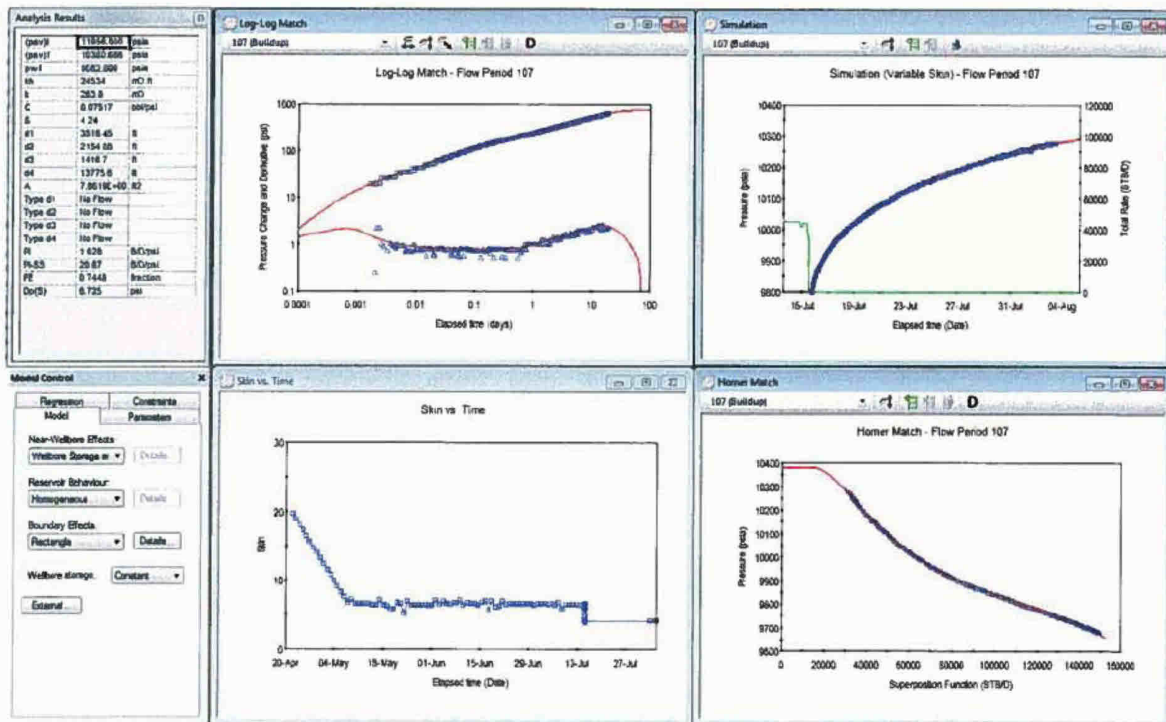Figure 120: Interpretation Model, Model Match and Analysis Results
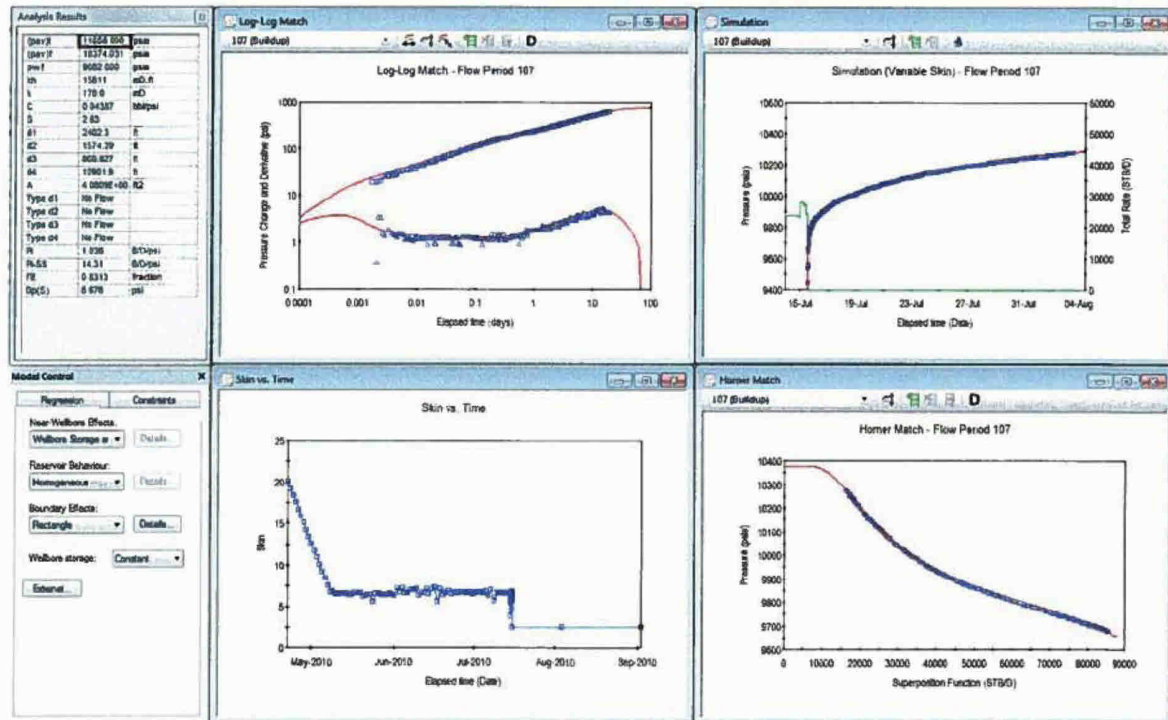
Figure 121: Interpretation Model, Model Match and Analysis Results (Zoom on Simulation – top left)
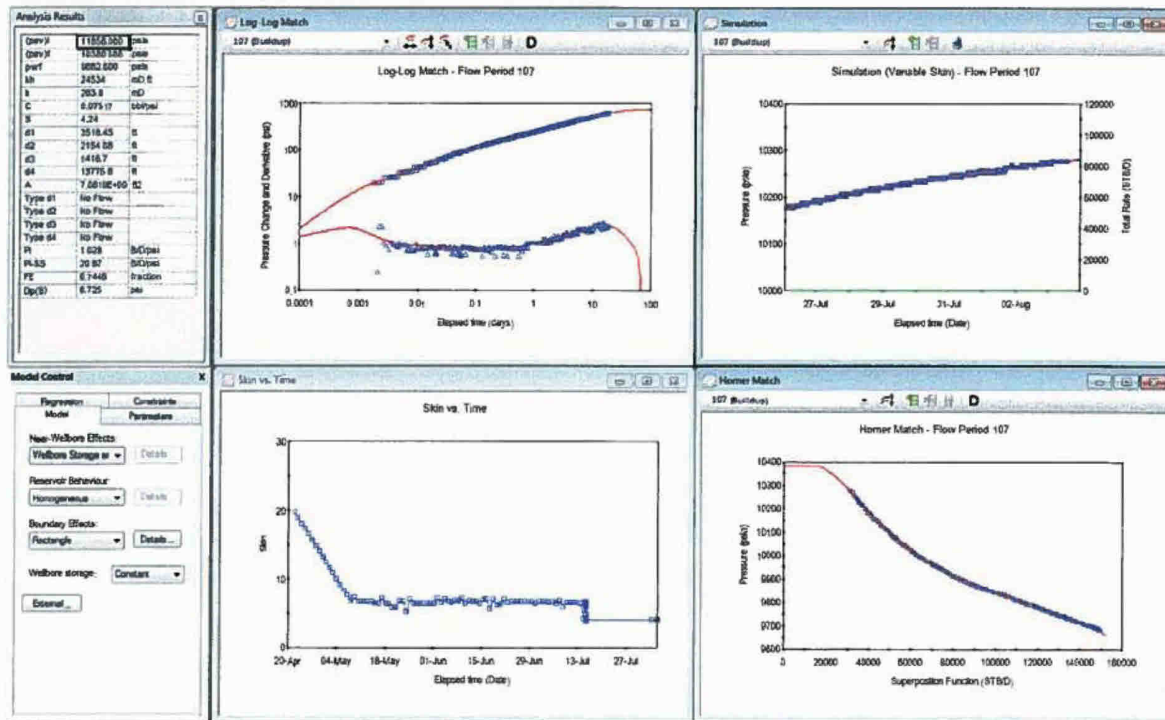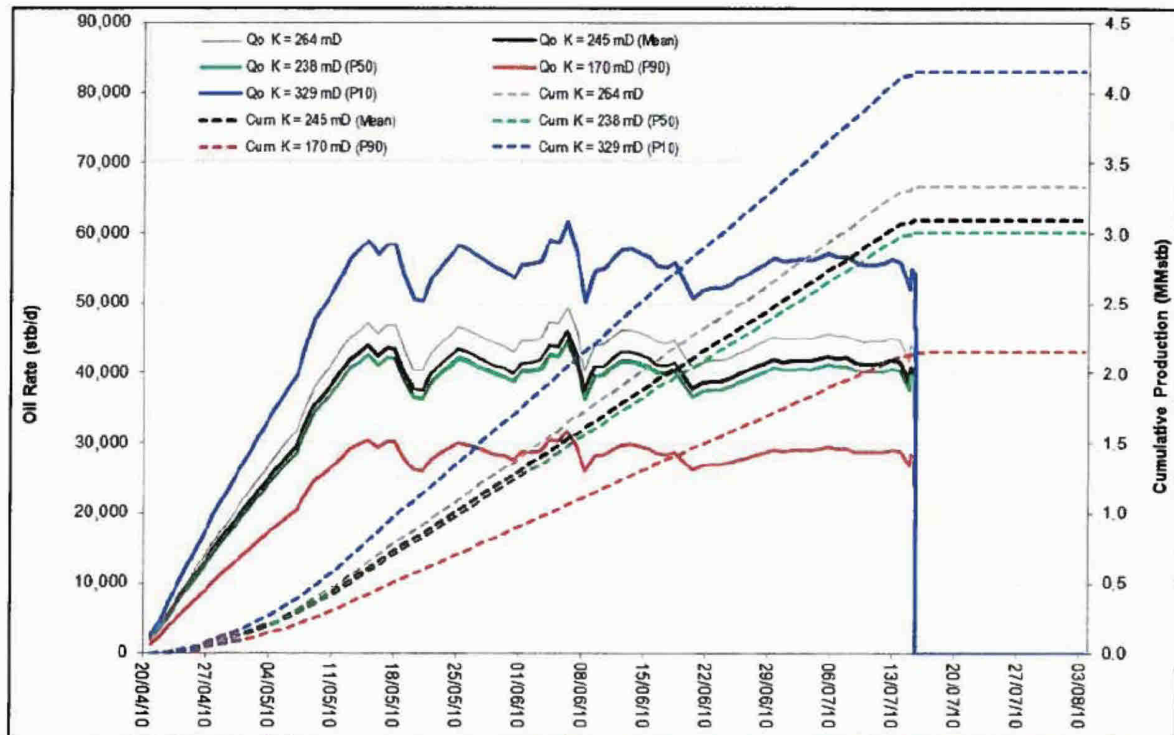
82
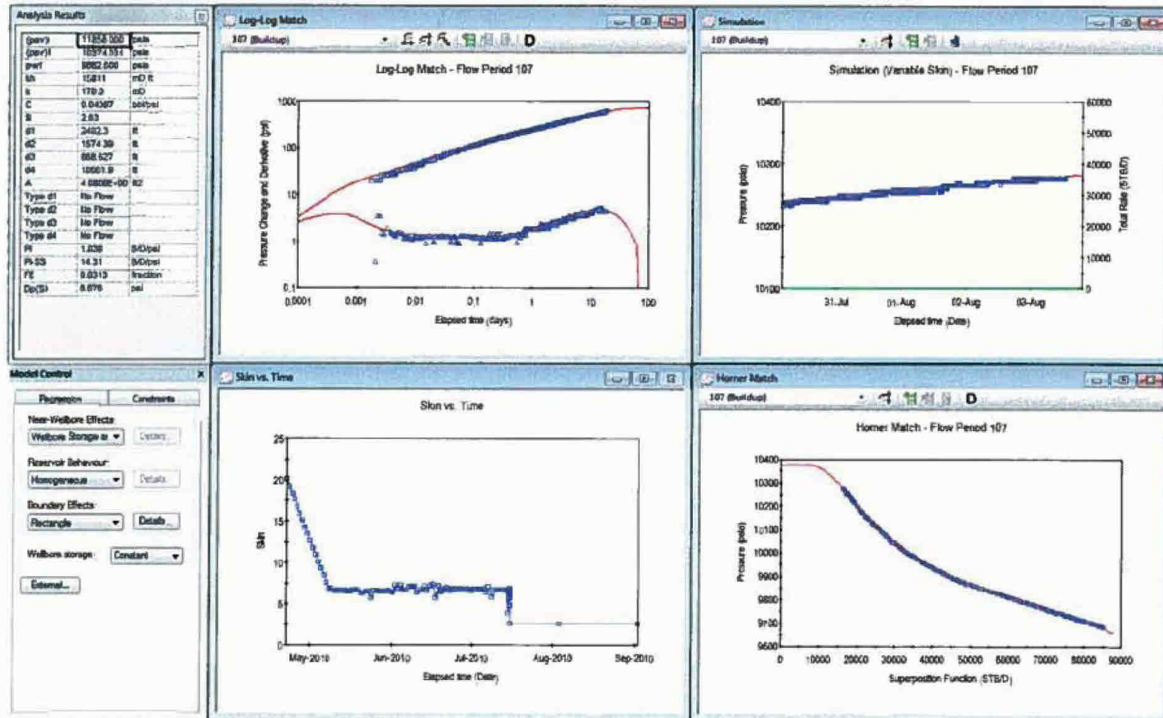
Figure 122: Interpretation Model, Model Match and Analysis Results (Further Zoom on Simulation – top left)

Analysis Model - Flow Period 107

Near Wellbore Effect: Wellbore Storage and Skin (C and S)
Reservoir Behaviour: Homogeneous
Boundary Effect: Rectangle

Initial average reservoir pressure, (pav)i	11856.000 psia
Final average reservoir pressure, (pav)f	10374.031 psia
Flowing pressure, pwf	9662.600 psia
Permeability Thickness, kh	15811 mD.ft
Permeability, k	170.0 mD
Wellbore storage coefficient, C	0.04387 bbl/psi
Wellbore skin factor, S	2.63
Distance to first boundary, d1	2402.3 ft
Distance to second boundary, d2	1574.39 ft
Distance to third boundary, d3	868.627 ft
Distance to fourth boundary, d4	10901.9 ft
Drainage area, A	4.0809E+007 ft2
Type of first boundary, Type d1	No Flow
Type of second boundary, Type d2	No Flow
Type of third boundary, Type d3	No Flow
Type of fourth boundary, Type d4	No Flow
Measured Productivity Index, PI	1.038 B/D/psi
Steady State Productivity Index, PI-SS	14.31 B/D/psi
Flow Efficiency, FE	0.8313 fraction
Pressure drop due to skin, Dp(S)	6.676 psi

Figure 123: P90 Model (Option-2 Drill Pipe Low) – Summary of Results

83

TREX-011696R.199

3.4.3.5 P10 Permeability Well Test Analysis

Shown in Figures 125 – 129 are the model diagnosis, interpretation model, model matches and analysis results which confirm a very good match to the pressure history, log-log pressure change and derivative, and the superposition (Horner) plot.

The match to the pressure history at various scales, further confirm a good match giving more validity to the analysis results and higher confidence predicting the Macondo well and reservoir properties using the matched interpretation model.

Figure 124: Diagnosis, Interpretation Model, Model Match and Analysis Results

Below are additional plots (Figures 126-129) showing the model match at various scales.

84

Figure 125: Interpretation Model, Model Match and Analysis Results

Figure 126: Interpretation Model, Model Match and Analysis Results (Zoom on Simulation – top left)
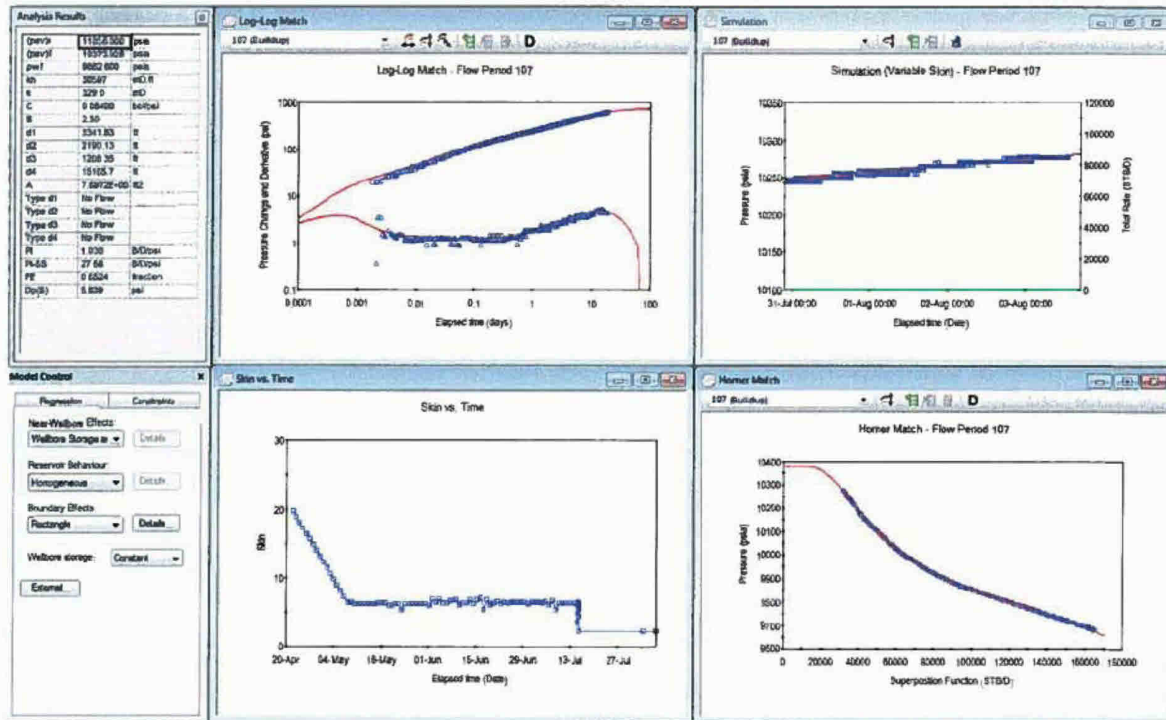
Figure 127: Interpretation Model, Model Match and Analysis Results (Further Zoom on Simulation – top left)

Analysis Model - Flow Period 107

Near Wellbore Effect: Wellbore Storage and Skin (C and S)
Reservoir Behaviour: Homogeneous
Boundary Effect: Rectangle

Initial average reservoir pressure, (pav)i	11856.000 psia
Final average reservoir pressure, (pav)f	10373.928 psia
Flowing pressure, pwf	9662.600 psia
Permeability Thickness, kh	30597 mD.ft
Permeability, k	329.0 mD
Wellbore storage coefficient, C	0.08490 bbl/psi
Wellbore skin factor, S	2.30
Distance to first boundary, d1	3341.83 ft
Distance to second boundary, d2	2190.13 ft
Distance to third boundary, d3	1208.35 ft
Distance to fourth boundary, d4	15165.7 ft
Drainage area, A	7.8972E+007 ft2
Type of first boundary, Type d1	No Flow
Type of second boundary, Type d2	No Flow
Type of third boundary, Type d3	No Flow
Type of fourth boundary, Type d4	No Flow
Measured Productivity Index, PI	1.038 B/D/psi
Steady State Productivity Index, PI-SS	27.68 B/D/psi
Flow Efficiency, FE	0.8524 fraction
Pressure drop due to skin, Dp(S)	5.839 psi

Figure 128: P10 Model (Option-2 Drill Pipe Low) – Summary of Results

86

TREX-011696R.202

3.4.3.6 K mean (245 mD) Permeability Well Test Analysis

Shown in Figures 130 – 134 are the model diagnosis, interpretation model, model matches and analysis results which confirm a very good match to the pressure history, log-log pressure change and derivative, and the superposition (Horner) plot.

The match to the pressure history at various scales, further confirm a good match giving more validity to the analysis results and higher confidence predicting the Macondo well and reservoir properties using the matched interpretation model.
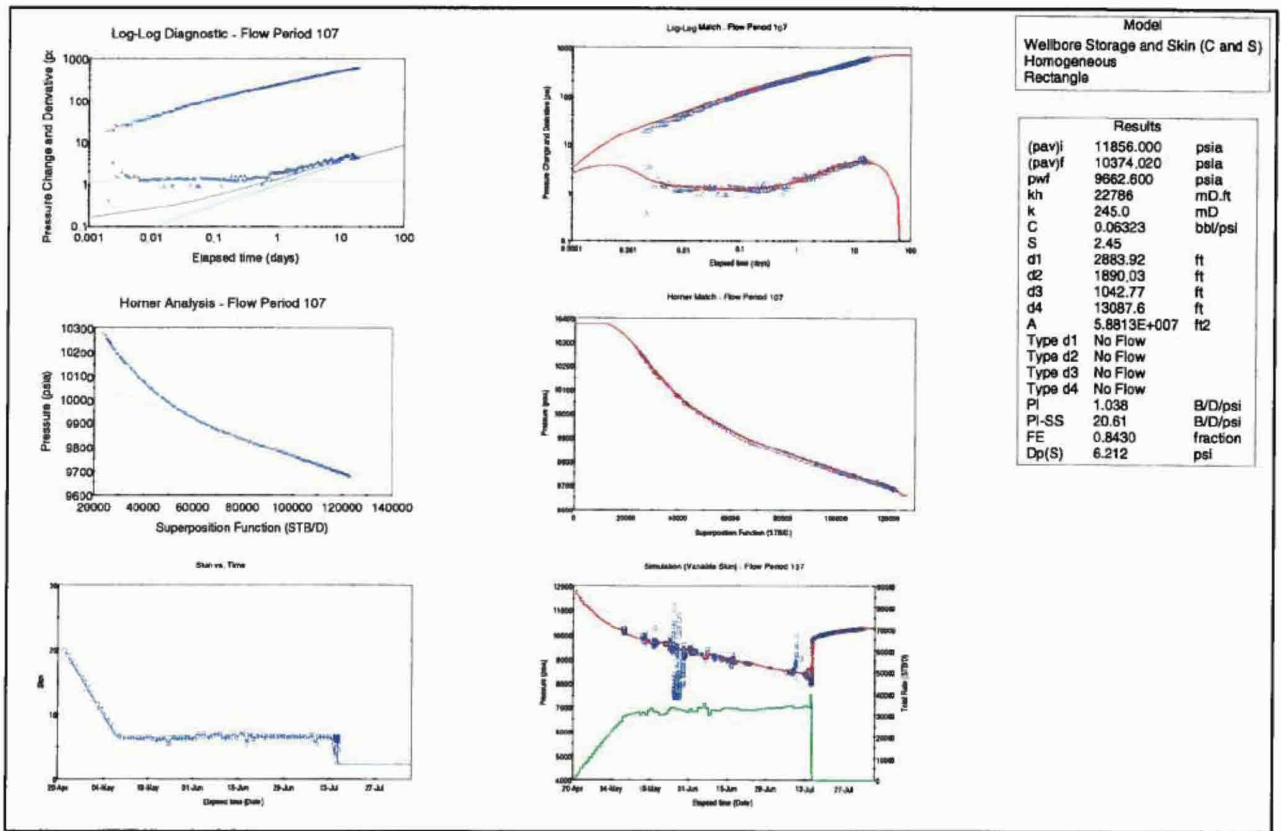
Figure 129: Diagnosis, Interpretation Model, Model Match and Analysis Results

Below are additional plots (Figures 131-134) showing the model match at various scales.
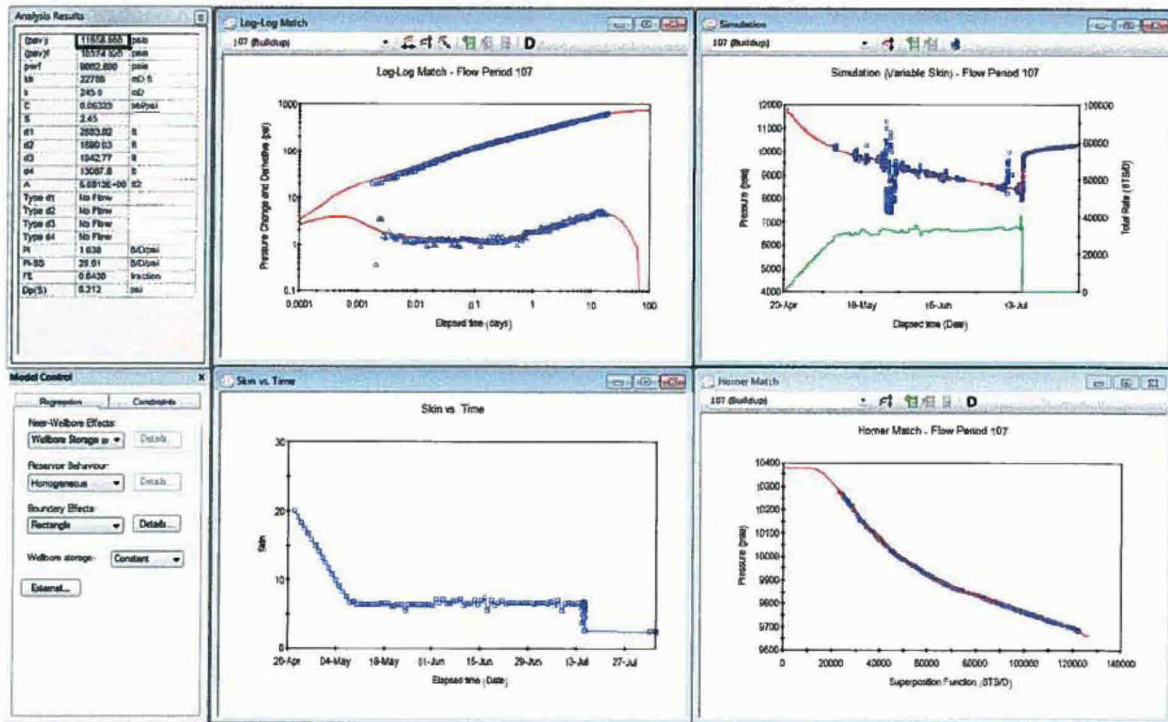
Figure 130: Interpretation Model, Model Match and Analysis Results
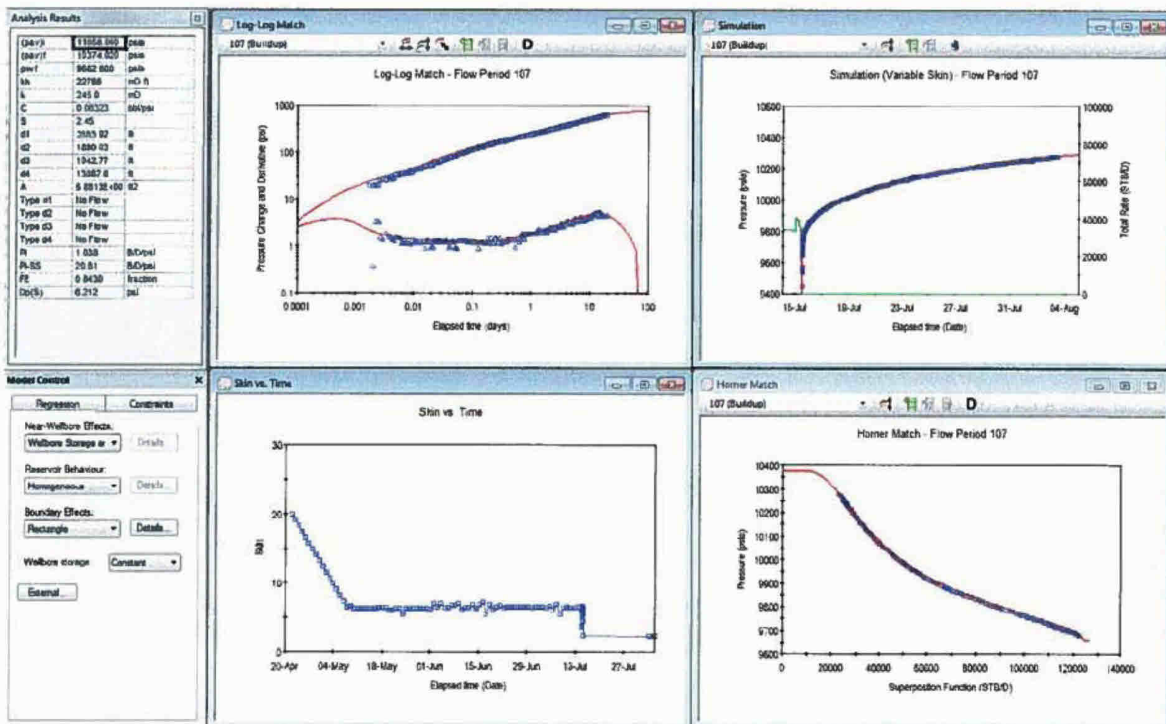
Figure 131: Interpretation Model, Model Match and Analysis Results (Zoom on Simulation – top left)

Figure 132: Interpretation Model, Model Match and Analysis Results (Further Zoom on Simulation – top left)

Analysis Model - Flow Period 107

Near Wellbore Effect: Wellbore Storage and Skin (C and S)
Reservoir Behaviour: Homogeneous
Boundary Effect: Rectangle

Initial average reservoir pressure, (pav)i	11856.000 psia
Final average reservoir pressure, (pav)f	10374.020 psia
Flowing pressure, pwf	9662.600 psia
Permeability Thickness, kh	22786 mD.ft
Permeability, k	245.0 mD
Wellbore storage coefficient, C	0.06323 bbl/psi
Wellbore skin factor, S	2.45
Distance to first boundary, d1	2883.92 ft
Distance to second boundary, d2	1890.03 ft
Distance to third boundary, d3	1042.77 ft
Distance to fourth boundary, d4	13087.6 ft
Drainage area, A	5.8813E+007 ft2
Type of first boundary, Type d1	No Flow
Type of second boundary, Type d2	No Flow
Type of third boundary, Type d3	No Flow
Type of fourth boundary, Type d4	No Flow
Measured Productivity Index, PI	1.038 B/D/psi
Steady State Productivity Index, PI-SS	20.61 B/D/psi
Flow Efficiency, FE	0.8430 fraction
Pressure drop due to skin, Dp(S)	6.212 psi

Figure 133: K-mean (245mD) Option-2 Drill Pipe Low – Summary of Results

89

3.4.3.7 K 321 mD Permeability Well Test Analysis

A sensitivity to 321mD was done by scaling the rates to match 45,000stb/d on the 14th of July, 2010.

Shown in Figures 135 – 139 are the model diagnosis, interpretation model, model matches and analysis results which confirm a very good match to the pressure history, log-log pressure change and derivative, and the superposition (Horner) plot.

The match to the pressure history at various scales, further confirm a good match giving more validity to the analysis results and higher confidence predicting the Macondo well and reservoir properties using the matched interpretation model.
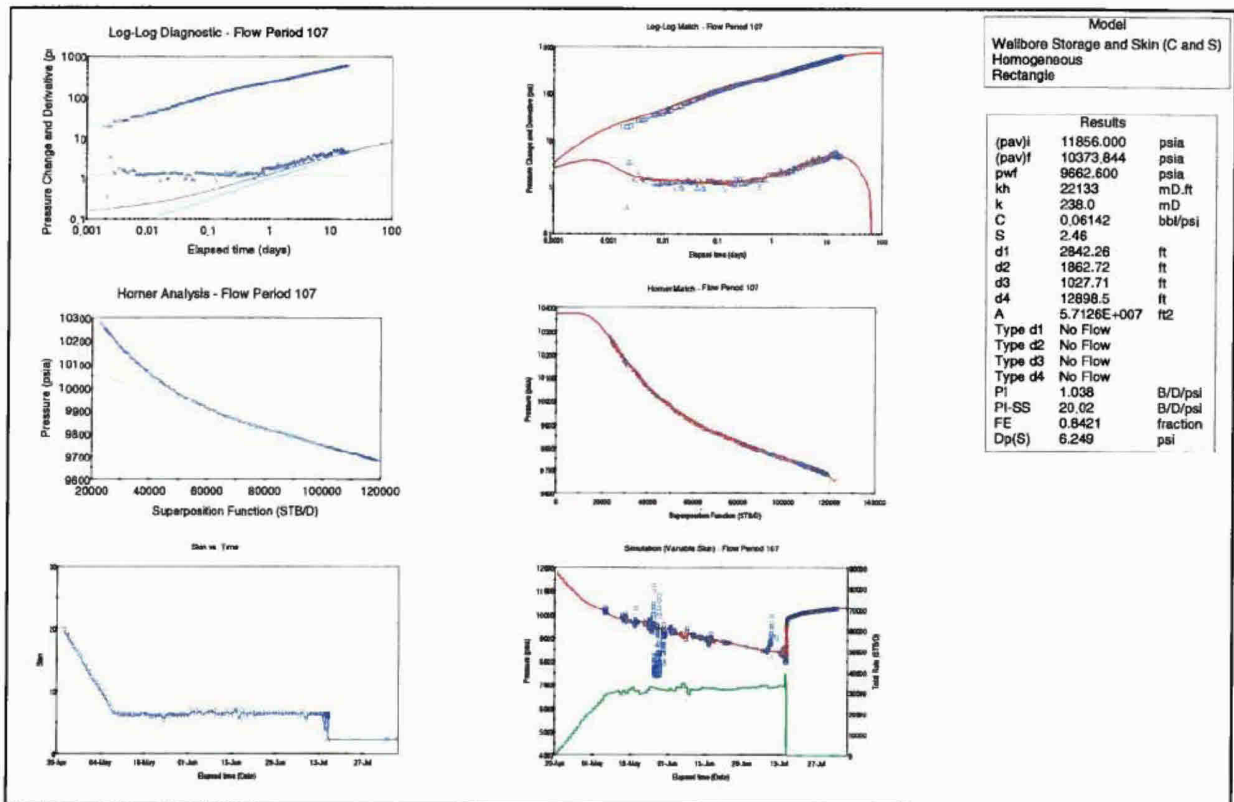

Figure 134: Diagnosis, Interpretation Model, Model Match and Analysis Results

Below are additional plots (Figures 136 – 139) showing the model match at various scales.
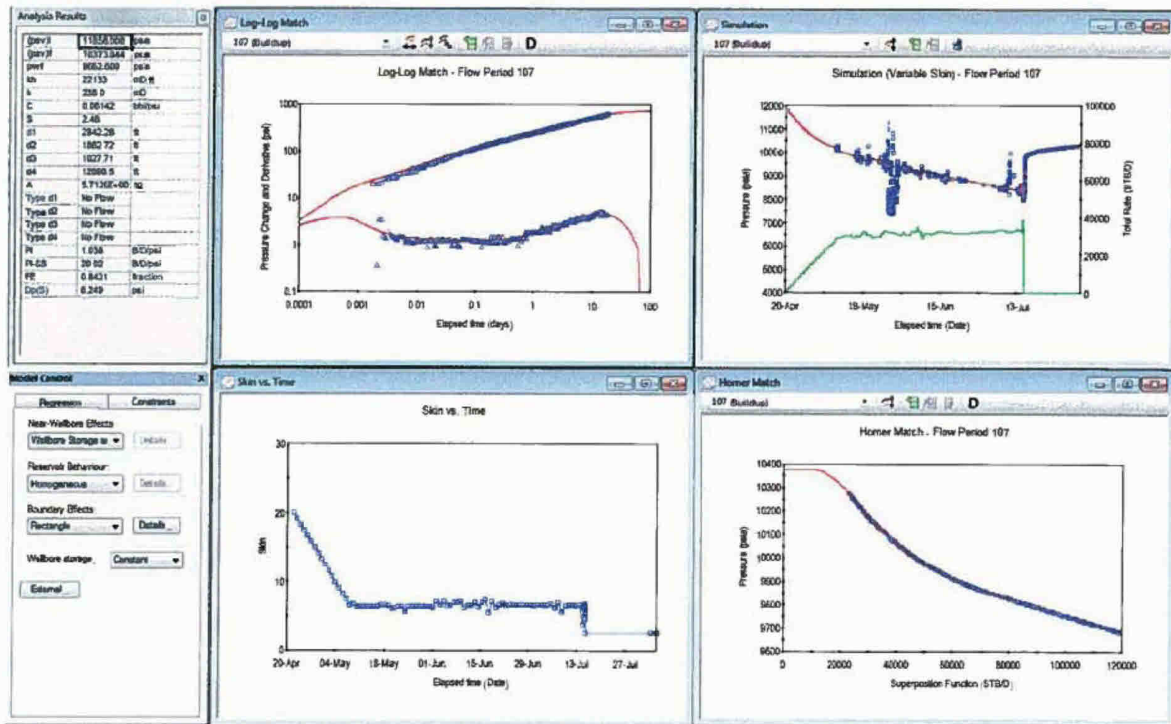
TREX-011696R.206

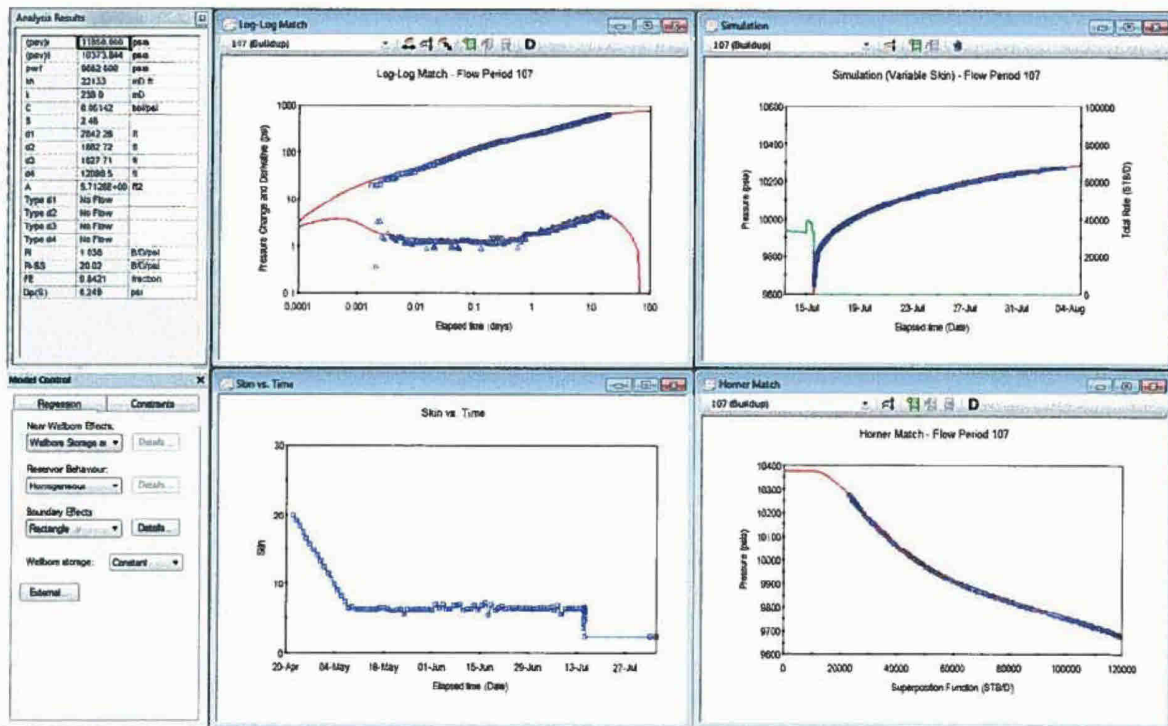Figure 135: Interpretation Model, Model Match and Analysis Results

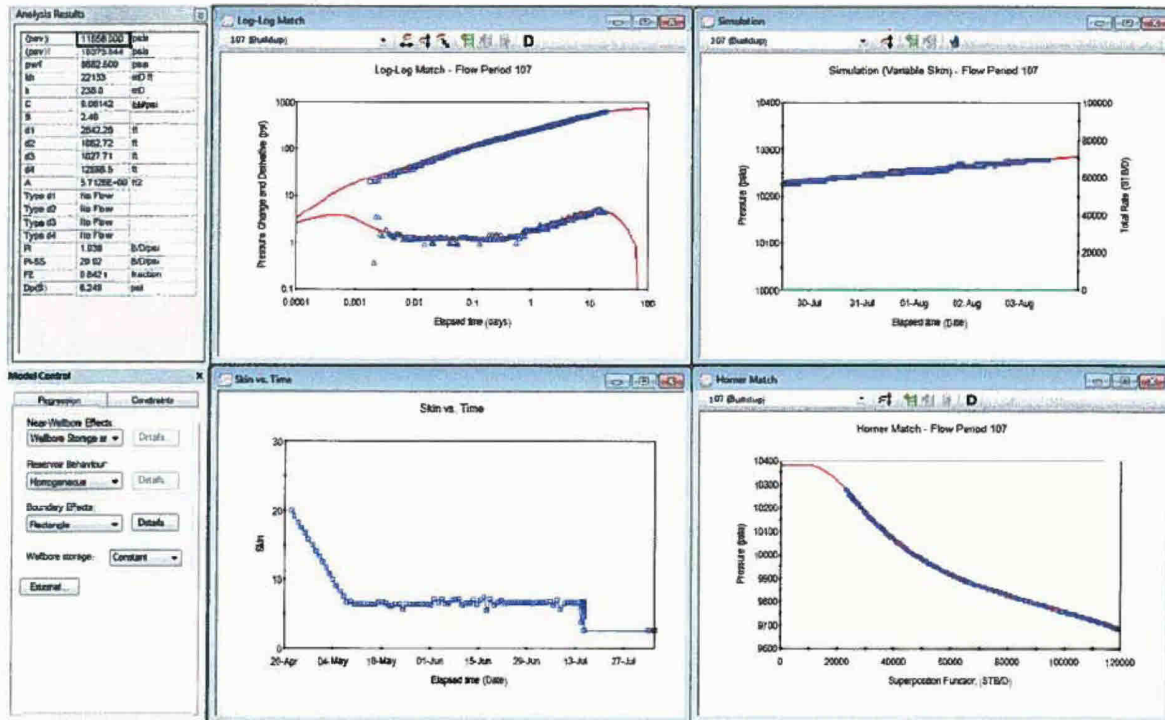Figure 136: Interpretation Model, Model Match and Analysis Results (Zoom on Simulation – top left)

Figure 137: Interpretation Model, Model Match and Analysis Results (Further Zoom on Simulation – top left)

Analysis Model - Flow Period 107

Near Wellbore Effect: Wellbore Storage and Skin (C and S)
Reservoir Behaviour: Homogeneous
Boundary Effect: Rectangle

Initial average reservoir pressure, (pav)i	11856.000 psia
Final average reservoir pressure, (pav)f	10373.972 psia
Flowing pressure, pwf	9662.600 psia
Permeability Thickness, kh	29826 mD.ft
Permeability, k	320.7 mD
Wellbore storage coefficient, C	0.08276 bbl/psi
Wellbore skin factor, S	2.32
Distance to first boundary, d1	3299.46 ft
Distance to second boundary, d2	2162.36 ft
Distance to third boundary, d3	1193.03 ft
Distance to fourth boundary, d4	14973.4 ft
Drainage area, A	7.6982E+007 ft2
Type of first boundary, Type d1	No Flow
Type of second boundary, Type d2	No Flow
Type of third boundary, Type d3	No Flow
Type of fourth boundary, Type d4	No Flow
Measured Productivity Index, PI	1.038 B/D/psi
Steady State Productivity Index, PI-SS	26.97 B/D/psi
Flow Efficiency, FE	0.8517 fraction
Pressure drop due to skin, Dp(S)	5.871 psi

Figure 138: K 321mD (Option-2 Drill Pipe Low) – Summary of Results

92

3.4.3.8 OPTION-2 DRILL PIPE LOW (SUMMARY AND RESULTS)

Parameters	P 90	P 50	P 10	Mean K	K-321
Initial Pressure @ Reservoir Depth (18,056 ft TVDss) psia	11,856	11,856	11,856	11,856	11,856
Final Pressure @ Reservoir Depth (18,056 ft TVDss) psia	10,374	10,374	10,374	10,374	10,374
Depletion (psi)	1,482.00	1,482.00	1,482.00	1,482.00	1,482.00
Reservoir Permeability (mD)	170	238	329	245	321
Skin	20 → 2	20 → 2	20 → 2	20 → 2	20 → 2
Boundary1 (d1) – ft	2,402	2,842	3,342	2,884	3,299
Boundary2 (d2) – ft	1,574	1,863	2,190	1,890	2,162
Boundary3 (d3) – ft	869	1,028	1,208	1,043	1,193
Boundary4 (d4) - ft	10,902	12,899	15,166	13,088	14,973
Reservoir Width - ft	3,271	3,870	4,550	3,927	4,492
Reservoir Length - ft	12,476	14,762	17,356	14,978	17,135
Area (MM ft^2)	40.8	57.1	79.0	58.8	77.0
Area (Acres)	937	1,312	1,813	1,350	1,767
STOIIP (MMstb)	56	78	107	80	105
Cumulative Production (MMstb)	1.74	2.43	3.36	2.50	3.27

Figure 139: OPTION-2 DRILL PIPE HIGH – Summary of Results

3.4.4   BUILD AND DRAWDOWN COMPARISON

Shown below (Figure 141) is a comparison of the buildup data and deconvolved derivative based on Option-1 Drill Pipe High. Also shown are the corresponding build up and drawdown type curves with identical permeabilities and boundary distances. This confirms a closed system at late times and consistency in with the buildup and drawdown data and models.
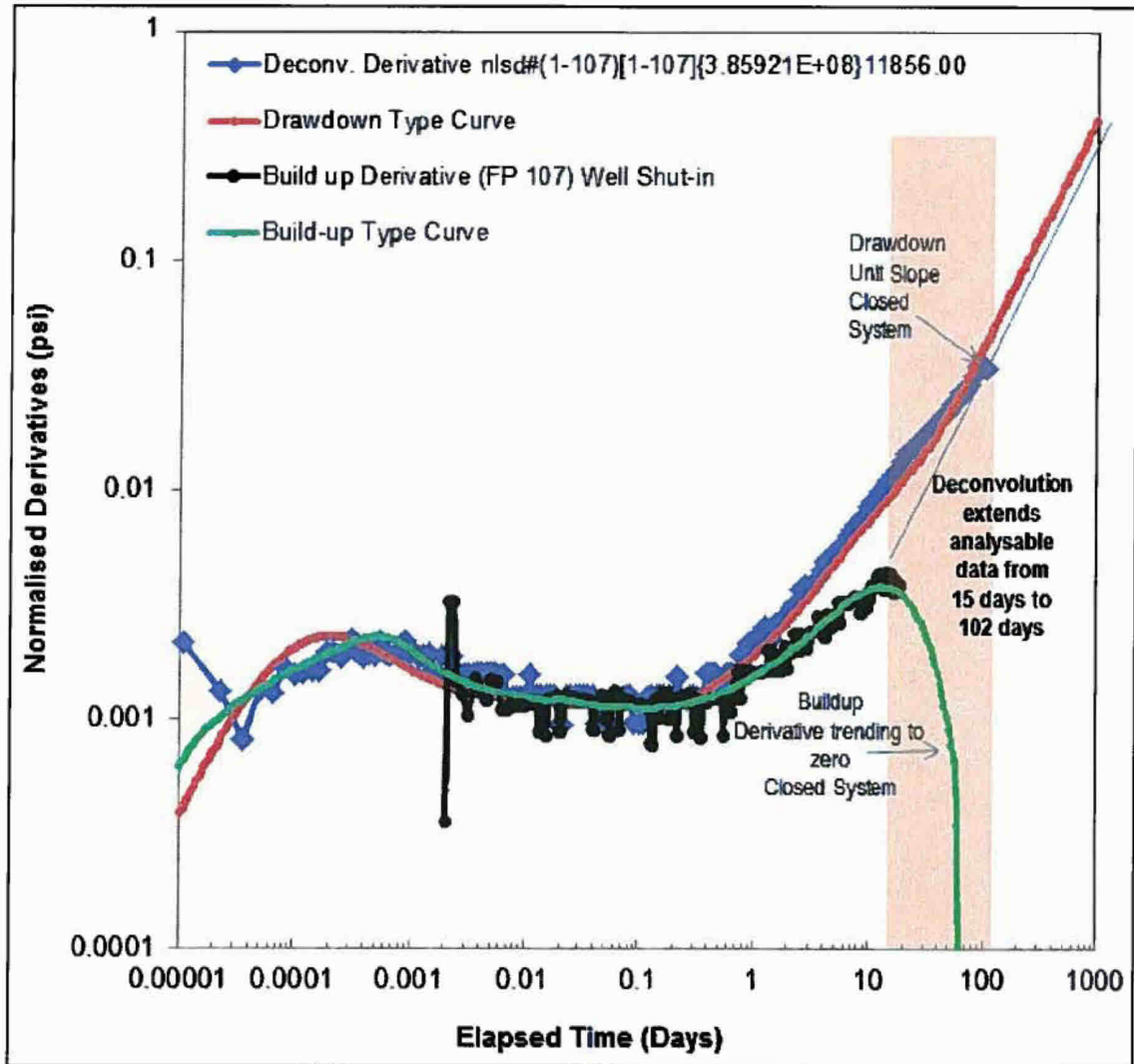
Figure 140: Comparison of Build and Drawdowns (Option-1 Drill Pipe High)

3.5 WELL TEST ANALYSIS on Well Head Pressures (WHP) – 4972 ft TVDss

3.5.1 Flow Period Selection

A total of 107 flow periods were also used to represent rate variations during the entire production and pressure history. The period when the Macondo well is full shut-in is flow period 107.

3.5.2 Deconvolution (Option -1)

The deconvolution results are shown in Figures 8 to 14 above. The convolved pressure match at the final iteration was near excellent and used as the rate profile for the well test analysis. The rates are scaled linearly to match the MDT uncertainty range of permeabilities (P50 238mD, P90 170mD, P10 329 mD and Mean Permeability 245mD).

3.5.2.1 P50 Permeability Well Test Analysis

Shown in Figures 142 – 146 are the model diagnosis, interpretation model, model matches and analysis results which confirm a very good match to the pressure history, log-log pressure change and derivative, and the superposition (Horner) plot.

The match to the pressure history at various scales, further confirm a good match giving more validity to the analysis results and higher confidence predicting the Macondo well and reservoir properties using the matched interpretation model.
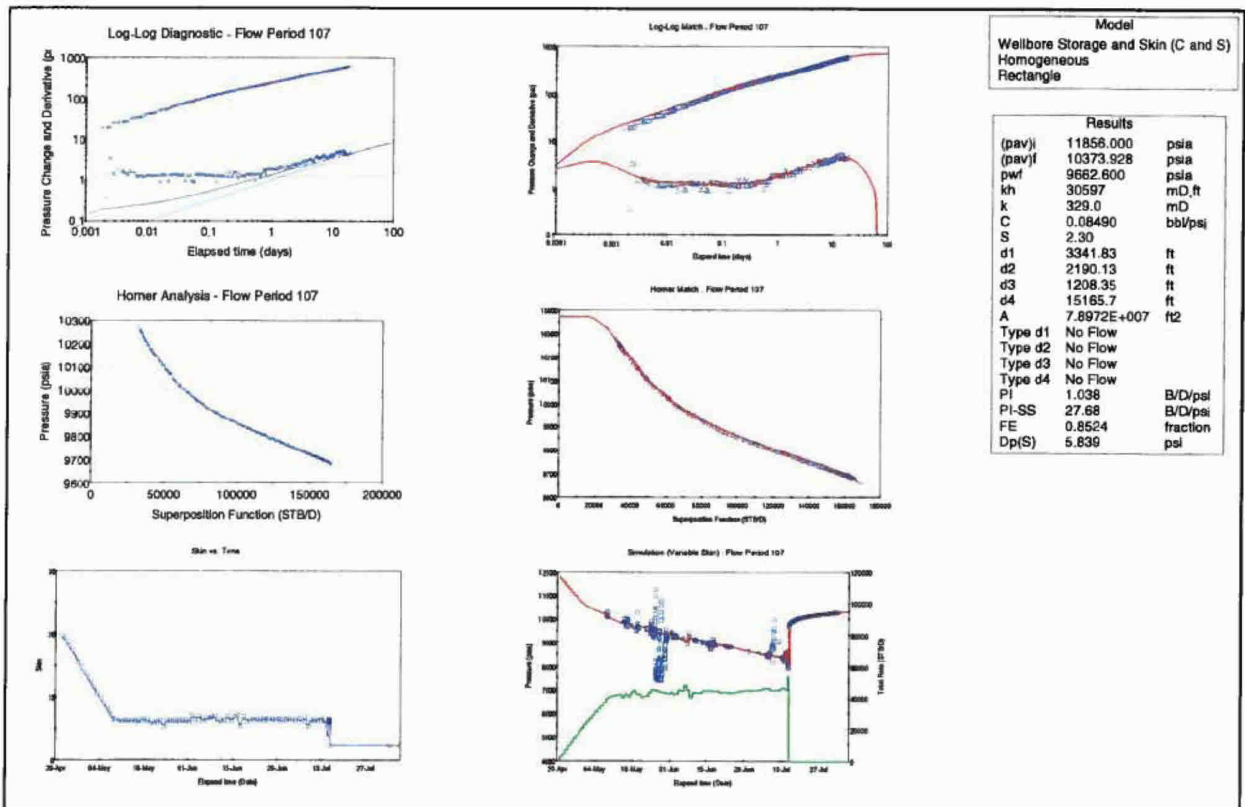

Figure 141: Diagnosis, Interpretation Model, Model Match and Analysis Results

Below are additional plots (Figures 143-146) showing the model match at various scales.
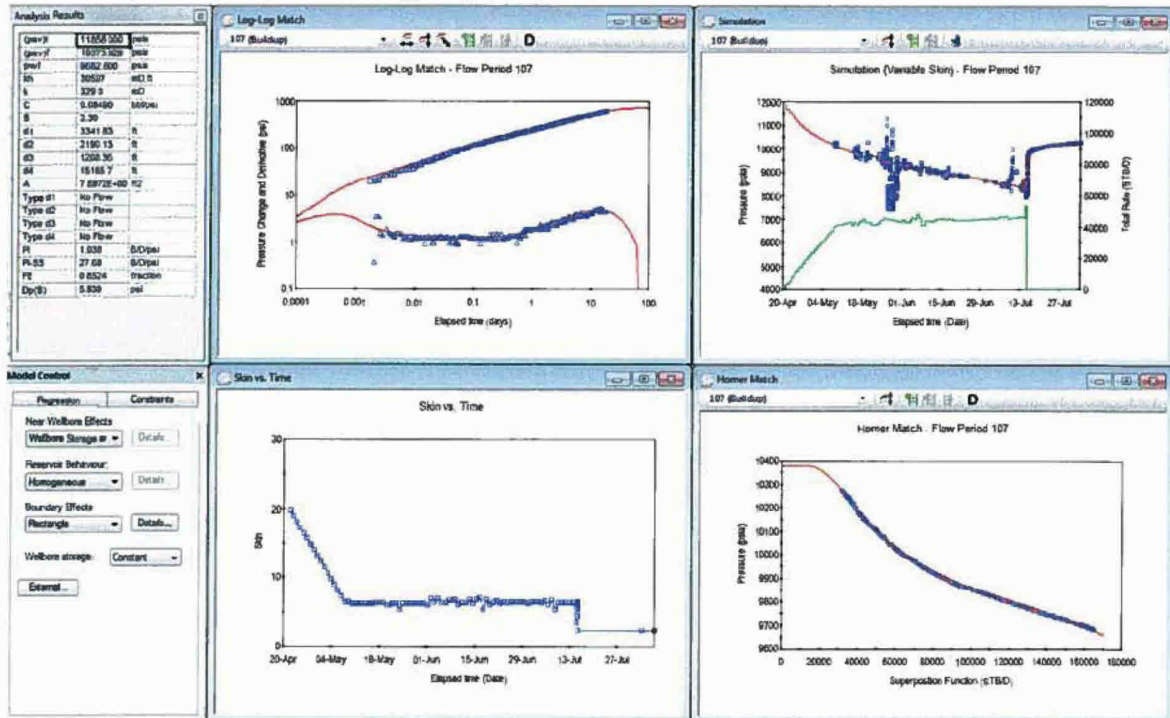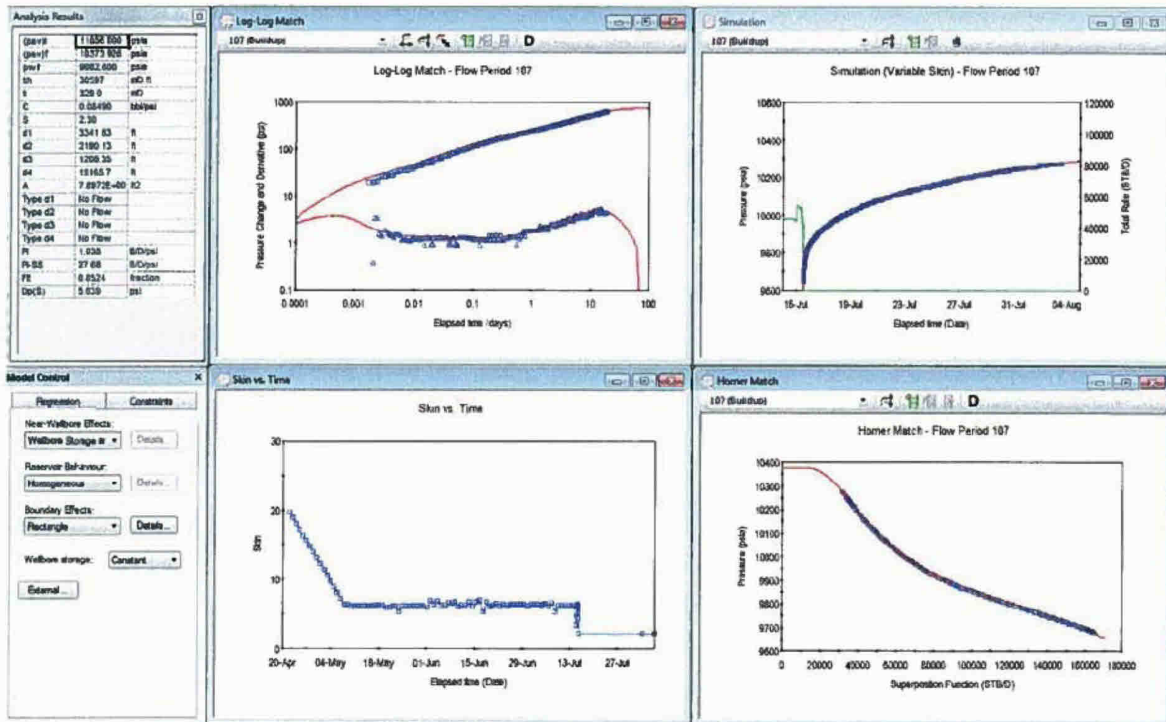
TREX-011696R.211
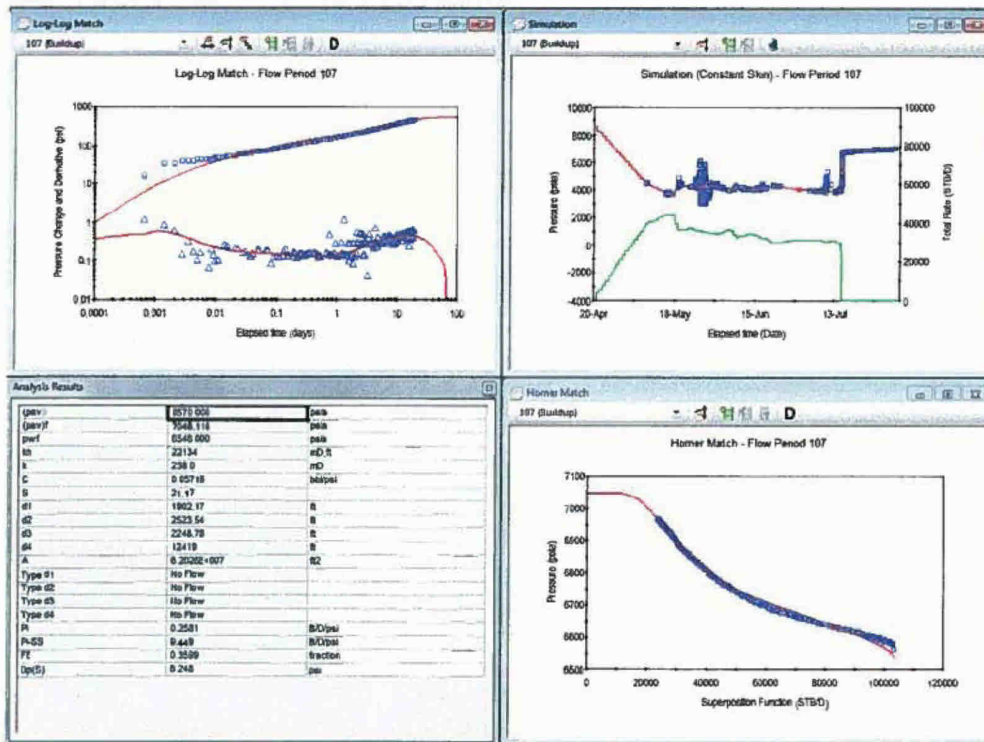
Figure 142: Interpretation Model, Model Match and Analysis Results

Figure 143: Interpretation Model, Model Match and Analysis Results (Zoom on Simulation – top left)

Log-Log Match

107 (Buildup)   D

Log-Log Match - Flow Period 107

(y-axis) Pressure Change and Derivative (psi); (x-axis) Elapsed time (days)

Simulation

107 (Buildup)

Simulation (Constant Skin) - Flow Period 107

(y-axis) Pressure (psia); (right y-axis) Total Rate (STB/D); (x-axis) Elapsed time (Date)

Analysis Results

(pav)i	8570.000	psia
(pav)f	7046.116	psia
pwf	6546.000	psia
kh	22134	mD.ft
k	238.0	mD
C	0.05718	bbl/psi
S	21.17	
d1	1902.17	ft
d2	2523.54	ft
d3	2248.78	ft
d4	12419	ft
A	6.2026E+007	ft2
Type d1	No Flow	
Type d2	No Flow	
Type d3	No Flow	
Type d4	No Flow	
PI	0.2581	B/D/psi
PI-SS	9.449	B/D/psi
FE	0.3599	fraction
Dp(S)	6.248	psi

Homer Match

107 (Buildup)   D

Homer Match - Flow Period 107

(y-axis) Pressure (psia); (x-axis) Superposition Function (STB/D)

Figure 144: Interpretation Model, Model Match and Analysis Results (Further Zoom on Simulation – top left)

Analysis Model - Flow Period 107

Near Wellbore Effect: Wellbore Storage and Skin (C and S)
Reservoir Behaviour: Homogeneous
Boundary Effect: Rectangle

Initial average reservoir pressure, (pav)i	8570.000 psia
Final average reservoir pressure, (pav)f	7046.116 psia
Flowing pressure, pwf	6546.000 psia
Permeability Thickness, kh	22134 mD.ft
Permeability, k	238.0 mD
Wellbore storage coefficient, C	0.05718 bbl/psi
Wellbore skin factor, S	21.17
Distance to first boundary, d1	1902.17 ft
Distance to second boundary, d2	2523.54 ft
Distance to third boundary, d3	2248.78 ft
Distance to fourth boundary, d4	12419 ft
Drainage area, A	6.2026E+007 ft2
Type of first boundary, Type d1	No Flow
Type of second boundary, Type d2	No Flow
Type of third boundary, Type d3	No Flow
Type of fourth boundary, Type d4	No Flow
Measured Productivity Index, PI	0.2581 B/D/psi
Steady State Productivity Index, PI-SS	9.449 B/D/psi
Flow Efficiency, FE	0.3599 fraction
Pressure drop due to skin, Dp(S)	6.248 psi

Figure 145: P50 Model (Pressures at BOP Datum) – Summary of Results

3.5.2.2 P90 Permeability Well Test Analysis

Shown in Figures 147 – 151 are the model diagnosis, interpretation model, model matches and analysis results which confirm a very good match to the pressure history, log-log pressure change and derivative, and the superposition (Horner) plot.

The match to the pressure history at various scales, further confirm a good match giving more validity to the analysis results and higher confidence predicting the Macondo well and reservoir properties using the matched interpretation model.

Figure 146: Diagnosis, Interpretation Model, Model Match and Analysis Results

Below are additional plots (Figures 148-151) showing the model match at various scales.
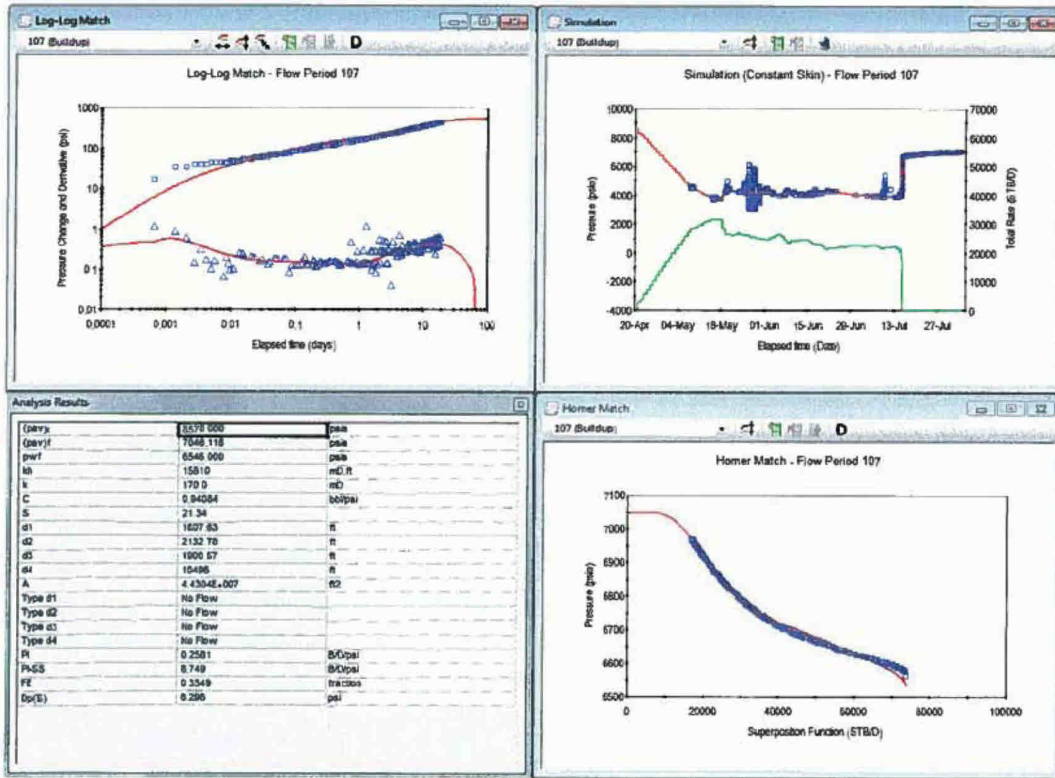
Figure 147: Interpretation Model, Model Match and Analysis Results
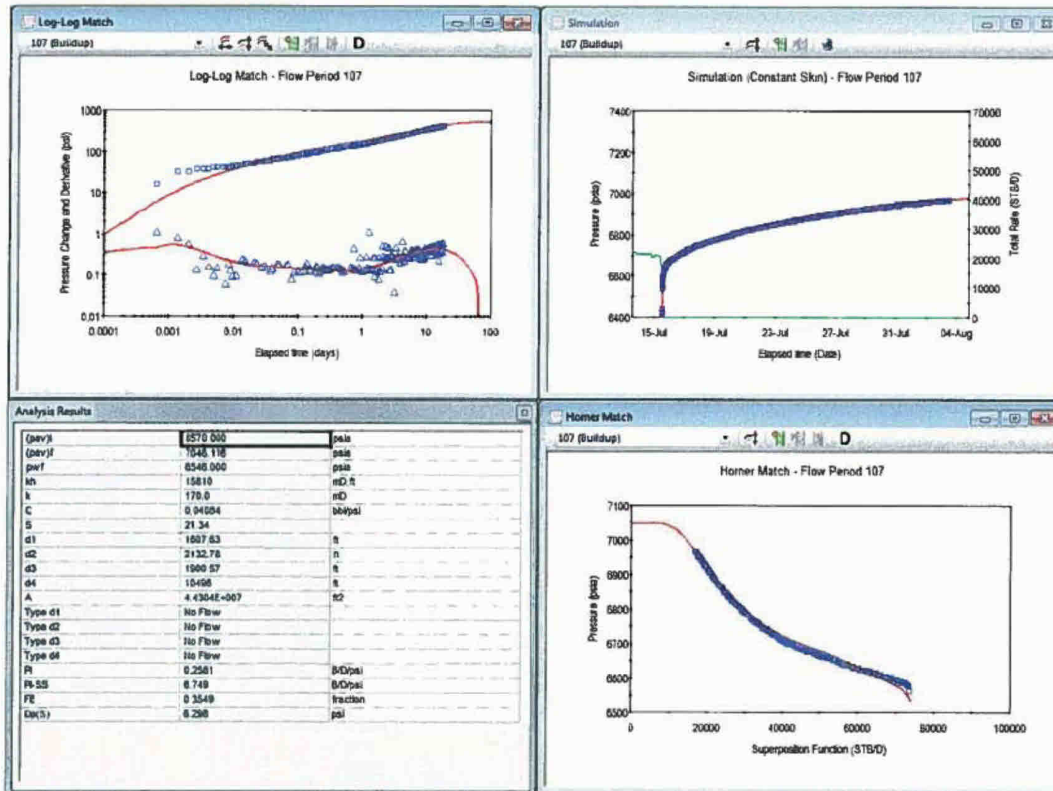
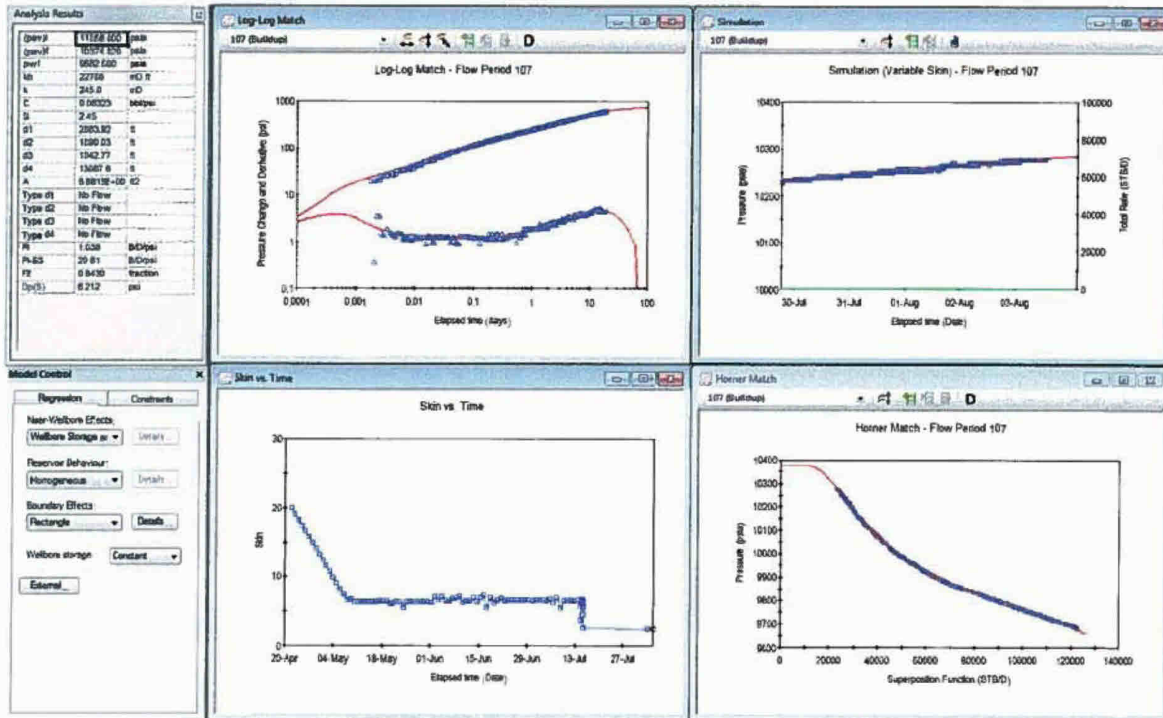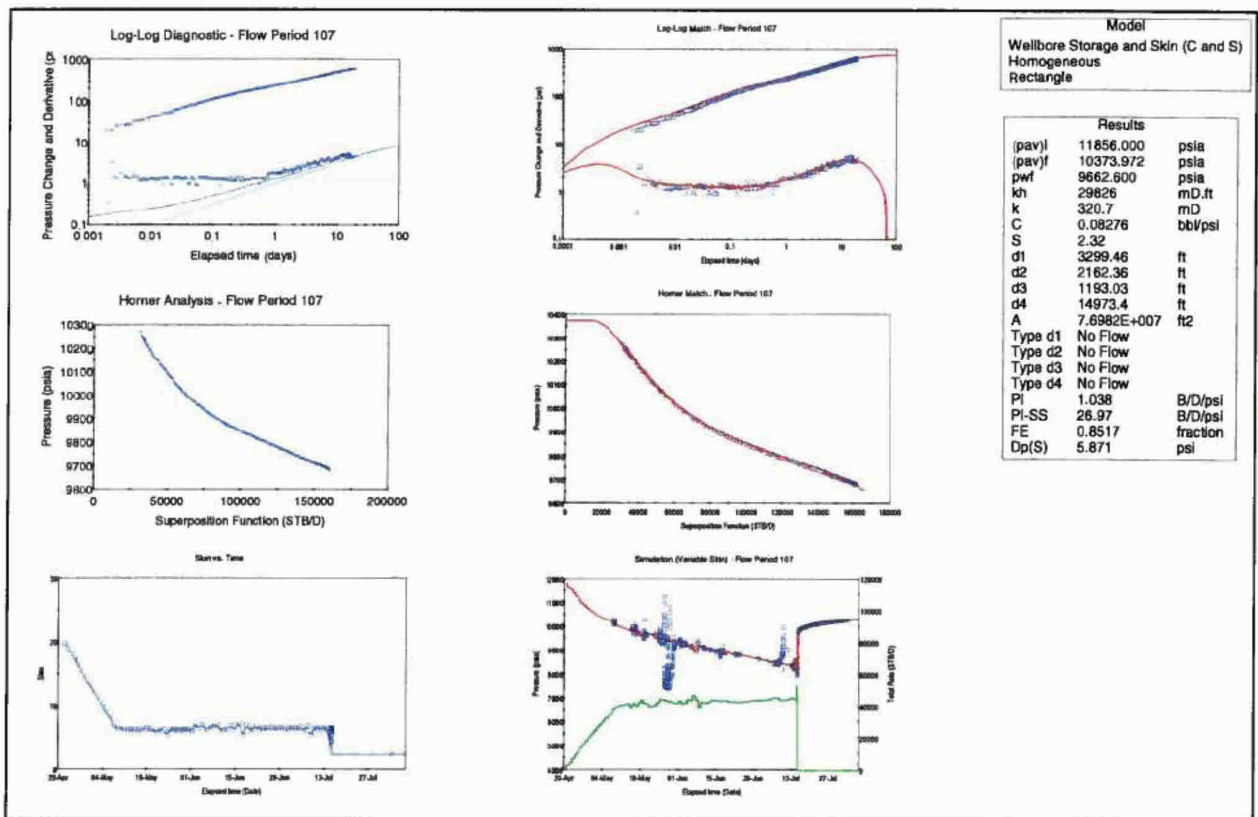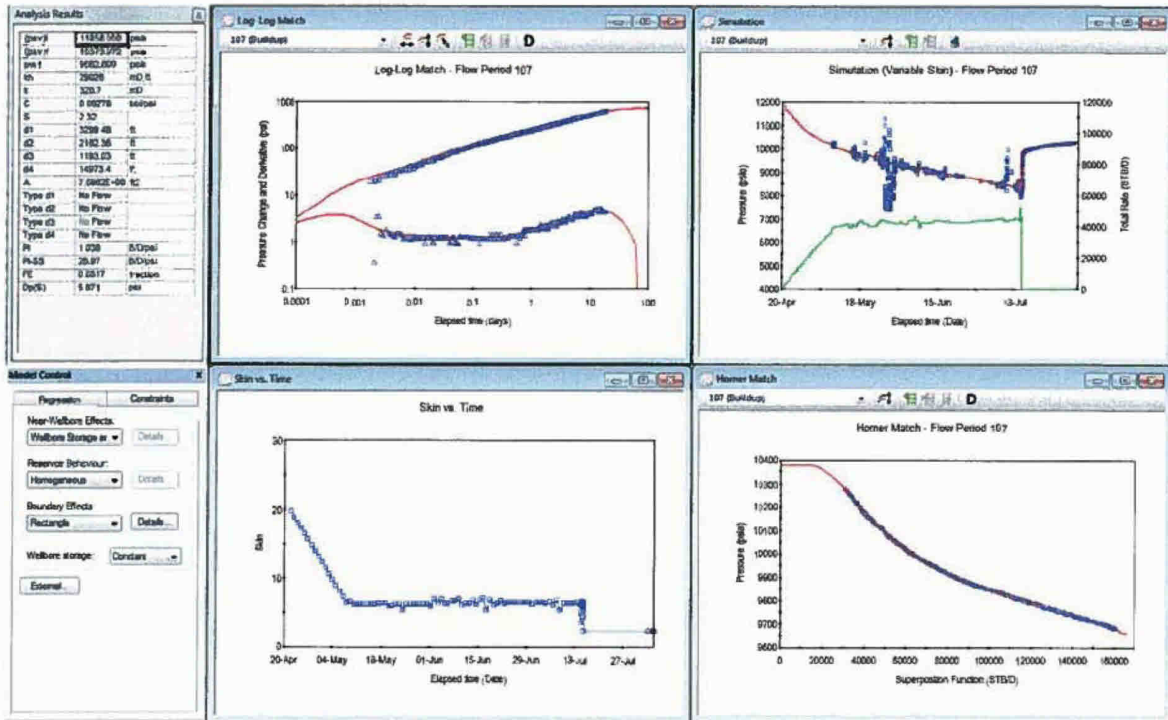**Figure 148: Interpretation Model, Model Match and Analysis Results (Zoom on Simulation – top left)**
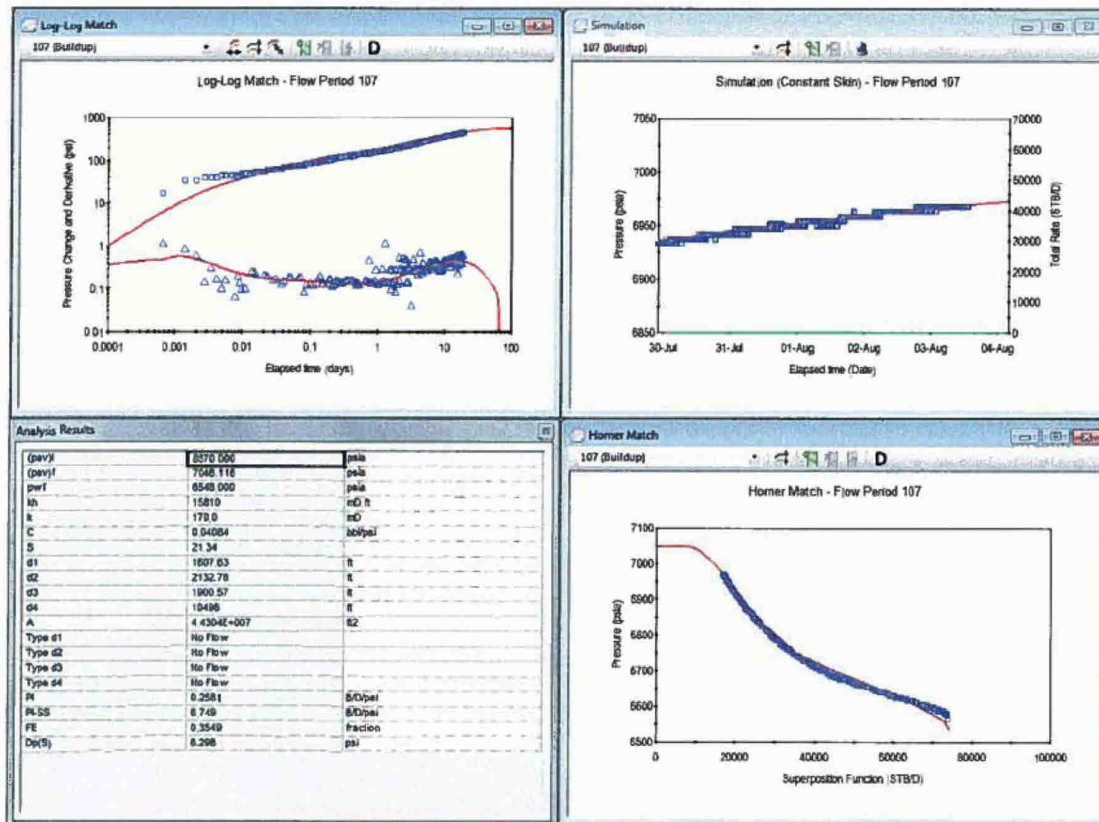
Figure 149: Interpretation Model, Model Match and Analysis Results (Further Zoom on Simulation – top left)

Analysis Model - Flow Period 107

Near Wellbore Effect: Wellbore Storage and Skin (C and S)
Reservoir Behaviour: Homogeneous
Boundary Effect: Rectangle

Initial average reservoir pressure, (pav)i	8570.000 psia
Final average reservoir pressure, (pav)f	7046.116 psia
Flowing pressure, pwf	6546.000 psia
Permeability Thickness, kh	15810 mD.ft
Permeability, k	170.0 mD
Wellbore storage coefficient, C	0.04084 bbl/psi
Wellbore skin factor, S	21.34
Distance to first boundary, d1	1607.63 ft
Distance to second boundary, d2	2132.78 ft
Distance to third boundary, d3	1900.57 ft
Distance to fourth boundary, d4	10496 ft
Drainage area, A	4.4304E+007 ft2
Type of first boundary, Type d1	No Flow
Type of second boundary, Type d2	No Flow
Type of third boundary, Type d3	No Flow
Type of fourth boundary, Type d4	No Flow
Measured Productivity Index, PI	0.2581 B/D/psi
Steady State Productivity Index, PI-SS	6.749 B/D/psi
Flow Efficiency, FE	0.3549 fraction
Pressure drop due to skin, Dp(S)	6.298 psi

Figure 150: P90 Model (Pressures at BOP Datum) – Summary of Results

100

TREX-011696R.216

3.5.2.3 P10 Permeability Well Test Analysis

Shown in Figures 152 – 156 are the model diagnosis, interpretation model, model matches and analysis results which confirm a very good match to the pressure history, log-log pressure change and derivative, and the superposition (Horner) plot.

The match to the pressure history at various scales, further confirm a good match giving more validity to the analysis results and higher confidence predicting the Macondo well and reservoir properties using the matched interpretation model.
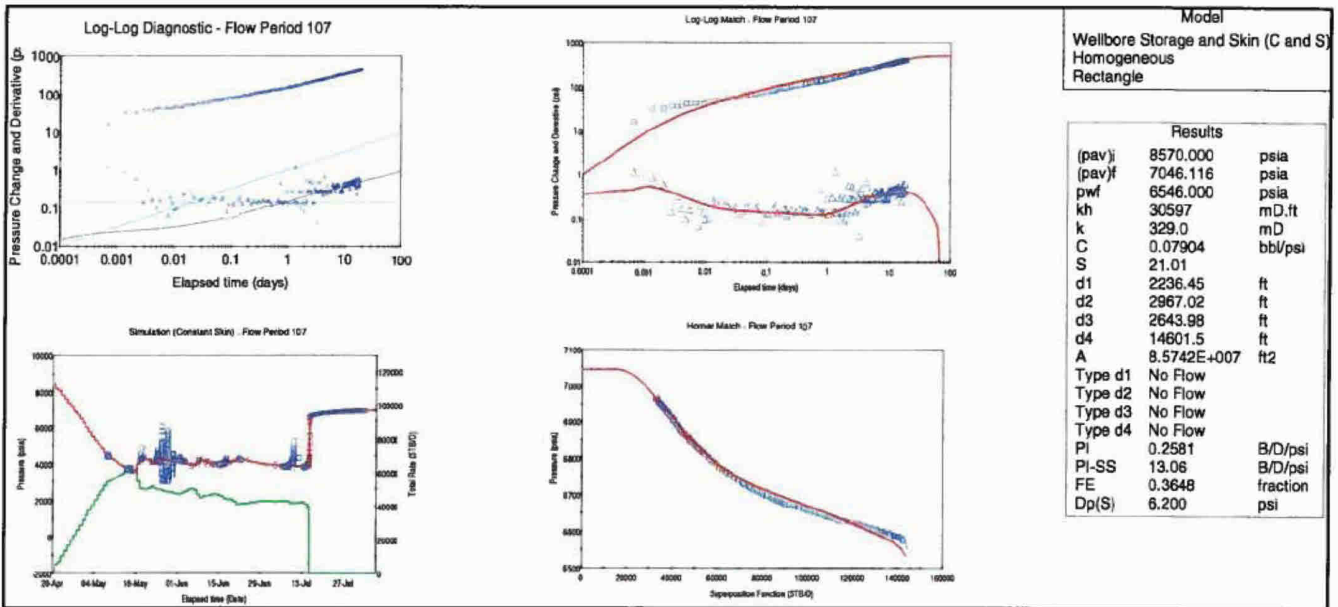
Figure 151: Diagnosis, Interpretation Model, Model Match and Analysis Results

Below are additional plots (Figures 153-156) showing the model match at various scales.
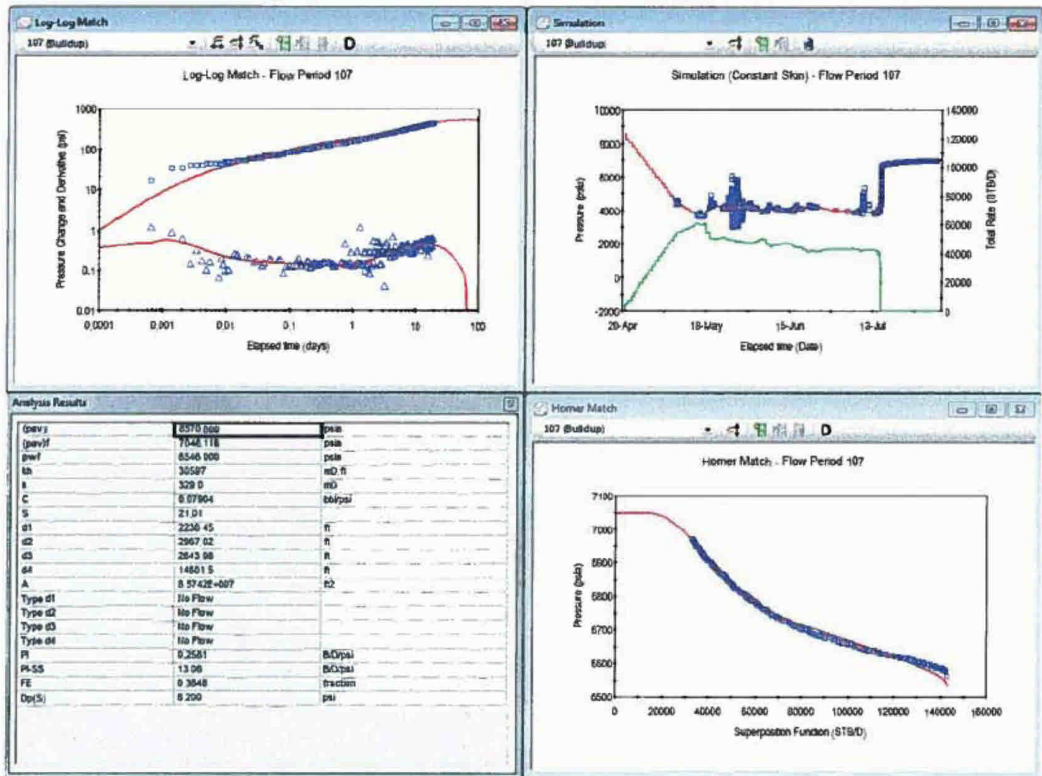
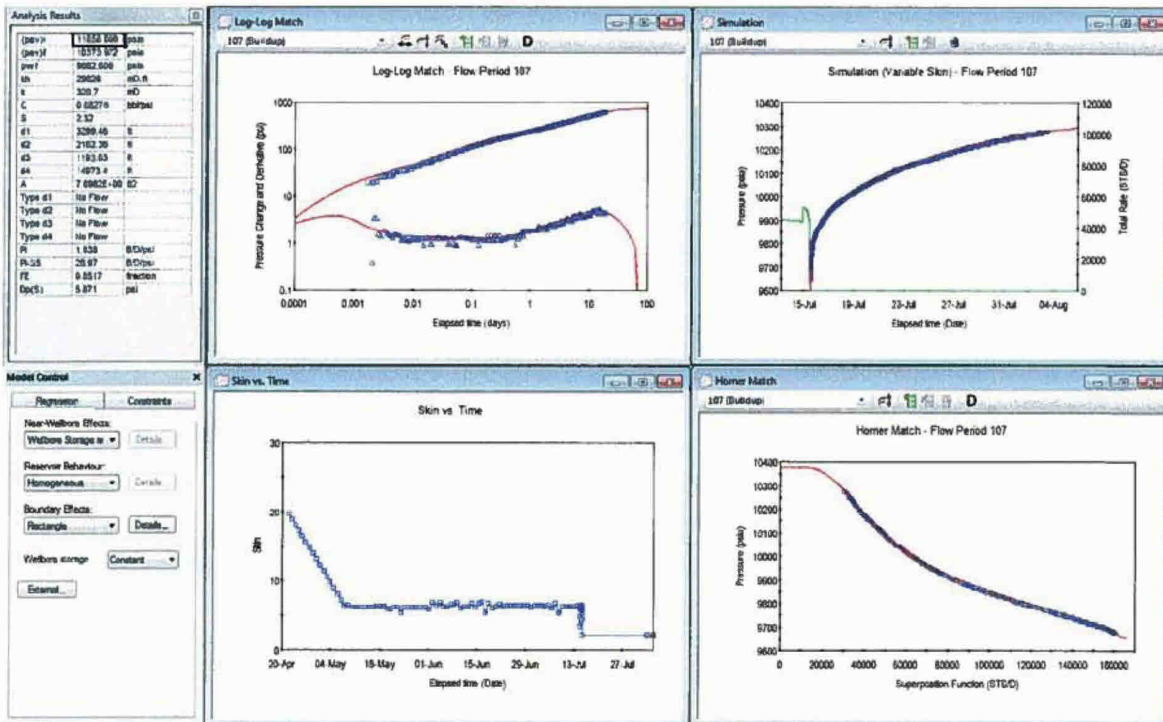Figure 152: Interpretation Model, Model Match and Analysis Results
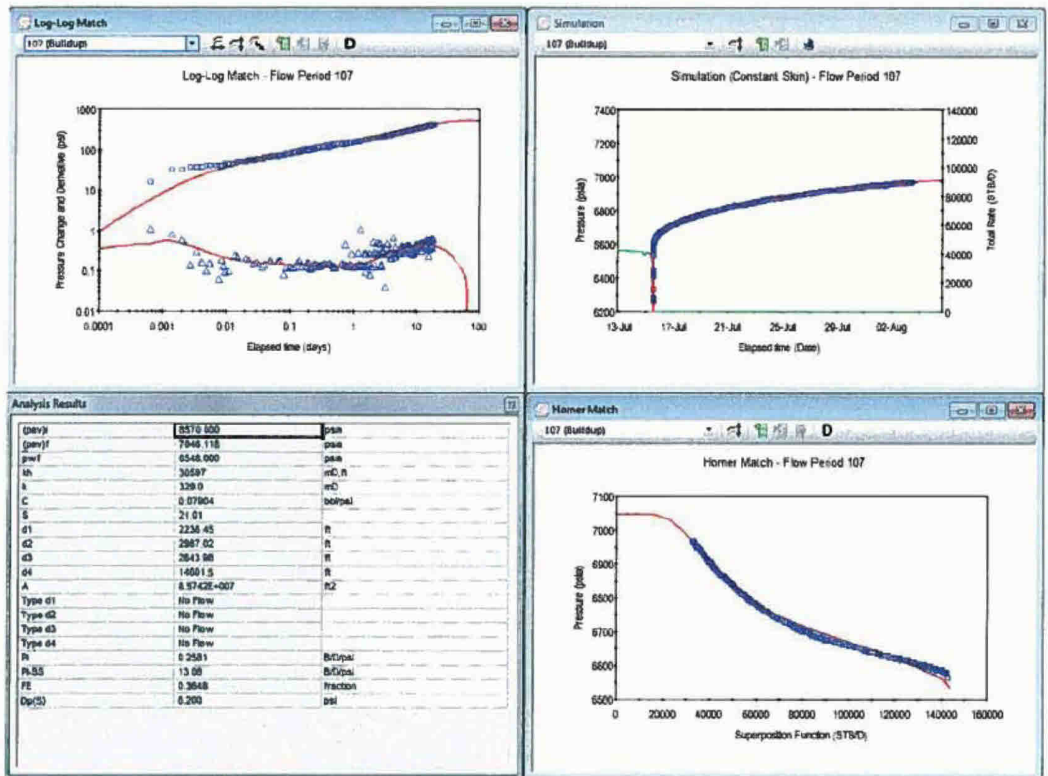
Figure 153: Interpretation Model, Model Match and Analysis Results (Zoom on Simulation – top left)
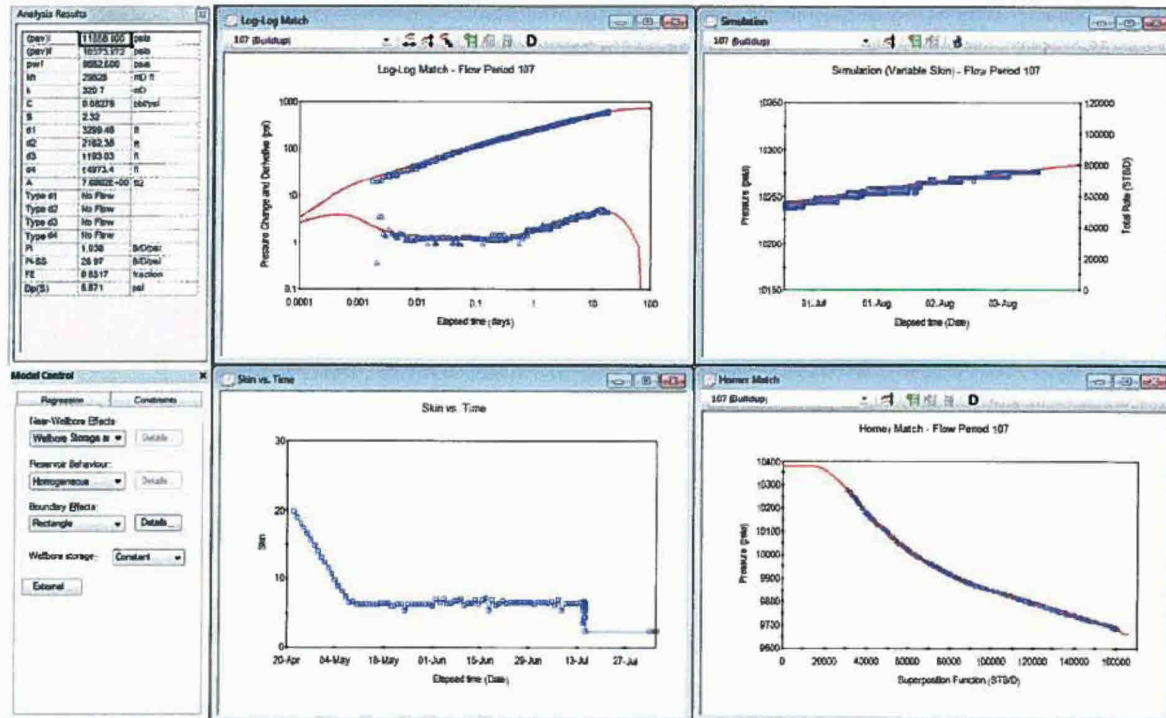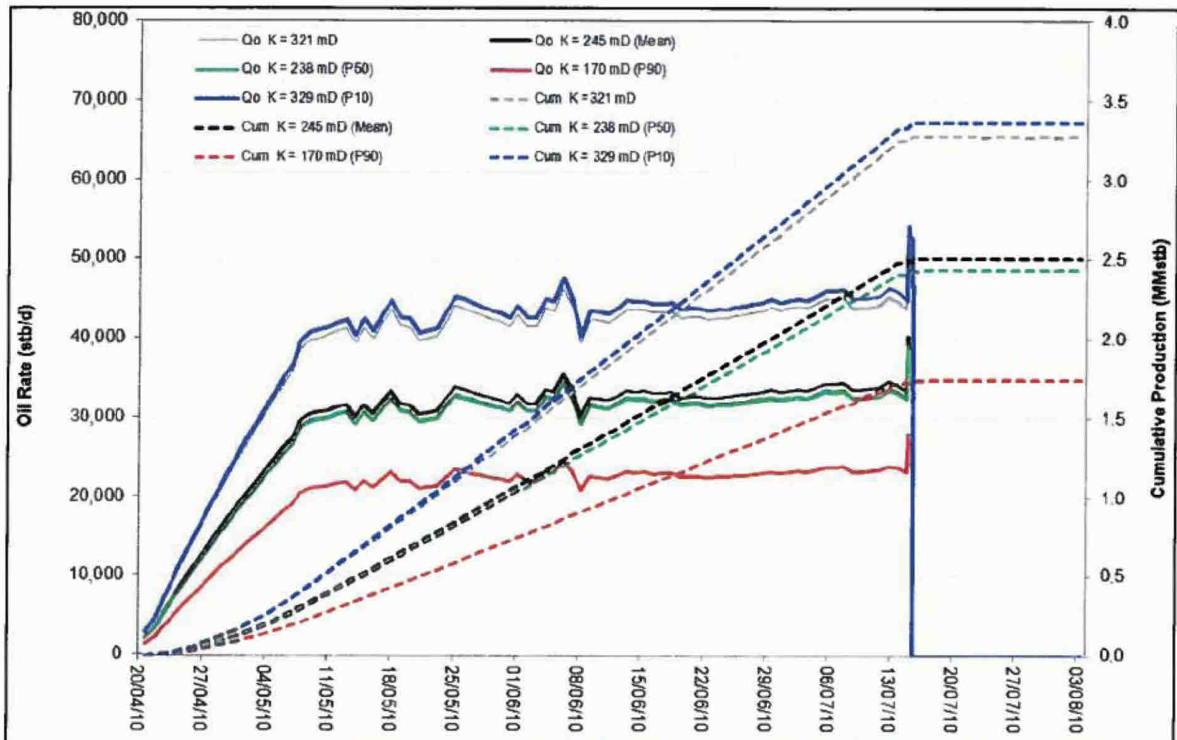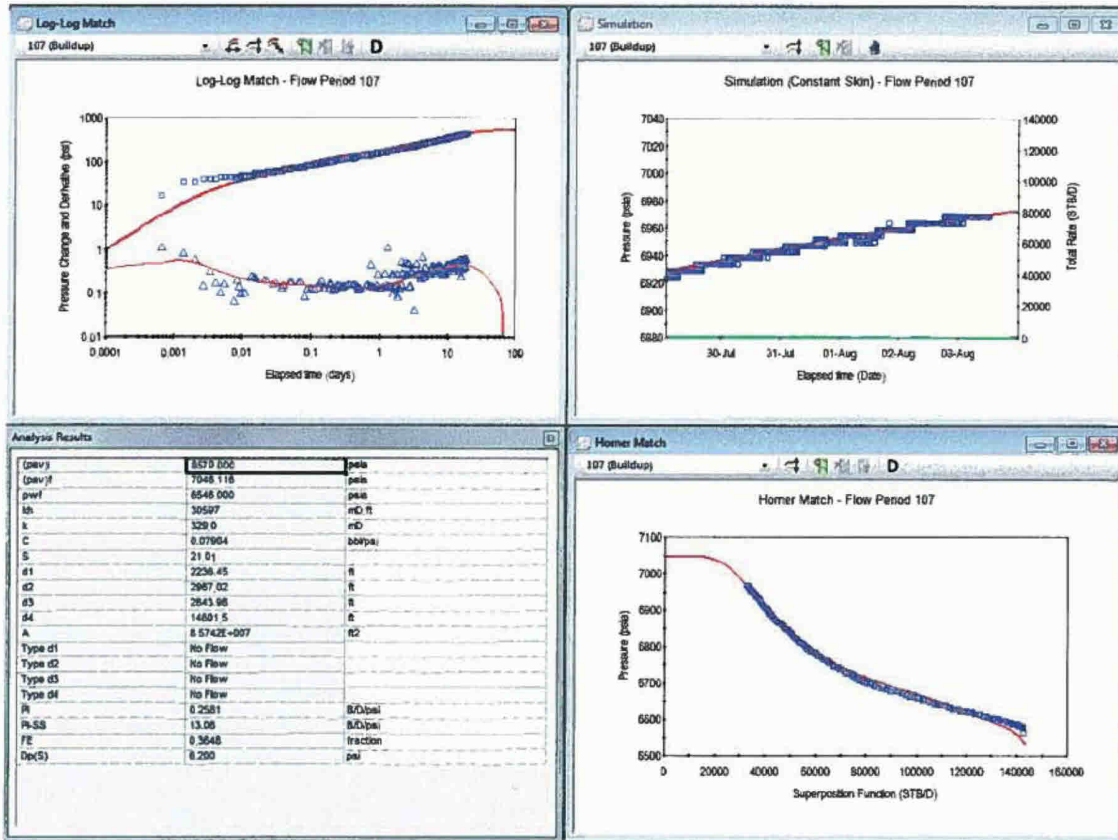
Figure 154: Interpretation Model, Model Match and Analysis Results (Further Zoom on Simulation – top left)

Analysis Model - Flow Period 107

Near Wellbore Effect: Wellbore Storage and Skin (C and S)
Reservoir Behaviour: Homogeneous
Boundary Effect: Rectangle

Initial average reservoir pressure, (pav)i	8570.000 psia
Final average reservoir pressure, (pav)f	7046.116 psia
Flowing pressure, pwf	6546.000 psia
Permeability Thickness, kh	30597 mD.ft
Permeability, k	329.0 mD
Wellbore storage coefficient, C	0.07904 bbl/psi
Wellbore skin factor, S	21.01
Distance to first boundary, d1	2236.45 ft
Distance to second boundary, d2	2967.02 ft
Distance to third boundary, d3	2643.98 ft
Distance to fourth boundary, d4	14601.5 ft
Drainage area, A	8.5742E+007 ft2
Type of first boundary, Type d1	No Flow
Type of second boundary, Type d2	No Flow
Type of third boundary, Type d3	No Flow
Type of fourth boundary, Type d4	No Flow
Measured Productivity Index, PI	0.2581 B/D/psi
Steady State Productivity Index, PI-SS	13.06 B/D/psi
Flow Efficiency, FE	0.3648 fraction
Pressure drop due to skin, Dp(S)	6.200 psi

Figure 155: P10 Model (Pressures at BOP Datum) – Summary of Results

103

3.5.2.4 K mean (245mD) Permeability Well Test Analysis

Shown in Figures 157 – 161 are the model diagnosis, interpretation model, model matches and analysis results which confirm a very good match to the pressure history, log-log pressure change and derivative, and the superposition (Horner) plot.

The match to the pressure history at various scales, further confirm a good match giving more validity to the analysis results and higher confidence predicting the Macondo well and reservoir properties using the matched interpretation model.
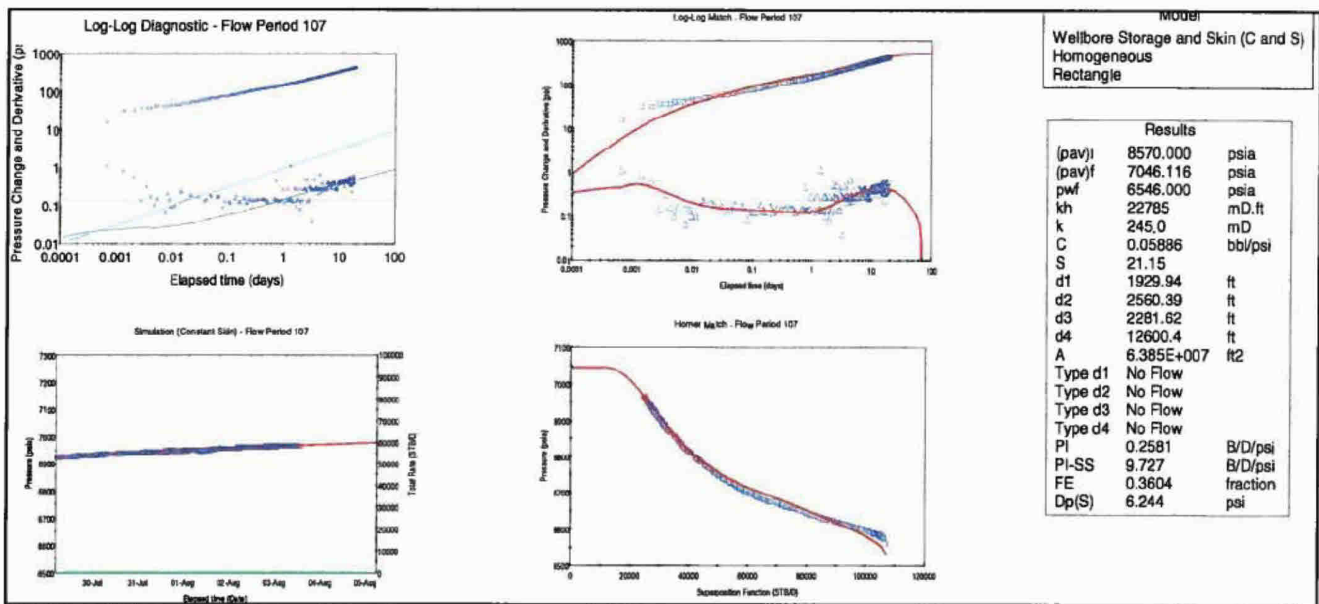
Figure 156: Diagnosis, Interpretation Model, Model Match and Analysis Results

Below are additional plots (Figures 158-161) showing the model match at various scales.
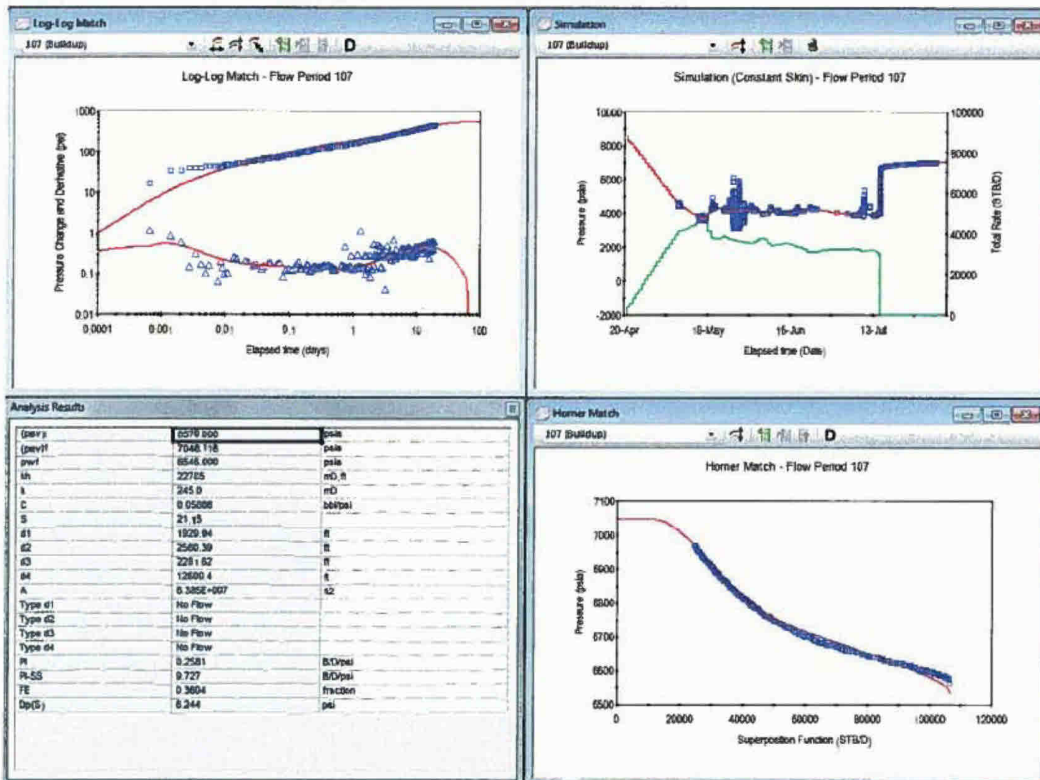
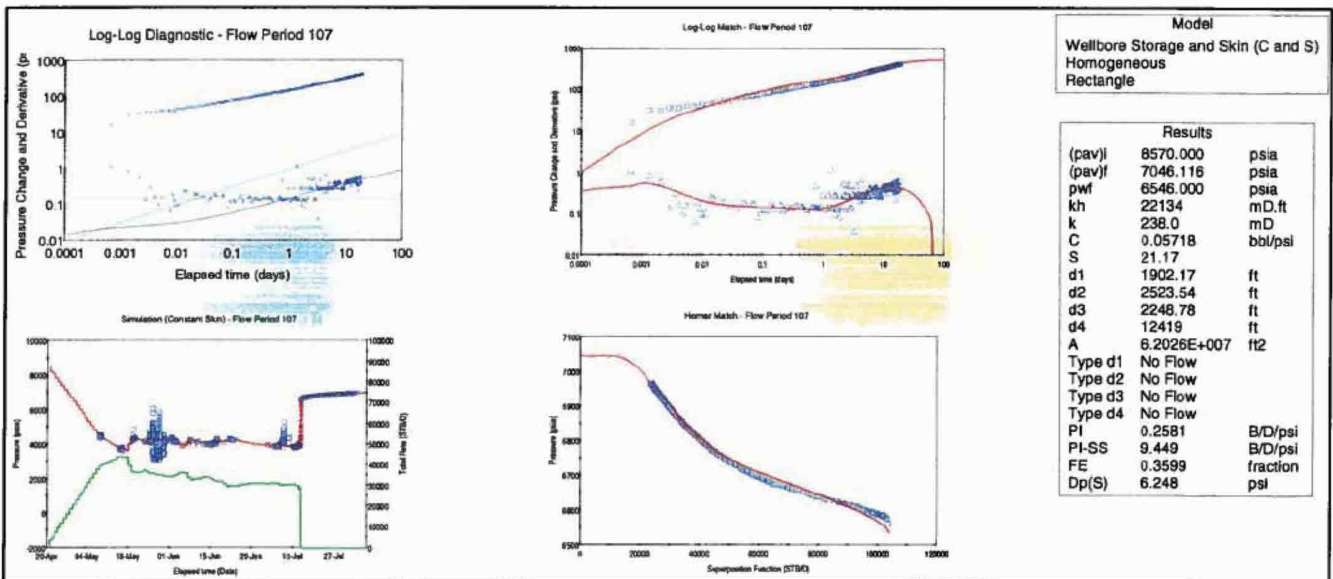Figure 157: Interpretation Model, Model Match and Analysis Results
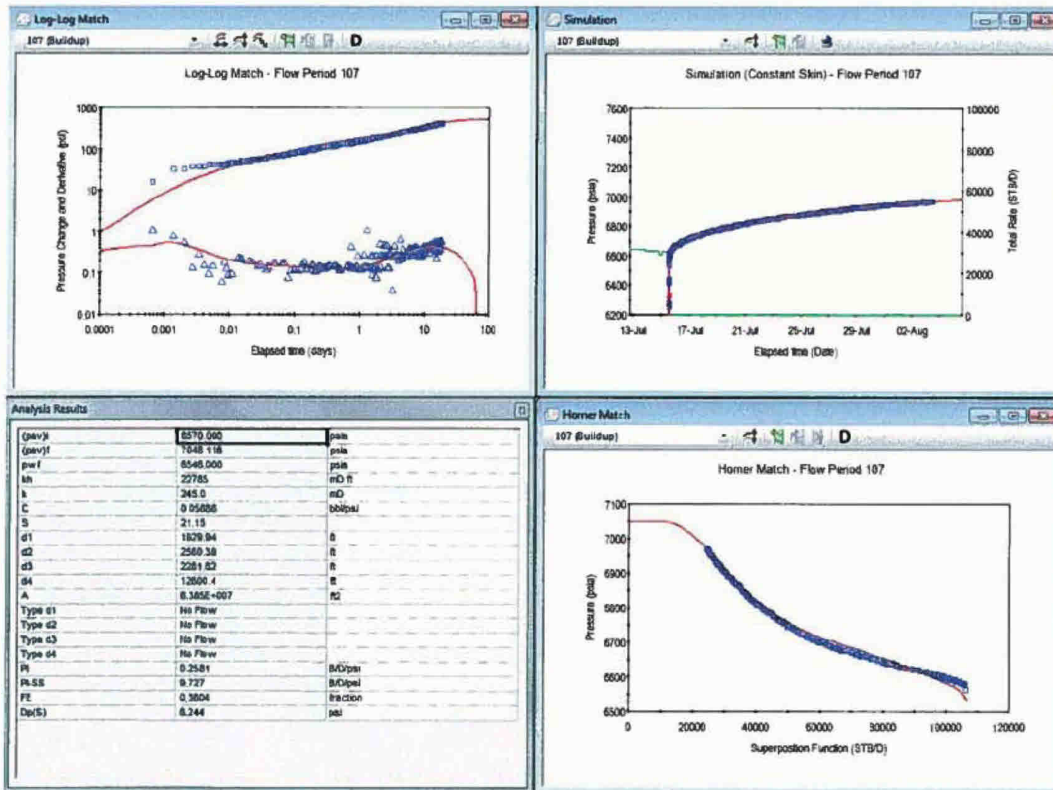
Figure 158: Interpretation Model, Model Match and Analysis Results (Zoom on Simulation – top left)

TREX-011696R.221
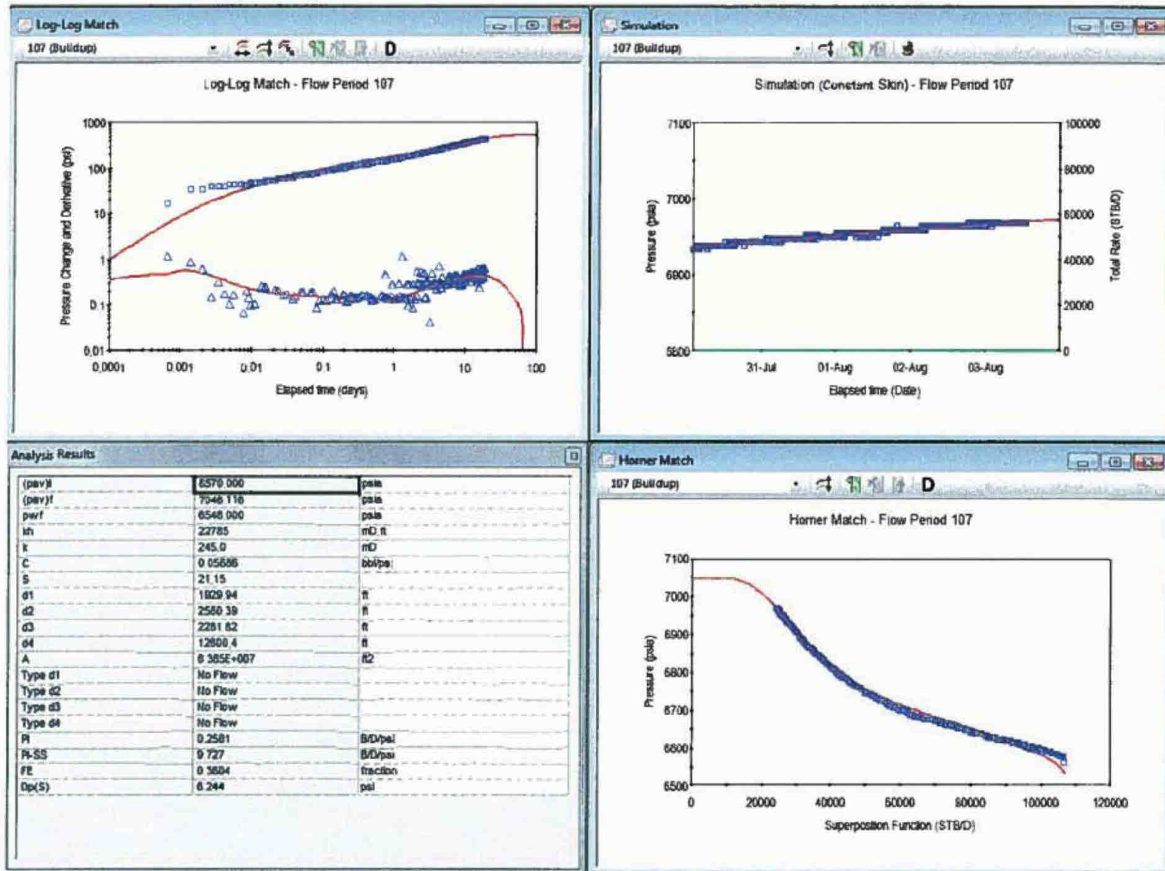
Figure 159: Interpretation Model, Model Match and Analysis Results (Further Zoom on Simulation – top left)

Analysis Model - Flow Period 107

Near Wellbore Effect:	Wellbore Storage and Skin (C and S)
Reservoir Behaviour:	Homogeneous
Boundary Effect:	Rectangle

Initial average reservoir pressure, (pav)i	8570.000 psia
Final average reservoir pressure, (pav)f	7046.116 psia
Flowing pressure, pwf	6546.000 psia
Permeability Thickness, kh	22785 mD.ft
Permeability, k	245.0 mD
Wellbore storage coefficient, C	0.05886 bbl/psi
Wellbore skin factor, S	21.15
Distance to first boundary, d1	1929.94 ft
Distance to second boundary, d2	2560.39 ft
Distance to third boundary, d3	2281.62 ft
Distance to fourth boundary, d4	12600.4 ft
Drainage area, A	6.385E+007 ft2
Type of first boundary, Type d1	No Flow
Type of second boundary, Type d2	No Flow
Type of third boundary, Type d3	No Flow
Type of fourth boundary, Type d4	No Flow
Measured Productivity Index, PI	0.2581 B/D/psi
Steady State Productivity Index, PI-SS	9.727 B/D/psi
Flow Efficiency, FE	0.3604 fraction
Pressure drop due to skin, Dp(S)	6.244 psi

Figure 160: K-mean (245mD) Model (Pressures at BOP Datum) – Summary of Results

106

3.5.2.5   K 333mD Permeability Well Test Analysis

A sensitivity to 333mD was done by scaling the rates to match 45,000stb/d on the 14th of July, 2010.

Shown in Figures 162 – 166 are the model diagnosis, interpretation model, model matches and analysis results which confirm a very good match to the pressure history, log-log pressure change and derivative, and the superposition (Horner) plot.

The match to the pressure history at various scales, further confirm a good match giving more validity to the analysis results and higher confidence predicting the Macondo well and reservoir properties using the matched interpretation model.
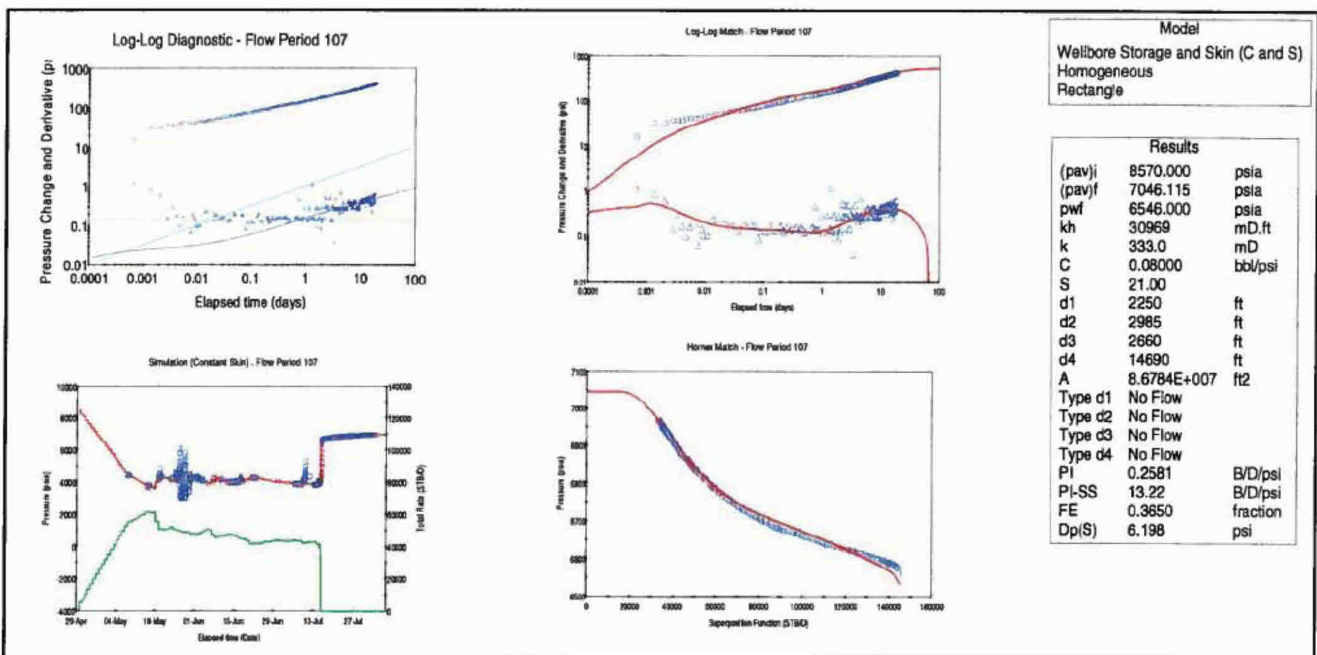
Figure 161: Diagnosis, Interpretation Model, Model Match and Analysis Results

Below are additional plots (Figures 163 – 166) showing the model match at various scales.
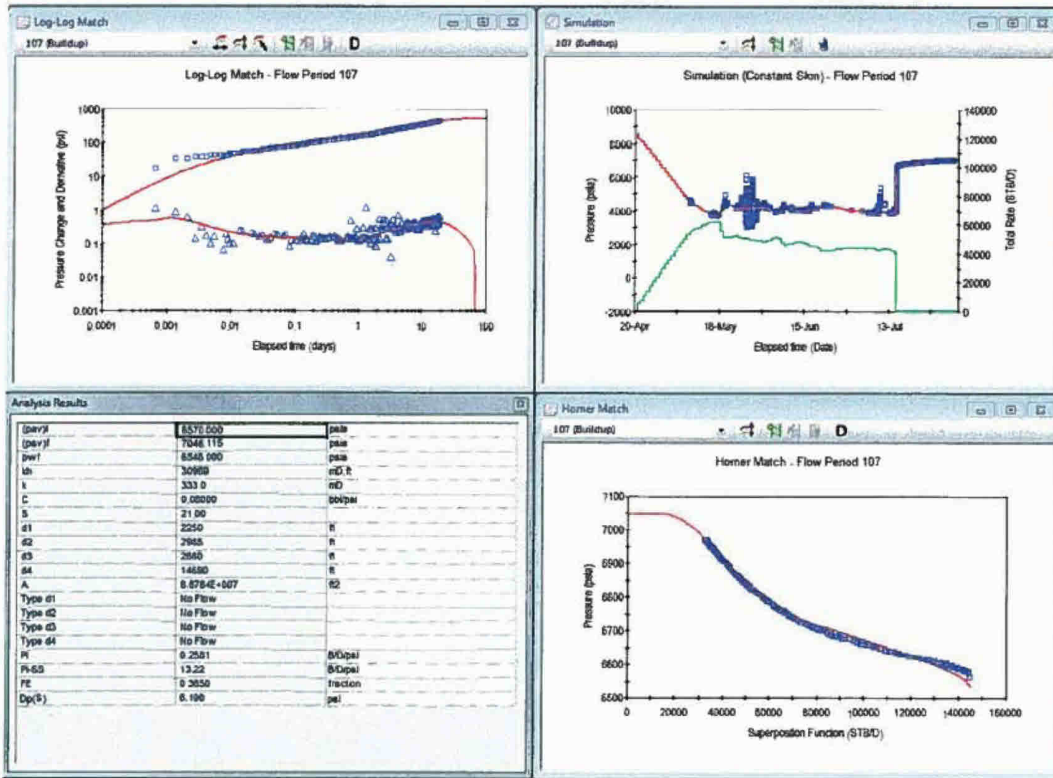
Figure 162: Interpretation Model, Model Match and Analysis Results
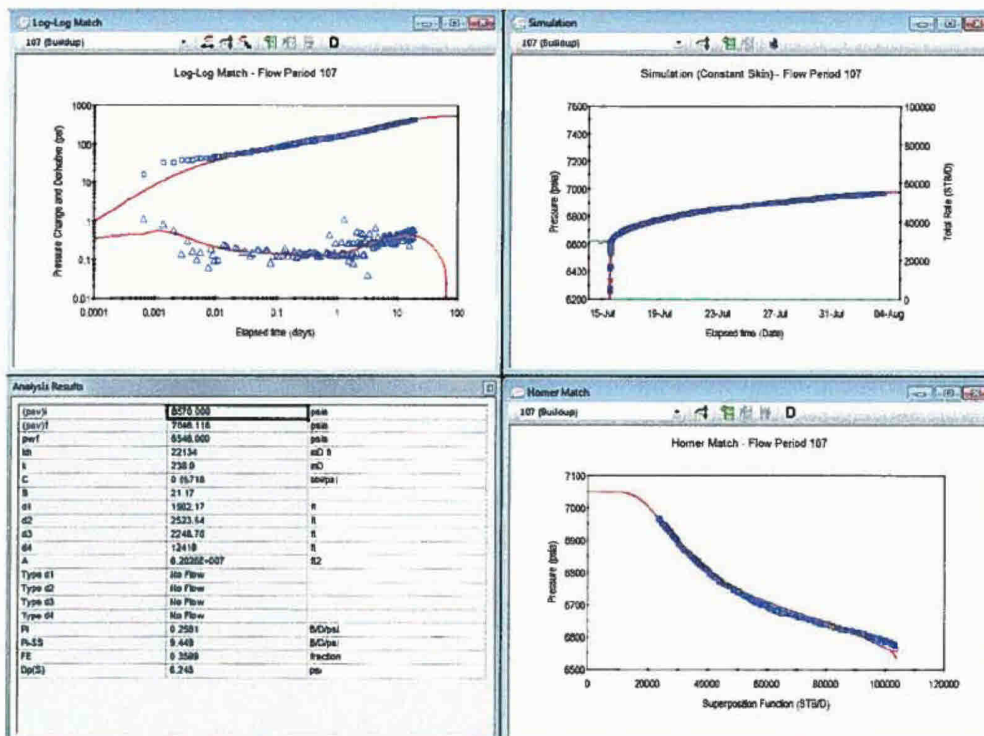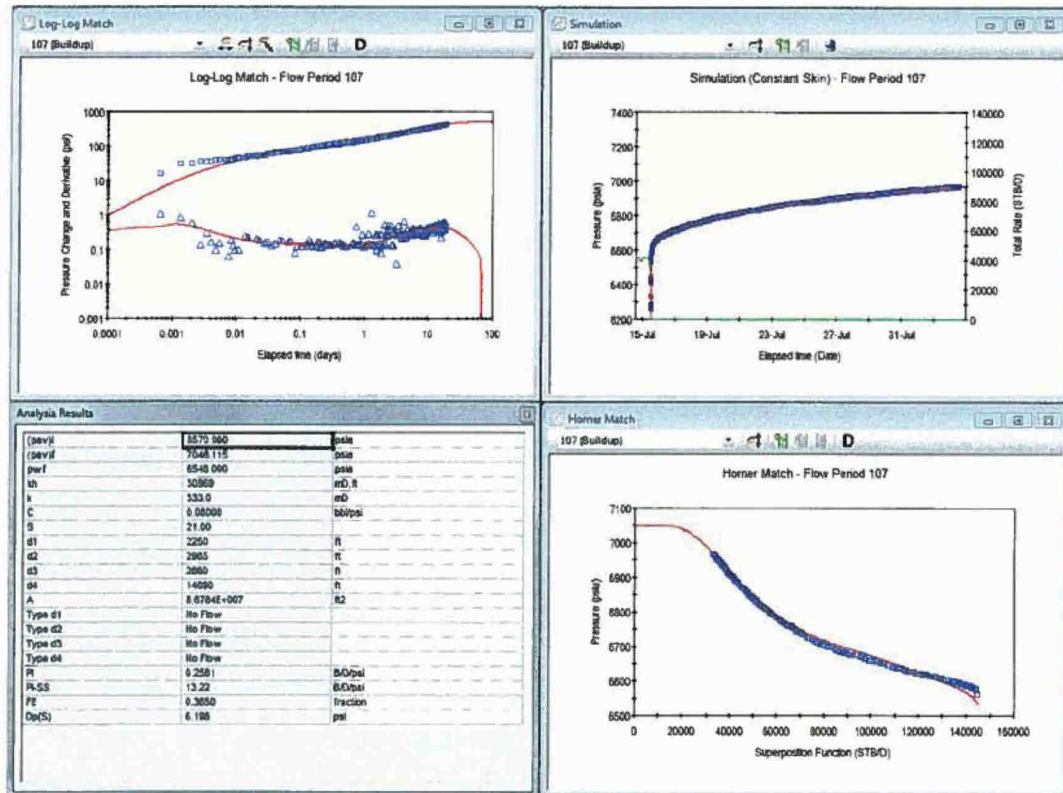

Figure 163: Interpretation Model, Model Match and Analysis Results (Zoom on Simulation – top left)
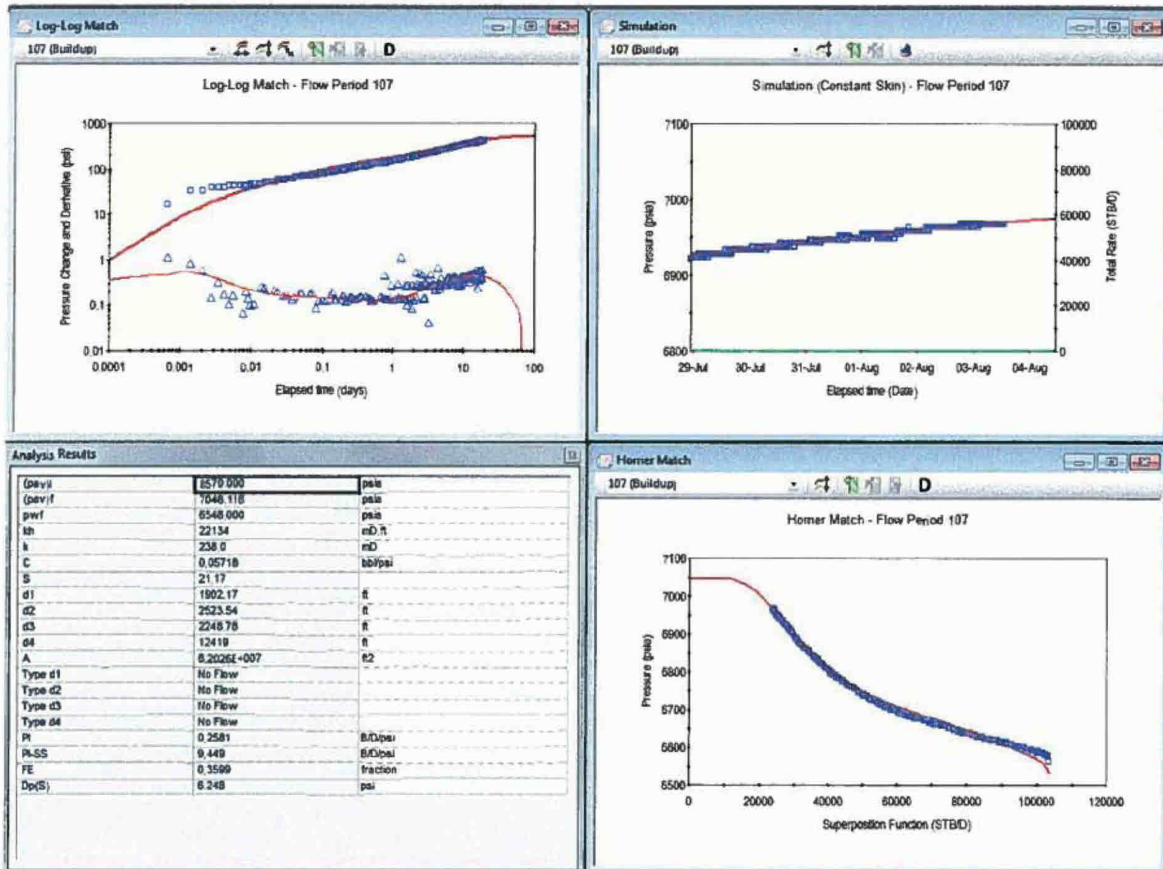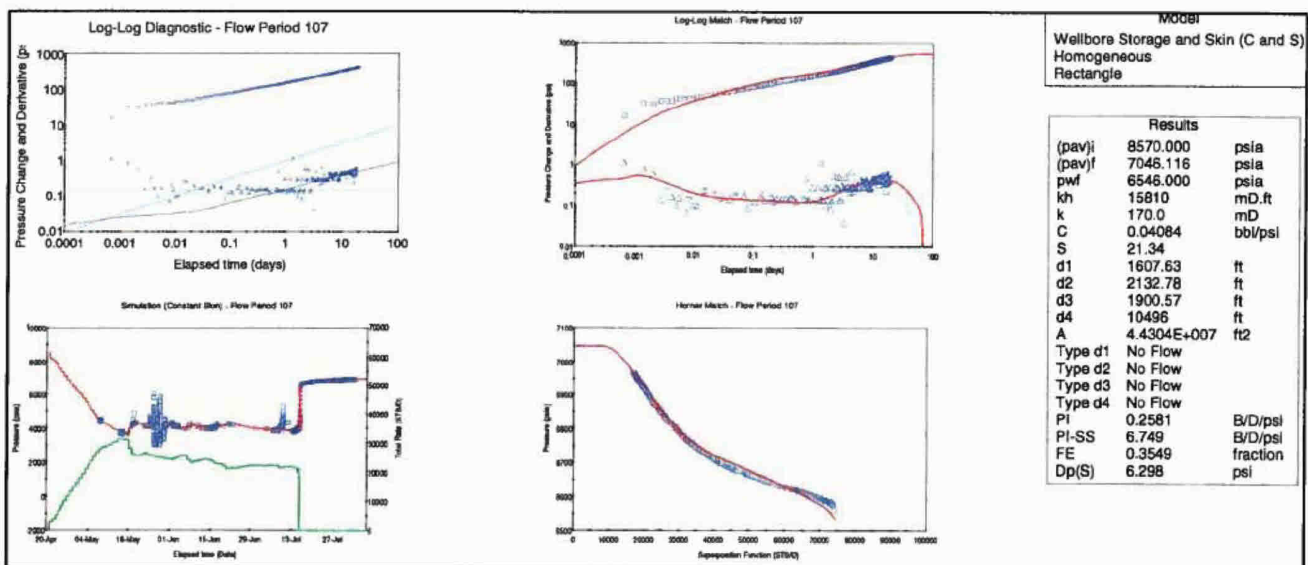
108
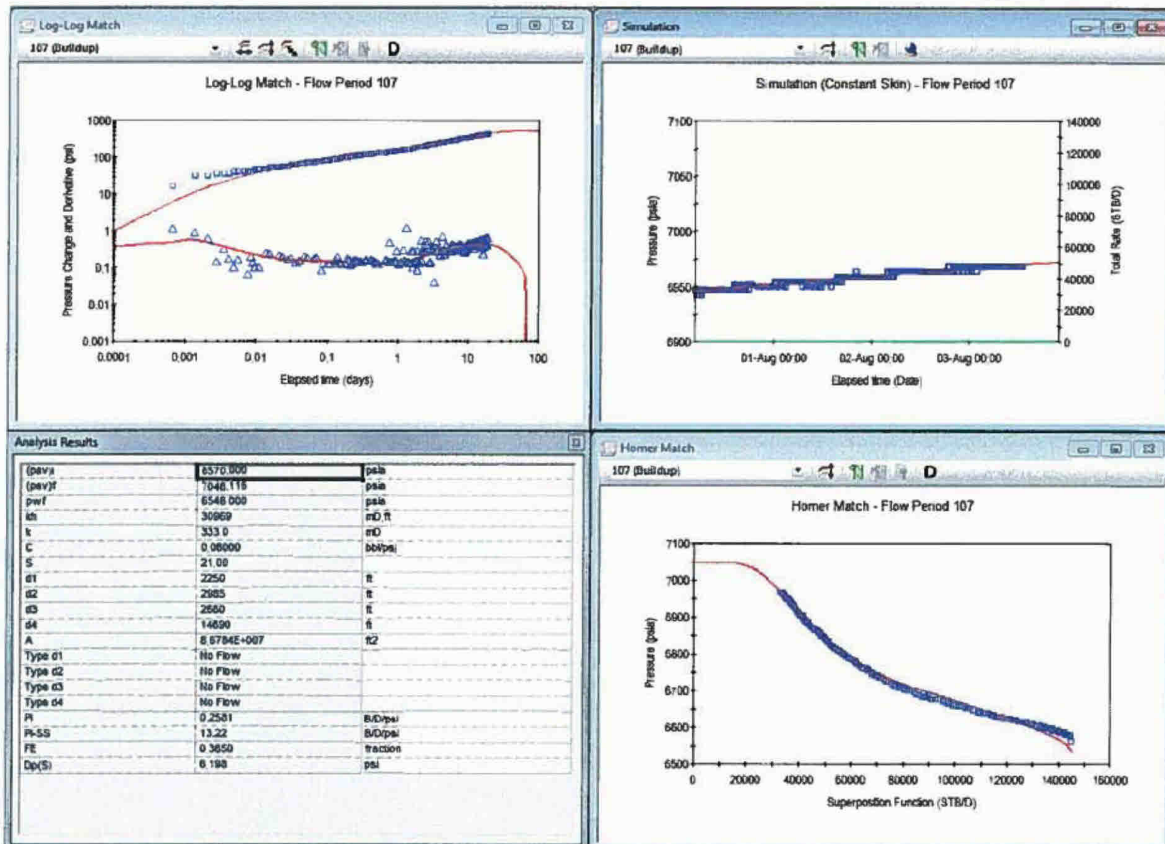
Figure 164: Interpretation Model, Model Match and Analysis Results (Further Zoom on Simulation – top left)

Analysis Model - Flow Period 107

Near Wellbore Effect: Wellbore Storage and Skin (C and S)
Reservoir Behaviour: Homogeneous
Boundary Effect: Rectangle

Initial average reservoir pressure, (pav)i	8570.000 psia
Final average reservoir pressure, (pav)f	7046.115 psia
Flowing pressure, pwf	6546.000 psia
Permeability Thickness, kh	30969 mD.ft
Permeability, k	333.0 mD
Wellbore storage coefficient, C	0.08000 bbl/psi
Wellbore skin factor, S	21.00
Distance to first boundary, d1	2250 ft
Distance to second boundary, d2	2985 ft
Distance to third boundary, d3	2660 ft
Distance to fourth boundary, d4	14690 ft
Drainage area, A	8.6784E+007 ft2
Type of first boundary, Type d1	No Flow
Type of second boundary, Type d2	No Flow
Type of third boundary, Type d3	No Flow
Type of fourth boundary, Type d4	No Flow
Measured Productivity Index, PI	0.2581 B/D/psi
Steady State Productivity Index, PI-SS	13.22 B/D/psi
Flow Efficiency, FE	0.3650 fraction
Pressure drop due to skin, Dp(S)	6.198 psi

Figure 165: K 333mD (Pressures at BOP Datum) – Summary of Results

109

3.5.2.6 WELL TEST ANALYSIS – BOP DATUM PRESSURES (SUMMARY AND RESULTS)

Parameters	P 90	P 50	P 10	Mean K	K-333
Initial Pressure @ BOP Depth (4,972 ft TVDss) psia	8,570	8,570	8,570	8,570	8,570
Final Pressure @ BOP Depth (4,972 ft TVDss) psia	7,046	7,046	7,046	7,046	7,046
Depletion (psi)	1,524.00	1,524.00	1,524.00	1,524.00	1,524.00
Reservoir Permeability (mD)	170	238	329	245	333
Skin	21	21	21	21	21
Boundary1 (d1) – ft	1,608	1,902	2,236	1,930	2,250
Boundary2 (d2) – ft	2,133	2,524	2,967	2,560	2,985
Boundary3 (d3) – ft	1,901	2,249	2,644	2,282	2,660
Boundary4 (d4) - ft	10,496	12,419	14,601	12,600	14,690
Reservoir Width - ft	3,509	4,151	4,880	4,212	4,910
Reservoir Length - ft	12,629	14,943	17,568	15,160	17,675
Area (MM ft^2)	44.3	62.0	85.7	63.9	86.8
Area (Acres)	1,017	1,424	1,968	1,466	1,992
STOIIP (MMstb)	60	84	117	87	118
Cumulative Production (MMstb)	1.94	2.71	3.75	2.79	3.80

Figure 166: WELL TEST ANALYSIS with PRESSURES at BOP DATUM – Summary of Results

110

3.6 OVERALL SUMMARY

Below is a summary of the overall results and the range of oil produced from the Macondo well based on the P50 and Mean Permeabilities determined from the MDT Analysis.

ANALYSIS OPTION / REFERENCE		Parameters	P 90	P 50	P 10	Mean K
		Reservoir Permeability (mD)	170	238	329	245
WHP (Well Head Pressure Analysis) ANALYSIS	4972 TVDss Initial Pressure 8570 psia	Final Reservoir Pressure	7,046			
		Depletion (psi)	1,524	1,524	1,524	1,524
		Reservoir Width - ft	3,509	4,151	4,880	4,212
		Reservoir Length - ft	12,629	14,943	17,568	15,160
		Area (Acres)	1,017	1,424	1,968	1,466
		STOIIP (MMstb)	60	84	117	87
		Cum. Production (MMstb)	1.94	2.71	3.75	2.79
OPTION-1 DRILL PIPE HIGH		Final Reservoir Pressure	10,364			
		Depletion (psi)	1,492	1,492	1,492	1,492
		Reservoir Width - ft	3,441	4,071	4,787	4,131
		Reservoir Length - ft	12,090	14,306	16,821	14,517
		Area (Acres)	955	1,337	1,848	1,377
		STOIIP (MMstb)	57	79	110	82
		Cum. Production (MMstb)	1.78	2.49	3.45	2.57
OPTION-2 DRILL PIPE HIGH	18056 TVDss Initial Pressure 11856 psia	Final Reservoir Pressure	10,381			
		Depletion (psi)	1,475	1,475	1,475	1,475
		Reservoir Width - ft	3,962	4,688	5,512	4,756
		Reservoir Length - ft	12,789	15,133	17,792	15,353
		Area (Acres)	1,163	1,629	2,251	1,676
		STOIIP (MMstb)	69	97	133	99
		Cum. Production (MMstb)	2.15	3.00	4.15	3.09
OPTION-2 DRILL PIPE LOW		Final Reservoir Pressure	10,374			
		Depletion (psi)	1,482	1,482	1,482	1,482
		Reservoir Width - ft	3,271	3,870	4,550	3,927
		Reservoir Length - ft	12,476	14,762	17,356	14,978
		Area (Acres)	937	1,312	1,813	1,350
		STOIIP (MMstb)	56	78	107	80
		Cum. Production (MMstb)	1.74	2.43	3.36	2.50

P50 & MEAN		Cumulative Production (MMstb)	RANGE	
			FROM	TO
P50	238 mD		2.4	3.0
MEAN	245 mD		2.5	3.1

[i] BP-HZN-2179MDL00477088; BP-HZN-2179MDL04440249.

[ii] PT-B Final Pressures.csv

[iii] BP-HZN-2179MDL00477088; BP-HZN-2179MDL04440249.

[iv] BP-HZN-2179MDL03290054.pdf

[v] OCS-G-32306 Well No. 1 ST00 BP01, BP-HZN-2179MDL01872218.xls

[vi] OCS-G-32306 Well No. 1 ST00 BP01, BP-HZN-2179MDL01872218.xls

[vii] PT3K2 SHUTIN DATA2.xlsx

[viii] OPTION1 P and Q for Translation (26-04-13) with BHPs.xlsx; OPTION2 P and Q for Translation (26-04-13) with BHPs.xlsx

APPENDIX G
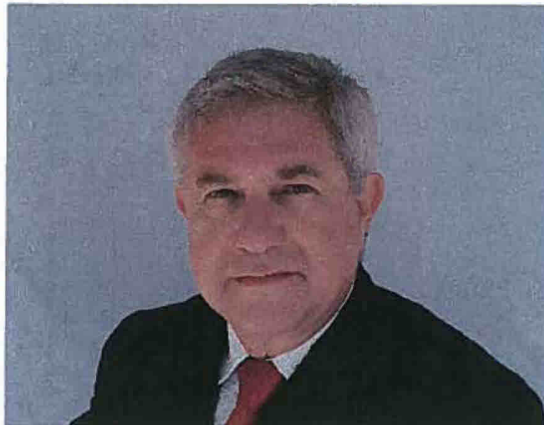
Alain C. Gringarten

Professor Alain C. Gringarten holds the Chair of Petroleum Engineering in the Department of Earth Science and Engineering at Imperial College in London, where he is also director of the Centre for Petroleum Studies. Prior to joining Imperial College in 1997, he spent fourteen years with Scientific Software-Intercomp; five years with Schlumberger; and five years with the Bureau de Recherches Géologiques et Minières in Orléans, France, in various senior technical and management positions.

Dr. Gringarten is a recognized expert in well test analysis and received the Society of Petroleum Engineers (SPE) Formation Evaluation award for 2001, the 2003 SPE John Franklin Carll award, the 2005 SPE Cedric K. Ferguson certificate for the best technical paper published in 2004, and the North Sea SPE Regional Service Award for 2009. He was a SPE Distinguished Lecturer for 2003-2004. He has published over ninety technical papers and was responsible for many advances in well test interpretation, including: the use of Greens functions; the "Gringarten type curves" for wells with wellbore storage and skin, fractured wells, and wells with double porosity behavior; the first major commercial computer-aided interpretation software; deconvolution; and a well test interpretation methodology which has become standard in the oil industry. He was also an early pioneer of multidisciplinary studies, both in industry and in academia. His research interests include shale gas and oil, gas condensate and volatile oil reservoirs, fissured fluid-bearing formations, hydraulically fractured wells, horizontal and multilateral wells, high and low enthalpy geothermal energy, Hot Dry Rocks, and radioactive waste disposal.

Prof. Gringarten has taught numerous well test interpretation industry courses around the world and has been involved in many consulting projects through his company Well Analysis Limited. A member of the Society of Petroleum Engineers (SPE) since 1969, he was elected a Distinguished Member in 2002 and an Honorary Member in 2009. He has chaired or organized many SPE Advanced Technology Workshops, and has been a member of the SPE International committees on: Research and Development (R&D) Advisory Committee (2010 -); Information and Management (2011 -); Honorary and Distinguished Member Awards (2011 -); Carll-Uren-Lester Awards (2009-2012); Nico van Wingen Fellowship (2013 -); PE Faculty Pipeline Award (2012 -); and was the 2011 chairman of the SPE Talent

Council (2009-2012). He holds a MSc. and a Ph.D. in Petroleum Engineering from Stanford University;
and an Engineer degree from Ecole Centrale, Paris, France.

Alain C. Gringarten

33 Melton Court   Birth date: 26 August 1945
Onslow Crescent   Tel: [+44](0)207 581 3301
London SW7 3 JQ UK   Email: a.gringarten@imperial.ac.uk

EDUCATION

1969-1970	Stanford University, Petroleum Engineering Department Master of Science, June 1969 Ph. D., April 1971
1965-1968	Ecole Centrale des Arts et Manufactures, Paris, France Engineer degree, July 1968

EMPLOYMENT HISTORY

Since 1997   **Imperial College London (UK)**

Director of the Centre for Petroleum Studies (Petroleum Engineering and GeoSciences)
Chair of Petroleum Engineering, Department of Earth Science and Engineering

1983-1996   **Scientific-Software Intercomp** (Consulting and Software for oil and gas production)

1994-1996	Executive Vice President, Software products and Consulting
1992-1994	Senior Vice President, Software products
1991	Senior Vice President, Strategic Planning
1989-1990	Senior Vice President, Special Projects
1987-1988	Senior Vice President, Corporate Marketing
1985-1987	Vice President, Well Performance products
1984	Senior Staff Advisor to the President
1983	Vice President, Research and Development (Intercomp UK)

1978-1983   **Schlumberger** (Oilfield services company)

1982	Director of Engineering (Johnston-Macco, USA)
1981	Department Head, Well test interpretation and PVT laboratories (Flopetrol, France)
1978-1980	Department Head, Well test interpretation (Flopetrol, France)

1973-1978   **BRGM, France** (French Geological Survey)

Principal Engineer
Scientific coordinator
Consultant to the Lawrence Berkeley Laboratory, Earth Science Division

1970-1972   University of California at Berkeley (USA)

Miller Research Fellow, Miller Institute for Basic Research in Science

EXPERIENCE

1- Management

- Various management assignments at SSI: P/L responsibility of the WorkBench Division Worldwide (marketing, development of software products including black oil, compositional and thermal simulators, sales, support) and of the Consulting Division (Americas and Far-East), with a budget of over 12 million dollars. Negotiation and implementation of joint ventures. Reorganization of SSI following the merger between Scientific Software Corp. and Intercomp Inc.

- General management of an engineering center for the development of tools and services for the production of oil and gas wells, including mechanical engineering, electronical engineering, reservoir engineering and computer hardware and software, with a budget of over 7 million dollars (Johnston-Macco-Schlumberger).

- Management of an international well test analysis service and PVT laboratories (Flopetrol-Schlumberger)

- Management of numerous development projects funded by the French government and the EEC (BRGM), for a total of over 1 million dollars.

2- Technical, and Research and Development

- Theoretical studies on fluid flow and heat transfer in porous and fissured media:
Application to oil and gas production, geothermal reservoirs, hydrogeology, geotechnical engineering and underground heat storage.

- Expertise in well testing
Author or co-author of over ninety technical articles and of many interpretation techniques that have become standard in the oil industry. Author of the first commercial well test analysis software product. Numerous consulting studies and courses worldwide.
Recipient of the SPE 2001 Formation Evaluation and 2003 John Franklin Carll awards. and the 2005 SPE Cedric K. Ferguson certificate for the best technical paper published in 2004. SPE Distinguished Lecturer 2003-2004.

- Reservoir Engineering projects, Reserve evaluations, Merger and Acquisitions

- Member of various professional or governmental committees for scientific research:
National Scientific Committee for Geothermal Energy of the Délégation Générale Scientifique et Technique, France (1974-1978); France representative at the NATO-CCMS for Hot Dry Rock and Solar Energy Research (1975-1978); Consultant to the European Economic Community and project manager for the EEC "Low Enthalpy" Geothermal Project (1975-1979); Advisor for underground heat storage to the Plan Construction, Ministry of Public Works, France (1976-1981); Member of the Scientific Advisory Committee for the EEC Hot Dry Rock Project in Soultz (1980-1983 and 1999-2005); Expert for the Skolkovo Foundation, Moscow (from 2012); Member of the ENI Awards Scientific Committee (from 2013)

- Principal Investigator
Consortium on "Well Testing without Emission "(3 companies, 1999-2002); Consortium on "Well test analysis in complex systems" (up to 7 oil companies, from 2000); Consortium on "Deconvolution" (up to 14 oil companies, from 2005)

- Owner and principal consultant, Well Analysis Limited
Consulting company specialized in well test analysis. Clients include Afren, AOC, Apache, Baker-Hughes, BP, BHP Billiton, ConocoPhillips, Deminex, Eastern American, Eni-AGIP, Eon, Exxon, Fairfield Energy, Gulf Canada, Hess, JNOC, Maersk, NIOC, Occidental Petroleum, PDVSA,

Petrobras, Petro-Canada, Perenco, Petro SA, POGC, Premier, RWA, RasGas, Sasol, Saudi Aramco, Schlumberger, Shell, Sondex, Total, Weatherford and Yukos.

3- Marketing and product development

- Reorganization of the Petroleum Engineering and Petroleum Geoscience curricula at Imperial College
  The MSc course in Petroleum Engineering has been reorganised in 1997 to follow the reservoir management process, with modules: Fundamentals; Reservoir Characterisation; Well Performance; and Field Development. The Fundamental and Reservoir Characterisation modules are mostly common with the MSc course in Petroleum Geoscience. The Reservoir Characterisation phase of the Group Field Development Project, based on real data from the North Sea, is performed with groups from the 3 petroleum disciplines (geology, geophysics and engineering), thus reproducing the environment of an asset team. The objective is to train students in the work flow concepts now prevailing in the oil industry and to produce petroleum professionals that are specialists in their field but are fully prepared to work effectively in multi-disciplinary teams.

- Definition and implementation of a marketing strategy for software products and consulting services (SSI):
  Definition and assessment of market segments, study of user requirements, definition of products, selection of hardware and software platforms, implementation of new structures, negotiation of marketing and development agreements, marketing and sales to international oil companies. Development of Interpret^{TM}, a well test analysis software product, and of WorkBench^{TM}, an integrated suite of products for the management of oil and gas reservoirs.

- Development of a Well Test Interpretation service (Flopetrol-Schlumberger):
  Definition of final product, development of new analysis methods, selection of computer hardware and development of software, hiring and training of engineers, preparation of a price list, organization and management of an international structure, marketing to international oil companies.

- Development of a program for the use of "low enthalpy" geothermal energy in France (BRGM):
  Definition and coordination of short-term and long term research in France and at the EEC; development of proposals for funded development; execution of feasibility studies, and pilot and full scale projects.

4- Additional information

- Extensive teaching and training experience (universities and oil companies, worldwide)

- Presentation of technical papers at numerous international conferences

- Member of the Society of Petroleum Engineers of the American Institute of Mining, Metallurgical and Petroleum Engineers since 1969, Distinguished Member since 2001, Honorary Member since 2009. Member of the Editorial review Committee (1982-1985); Board member, London Section (since 1997); Member of the Steering Committee, 1998 SPE Forum Series in Asia Pacific on "Integrated Well testing and Reservoir Characterization"; Member of the Technical Update Committee (1998-2001); Member of the Committee on Education and Professionalism (1998-2001); Chairman, SPE UK Workshops on Well Testing (November 2001), Gas Condensates (November 2002), Fractured Reservoirs (November 2003), Multilateral Wells (December 2004), Measurements while drilling (2006) and Multilayered reservoirs (2008); Co-convenor, EAGE/SPE workshop on Well testing and Seismics (Berlin, 2009); EAGE/Europec: Local Action Committee, Paris 2004 and London 2007; Technical Program Committee, Madrid 2005, London (Europec Chairman) 2007, Rome 2008, Amsterdam 2009, Barcelona 2010, Vienna 2011, Copenhagen 2012, London 2013;; Technical program Committee, 2005 IPTC (Qatar); Project Awards Committee, 2009 IPTC (Qatar); Chairman, Offshore Europe 2011 - Reservoir Management Programme Committee; Member, 2013 ATCE Education, Training and Professionalism Committee.

- Board member of (1) Moscow based Rock Flow Dynamics (RFD) a company founded in Spring 2005 for developing software for the petroleum industry and a member of the "Skolkovo" innovation centre; and (2) US based Reservoir Engineering Research Institute (RERI), a nonprofit research

and educational organization founded in January 1990 to carry out in-depth research in some key areas of petroleum reservoir engineering

- Fluent in French

ALAIN C. GRINGARTEN

List of Publications

Presented at conferences and published or accepted for publication:

1. Ogunrewo, O., Herens, T. and Gringarten, A. C.:" Well deliverability forecasting of gas condensate and volatile oil wells below saturation pressure", paper SPE 164869 to be presented at SPE Europec/EAGE Annual Conference, London, United Kingdom, 10–13 June 2013

2. Spyrou, C. E., Nurafza, P. and Gringarten, A. C.:" Well-head Pressure Transient Analysis", paper SPE 164871 to be presented at SPE Europec/EAGE Annual Conference, London, United Kingdom, 10–13 June 2013

3. Alshawaf, M. H. A. and Gringarten, A. C.:" Impact of Completion on Wellbore Skin Effect", paper SPE 164872 to be presented at SPE Europec/EAGE Annual Conference, London, United Kingdom, 10–13 June 2013

4. Cumming, J. A., Wooff, D. A., Whittle, T. M., Crossman, R. J., and Gringarten, A. C.:" Assessing the Non-Uniqueness of the Well Test Interpretation Model Using Deconvolution", paper SPE 164870 to be presented at SPE Europec/EAGE Annual Conference, London, United Kingdom, 10–13 June 2013

5. Green, A. J., Whittle, T. M, and Gringarten, A. C.:" Multi-phase Well Testing to Calibrate Relative Permeability Measurements for Reservoir Simulation", paper SPE 154851 presented at SPE Europec/EAGE Annual Conference, Copenhagen, Denmark, 4-7 June 2012.

6. Laoroongroj, A., Zechner M., Clemens, T., and Gringarten, A. C.:" Determination of the In-Situ Polymer Viscosity from Fall-Off Tests", paper SPE 154832 presented at SPE Europec/EAGE Annual Conference, Copenhagen, Denmark, 4-7 June 2012.

7. Kgogo, T. C. and Gringarten, A. C.:" Well Test Analysis of Medium-Rich to Rich Gas-Condensate Layered Reservoirs", paper SPE 143621 presented at the 2011 SPE EUROPEC/EAGE Annual Conference and Exhibition in Vienna, Austria, 23–26 May 2011.

8. Gringarten, A.C., Ogunrewo, O., and Uxukbayev, G.:" Assessment of Rate-Dependent Skin Factors in Gas Condensate and Volatile Oil Wells," paper SPE 143592 presented at the 2011 SPE EUROPEC/EAGE Annual Conference and Exhibition in Vienna, Austria, 23–26 May 2011.

9. Kgogo, T. C. and Gringarten, A. C.:" Comparative Well-Test Behaviours in Low-Permeability Lean, Medium-rich, and Rich Gas-Condensate Reservoirs", paper SPE 134452 presented at the 2010 SPE Annual Technical Conference and Exhibition held in Florence, Italy, 19–22 September 2010.

10. Gringarten, A. C.:"Practical use of well test deconvolution," paper SPE 134534 presented at the 2010 SPE Annual Technical Conference and Exhibition held in Florence, Italy, 19–22 September 2010

11. Madahar, A., Stewart G. and Gringarten, A.C.:" Effect of Material Balance on Well Test Analysis", paper SPE 124524 presented at the 2009 SPE Annual Technical Conference and Exhibition held in New Orleans, Louisiana, USA, 4–7 October 2009.

12. Mavromoustaki A., Lim B., Ng B., Mirza S.M., Hale C.P., Manolis I., Gringarten A.C., Hewitt G.F. and Matar O.K.:"An experimental study of wellbore phase redistribution effects in gas condensate reservoirs", presented at the 14th BHRG International Conference on Multiphase Production Technology, Cannes, France, 17-19 June 2009.

13. Whittle, T., Jiang, H., Young, S. and Gringarten A. C.:"Well Production Forecasting by Extrapolation of the Deconvolution of the Well Test Pressure Transients," paper SPE 122299 presented at the 2009 SPE EUROPEC/EAGE Annual Conference and Exhibition held in Amsterdam, The Netherlands, 8–11 June 2009.

14. Krukrubo G. J., and Gringarten, A.C.:" Predicting the onset of condensate accumulation near the wellbore in a gas condensate reservoir," paper SPE 121326 presented at the 2009 SPE EUROPEC/EAGE Annual Conference and Exhibition held in Amsterdam, The Netherlands, 8–11 June 2009.

15. Aluko, O.A. and Gringarten, A.C.:" Well Test Dynamics in Rich Gas Condensate Reservoirs under Gas Injection," paper SPE 121848 presented at the 2009 SPE EUROPEC/EAGE Annual Conference and Exhibition held in Amsterdam, The Netherlands, 8–11 June 2009.

16. Sanni, M. and Gringarten A. C.:" Application of Well Testing for Well Deliverability Forecasting in Volatile Oil Reservoirs," paper SPE 118377,

presented at the 2008 Abu Dhabi International Petroleum Exhibition and Conference, Abu Dhabi, UAE, 3–6 November 2008.

17. Sanni, M. and Gringarten A. C.:" Well Test Analysis in Volatile Oil Reservoirs," paper SPE 116239, presented at the 2008 SPE Annual Technical Conference and Exhibition, Denver, Co., U.S.A., 21–24 September 2008.

18. Whittle, T. and Gringarten A. C.:" The Determination of Minimum Tested Volume from the Deconvolution of Well Test Pressure Transients," paper SPE 116239, presented at the 2008 SPE Annual Technical Conference and Exhibition, Denver, Co., U.S.A., 21–24 September 2008.

19. Azi, A. C., Gbo, A., Whittle, T and Gringarten, A.C.:" Evaluation of confidence intervals in well test interpretation results," paper SPE 113888 presented at the 2008 SPE Europec/EAGE Annual Conference and Exhibition, Italy, 9–12 June 2008.

20. Mijinyawa, A., and Gringarten, A.C.:" Influence of Geological Features on Well Test Behavior," paper SPE 113877 presented at the 2008 SPE Europec/EAGE Annual Conference and Exhibition, Rome, Italy, 9–12 June 2008.

21. T. von Schroeter and A. C. Gringarten: "Superposition Principle and Reciprocity for Pressure Transient Analysis of Data from Interfering Wells," paper SPE 110465 presented at the 2007 SPE Annual Technical Conference and Exhibition, Anaheim, California, 11-14 November 2007.

22. Gringarten A. C.:" From Straight lines to Deconvolution: the Evolution of the State of the art in Well Test Analysis," paper SPE 102079, presented at the 2006 SPE Annual Technical Conference and Exhibition, San Antonio, Texas, U.S.A., 24–27 September 2006.

23. Gringarten A. C., Daungkaew S., Hashemi S. and Bozorgzadeh, M: "Well Test Analysis in Gas Condensate Reservoirs: Theory and Practice," paper SPE 100993, presented at the 2006 SPE Russian Oil and Gas Technical Conference and Exhibition, Moscow, Russia, 3–6 October 2006.

24. Amudo C., Turner, J., Frewin J.; Kgogo, T., and Gringarten A. C.:"Integration of Well Test Deconvolution Analysis and Detailed Reservoir Modelling in 3D Seismic Data Interpretation: A Case Study," paper SPE 100250 presented at the SPE Europec/EAGE Annual Conference and Exhibition, Vienna, Austria, 12–15 June 2006

25. Gringarten, A. C.:" Well Test Analysis in Low Permeability Multilateral Wells," paper IPTC-10686, presented at the International Petroleum Technology Conference, Doha, Qatar, 21-23 November 2005.

26. Ali, A. M, Falcone, G., Bozorgzadeh, M., Gringarten, A. C. and Hewitt, G. F: "Experimental Investigation of Wellbore Phase Redistribution Effects on Pressure-Transient Data" SPE-96587 presented at the 2005 SPE Annual Technical Conference and Exhibition, Dallas, Tx, 9-12 Oct-2005.

27. Tarik Baig, Uwe Droegemueller and Alain C. Gringarten:"Productivity Assessment of Fractured and Non-Fractured Wells in a Lean/Intermediate Low Permeability Gas Condensate Reservoir", Paper SPE 93136 presented at the 14th Europec Biennial Conference, Madrid, Spain, 13-16 June 2005.

28. Manijeh Bozorgzadeh and Alain C. Gringarten:"Application of Build-Up Transient Pressure Analysis to Well Deliverability Forecasting in Gas Condensate Reservoirs Using Single-Phase and Two-Phase Pseudo-Pressures", paper SPE/IADC 94018 presented at the 14th Europec Biennial Conference, Madrid, Spain, 13-16 June 2005.

29. Abdolnabi Hashemi and Alain C. Gringarten:"Comparison of Well Productivity between Vertical, Horizontal and Hydraulically Fractured Wells in Gas-Condensate Reservoirs" paper SPE 94178 presented at the 14th Europec Biennial Conference, Madrid, Spain, 13-16 June 2005.

30. Alain C. Gringarten:" Analysis of an Extended Well Test to Identify Connectivity Between Adjacent Compartments in a North Sea Reservoir," paper SPE 93988 presentated at the 14th Europec Biennial Conference, Madrid, Spain, 13-16 June 2005.

31. T. von Schroeter and A.C. Gringarten: "Estimates For The Radius Of A Condensate Zone From A Simple Compositional Model" in Proc. 2004 SPE Ann. Tech. Conf. Exh., Soc. Pet. Eng., Houston, paper SPE 89911 (2004).

32. A. Hashemi, L.M. Nicolas and A.C. Gringarten: "Well Test Analysis of Horizontal wells in Gas-Condensate Reservoirs" in Proc. 2004 SPE Ann. Tech. Conf. Exh., Soc. Pet. Eng., Houston, paper SPE 89905 (2004).

33. M.Bozorgzadeh and A.C. Gringarten: "New Estimate for the Radius of a Condensate Bank from Well Test Data Using the Dry Gas Pseudopressure" in Proc. 2004 SPE Ann. Tech. Conf. Exh., Soc. Pet. Eng., Houston, paper SPE 89904 (2004).

34. Alain C. Gringarten, Thomas von Schroeter, Trond Rolfsvaag and John Bruner: "Use of downhole permanent pressure gauge data to

diagnose production problems in a North Sea horizontal well" in *Proc. 2003 SPE Ann. Tech. Conf. Exh.*, Soc. Pet. Eng., Denver, paper SPE 84470 (2003).

35. T. M. Whittle, J. Lee and A.C. Gringarten: "Will Wireline Formation Tests Replace Well Tests?" in *Proc. 2003 SPE Ann. Tech. Conf. Exh.*, Soc. Pet. Eng., Denver, paper SPE 84086 (2003).

36. Hoellander, F., P. Hammond and Gringarten, A. C: "Harmonic Testing for Continuous Well and Reservoir Monitoring" in *Proc. 2002 SPE Ann. Tech. Conf. Exh.*, Soc. Pet. Eng., San Antonio, paper SPE 77692, (2002).

37. von Schroeter, T., Hoellander, F. and Gringarten, A. C: "Analysis of Well Test Data From Permanent Downhole Gauges by Deconvolution" in *Proc. 2002 SPE Ann. Tech. Conf. Exh.*, Soc. Pet. Eng., San Antonio, paper SPE 77688, (2002).

38. Florian Hollaender, Jim G. Filas, Curtis O. Bennett and Alain C. Gringarten: "Use of Downhole Production/Reinjection for Zero-Emission Well Testing: Challenges and Rewards" in *Proc. 2002 SPE Ann. Tech. Conf. Exh.*, Soc. Pet. Eng., San Antonio, paper SPE 77620, (2002).

39. S. Daungkaew, F. Ross and A. C. Gringarten: "Well Test Investigation of Condensate Drop-Out Behavior in a North Sea Lean Gas Condensate Reservoir" in *Proc. 2002 SPE Ann. Tech. Conf. Exh.*, Soc. Pet. Eng., San Antonio, paper SPE 77548, (2002).

40. von Schroeter, T., Hoellander, F. and Gringarten, A. C.:"Deconvolution of Well test Data as a Non-linear Total Least Square Problem", in *Proc. 2001 SPE Ann. Tech. Conf. Exh.*, Soc. Pet. Eng., Dallas, paper SPE 71574, (2001).

41. Romero, C. E., Carter J. N., Gringarten, A. C. and Zimmerman, R. W.:"A modified genetic algorithm for reservoir characterization", *Proc. 2000 SPE Int. Oil Gas Conf*, Beijing, 7-10 Nov., Soc. Pet. Eng., Dallas, paper SPE 64765, (2000).

42. Gringarten, A. C., Bond, D. J., Jackson, M. D., Jing, X., Ala, M. and Johnson, H. D.:" A Petroleum Engineering Educational Model Based on the Maureen Field UKCS", in *Proc. 2000 SPE Ann. Tech. Conf. Exh.*, Soc. Pet. Eng., Dallas, paper SPE 64311, (2000).

43. Gringarten, A. C., Al-Lamki, A., Daungkaew, S., Mott, R. and Whittle, T. M.:" Well Test Analysis in Gas-Condensate Reservoirs", ", in *Proc. 2000 SPE Ann. Tech. Conf. Exh.*, Soc. Pet. Eng., Dallas, paper SPE 62920, (2000).

44. Daungkaew, S., Hollaender, F. and Gringarten, A. C. :"Frequently Asked Questions in Well Test Analysis", in *Proc. 2000 SPE Ann. Tech. Conf. Exh.*, Soc. Pet. Eng., Dallas, paper SPE 63077, (2000).

45. Romero, C. E., Carter, J. N., Zimmerman, R. W. and Gringarten, A. C.:"Improved reservoir characterization through evolutionary computation", in *Proc. 2000 SPE Ann. Tech. Conf. Exh.*, Soc. Pet. Eng., Dallas, paper SPE 62942, (2000).

46. Zambrano, J., Zimmerman, R. W. and Gringarten, A. C.:"Influence of Geological Features on Well Test Behavior" SPE 59398, proceedings of the 2000 SPE Asia Pacific Conference on Integrated Modelling for Asset Management held in Yokohama, Japan, 25-26 April (2000).

47. Gringarten, A. C.:"Evolution of Reservoir Management Techniques: From Independent Methods to an Integrated Methodology. Impact on Petroleum Engineering Curriculum, Graduate Teaching and Competitive Advantage of Oil Companies" SPE 39713, proceedings of the 1998 SPE Asia Pacific Conference on Integrated Modelling for Asset Management held in Kuala Lumpur, Malaysia, 23-24 March (1998).

48. Bidaux, P., Whittle, T. M., Coveney, P. J. and Gringarten, A. C.: "Analysis of Pressure and Rate Transient Data From Wells in Multilayered Reservoirs," SPE paper 24679 presented at the 67th Annual Technical Conference and Exhibition of SPE, Washington, DC, Oct. 4-7, 1992.

49. Gringarten, A. C.: "Computer-aided Well Test Analysis," SPE paper 14099 presented at the Second International Petroleum Exhibition and Technical Symposium of SPE, Beijing, China, March 17-20, 1986.

50. Gringarten, A. C.: "Flow-test Evaluation of Fractured Reservoirs," *Special Paper 189* Geological Society of America, 1982.

51. Gringarten, A. C.: "Interpretation of Tests in Fissured Reservoirs and Multilayered Reservoirs with Double Porosity Behavior: Theory and Practice," paper SPE 10044 presented at the International Petroleum Exhibition and Technical Symposium of SPE, Beijing, China, March 18-26, 1982.

52. Gringarten, A. C., Burgess, T. M., Viturat, D., Pelissier, J. and Aubry, M.: "Evaluating Fissured Formation Geometry from Well Test Data: A Field Example," paper SPE 10182 presented at the Fifty-sixth Annual Fall Technical Conference and Exhibition of SPE, San Antonio, Texas, Oct. 5-7, 1981.

53. Bourdet, D. and Gringarten, A. C.: "Determination of Fissure Volume and Block Size in Fractured Reservoirs by Type-curve Analysis," paper SPE 9293 presented at the Fifty-fifth Annual Technical Conference and Exhibition of SPE, Dallas, Texas, Sept. 21-24, 1980.

54. Gringarten, A. C., Sauty, J. P., Landel, P. A. and Menjoz, A.: "Lifetime Optimization of Low Enthalpy Geothermal Doublets," *Advances in European Geothermal Research*, Proceedings of the Second Invitational Seminar on the Results of E. C. Geothermal Energy Research, Strasbourg, March 4-6, Dordrect, D. Reidal, 1980.

55. Gringarten, A. C. and Sauty, J. P.: "Stockage de Chaleur Sous Forme de Chaleur Sensible," Collogue DGRST sur le Transport et Stockagede l'Energie, Comité Thermique et Thermo-dynamique, Sofia Antipolis, France, October 12-13, 1979.

56. Gringarten, A. C., Bourdet, D. P., Landel, P. A., and Kniazeff, V. J.: "A Comparison Between Different Skin and Wellbore Storage Type-curves for Early-time Transient Analysis," paper SPE 8025 presented at the Fifty-fourth Annual Fall Technical Conference and Exhibition of SPE, Las Vegas, Nevada, Sept. 23-26, 1979.

57. Gringarten, A. C., Landel, P. A., and Sauty, J. P.: "The Effect of Thermal Dispersion on Injection of Hot Water in Aquifers," Second Invitational Well Testing Symposium, Berkeley, California, pp. 25-27, October 1978.

58. Gringarten, A. C.: "Well Testing in Two-Phase Geothermal Wells," paper SPE 7480 presented at the Fifty-third Annual Fall Technical Conference and Exhibition of SPE, Houston (USA), Oct. 1-3, 1978.

59. Gringarten, A. C.: "Reservoir Limit Testing for Fractured Wells," paper SPE 7452 presented at the Fifty-third Annual Fall Technical Conference and Exhibition of SPE, Houston (USA), Oct. 1-3, 1978.

60. Gringarten, A. C.: "Reservoir Life and Heat Recovery Factor in Geothermal Aquifers Used for Urban Heating," IASPEI/IAVCEI Durham Symposium on Geothermics and Geothermal Energy, Durham (Great Britain), August 1977, *Pure and Applied Geophysics* (1978-1979) **117**, Nos. 1-2.

61. Gringarten, A. C., Landel, P. A. and Peaudecerf, P.: "Pollution Thermique des Nappes par Réinjection d'Eau des Circuits de Climatisation," Société Hydrotechnique de France, XIVème Journées de l'Hydraulique, Question IV, rapport 3, Paris, 1976.

62. Gringarten, A. C. and Stieltjes, L.:"Study of a Geothermal Field in the ASAL Active Volcanic Rift Zone (French Territory of Afars and Issas, East Africa)," Workshop on Geothermal Reservoir Engineering, Stanford, Stanford University Press, 1975, 113-116.

63. Gringarten, A. C. and Sauty, J. P.: "Recovery of Heat Energy from Deep or Shallow Aquifers," Eighth International Seminar on Heat and Mass Transfer, Dubrovnik, Yugoslavia, August 18-23, 1975.

64. Gringarten, A. C. and Sauty, J. P.: "Influence de la Réinjection sur la Température d'un Réservoir Géothermique Utilisé pour le Chauffage Urbain," Second U.S. Symposium of the Development and Use of Geothermal Resources, San Francisco, May 20-29, 1975.

65. Ramey, H. J., Jr. and Gringarten, A. C.: "Effect of High Volume Vertical Fractures on Geothermal Steam Well Behavior," Second U.N. Symposium on the Development and Use of Geothermal Resources, San Francisco, May 20-29, 1975.

66. Gringarten, A. C. and Witherspoon, P.A.: "A Method of Analyzing Pump Test Data for Fractured Aquifers." *Symposium on Percolation Through Fissured Rock* at the International Society of Rock Mechanics, Stuttgart, Germany, September 18-19, 1972.

Presented at conferences, available as abstracts only:

67. Auzet, J. P., Drogue, C., and Gringarten, A. C.: "Analyse d'Essais de Pompage dans les Massifs Calcaires Fissurés. Interpretation du Début du Régime Transitoire," Troisième réunion des Sciences de la Terre, Montpellier, France, April 23-25, 1975.

68. Gringarten, A. C., et al: "Horner Type-curve Analysis," paper SPE 9291 presented at the Fifty-fifth Annual Technical Conference and Exhibition of SPE, Dallas, Texas, Sept. 21-24, 1980.

69. Ramey, H. J. and Gringarten, A. C.: "Well Tests in Fractured Reservoirs," Circum Pacific Conference of SPE, Honolulu, Hawaii, August 20, 1982.

70. Gringarten, A. C.: "Future Direction of Reservoir Description, Reservoir Simulation and Integrated Reservoir Management," SPE paper 25557 presented at the International Symposium on Reservoir Management of the Society of Indonesian Petroleum Engineers (IATMI), Yogyakarta, Indonesia, July 1, 1993.

71. Gringarten, A. C.: "Well Test Analysis in the 1990's", presented at the Latin America Caribbean Petroleum Engineering Conference

(LACPEC), Porto la Cruz, Venezuela, 20 Oct. 1993.

72.Gringarten, A. C.: "Geological aspects of well test analysis", presented at the PETEX 2000 Conference, London, UK, 28-30 Nov. 2000.

Published in Technical Journals:

73. Gringarten, A. C. and Witherspoon, P. A.: "Extraction of Heat from Multiple Fractured Dry Hot Rock." *Geothermics* (1973) **Vol. 2**, 3-4, p. 119.

74. Gringarten, A. C. and Ramey, H. J. Jr.: "The Use of the Point Source Solution and Green's Function for Solving Unsteady Flow Problems in Reservoirs," *Soc. Pet. Eng. J.* (October 1973) 285.

75. Gringarten, A. C. and Ramey, H. J., Jr.: "Unsteady-state Pressure Distributions Created by a Well with a Single Infinite Conductivity Vertical Fracture," *Soc. Pet. Eng. J.* (August 1974) 347.

76. Gringarten, A. C. and Ramey, H. J., Jr.: "Unsteady-state Pressure Distributions Created by a Well with a Single Horizontal Fracture, Partial Penetration, or Restricted Entry," *Soc. Pet. Eng. J.* (August 1974) 413.

77. Gringarten, A. C., Raleigh, C. B., Witherspoon, P. A. and Onishi, Y.: "Multiple Hydraulic Fracturing for the Recovery of Geothermal Energy," *EOS Transactions*, AGU (1974) **55**, No. 4, p. 4025.

78. Gringarten, A. C. and Ramey, H. J., Jr.: "An Approximate Infinite Conductivity Solution for a Partially Penetrating Line-Source Well," *Soc. Pet. Eng. J.* (April 1975) 141.

79. Gringarten, A. C., Witherspoon, P. A. and Onishi, Y.: "Theory of Heat Extraction From Fractured Hot Dry Rock," *J. Geoph. Res.* (March 1975) **80**, No. 8, 1120.

80. Gringarten, A. C., Ramey, H. J. and Raghavan, R.: "Applied Pressure Analysis for Fractured Wells," *J. Pet. Tech.* (July 1975) 887.

81. Gringarten, A. C. and Sauty, J. P.: "A Theoretical Study of Heat Extraction from Aquifers with Uniform Regional Flow," *J. Geoph. Res.* (Dec. 10, 1975) **80**, No. 35, 4956.

82. Gringarten, A. C.: "Simulation des Transferts de Chaleur dans les Aquifères," *Bull.*, B.R.G.M. (2) **III**, 1-1975.

83. Clouet d'Orval, M., Dieulin, A., Fabris, H., Goblet, P., Gringarten, A. C., Iris, P., Ledoux, E., and de Marsily, G.: "Détermination des Paramètres Thermiques d'un Aquifère Captif et de Ses Epontes," *Mémoires du BRGM* (1978) **91**, 307.

84. Gringarten, A. C., Sauty, J. P., Menjoz, A. and Landel, P.A.: "Sensible Energy Storage in Aquifers - Part I: Theoretical Study," *Water Resour. Res.* (April 1982) **18** (2).

85. Gringarten, A. C., Sauty, J. P., Menjoz, A. and Landel, P. A.: "Sensible Energy Storage in Aquifers - Part II: Field Experiments and Comparison with Theoretical Results," *Water Resour. Res.* (April 1982) **18** (2).

86. Gringarten, A. C.: "Interpretation of Tests in Fissured and Multilayered Reservoirs with Double Porosity Behavior: Theory and Practice," Distinguished Author Series Paper, *J. Pet. Tech.* (April 1984), 549-564.

87. Gringarten, A. C.: "Type-curve Analysis: What It Can and Cannot Do," Technology Today Series, *J. Pet. Tech.* (January 1987).

88. Gringarten, A. C.: "Recognizing Double Porosity Systems from Well Tests," Technology Today Series, *J. Pet. Tech.* (June 1987).

Books or Chapters in books:

89. Peube, J.L.; Hewitt, G.F.; Eckert, E.R.G.; Hahne, E.; Hoffman, H.W.; Le Goff, P.; Sandner, H.;Stephenson, D.G.; Gringarten, A. C.; Kurti, N.:"Heat transfer and thermal energy transport", in *Thermal energy storage* NATO Science Committee Conference, Turnberry, Scotland, March 1-5, 1976, Report (A76-45543 23-44) Brussels, NATO, 1976, p. 35-48.

90. Gringarten, A. C.: "Man-made Geothermal Reservoirs," published in *Geophysical Aspects of Energy Problem*, edited by A. Rapolla, G. V. Keller and D. J. Moore, Energy Research 1, Elsevier Scientific Publishing Company, Amsterdam, Oxford, New York, 1980.

91. Gringarten, A. C.: "Interpretation of Transient Well Test Data," published in *Developments in Petroleum Engineering - 1*, edited by R. A. Dawe and D. C. Wilson, Elsevier Applied Science Publishers, London and New York, 1985.

Unsolicited articles accepted for publication:

92. Gringarten, A.C., and Ramey, H.J., Jr.:"Application of the P function to heat conduction and flow problems," SPE paper 3816, 3 Nov. 1971.

93. Gringarten, A.C., and Ramey, H.J., Jr.:"A comparison of different solutions to the radial flow problem," SPE paper 3817, 3 Nov. 1971.

Patents:

94. Gringarten, A. C.: "Method of Determining Characteristics of a Fluid Producing Underground Formation," United States Patent 4, 32B, 705 May 11, 1982.

95. Gringarten, A. C.: "Method for Obtaining Dimensionless Representation of Well Pressure Data without the Use of Type-curves," United States Patent 4,607,524, August 1985.

APPENDIX H

Gringarten Consideration Materials

Aluko, O. A. and Gringarten, A.C. 2009: "Well Test Dynamics of Rich Gas Condensate Reservoirs under Gas Injection," Paper 121848 presented at 2009 SPE EUROPEC/EAGE Annual Conference and Exhibition held in Amsterdam, The Netherlands, 8-11 June.

Evgeny Pimonov, SPE and Cosan Ayan, SPE, Schlumberger, Mustafa Onur, SPE, Istanbul Technical University and Fikri Kuchuk, SPE, Schlumberger. A New Pressure/Rate-Deconvolution Algorithm to Analyse Wireline Formation-Tester and Well Test data. SPE 123982-PA-P1, August 2010 SPE Reservoir Evaluation and Engineering.

Gray, K. E: Approximating Well-to Fault Distance From Pressure Build-up Tests, J.Pet.Tech (July 1965).

Levitan, M. M., 2003:"Practical Application of Pressure-Rate Deconvolution to Analysis of Real Well Tests", paper SPE 84290, presented at the 2003 SPE Annual Technical Conference and Exhibition, Denver, CO, Oct. 5 – Oct. 8.

Meunier, D.F., Kabir, C.S., and Wittmann, M.J. 1987:"Gas Well Test Analysis: Use of Normalized Pressure and Time Functions", *SPEFE* 2 (4): 629–636. SPE-13082-PA. DOI: 10.2118/13082-PA.

Sanni, M. and Gringarten, A.C., 2008: "Well Test Analysis in Volatile Oil Reservoirs," Paper SPE 116239 presented at the 2008 SPE Annual Technical Conference and Exhibition, Denver, 21-24 September.

von Schroeter, T., Hollaender, F., Gringarten, A., 2002:"Analysis of Well Test Data From Permanent Downhole Gauges by Deconvolution," paper SPE 77688, presented at the 2002 SPE Annual Technical Conference and Exhibition, San Antonio, TX, Sept. 29 –Oct. 2.

(May-June) Hsieh, P - Application of Transient Analyiss to Macondo

(May-June) Hsieh, P - Application of Transient Analyiss to Macondo

20101208 - DOE-NL -- DJB marked with proprietary marked OUO -SAND Report on Flow Analysis Studies 12-08-10

40905 SIGNATURE LETTER AND ERRATA SHEET OF JASON LEBLANC

A New Method for Determination of Reservoir Pressure SPE 56418

A Practical Approach to Transient Pressure Behavior SPE 9901

ADR032-061971

AE-HZN-2179MDL00078658

AE-HZN-2179MDL00078658

ALL-T=160F-SSF.ecl.xls

ALL-T=180F-SSF.ecl.xls

ALL-T=200F-SSF.ecl.xls

ALL-T=210-SSF.ecl.xls

ALL-T=220F-SSF.ecl.xls

ALL-T=35-SSF.ecl.xls

Amudo C., Turner, J., Frewin J.; Kgogo, T., and Gringarten A. C., 2006:"Integration of Well Test Deconvolution Analysis and Detailed Reservoir Modelling in 3D Seismic Data Interpretation: A Case Study," paper SPE 100250 presented at the SPE Europec/EAGE Annual Conference and Exhibition, Vienna, Austria, 12–15 June

Analyzing Pressure Buildup Data by the Rectangular Hyperbola Approach SPE 13079

Appendix W to BP Deepwater Horizon Accident Investigation Report
Bozorgzadeh, M. and Gringarten, A.C. 2005: "Application of Build-up Transient Pressure Analysis to Well deliverability Forecasting in Gas Condensate Reservoirs Using Single-Phase and Two Phase Pseudo-pressure," Paper SPE 94018, presented at the 14th SPE Europec Technical Conference and Exhibition held in Madrid, Spain, 13-16 June; "Estimating Productivity-Controlling Parameters in Gas/Condensate Wells From Transient Pressure Data", *SPEREE* (APR. 2007) 100-111.
Bozorgzadeh, M. and Gringarten, A.C. 2006. Condensate-Bank Characterization from Well-Test Data and Fluid PVT Properties. *SPEREE* 9 (5): 596-611
BP Deepwater Horizon Accident Investigation Report
BP-HZN-2179MDL04440732
BP-HZN-2179MDL00004086
BP-HZN-2179MDL00058226
BP-HZN-2179MDL00058394
BP-HZN-2179MDL00059282
BP-HZN-2179MDL00059520
BP-HZN-2179MDL00059910
BP-HZN-2179MDL00062806
BP-HZN-2179MDL00063016
BP-HZN-2179MDL00063038
BP-HZN-2179MDL00063084
BP-HZN-2179MDL00063242
BP-HZN-2179MDL00063313
BP-HZN-2179MDL00063323
BP-HZN-2179MDL00063404
BP-HZN-2179MDL00063505
BP-HZN-2179MDL00063693
BP-HZN-2179MDL00159242
BP-HZN-2179MDL00159246
BP-HZN-2179MDL00159252
BP-HZN-2179MDL00159257
BP-HZN-2179MDL00159262
BP-HZN-2179MDL00159266
BP-HZN-2179MDL00251209
BP-HZN-2179MDL00251213
BP-HZN-2179MDL00251218
BP-HZN-2179MDL00251222
BP-HZN-2179MDL00251227
BP-HZN-2179MDL00251231
BP-HZN-2179MDL00251235

BP-HZN-2179MDL00251239
BP-HZN-2179MDL00251243
BP-HZN-2179MDL00251247
BP-HZN-2179MDL00251251
BP-HZN-2179MDL00251256
BP-HZN-2179MDL00251260
BP-HZN-2179MDL00251266
BP-HZN-2179MDL00309089
BP-HZN-2179MDL00470598
BP-HZN-2179MDL00470599
BP-HZN-2179MDL00477088
BP-HZN-2179MDL01530342
BP-HZN-2179MDL01594162
BP-HZN-2179MDL01608973
BP-HZN-2179MDL01872218
BP-HZN-2179MDL01872218
BP-HZN-2179MDL01945241
BP-HZN-2179MDL02107723
BP-HZN-2179MDL02107724
BP-HZN-2179MDL02172464
BP-HZN-2179MDL02393883
BP-HZN-2179MDL02394182
BP-HZN-2179MDL02394183
BP-HZN-2179MDL02394185
BP-HZN-2179MDL02394186
BP-HZN-2179MDL02394187
BP-HZN-2179MDL02900640
BP-HZN-2179MDL03139594
BP-HZN-2179MDL03198892
BP-HZN-2179MDL03290054
BP-HZN-2179MDL03742328
BP-HZN-2179MDL03742328
BP-HZN-2179MDL03807359
BP-HZN-2179MDL04440100
BP-HZN-2179MDL04440168
BP-HZN-2179MDL04440192
BP-HZN-2179MDL04440238
BP-HZN-2179MDL04440249

BP-HZN-2179MDL04440262
BP-HZN-2179MDL04440263
BP-HZN-2179MDL04440267
BP-HZN-2179MDL04440368
BP-HZN-2179MDL04440382
BP-HZN-2179MDL04440431
BP-HZN-2179MDL04440456
BP-HZN-2179MDL04440466
BP-HZN-2179MDL04440533
BP-HZN-2179MDL04440557
BP-HZN-2179MDL04440584
BP-HZN-2179MDL04440613
BP-HZN-2179MDL04440614
BP-HZN-2179MDL04440689
BP-HZN-2179MDL04440691
BP-HZN-2179MDL04440733
BP-HZN-2179MDL04440775
BP-HZN-2179MDL04440804
BP-HZN-2179MDL04440967
BP-HZN-2179MDL04440968
BP-HZN-2179MDL04440969
BP-HZN-2179MDL04440977
BP-HZN-2179MDL04440978
BP-HZN-2179MDL04549798
BP-HZN-2179MDL04578057
BP-HZN-2179MDL04826982
BP-HZN-2179MDL04826982
BP-HZN-2179MDL04884268
BP-HZN-2179MDL04884268
BP-HZN-2179MDL04927171
BP-HZN-2179MDL04940401
BP-HZN-2179MDL05187231
BP-HZN-2179MDL05796332
BP-HZN-2179MDL06314451
BP-HZN-2179MDL06424832
BP-HZN-2179MDL06666023
BP-HZN-2179MDL06666023
BP-HZN-2179MDL06666023

Appendix H (Materials Considered) - 2013-05-01-1931.docx

BP-HZN-2179MDL06741948
BP-HZN-2179MDL06742178
BP-HZN-2179MDL06742179
BP-HZN-2179MDL06742232
BP-HZN-2179MDL06742233
BP-HZN-2179MDL06742234
BP-HZN-2179MDL06742238
BP-HZN-2179MDL06742239
BP-HZN-2179MDL06742608
BP-HZN-2179MDL06742609
BP-HZN-2179MDL06742613
BP-HZN-2179MDL06742614
BP-HZN-2179MDL06742720
BP-HZN-2179MDL06742721
BP-HZN-2179MDL06742965
BP-HZN-2179MDL06742966
BP-HZN-2179MDL06742968
BP-HZN-2179MDL06742969
BP-HZN-2179MDL06742970
BP-HZN-2179MDL06742973
BP-HZN-2179MDL06742974
BP-HZN-2179MDL06743166
BP-HZN-2179MDL06743280
BP-HZN-2179MDL06743284
BP-HZN-2179MDL06743478
BP-HZN-2179MDL06743479
BP-HZN-2179MDL06743482
BP-HZN-2179MDL06744009
BP-HZN-2179MDL06744010
BP-HZN-2179MDL06744011
BP-HZN-2179MDL06744066
BP-HZN-2179MDL06744067
BP-HZN-2179MDL06744204
BP-HZN-2179MDL06744773
BP-HZN-2179MDL06744880
BP-HZN-2179MDL06744882
BP-HZN-2179MDL06744883
BP-HZN-2179MDL06744884

Appendix H (Materials Considered) - 2013-05-01-1931.docx

TREX-011696R.249

BP-HZN-2179MDL06744885
BP-HZN-2179MDL06744992
BP-HZN-2179MDL06745326
BP-HZN-2179MDL06745327
BP-HZN-2179MDL06745329
BP-HZN-2179MDL06746267
BP-HZN-2179MDL06746268
BP-HZN-2179MDL06947352
BP-HZN-2179MDL07129522
BP-HZN-2179MDL07279438
BP-HZN-2179MDL07279439
BP-HZN-2179MDL07279440
BP-HZN-2179MDL07279441
BP-HZN-2179MDL07279442
BP-HZN-2179MDL07279443
BP-HZN-2179MDL07279444
BP-HZN-2179MDL07279445
BP-HZN-2179MDL07279446
BP-HZN-2179MDL07279447
BP-HZN-2179MDL07279448
BP-HZN-2179MDL07279449
BP-HZN-2179MDL07279450
BP-HZN-2179MDL07383106
BP-HZN-2179MDL07383108
BP-HZN-2179MDL07383109
BP-HZN-BLY00000526
BP-HZN-BLY00120160
BP-HZN-BLY00120160
BP-HZN-BLY00134336
BP-HZN-BLY00138899
BP-HZN-BLY00269184
BP-HZN-MBI00023865
CAM_CIV_0148046
Camilli - WHOI Prepared Congressional Statement
Camilli WHOI Presentation Plan
Computer Simulation of Reservoir Depletion and Oil Flow from the Macondo Well Following the Deepwater Horizon Blowout
Congressional Hearing - Sizing Up the BP Oil Spill - Transcript (Original)

6

Consideration Materials List of Aaron Zick
Consideration Materials List of Mehran Pooladi-Darvish
Consideration Materials List of Mohan Kelkar and Rajagopa Raghavan
Consideration Materials List of Mohan Kelkar and Rajagopa Raghavan (Revised)
Crone - Science Express - Magnitude of the 2010 Gulf of Mexico Oil Leak
Crone, Chiang, Wereley -- NPR - Gulf Oil Spill May Far Exceed Government, BP Estimates _ NPR
Crone, Chiang, Wereley -- NPR - Transcript
Deepwater Horizon - BP Oil Budget - What happened to the oil
Deepwater Horizon MC252 Gulf Incident Oil Budget
Deposition and Exhibits of E. Shtepani
Deposition and Exhibits S. McArthur
Deposition of A. Ballard
Deposition of D. Barnett
Deposition of F. Saidi
Deposition of G. Guthrie
Deposition of M. Gochnour
Deposition of M. Levitan
Deposition of M. Mason
Deposition of O. Rygg
Deposition of P. Hsieh
Deposition of P. Tooms
Deposition of Robert Merrill
Deposition of S. Bishop
Deposition of S. Pelphrey
Deposition of T. Gansert
Deposition of T. Hill
Deposition of T. Liao
Deposition of T. Lockett
Deposition of Y. Wang
DOE-NL -- DJB marked with proprietary marked OUO -SAND_Report_on_Flow_Analysis_Studies
DOE-NL DWH Oil Re (Griffiths)
Evaluations of confidence intervals in well test interpretation results SPE 113888
Exhibit 8620
Expert Report of A.E. Johnson PhdD Ceng
Expert Report of Aaron Zick
Expert Report of Mehran Pooladi-Darvish
Expert Report of Mohan Kelkar and Rajagopal Raghavan
Expert report of Morten Emilsen

Expert report prepared by Carlos Torres-Verdin
Expert report prepared by Curtis Whitson
Expert report prepared by Martin Blunt
Expert report prepared by Martin Trusler
Expert report prepared by Robert Zimmerman
████████████
Expert report of M. Zaldivar
FEESA Expert Report
FRTG - Assessment of Flow Rate Estimates for the Deepwater Horizon-Macondo Oil Spill - (Combined)
FRTG - Assessment of Flow Rate Estimates for the Deepwater Horizon-Macondo Oil Spill - (Combined)
FRTG - Jun 8 - Pooling Report
FRTG - Plume Team Statement
FRTG - Refined Estimate
FRTG - Summary Preliminary Report
FRTG - US Scientific Team Draws on New Data
FRTG Plume Team - PIV Report (Revised)
FRTG Press Release
FRTG -Press Release McNutt Provide Updates on Progress of Scientific Teams
Griffiths_Revised_6_2011
Gringarten A. C., 2006:" From Straight lines to Deconvolution: the Evolution of the State of the art in Well Test Analysis," paper SPE 102079, presented at the 2006 SPE Annual Technical Conference and Exhibition, San Antonio, Texas, U.S.A., 24–27 September 2006; SPEREE (Feb. 2008).
Gringarten, A. C., Bozorgzadeh, M., Daungkaew, S. and Hashemi, A. 2006:" Well Test Analysis in Lean Gas Condensate Reservoirs: "Theory and Practice," Paper SPE 100993 presented at the 2006 SPE Russian Oil and Gas Technical Conference and Exhibition, Moscow, 3-6 October.
Gringarten, A. C., Well-head Pressure Transient Analysis SPE 164871
Gringarten, A.C. 2008. "Additional Well Test Analysis of Well E-M02Pa for PetroSA", Consulting report for PetroSA, May
Gringarten, A.C., Ogunrewo, O. and Uxukbayev, G. 2011: "Assessment of Rate-Dependent Skin Factors in Gas Condensate and Volatile Oil Wells, SPE 143592, presented at SPE EUROPEC/EAGE Annual Conference Vienna, Austria, 23-26 May 2011
Gringarten, A.C., T. von Schroeter, Rolfsvaag, T., Bruner, J. 2003. "Use of Downhole Permanent Pressure Gauge Data to Diagnose Production Problems in a North Sea Horizontal Well", SPE paper 84470.
Gringarten, A.C.: "Practical use of well test deconvolution", SPE paper 134534, September 2010.
Haddad, S., So What is the Reservoir Permeability? SPE 63138
Ian MacDonald -- SkyTruth - Gulf Oil Spill - New Spill Calculation
IGS629-003048
IGS642-000215
IGS770-000026
John Amos - SkyTruth - Gulf Oil Spill Rate Must be Much Higher than Stated

Kelkar Raghavan Consideration Materials List 20130401.pdf
Kuchuck, F.J., Carter, R.G., and Ayestaran, L.: "Deconvolution of Wellbore Pressure and Flow Rate," SPEFE 53, March, 1990.
LeBlanc Jason - FULL - FINAL 2012-09-10
LeBlanc Jason compressed
Lehr IOSC - Computing Mass Balance for the Deepwater Horizon Spill (Presented May 26, 2011)
Lehr IOSC Poster- Spill Response 10 Years Later
Levitan, M. M., Crawford, G. E., and Hardwick, A., 2004:" Practical Considerations for Pressure-Rate Deconvolution of Well Test Data," paper SPE 90680 presented at the SPE Annual Technical Conference and Exhibition held in Houston, Texas, U.S.A., 26–29 September.
Levitan, M.M. and Wilson, M.R., 2010:" Deconvolution of Pressure and Rate Data From Gas Reservoirs With Significant Pressure Depletion," paper SPE 134261 presented at the 2010 Annual Conference and Exhibition held in Florence, Italy, 19-22 September
MDL 2179 Deposition Exhibit 8580
MDL 2179 Deposition Exhibit 8581
MDL 2179 Deposition Exhibit 8582
MDL 2179 Deposition Exhibit 8583
MDL 2179 Deposition Exhibit 8584
MDL 2179 Deposition Exhibit 8585
MDL 2179 Deposition Exhibit 8586
MDL 2179 Deposition Exhibit 8587
MDL 2179 Deposition Exhibit 8588
MDL 2179 Deposition Exhibit 8589
MDL 2179 Deposition Exhibit 8590
MDL 2179 Deposition Exhibit 8591
MDL 2179 Deposition Exhibit 8592
MDL 2179 Deposition Exhibit 8593
MDL 2179 Deposition Exhibit 8594
MDL 2179 Deposition Exhibit 8595
MDL 2179 Deposition Exhibit 8596
MDL 2179 Deposition Exhibit 8597
MDL 2179 Deposition Exhibit 8598
MDL 2179 Deposition Exhibit 8599
MDL 2179 Deposition Exhibit 8700
MDL 2179 Deposition Exhibit 8701
MDL 2179 Deposition Exhibit 8702
MDL 2179 Deposition Exhibit 8703
MDL 2179 Deposition Exhibit 8704
MDL 2179 Deposition Exhibit 8705

MDL 2179 Deposition Exhibit 8706
MDL 2179 Deposition Exhibit 8707
MDL 2179 Deposition Exhibit 8708
MDL 2179 Deposition Exhibit 8709
MDL 2179 Deposition Exhibit 8710
MDL 2179 Deposition Exhibit 8711
MDL 2179 Deposition Exhibit 8712
MDL 2179 Deposition Exhibit 8713
Mendes, L.C.C., Tygel, M., and Correa, A.C.F.: "A Deconvolution Algorithm for Analysis of Variable Rate Well Test Pressure Data," paper SPE 19815, presented at the SPE ATCE, San Antonio, Texas, 1989.
M-I 00008408
M-I 00008408
NYT Article Reporting 5000 bbl a day NOAA Estimate
Ogunrewo, O. 2013. "Well test analysis of gas condensate and volatile oil below saturation pressure", an unpublished PhD thesis, Imperial College London.
Oil Release from Well MC252 Following the Deepwater Horizon Accident.pdf
Oil Spill Calculator - Technical Documentation
OPTION1 P and Q for Translation (26-04-13) with BHPs.xlsx
OPTION2 P and Q for Translation (26-04-13) with BHPs.xlsx
Pimonov, E.,A New Pressure/Rate-Deconvolution Algorithm to Analyze Wireline-Formation-Tester and Well-Test Data
PNAS Simulation Report
Pooladi-Darvish, Mehran Expert Modeling Runs
Practical use of well test deconvolution SPE 134534
PresComm - BP Comments to Oct 6 Working Paper No 3 - Amount and Fate of Oil
PresComm - BP Comments to Oct 6 Working Paper No 3 - Amount and Fate of Oil
PresComm - Flow Rate - Amount and Fate of Oil
PresComm - The Amount and Fate of the Oil (Revised)
PresComm - The Amount and Fate of the Oil (Revised)
Trusler PT-3K-1 Final Pressures.csv
Trusler PT-3K-2 Final Pressures.csv
PT3K2 SHUTIN DATA2.xlsx
PT-B Final Pressures.csv
Revised_Ratzel_9_2011
Roumboutsos, A., and Stewart, G.: "A Direct Deconvolution or Convolution Algorithm for Well Test Analysis," paper SPE 18157, presented at the SPE ATCE, Houston, 2-5 October, 1988.
Single-phase-density-20130306.xls
SNL043-007022
SNL043-007023

Appendix H (Materials Considered) - 2013-05-01-1931.docx

TREX-011696R.254

SNL043-007034
SNL043-007524
SNL111-002483
SNL111-002485
T=243F-SSF-ALL.xls
Thompson, L. and Reynolds, A.: "Analysis of Variable-Rate Well-Test Pressure Data using Duhamels Principle", Society of Petroleum Engineers Formation Evaluation, (October 1986).
Tiwari, R.R., "New Generation Permeability Logs," 7th International Conference & Exposition on Petroleum Geophysics
TRN-INV-01275508
Understanding the Muskat Method of Analysing Pressure Build-up Curves
Use of Data on the Build-up of Bottom-hole Pressures
von Schroeter, T., Hollaender, F., and Gringarten, A. C., 2001: "Deconvolution ofWell Test Data as a Nonlinear Total Least Squares Problem," paper SPE 71574 presented at the 2001 SPE Annual Technical Conference and Exhibition, New Orleans, Louisiana, 30 September – 3 October; SPEJ (Dec. 2004).
von Schroeter, T., Hollaender, F., and Gringarten, A. C., 2001: "Deconvolution ofWell Test Data as a Nonlinear Total Least Squares Problem," paper SPE 71574 presented at the 2001 SPE Annual Technical Conference and Exhibition, New Orleans, Louisiana, 30 September – 3 October; SPEJ (Dec. 2004)
Werely - Congressional Presentation
WHOI Preliminary Report
Will Wireline Formation Tests Replace Well Tests? SPE 84086
William D. McCain, The Properties of Petroleum Fluids, 2nd Edition tn870.5.m386 (1989).